NUREG/CR–5978
SAND92–2688

Source Term Attenuation by Water in the Mark I Boiling Water Reactor Drywell

Prepared by
D. A. Powers

Sandia National Laboratories
Operated by
Sandia Corporation

Prepared for
U.S. Nuclear Regulatory Commission

AVAILABILITY NOTICE

Availability of Reference Materials Cited in NRC Publications

Most documents cited in NRC publications will be available from one of the following sources:

1. The NRC Public Document Room, 2120 L Street, NW, Lower Level, Washington, DC 20555-0001
2. The Superintendent of Documents, U.S. Government Printing Office, Mail Stop SSOP, Washington, DC 20402-9328
3. The National Technical Information Service, Springfield, VA 22161

Although the listing that follows represents the majority of documents cited in NRC publications, it is not intended to be exhaustive.

Referenced documents available for inspection and copying for a fee from the NRC Public Document Room include NRC correspondence and internal NRC memoranda; NRC Office of Inspection and Enforcement bulletins, circulars, information notices, inspection and investigation notices; Licensee Event Reports; vendor reports and correspondence; Commission papers; and applicant and licensee documents and correspondence.

The following documents in the NUREG series are available for purchase from the GPO Sales Program: formal NRC staff and contractor reports, NRC-sponsored conference proceedings, and NRC booklets and brochures. Also available are Regulatory Guides, NRC regulations in the *Code of Federal Regulations*, and *Nuclear Regulatory Commission Issuances*.

Documents available from the National Technical Information Service include NUREG series reports and technical reports prepared by other federal agencies and reports prepared by the Atomic Energy Commission, forerunner agency to the Nuclear Regulatory Commission.

Documents available from public and special technical libraries include all open literature items, such as books, journal and periodical articles, and transactions. *Federal Register* notices, federal and state legislation, and congressional reports can usually be obtained from these libraries.

Documents such as theses, dissertations, foreign reports and translations, and non-NRC conference proceedings are available for purchase from the organization sponsoring the publication cited.

Single copies of NRC draft reports are available free, to the extent of supply, upon written request to the Office of Information Resources Management, Distribution Section, U.S. Nuclear Regulatory Commission, Washington, DC 20555-0001.

Copies of industry codes and standards used in a substantive manner in the NRC regulatory process are maintained at the NRC Library, 7920 Norfolk Avenue, Bethesda, Maryland, and are available there for reference use by the public. Codes and standards are usually copyrighted and may be purchased from the originating organization or, if they are American National Standards, from the American National Standards Institute, 1430 Broadway, New York, NY 10018.

DISCLAIMER NOTICE

NUREG/CR-5978
SAND92-2688

Source Term Attenuation by Water in the Mark I Boiling Water Reactor Drywell

Manuscript Completed: August 1993
Date Published: September 1993

Prepared by
D. A. Powers

Sandia National Laboratories
Albuquerque, NM 87185

Prepared for
Division of Systems Research
Office of Nuclear Regulatory Research
U.S. Nuclear Regulatory Commission
Washington, DC 20555-0001
NRC FIN L1484

Abstract

Analyses are presented to show that water admitted to the drywell of a Mark I boiling water reactor can significantly attenuate radionuclide releases during severe reactor accidents. This attenuation can be achieved whether or not water is able to prevent or delay failure of the drywell. Attenuation of releases of radioactive materials is achieved by the actions of water pools maintained over core debris interacting with concrete in the drywell and by the actions of drywell sprays.

A mechanistic model is formulated of the aerosol scrubbing by a water pool overlying core debris that is interacting with concrete. Eighteen uncertain features of the model are identified. A quantitative uncertainty analysis of the model is described. Cumulative probability distribution functions are developed at confidence levels of 50, 90, and 95 percent for the decontamination factors that can be achieved by water pools 30 and 50 cm deep with subcooling of 0, 2, 5, 10, 20, 30, 50, and 70°C. These distribution functions show with high confidence that the radionuclide emissions during core debris interactions with concrete can be reduced by a factor of 10 and perhaps by a factor in excess of 100 by shallow, subcooled water pools. It is argued that similar decontamination factors would be realized even if core debris penetrated the Mark I liner and flowed into the reactor torus room.

Features of spray systems in the drywells of Mark I containments are described. A mechanistic model is formulated of the aerosol scrubbing that can be achieved by drywell sprays. Nineteen uncertain features of the model are identified and quantities are defined to describe the uncertainty of these features. Ranges of values for uncertain quantities and distributions for values within these ranges are defined. A quantitative uncertainty analysis of the model is described. Cumulative probability distribution functions are developed at confidence levels of 50, 90 and 95 percent for the decontamination coefficient produced by sprays for water fluxes into the drywell of 0.002, 0.01 and 0.25 cm^3/cm^2-s. Rapid removal of aerosols by spray droplets can be expected with high confidence only for the highest water fluxes ($\sim$0.25 cm^3 H_2O/cm^2-s). These high water fluxes are within the capabilities of spray systems in some Mark I drywells. At lower water fluxes, decontamination of the drywell atmosphere can be achieved if drywell failure is delayed and the leak rate following drywell failure is not large.

Correlations of the results obtained in the uncertainty analyses of decontamination by water pools and by sprays are used in an example analysis of a hypothetical accident at a Mark I boiling water reactor.

Contents

Contents (Concluded)

Figures

Figures (Continued)

Figures (Concluded)

Tables

Acknowledgements

The author acknowledges the final editorial assistance he has received in the course of preparing this work from R. Cochrell and the graphic arts work of T. Salazar. The author also acknowledges the sacrifice by S. Powers of her kitchen and dining room tables for six months to the masses of paper generated during this work.

Executive Summary

The document describes the effects on the source term that water pools and sprays in the Mark I boiling water reactor would have. Detailed phenomenological models of the decontamination of aerosol-laden gas bubbles rising through a water pool and of the removal of aerosols by spray droplets are developed. The decontamination of bubbles by water pools occurs by:

- condensation of excess steam in subcooled water pools,
- sedimentation of aerosols within bubbles,
- diffusion of aerosol particles to bubble walls, and
- inertial impaction of aerosol particles with bubble walls in the cases where gases within the bubble circulate.

Spray droplets remove aerosols from the drywell atmosphere by:

- impaction of particles too big to follow stream lines of flow around the droplets,
- interception of particle whose size is big enough that the particle extends across stream lines to contact the droplets, and
- diffusion of particles to droplet surface.

Eighteen uncertain features of the model of decontamination of aerosol-laden gases by water pools are identified. Nineteen uncertain features of the model of spray removal of aerosols from the drywell atmosphere are identified. These uncertainties include:

- uncertainties in the quantitative description of phenomena and processes responsible for trapping of aerosol particles by water in the form of pools or spray droplets,
- uncertainty in the physical properties of the drywell atmosphere, contaminated water and aerosol particles, and
- uncertainty in the boundary conditions and initial conditions dictated by the progression of severe accidents in Mark I boiling water reactors.

Parametric quantities are defined to describe these various uncertainties. Credible ranges for the values of the parametric quantities are established based on data, analyses and, where necessary, judgement. Subjective probability density functions for values of the parametric quantities within these ranges are assigned according to a set of rules:

- a uniform probability density function is assigned to a parameter whose meaningful range of values spans less than one order of magnitude,
- a uniform probability density function is assigned to the logarithm of a parameter whose meaningful range of values spans more than one order of magnitude, and

- a lognormal distribution is assigned to parameters for which there are data or other reasons to believe the probability densities are more peaked around a median value than would be indicated by a uniform or log-uniform probability density function.

Because of the uncertain features of the respective models, decontamination factors that can be produced by water pools and the rates of aerosol removal by sprays in the drywells of Mark I containments are uncertain. Uncertainty distributions for the decontamination factors and spray removal rate constants are constructed from samples of the distributions obtained using a Monte Carlo sampling. The samples were of a size that there was a 99 percent confidence that 95 percent of the possible range of values of the predicted quantity was sampled. The uncertainty distributions were constructed using a nonparametric statistical analysis to distinguish between phenomenological uncertainty and stochastic uncertainty that arises from the use of finite samples of the distribution.

Uncertainty distributions were obtained for the decontamination of gases produced during core debris/concrete interactions by water pools 30 and 50 cm deep subcooled by 0 to 70 degrees Kelvin.

The rate constant for spray decontamination of a drywell atmosphere was found to depend on the extent of atmosphere decontamination as well as water flux through the atmosphere. Uncertainty distributions are developed for the rate constants for spray removal of aerosols for water fluxes of 0.25, 0.01 and 0.002 cm^3 H_2O/cm^2-s and decontamination factors of 1.1, 2, 3.3, 10, 100 and 1000.

Results obtained in these uncertainty analyses are applied to several hypothetical severe accident situations. The calculations done for these cases show that the amount of radioactive material available for release in the event of failure of the Mark I liner can be reduced substantially by water in the drywell. Appropriate design for water pool depth, subcooling, spray water flux and spray operation time can produce decontamination factors of over 100 relative to cases in which water is not available in the drywell. Thus, even if water in the drywell is unable to prevent containment failure the water can reduce substantially the amount of radioactive material released from the nuclear plant and consequently, the consequences of a severe reactor accident.

I. Introduction

Risk to the public from the use of nuclear power was shown as early as 1975 to be small and to come predominantly from severe accidents that exceed the design basis of the power plants [1]. Public consequences of severe accidents come about only if the accident leads to the failure of the protective barriers in a plant and if large quantities of radioactive materials are released from the plant. This usually means that to produce large consequences the severe accident must cause the protective containment of the nuclear reactor to rupture. There must, however, also be a substantial amount of radioactivity suspended in the containment atmosphere at the time of containment rupture or following containment rupture for these large public consequences to develop. The so-called NUREG-1150 study [2] has confirmed these general conclusions for five different types of nuclear power plants. The study provides quantitative analyses of both the probability of containment failure and the probability of a large radioactivity release following containment failure at each of these nuclear power plants.

Findings in the NUREG-1150 study for the specific case of a Mark I boiling water reactor present an interesting example. Relative to other types of nuclear power plants, the probability that Mark I boiling water reactors will have accidents that go beyond the design basis is low. The boiling water reactors have automatic depressurization capabilities. Once depressurized, the reactor coolant system can be supplied coolant from a variety of low-pressure sources to prevent core meltdown. If, despite the many sources of water, an accident progresses to core melting, there are still many protective features of the Mark I containment that can prevent the release of large amounts of radioactivity. In most severe accidents hypothesized as possible in the Mark I reactors, effluents produced during core degradation within the reactor coolant system including radioactive vapors and aerosols released from overheated fuel must pass through the reactor's steam suppression pool. This pool will scrub particulate and soluble radioactive materials from the effluent [3-5]. The effluent stream of hydrogen and steam is substantially cleansed of radioactive materials except, perhaps, for noble gases.

Safety concerns with the Mark I boiling water reactor increase if severe accidents can progress to the point that core debris penetrates the reactor vessel and falls into the reactor drywell (see Figure 1). Though the drywell of a Mark I containment has a very strong, steel, pressure boundary [6], the drywell is of small volume ($< 200{,}000$ ft^3 or < 5100 m^3). The drywell can be pressurized quickly once core debris is outside the reactor vessel. An example of the pressurization of the drywell calculated to take place in a particular, hypothetical severe accident [7] is shown in Figure 2. Gases and heat partitioned into the containment atmosphere as the core materials expelled from the vessel interact with the concrete are responsible for this pressurization. With continued pressurization, the Mark I boiling water reactor containment can rupture and radioactive materials suspended in the containment atmosphere can be released into the reactor building and eventually outside the plant [8].

The Mark I containments also use elastomeric seals. Overheating of these seals, especially in the presence of ionizing radiation from radionuclides released from the fuel, can also cause a loss of containment integrity [8-10] and a release of radioactivity.

Threats to the integrity of the Mark I containment are of keen interest. In 1985, an alternate mechanism for containment failure in the Mark I boiling water reactor was identified. Greene et al. [11] showed that core debris expelled from the reactor coolant system could spread out of the pedestal region, across the drywell floor of a Mark I containment, and come into direct contact with the steel liner that constitutes the containment pressure boundary. For most of the accident cases considered, contact between the core debris and the liner was predicted to lead to liner melting and a loss of containment

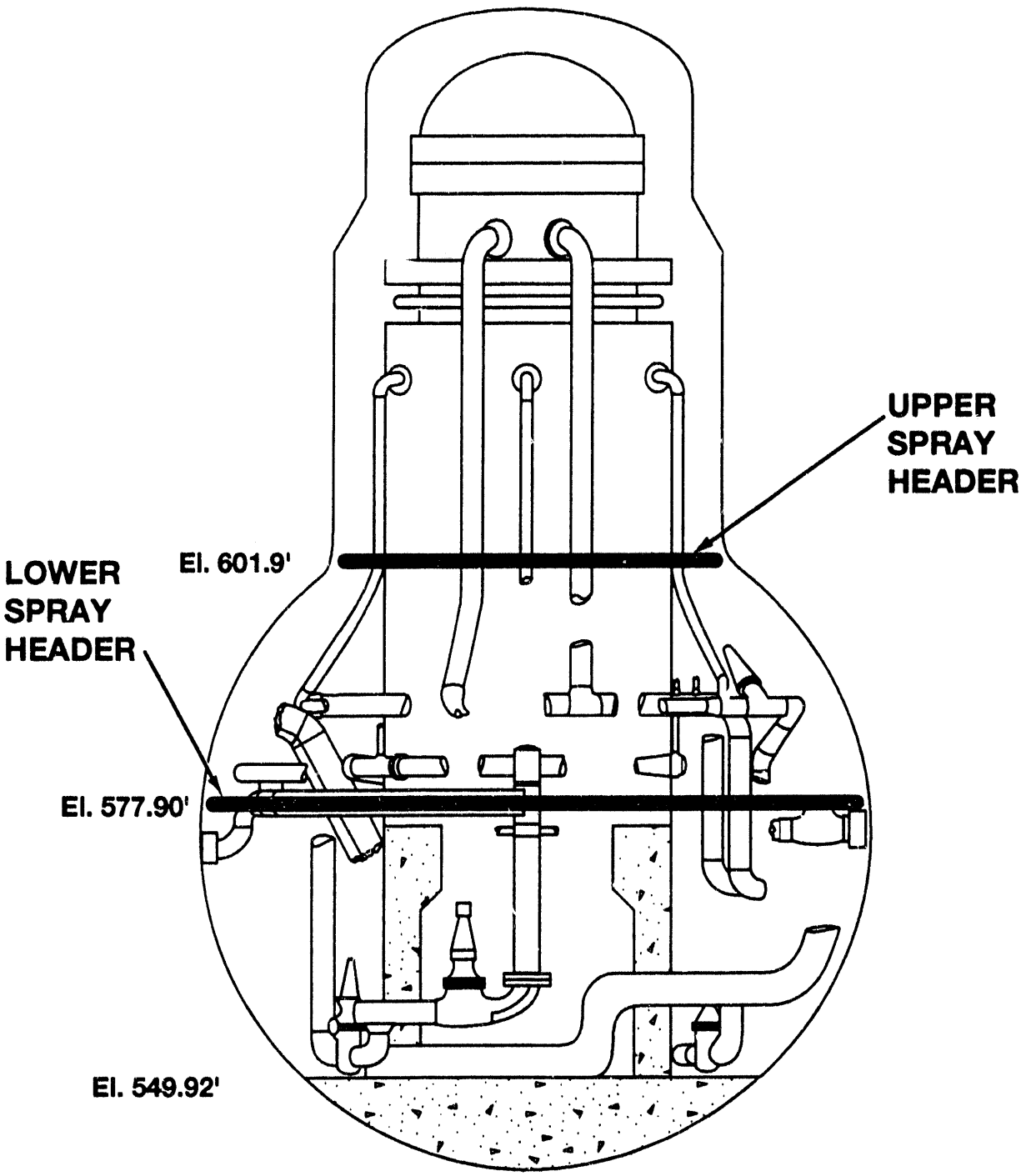

Figure 1 Schematic diagram of the Mark I containment for a boiling water reactor. Much of the piping and other structures within the drywell has been deleted for the purposes of clarity. Note that elevations are given in feet where 1 ft = 30.48 cm.

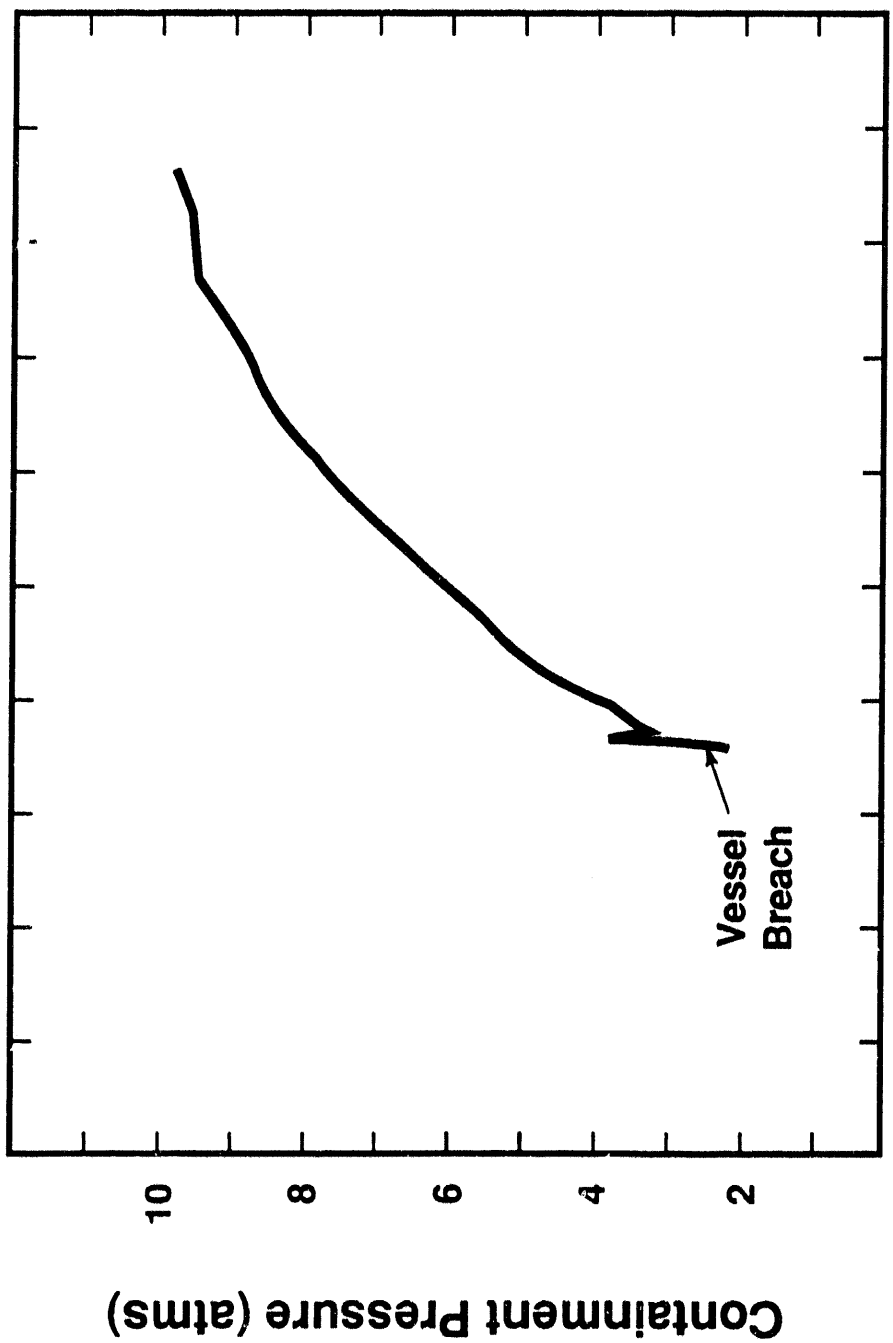

Figure 2 Pressure within a Mark I boiling water reactor containment during a severe reactor accident. Details of this calculation are described in Reference 8. Times are from accident initiation. Core debris attack on concrete was assumed to begin immediately after vessel failure.

integrity. Some attempts have been made to contradict these findings [12]. Most other analyses have tended to support the contention that contact of high-temperature core debris with the Mark I drywell liner without water present causes containment failure [?, 13]. The probability of containment failure in the event of a core meltdown or severe accident in a Mark I boiling water reactor is high relative to this conditional probability in other reactors [2]. In pursuit of defense-in-depth against risks associated with the use of nuclear power there is interest in mitigating the threat of liner failure as a result of interactions with core debris on the drywell floor.

Several mitigation schemes have been suggested including the installation of a refractory barrier at the openings from the pedestal region of the drywell to prevent core debris contact with the liner [14]. The simplest mitigation strategy that has been suggested is to assure that water is present in the drywell at the time core debris is expelled from the reactor coolant system into the reactor cavity. It has been hypothesized that a water pool on the drywell floor might prevent or at least it might delay contact between molten core debris and the liner. Furthermore, with an overlying water present, the liner would act as a "cooling fin." Heat imparted to the liner would conduct up through the liner and be removed by boiling water. Again, even if the water did not ultimately prevent liner failure, it would surely delay failure. Delays in the time of containment failure are significant. They provide time to implement emergency response measures. They also allow time for natural processes to attenuate the amount of radioactivity suspended in the containment atmosphere and available for release when containment integrity is lost.

Qualitative arguments on the mitigation by water of the threat posed to the drywell liner by core debris were not persuasive during the analyses of uncertainty done for the NUREG-1150 study [2]. Some of the experts elicited during this study felt that water would have a powerful mitigating effect on core debris interactions with the liner. Others believed that the potential effects of water were overestimated and the threat to the liner was little altered by presence of water on the drywell floor. As a result of this disparity in expert opinions, the conditional probability of containment failure estimated in NUREG-1150 remained high for the Mark I boiling water reactor relative to other types of containment.

The U.S. Nuclear Regulatory Commission has initiated a more thorough, probabilistic examination of the effects water can have on melt/liner interactions [15]. Preliminary results of this work have been subjected to intense expert scrutiny. The results do support the contention that water on the drywell floor will reduce dramatically the probability of early containment failure during a severe accident in a Mark I boiling water reactor.

The analyses of core debris/liner interactions now being done do not indicate that the possibility of eventual failure of the Mark I containment by some mechanism is reduced. Nor do the studies consider all possible interactions of core debris with the liner. Such things as splashing melt onto the liner by pressure-driven melt expulsion or as a result of energetic melt/water interactions are not considered. It is, however, useful to notice that water in the drywell can mitigate severe accidents at Mark I boiling water reactors in ways other than preservation of liner integrity during interactions with core debris. In particular, water in the drywell could attenuate substantially the amount of radioactive material that could escape the plant in the event that containment did fail by whatever mechanism. That is, a reduction in the source term of radioactivity from the containment can be achieved whether or not water can prevent liner melt-through or mitigate pressurization within the containment.

Radioactive aerosols are injected into the drywell atmosphere by three important processes:

- release of radioactive species during core debris interactions with concrete,
- release of radioactive species from residual fuel in the reactor coolant system after core debris has penetrated the reactor vessel, and
- revaporization or resuspension of radionuclides deposited in the reactor coolant system during core degradation early in the reactor accident.

Once core debris has penetrated the reactor vessel, released radionuclides accumulate in the drywell atmosphere rather than being forced through the steam suppression pool. The very effective scrubbing of radioactive materials from the effluents by the suppression pool is no longer possible. Only the slower processes of aerosol sedimentation and deposition naturally attenuate the amount of radioactive material suspended in the drywell atmosphere and available for release from the nuclear plant should the drywell rupture.

Introduction of water into the drywell provides additional mechanisms to reduce the amount of radioactivity available for release from the plant in the event of drywell failure. A water pool overlying core debris in the drywell will scrub aerosols from gases evolved during core debris interactions with concrete. Though the overlying water pool will typically be shallower than a steam suppression pool, the physical phenomena responsible for mitigating the radionuclide release during core debris interactions with concrete are quite similar to the physical phenomena responsible for decontamination by steam suppression pools. Decontamination can be achieved by a water pool overlying core debris interacting with concrete even though the water does not quench and cool the core debris [16]. This decontamination can be substantial especially if the water pool is subcooled.

Water pools overlying core debris in the Mark I drywell have the very attractive feature that they will follow the debris should the debris penetrate the liner. Were core debris to penetrate the liner, it would seem likely that debris would flow along the annulus between the steel liner and the concrete shield building. Eventually the debris would encounter an opening for a downcomer for the steam suppression pool. Debris would flow through this opening into the so-called "torus room." (See Figure 3.) Once core debris had drained from the drywell along this route, water would surely follow if not accompany the debris. Except, perhaps, for a brief transient period, the core debris would remain covered with water. In the torus room core debris could be spread over a very broad area which might be expected to further mitigate some of the release of radioactivity from the debris. Also, the continued supply of water could lead to very deep water pools overlying debris in the torus room and, consequently, very extensive scrubbing of aerosol-laden gases being evolved from the debris.

Additional mitigation of the radionuclide source term can be achieved depending on how water is admitted to the Mark I drywell. Essentially, there are two ways readily available to supply this water. Water can be injected into the reactor coolant system via the normal routes. Core debris will have penetrated the reactor vessel at this stage in an accident. The water, then, will drain from the reactor coolant system into the drywell. Or, water can be admitted to the drywell by the drywell sprays.

Either mechanism for water admission could attenuate the release of radioactivity beyond the attenuation provided by the water pool overlying core debris on the drywell floor. Water injected into the reactor

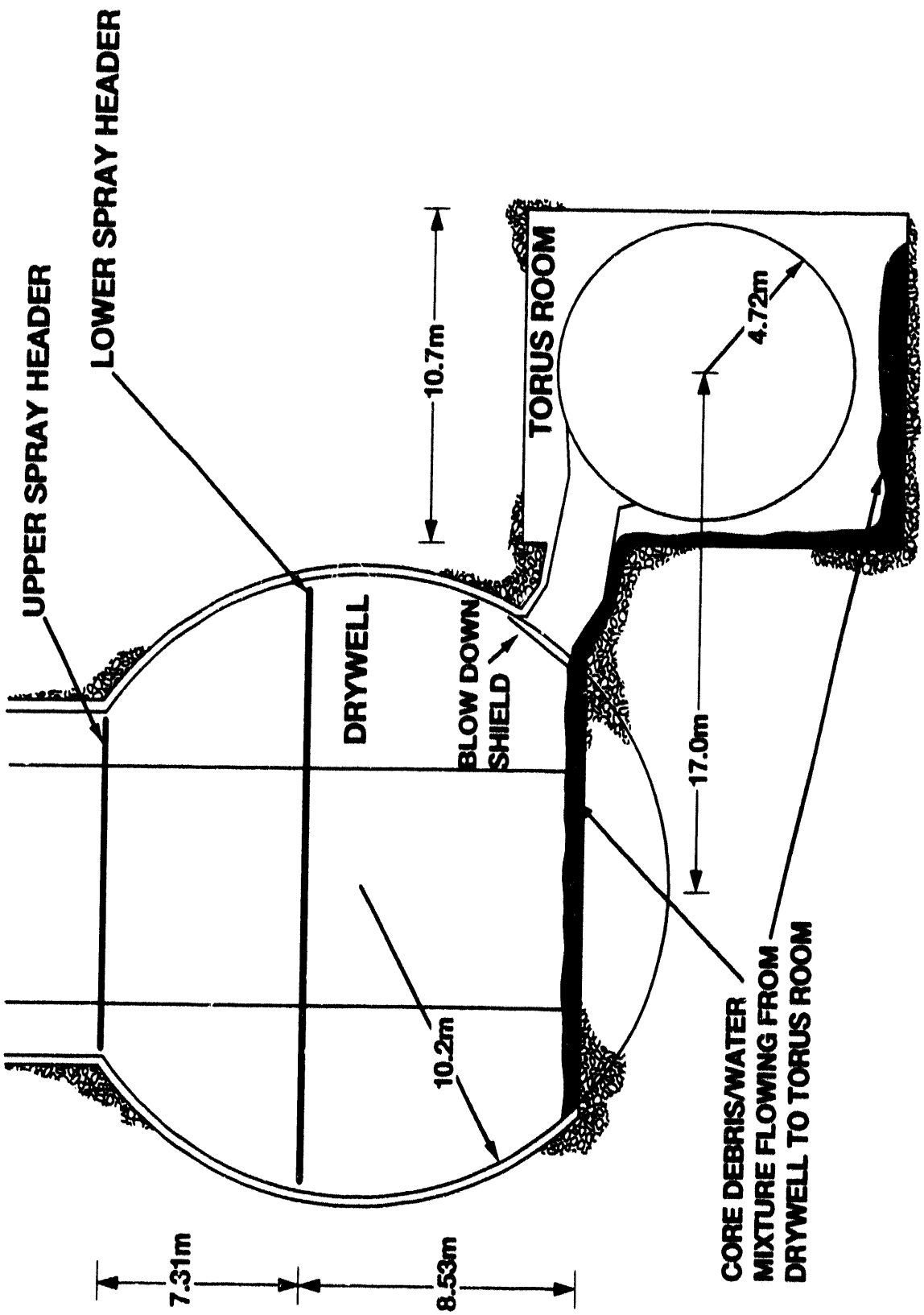

Figure 3 Conceptual drawing of core debris draining from the Mark I drywell into the torus room.

coolant system would cool the surfaces of the reactor coolant system and reduce or delay the revaporization of radionuclides deposited on these surfaces. Depending on the precise routes taken by the water flow, a substantial fraction of the deposited radionuclides might be leached or dissolved from the reactor coolant system so that they could not revaporize. Water added to the reactor coolant system by the core sprays might cool residual fuel sufficiently that there would be no significant additional releases of radionuclides from this residual fuel. The biggest additional source term attenuation would be achieved by admitting water to the drywell with the drywell sprays. The sprays would, of course, cool the drywell atmosphere, thus reducing loads on the containment and at least delaying containment failure by overpressurization. The sprays would cool the reactor vessel and at least reduce the heating that drives revaporization. But, the most important effects of spray would be to sweep aerosol particles from the containment atmosphere regardless of whether these particles were produced by core degradation, revaporization or the interactions of core debris with concrete. The drywell sprays augment the attenuation of the radionuclide release during core debris interactions with concrete in the drywell provided by the overlying water pool. Sprays replace the attenuation of the radionuclide release from other sources provided by the steam suppression pool earlier in a severe accident before core debris penetrated the reactor vessel.

Studies at the systems level to indicate which of the two routes of water addition is most likely to be available and which is to be preferred have not appeared. Injection via the normal routes into the reactor coolant system most likely will not be available for accidents in which automatic depressurization of the reactor coolant system occurred. Were these water sources available, it is likely that the reactor incident could not have progressed to a severe accident. On the other hand, the normal, low pressure water injection routes may become available for accident management in cases in which the core degradation processes take place at elevated pressure. Only after core debris has penetrated and depressurized the reactor vessel would the low pressure water sources be available for accident mitigation. Or, the low pressure water injection may become available only as a result of accident recovery efforts that were successful too late to prevent meltdown of the core and expulsion of the core into the drywell. Use of drywell sprays may be resisted because, at least at some plants, water for these sprays is drawn from the low pressure injection system. Operators may prefer to retain the full capability of the low pressure injection in the hope that recovery efforts would make these capabilities available to them.

Despite issues concerning the way water can be provided to the drywell, the qualitative arguments made above show that water additions to the drywell could provide substantial risk reduction by attenuating the inventory of suspended radioactivity available for release from the plant should containment fail. This attenuation can be achieved whether the drywell water significantly delays containment failure or not. Attenuation can continue even after containment failure. The issue, then, is to ascertain how much attenuation of radionuclide release can be achieved by drywell water. Source term attenuation by water pools overlying core debris in the Mark I drywell and source term attenuation by drywell sprays are examined quantitatively in the balance of this document.

There are uncertainties in the prediction of decontamination that can be achieved by water pools and sprays in the Mark I containments. These uncertainties arise from a variety of sources. Boundary and initial conditions needed for the predictions are highly variable among the many types of accidents hypothesized to occur in Mark I boiling water reactors [2, 15]. Even for a specified accident at a specified nuclear power plant the details of accident progression are not so perfectly known that boundary and initial conditions can be accurately specified. Models now available to predict the

performance of sprays and water pools are not perfect. Some uncertainty must be ascribed to predictions obtained with these models.

With these uncertainties in mind, the analyses presented below were developed following a procedure successfully used to analyze other uncertain severe accident source term issues [17-21]. Physical phenomena that lead to decontamination by overlying water pools and by sprays are briefly described. The various sources of uncertainty are identified. Quantitative uncertainty analyses of the decontamination processes are described. The uncertainty analysis is conducted by a Monte Carlo sampling of the predictions of mechanistic models of the processes. The results of the Monte Carlo sampling are then analyzed with non-parametric, order statistics methods. This analysis is used to construct quantitatively characterized uncertainty distributions for the predictions of the decontamination that can be achieved by overlying water pools and by sprays in the Mark I containment. In Chapters II and III the physical phenomena responsible for source term attenuation are described. In Chapters IV and V similar discussions are presented for source term attenuation by sprays. Chapter VI is a description of likely source term reductions that can be achieved with drywell water in reactor accidents.

II. Source Term Attenuation by an Overlying Water Pool

A. Background

By hypothesis, water is to be supplied to the drywell of a Mark I boiling water reactor at a rate sufficient to maintain a water pool over the core debris. The physical phenomena that lead to scrubbing of aerosols from gases sparging through this water pool are described in this chapter.

Early in the course of core debris expulsion from the reactor coolant system it may not be physically possible to maintain a coolant layer over the core debris. A core debris stream is hypothesized [15] to fall some 10 m from the reactor vessel into the pedestal region. If water is present on the drywell floor at the time core debris penetrates the vessel, a very dynamic interaction between water and core debris will take place. Large volumes of steam will be generated which might push water out of the pedestal region or even elutriate debris droplets out of the pedestal region. This dynamic period is not considered here. Rather, the quasi-steady state in which a coherent water pool overlies a pool of core debris is the situation of interest.

An inherent conservatism in the analysis is developed because attention is directed toward cases in which a very large fraction of the core inventory has been expelled from the reactor coolant system. Spreading of the core debris over the drywell floor is assumed to be complete. The water supply and the overflow of water into downcomers for the steam suppression pool are assumed to be in balance. Water is presumed not capable of completely quenching the core debris. This is consistent with all data now available concerning the simultaneous interactions of core debris with concrete and coolant (see for example References 16 and 22). There are, however, suggestions that tests done to date are not sufficiently representative of the real interactions that would take place in the drywell under severe accident conditions [23]. Under sufficiently representative conditions, it is contended, water will quench the core debris. Were this quenching to occur, source terms from the ex-vessel interactions of core debris would, of course, be negligible. Radioactivity releases from residual fuel in the ruptured reactor vessel or releases by revaporization of materials deposited on surfaces of the reactor coolant system would still be possible.

Early in the course of core debris interactions with concrete in the drywell, the water supply necessary to maintain a water pool over the core debris would have to be relatively large. The water supply would have to compensate for boiling losses as a result of both decay heat and exothermic chemical reactions in the core debris. Core debris produced in severe reactor accidents is usually calculated [7] to be rich in metallic zirconium. This metallic zirconium is highly reactive toward the condensed and gaseous products of concrete decomposition:

$$Zr + 2H_2O \rightarrow ZrO_2 + 2H_2$$
$$\Delta H(rxn) = -580321 \text{ J}$$

$$Zr + 2CO_2 \rightarrow ZrO_2 + 2CO$$
$$\Delta H(rxn) = -527887 \text{ J}$$

$$Zr + SiO_2(l) \rightarrow ZrO_2 + Si(l)$$
$$\Delta H(rxn) = -148377 \text{ J}$$

where $\Delta H(rxn)$ is the enthalpy of reaction using the chemical convention so that when heat is produced by a chemical reaction the value of $\Delta H(rxn)$ is negative. The exoergic reactions of zirconium can produce heating rates in core debris that are several times heating rates produced by radioactive decay.

Once the highly reactive species in the core debris are consumed, the water supply necessary to maintain a water pool must only compensate for boiling that comes from decay heating in the debris. In fact, there are water supply capabilities in some Mark I containments that are sufficient to maintain the water pool subcooled at least once vigorous, exoergic chemical reactions have ceased. For instance, drywell sprays at the Brown's Ferry units 1 and 2 can supply 517 liters of water per second. At unit 3, the sprays can supply 577 liters per second. On the other hand, some Mark I drywell sprays have been modified to curtail the flow of water to about 50 liters per second out of concern that under some circumstances the sprays might cool the drywell atmosphere so much that pressure within the drywell is less than the external atmospheric pressure. The Mark I pressure boundary is not designed to withstand external pressurization.

The mechanics available for supplying water to the drywell are not the issues of interest here. The basis for the discussions below is that a water pool can be maintained over the core debris. It is evident that the water pool can be saturated or subcooled.

Water pools that can be maintained in the drywells of Mark I boiling water reactors will not be deep. Without some modifications, water will flow into the downcomers for the steam suppression pool. The lower lips for the downcomers in the Brown's Ferry Mark I boiling water reactors are 61 cm above the floor. At other Mark I boiling water reactors, the lower lip for the downcomers may be at other elevations above the drywell floors. A relatively complete meltdown of the Mark I reactor core would produce a debris bed with a "collapsed height" of about 22 cm. The depth of the water pool, if gas holdup in the debris is considered, might then be only 30 cm. Given that the lower lips of the steam suppression pool downcomers are 60 cm above the flow, it is unlikely that overlying water pools will be deeper than about 50 cm. It is possible to get deeper water pools in the drywell by completely flooding the steam suppression pool torus. This, however, requires steps to be taken that are outside the scope of analysis undertaken here. Consequently, very deep water pools are not considered here. Deep water pools can develop if molten core debris flows into the torus room (see above).

Were there no water present, core debris interacting with concrete would be expected to inject enormous quantities of aerosol into the reactor containment atmosphere. Predictions of the rates of aerosol generation during core debris interactions with concrete in a Mark I boiling water reactor are shown in Figure 4 [8]. Core debris first deposited on the drywell floor is usually predicted to be at a fairly low temperature. Aerosol generation increases as the core debris heats because of radioactive decay and the exoergic reactions of concrete decomposition products with zirconium in the core debris. Core debris produced in severe accidents at Mark I boiling water reactors is often predicted to be quite rich in zirconium so heating of the core debris by chemical reactions can be prolonged. Very intense release of aerosols from the core debris lasts for 4 to 5 hours after core debris first contacts the concrete. (Note that for the calculations shown in Figures 4 and 5, core debris was not allowed to spread outside the pedestal region of the drywell. Spreading of the debris might accentuate the rates of chemical reaction of debris constituents and thus shorten the period of intense radionuclide release and aerosol generation. On the other hand slow deposition of debris into the drywell might prolong the period of high aerosol generation by renewing the concentration of reactive zirconium in the core debris.) Once the reactive constituents of core debris are consumed, temperatures in the core debris drop rapidly. A fairly steady,

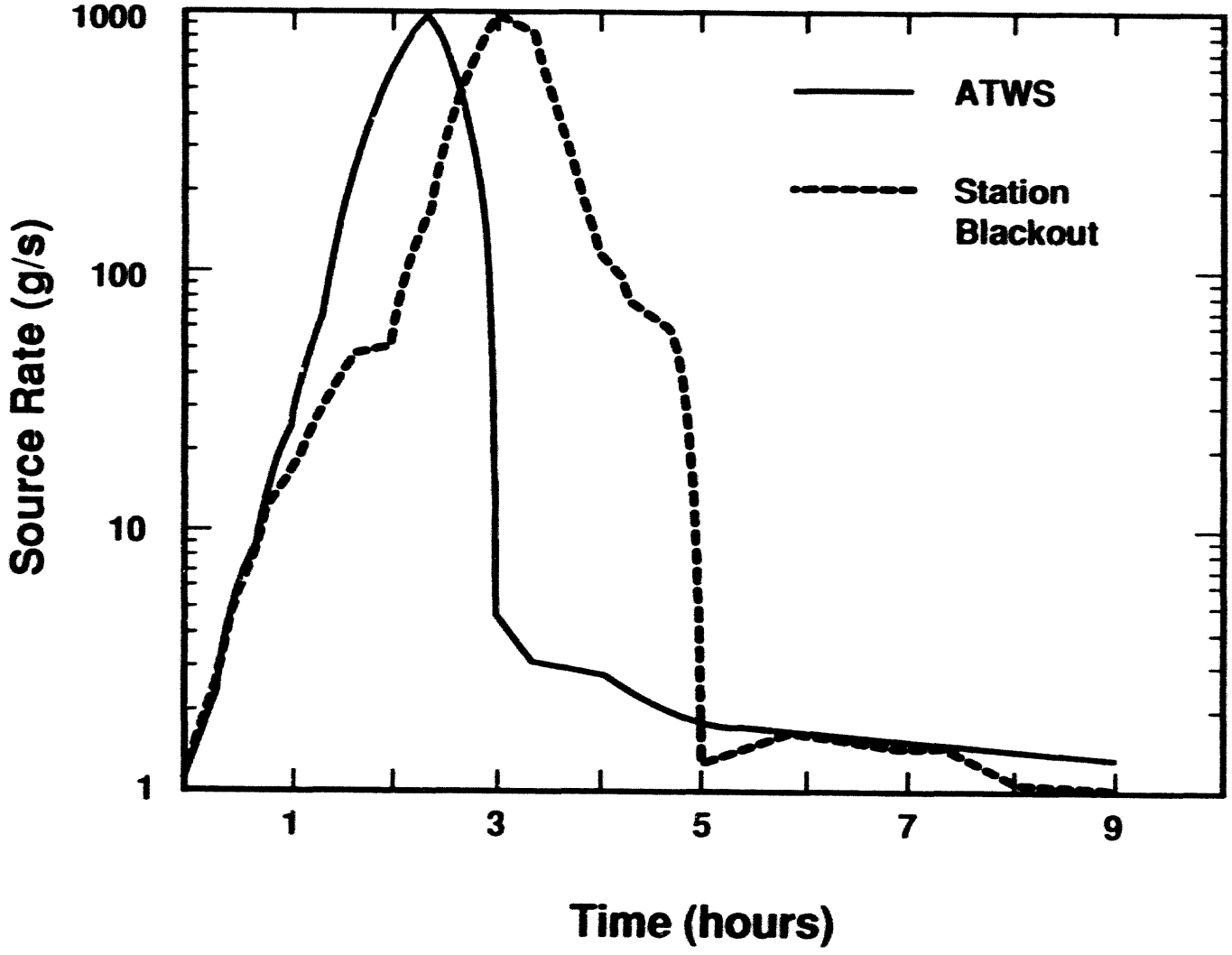

Figure 4 **Calculated rates of aerosol generation during core debris interactions with concrete in a Mark I boiling water reactor drywell. The solid line is for an anticipated transient without scram accident (a so-called TC2) accident. The dashed line is for an accident initiated by loss of on-site and off-site power (a so-called station blockout or TB1 accident). Times are from the start of core debris attack on concrete. Other details of the calculation are to be found in Reference 7.**

low, aerosol generation rate develops. Though aerosol generation is shown only for about 10 hours in Figure 4, aerosol generation can continue for days at these low rates. Most of the radionuclide release occurs during the high temperature phase of the core debris interactions. But, tellurium release persists even into the long term, low intensity, release phase of the interactions [24]. Consequently, from a radionuclide source term perspective, mitigation by an overlying water pool of even the late phase releases is still of interest.

B. Attenuation Mechanisms

The predominant mode by which aerosols are generated during core debris interactions with concrete is the vaporization of volatile constituents of the melt. Water vapor and carbon dioxide released from the concrete sparge through and react with the molten core debris. Bubbles of gas in the melt provide free surfaces for the vaporization of species from the melt. At the temperatures expected to exist in mixtures of core debris and concrete decomposition products, nearly all the melt constituents have significant vapor pressures and will contribute vapor to the bubbles. When bubbles emerge from the core debris, the vapors are released into a cooler environment, and they condense to form aerosol particles. When bubbles burst at the surface of core debris, aerosols can be formed by mechanical processes. Typically, mechanical generation of aerosols is a small fraction of the aerosol generation by vaporization [25]. Late in the course of core debris interactions with concrete when melt temperatures are quite low, the mechanical generation of aerosols can become comparable to aerosol generation by vaporization. Mechanical aerosol generation becomes the predominant mode of radionuclide release at very low core debris temperatures.

In principle, the essential phenomena responsible for aerosol generation are not greatly changed when a water pool overlies the core debris if water does not quench the debris. The one complication arises because water will cause a crust of solidified material to form at the interface between the water and the core debris.* The crusts are quite porous so aerosol-laden gases readily pass through the crusts. Crusts might interfere in the mechanical formation of aerosols by bubbles bursting at the surface of molten debris. The fine pore structure of the crusts might provide excellent surfaces for the deposition of aerosols. None of these effects are considered here. The only attenuation of aerosol generation attributed to water pools is the scrubbing of aerosols from gas bubbles rising through the water pools.

Gases produced by melt attack on concrete are assumed here to mix with steam produced by the boiling of water on the crust surface. The mixing is easiest to imagine if water is in film boiling on the crust surface. Then, gases emerging through the pores in the crust combine in the steam film at the interface with water. Taylor instability of the low density gas layer below the liquid water leads to bubble formation. Available experimental information suggests, however, that water on core debris crusts is in nucleate rather than film boiling. It must, then, be imagined that free surfaces formed by gases emerging from the pore structure provide excellent water vapor generation sites induced by the heat flux from the crust. When enough gas and steam has entered a bubble, the bubble detaches form the crust and rises through the water pool.

---

*Some specialists have suggested that such crusts are unstable and will fragment into coolable debris. The many tests that have now been done of combined core debris-concrete-coolant interactions have not shown this phenomenon. It is neglected here. Crusts are assumed to be stable for this work, as has been shown in all tests to date.

Aerosols within a gas bubble rising through the water pool can be "scrubbed" from the gas because:

- aerosols sediment onto the walls of the bubble,
- aerosols diffuse to the walls of the bubble, and
- aerosols inertially impact the walls of the bubble.

Sedimentation is just the gravitational settling of particles within the bubble. Sedimentation rates are significant only for the larger aerosol particles such as those generated by mechanical processes at the surface of the molten core debris. Diffusion of aerosol particles is the result of the spatially stochastic impulses imparted to the particles by collisions with gas molecules. Diffusion efficiently transports only very small particles (diameters ≤ 0.1 μm) to the bubble walls on the time scales of interest. Impaction of aerosol particles with the bubble walls occurs because the gases within the bubble can circulate as the bubble rises. Particles that are too big to respond to the accelerations involved in the circulatory motion of the gas can be carried into the bubble walls. Circulation of the gases is thought to depend on the purity of the water as well as the size of the bubble [26]. Impurities in the water can accumulate on the bubble surface and retard circulation of gas within the bubble.

It is assumed here that once a particle contacts the water it is permanently trapped in the water. Surface tension and van der Waals forces are thought to be sufficiently strong to preclude bounce or re-entrainment of the particles.

Consider a bubble containing a mass M(x) of aerosols of particle size d_p. The bubble is distorted into an oblate ellipsoid of eccentricity E and has a volume equivalent to a spherical bubble of size D_b. The extent to which particles are scrubbed from the bubble by sedimentation, diffusion and impaction per unit of rise distance is given by:

$$\frac{dM(x)}{dx} = -\left\{ \alpha_s \left(D_b, d_p\right) + \alpha_D \left(D_b, d_p\right) + \alpha_I \left(D_b, d_p\right) \right\} M(x)$$

where

x = distance of the bubble from the point of release into the water pool.

$\alpha_s\left(D_b, d_p\right)$ = aerosol trapping coefficient for the sedimentation of particles in the bubble.

$\alpha_D\left(D_b, d_p\right)$ = aerosol trapping coefficient for the diffusion of particles within the bubble.

$\alpha_I\left(D_b, d_p\right)$ = aerosol trapping coefficient for the inertial impaction of particles within the bubble.

The coefficients in this differential equation for particle scrubbing are given by [18, 27]:

Source Term

- Sedimentation:

$$\alpha_s(D_b,d_p) = 1.5\ E^{2/3}\ J\ /\ D_b\ U_T$$

where

E = ratio of the maximum bubble axis divided by the minimum bubble axis (see discussion of bubble shapes)

$J = g\rho_p\ d_p^2\ \bar{c}\ /\ 18\ \mu g$

g = acceleration due to gravity = 980 cm/s^2

ρ_p = density of the material making up the aerosol particle

$\bar{c}$ = Cunningham slip correction

$$= 1 + \left(\frac{2\lambda}{d_p}\right)\left[1.257 + 0.4\ \exp\ (-0.55\ d_p/\lambda)\right]$$

λ = mean free path of a gas molecule $\approx \left[\sqrt{2}\ \pi\ d_g^2\ N_A\ P\ /\ 82.06\ T\right]^{-1}$ cm

d_g = diameter of a gas molecule

N_A = Avogadro's number = 6.022 x 10^{23}

P = absolute pressure in atmospheres (101325 Pa)

μ_g = viscosity of gas

U_T = terminal rise velocity of the bubble

- Diffusion:

$$\alpha_D\ (D_b,d_p) = 6\sqrt{\frac{8\theta}{\pi U_T\ D_b^3}}\left\{\frac{(E^2 - 1)\ f(E)}{1 + \sqrt{4 + 2(E^2 - 1)}}\right\}$$

where

θ = particle diffusion coefficient = $kT\,\bar{c} / 3\pi\mu_g d_p$

k = Boltzmann's constant = 1.3807×10^{-16} ergs/K

T = absolute temperature in Kelvin

$$f(E) = \left[\frac{1.76E^2}{E^2 - 1} - \sqrt{(2)}\right]^{1/2} \left[\frac{E^2 \tan^{-1}\left(\sqrt{E^2 - 1}\right)}{\sqrt{E^2 - 1}} - 1\right]^{-1/2}$$

Note that f(E) approaches $1.625/(E^2 - 1)$ as E approaches 1.

- Inertial Impaction:

$$\alpha_I (D_b, d_p) = 6\, U_T\, \tau\, g(E) / D_b^2$$

where

$$\tau = \rho_p\, d_p^2\, \bar{c} / 18\, \mu g$$

$$g(E) = \frac{E^{4/3}\left[\left(E^2 - 1\right) + \left(E^2 - 1\right)^{3/2}\left(E^2 - 2\right)\tan^{-1}\left(\sqrt{E^2 - 1}\right)\right]}{\left[E^2 - 1 - E^2 \tan^{-1}\left(\sqrt{E^2 - 1}\right)\right]^2}$$

Note: $g(E = 1) = 3$

The dependencies of these aerosol trapping coefficients on particle size and bubble size are shown in Figures 5 and 6, respectively. Diffusion is, as expected, most efficient for trapping very small particles. Impaction and sedimentation increase with increasing aerosol particle size. In sum, the three trapping mechanisms yield an overall trapping coefficient that passes through a minimum when plotted against aerosol particle size. The precise location of this minimum depends on bubble size and properties of the system in question, but, typically the minimum trapping is for particles about 0.3 μm in diameter.

The variation in the overall trapping coefficient has enormous ramifications on the decontamination that can be achieved by a water pool overlying core debris. Evolved aerosols with a distribution of sizes will not be uniformly scrubbed from rising bubbles. Rather, very large and very small particles will be removed much more easily than particles having sizes in the vicinity of the minimum in the overall trapping coefficient. Thus, not only does a water pool attenuate the magnitude of the aerosol production, it also changes the particle size distribution of what aerosols do pass through the water pool.

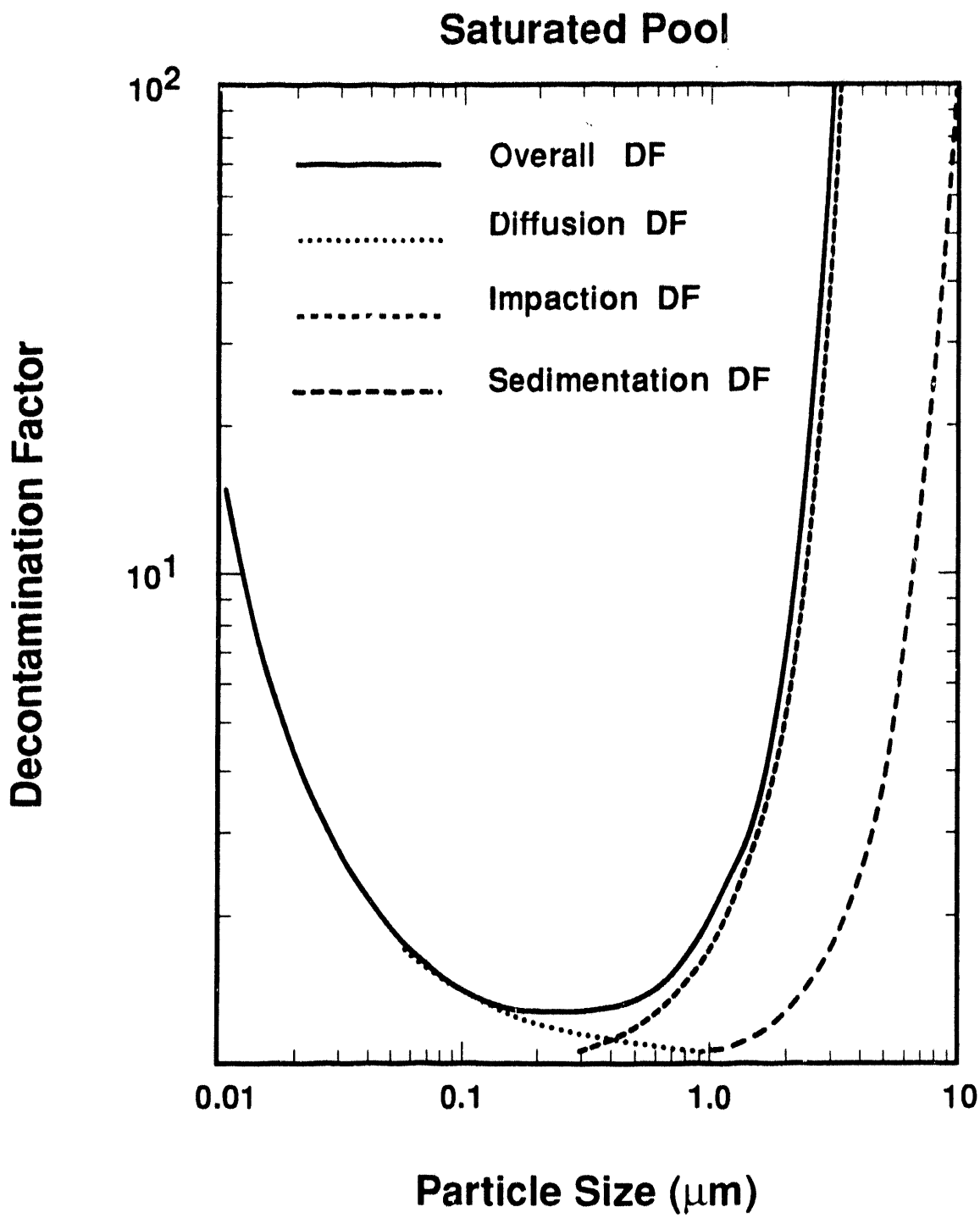

Figure 5 Decontamination factors produced by sedimentation, diffusion, and inertial impaction as functions of aerosol particle size (D_b = 1.0 cm)

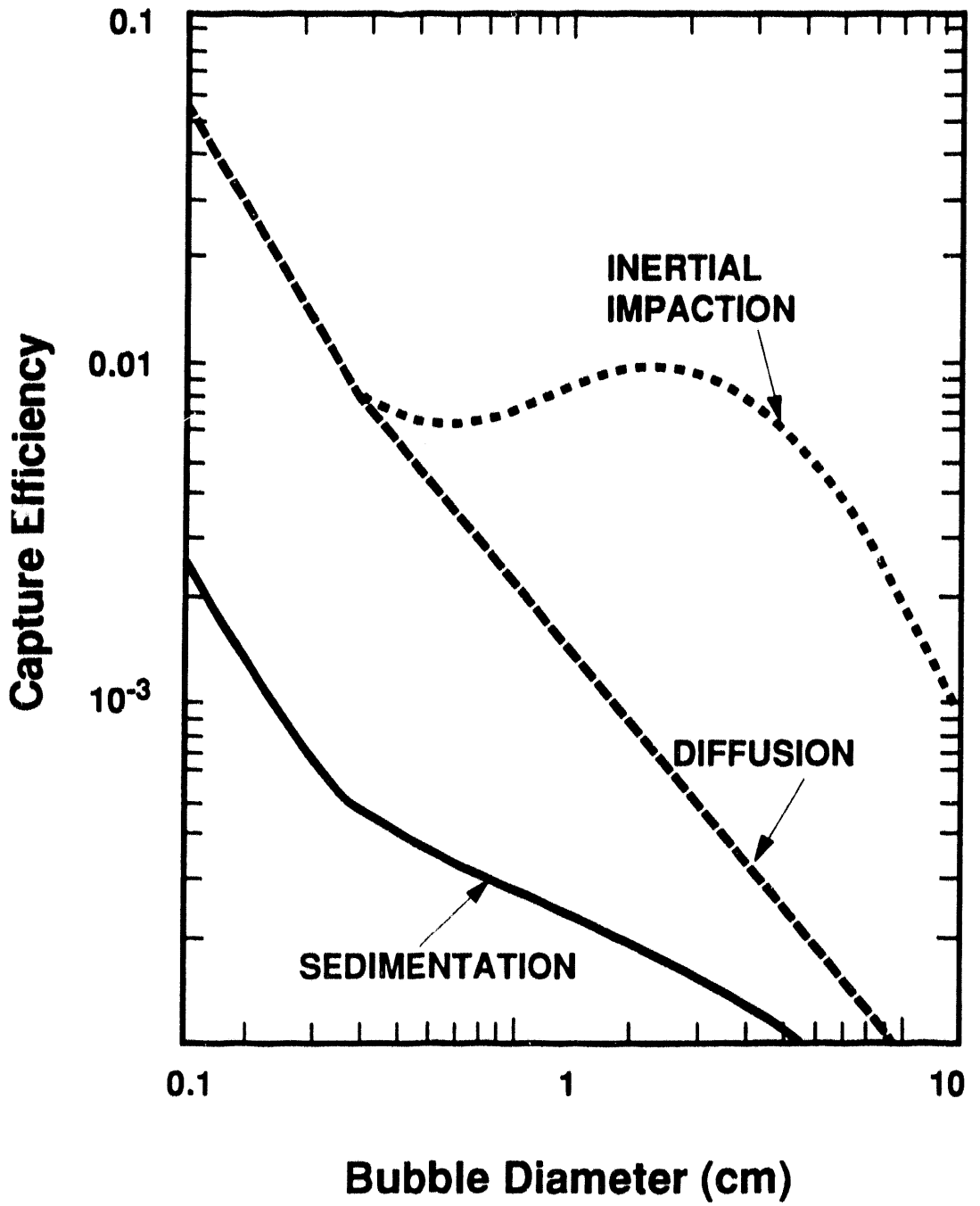

Figure 6 Aerosol capture efficiencies for sedimentation, diffusion, and inertial impaction as functions of bubble size (d_p = 0.5 μm)

All three of the mechanisms for aerosol trapping by a water pool increase in efficiency as the size of the bubble decreases. The increase in the efficiency of trapping by inertial impaction is not continuous since gases within very small bubbles (<0.2 cm) are thought not to circulate [26].

The sensitivities of the trapping coefficients to bubble size is thought to be responsible for the efficient decontamination that can be achieved by subcooled water pools. Bubbles of steam and gases from the concrete will shrink when injected into a subcooled water pool as excess steam condenses on the bubble walls. It is presumed that the Stefan flows created during the condensation will sweep aerosols to the bubble walls with an efficiency that is independent of the aerosol particle size. The amount of decontamination of the bubble achieved as the bubble equilibrates with the subcooled water pool is just proportional to the volume change of the bubble. This can be a significant decontamination. A more important factor is, however, that the final bubble is smaller. Aerosol trapping is more efficient as this smaller bubble rises through the pool than in a corresponding case in which the pool is not subcooled.

This view of bubble formation and collapse in a subcooled pool can be questioned. The only support for the model is that it does lead to fairly accurate predictions of the decontamination achieved in the SWISS-2 test [16].

It is evident from the models for the trapping coefficients that the decontamination that can be achieved by an overlying water pool depends on:

- characteristics of the bubbles
- characteristics of the aerosol particles, and
- properties of the liquid phase and the gas.

These topics are discussed in the subsections below.

C. Characteristics of the Bubbles

There has been little careful study of the bubbles formed when water boils on core debris. An experimental technique developed by Brockmann et al. [28] holds the promise of being capable of providing the data needed to more accurately define the initial sizes of bubbles that rise up through a water pool overlying core debris. Until better data are available, a simple intuitive model is adopted:

a. At low gas generation rates the porous crust that separates the molten core debris from the overlying water pool would behave much like a porous plate. The size of bubbles escaping from such a porous plate is given by the Fritz equation [29]:

$$D_b = 0.0105\ \psi \left[\sigma_l \,/\, g\left(\rho_l - \rho_g\right)\right]^{1/2}$$

where

ψ = contact angle (degrees) between water and the frozen core debris

σ_l = surface tension of the liquid

ρ_l = density of the liquid

ρ_g = density of the gas

b. At very high rates of gas generation, the size of the bubbles initially released into the water pool is determined by Taylor instability [30]:

$$D_b = 2\ C \left[\sigma_l / \left(\rho_l - \rho_g\right)g\right]^{1/2}$$

where C is a constant given various values between 1.9 and 4.

c. Between these limiting values for very high and very low gas generation rates, the initial bubble diameter is thought to depend on the rate of gas generation as described by the Davidson-Schular equation for low viscosity fluids [31]:

$$D_b = 1.11\left(\frac{6}{\pi}\right)^{1/3} \frac{V_s^{0.4}}{g^{0.2}} \quad \text{cm}$$

where V_s is the total superficial vapor velocity (gas and steam) from the crust surface.

Initial bubble diameter as a function of the superficial gas velocity is shown in Figure 7. The initial bubble diameters shown in this figure are, in fact, the diameters of spherical bubbles with the same volumes as the actual bubbles. An actual bubble is thought to distort into oblate ellipsoid with semi-major axis a and semi-minor axis b. Then,

$$D_b = 2a / E^{1/3}$$

where E = a/b is the eccentricity of the bubble. The eccentricities of bubbles rising in wat · have been correlated by [32]:

$$1/E = \begin{cases} 1 & \text{for } Ta \le 1 \\ \left\{0.81 + 0.206 \tanh\left[2\left(0.8 - \log_{10}Ta\right)\right]\right\}^3 & \text{for } 1 < Ta \le 39.8 \\ 0.24 & \text{for } Ta > 39.8 \end{cases}$$

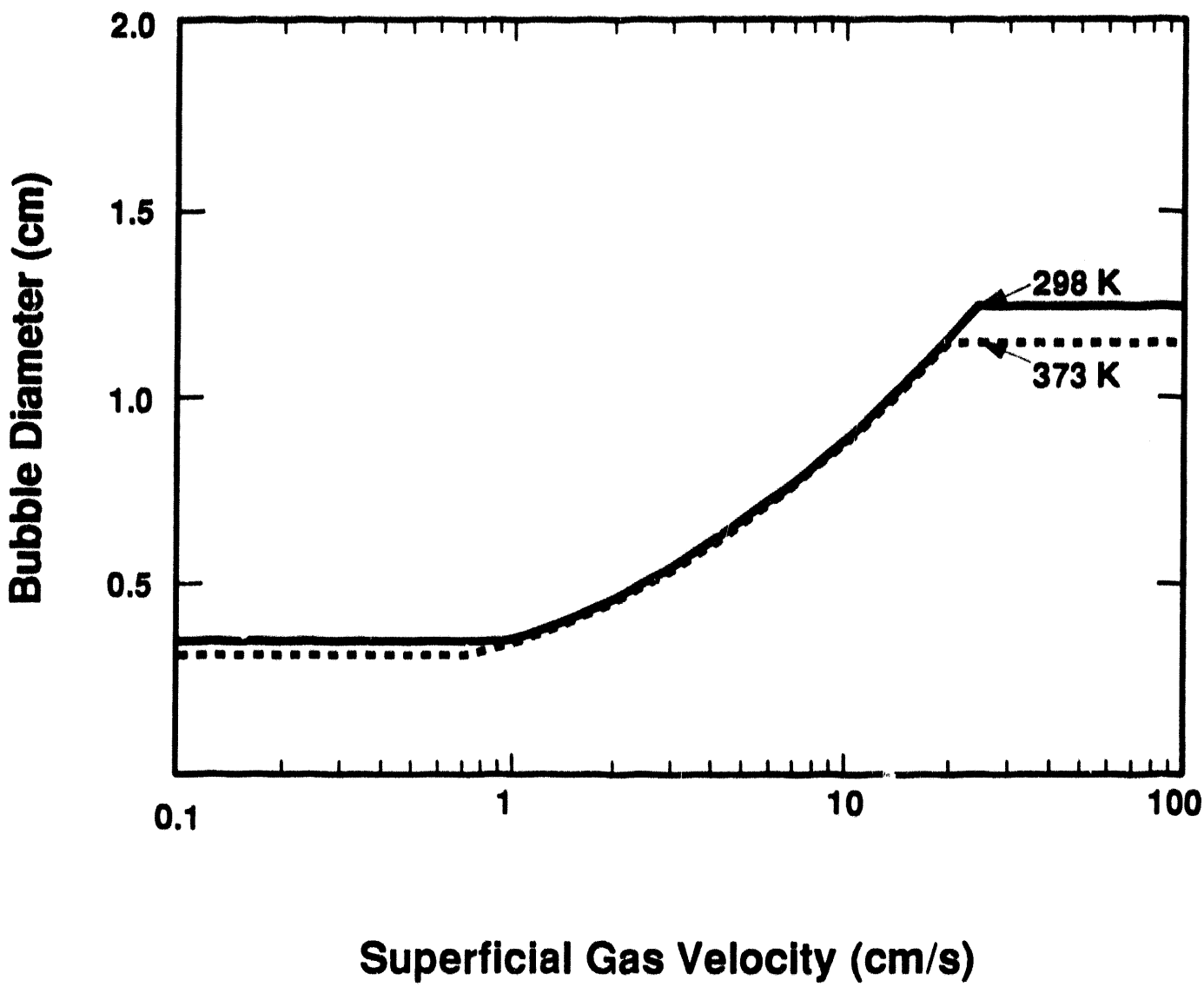

Figure 7 Initial bubble size as a function of the superficial gas velocity

where

$$Ta = Re\ M^{0.23}$$

$$M = \text{Morton number} = g\ \mu_l^4 / \rho_l \sigma_l^3$$

$$Re = \text{Reynolds number} = U_T\ \rho_l\ D_b / \mu_l$$

$$\mu_l = \text{viscosity of the liquid phase}$$

Note that bubbles with Ta > 39.8 are actually spherical-cap or ellipsoidal-cap bubbles.

Terminal velocities of rising bubbles have a complex dependence on bubble size and liquid properties in very pure water [26]. Water pools overlying core debris that is interacting with concrete will not be pure for long. Water pools used in the SWISS tests [16] very quickly became heavily contaminated by dissolved and suspended solids. The contamination did not all come from aerosols trapped in the water pool. Much of the contamination was the result of the actions hot water has on concrete and the solidified crust of core debris. Terminal velocities of bubbles rising through contaminated water have been correlated by [33]:

$$U_T = \mu_l\ M^{-0.149}\ (J_o - 0.857) / \rho_l\ D_b$$

where

$$J_o = \begin{cases} 0.94\ H^{0.757} & \text{for } 2 \le H \le 59.3 \\ 3.42\ H^{0.441} & \text{for } H > 59.3 \end{cases}$$

$$H = (4/3)\ E_o\ M^{-0.149}\ (\mu_l / \mu_w)^{-0.1}$$

$$E_o = \text{Eotvos number} = g \rho_l\ D_b^2 / \sigma_l$$

$$\mu_w = 0.009 \text{ Poises}$$

The terminal velocities of bubbles of various sizes rising through water are shown in Figure 8.

As a bubble rises through the water pool, it grows as a result of the loss of hydrostatic head. At the level of approximation adopted here, the growth of the bubble during its rise through the water pool is described by [25]:

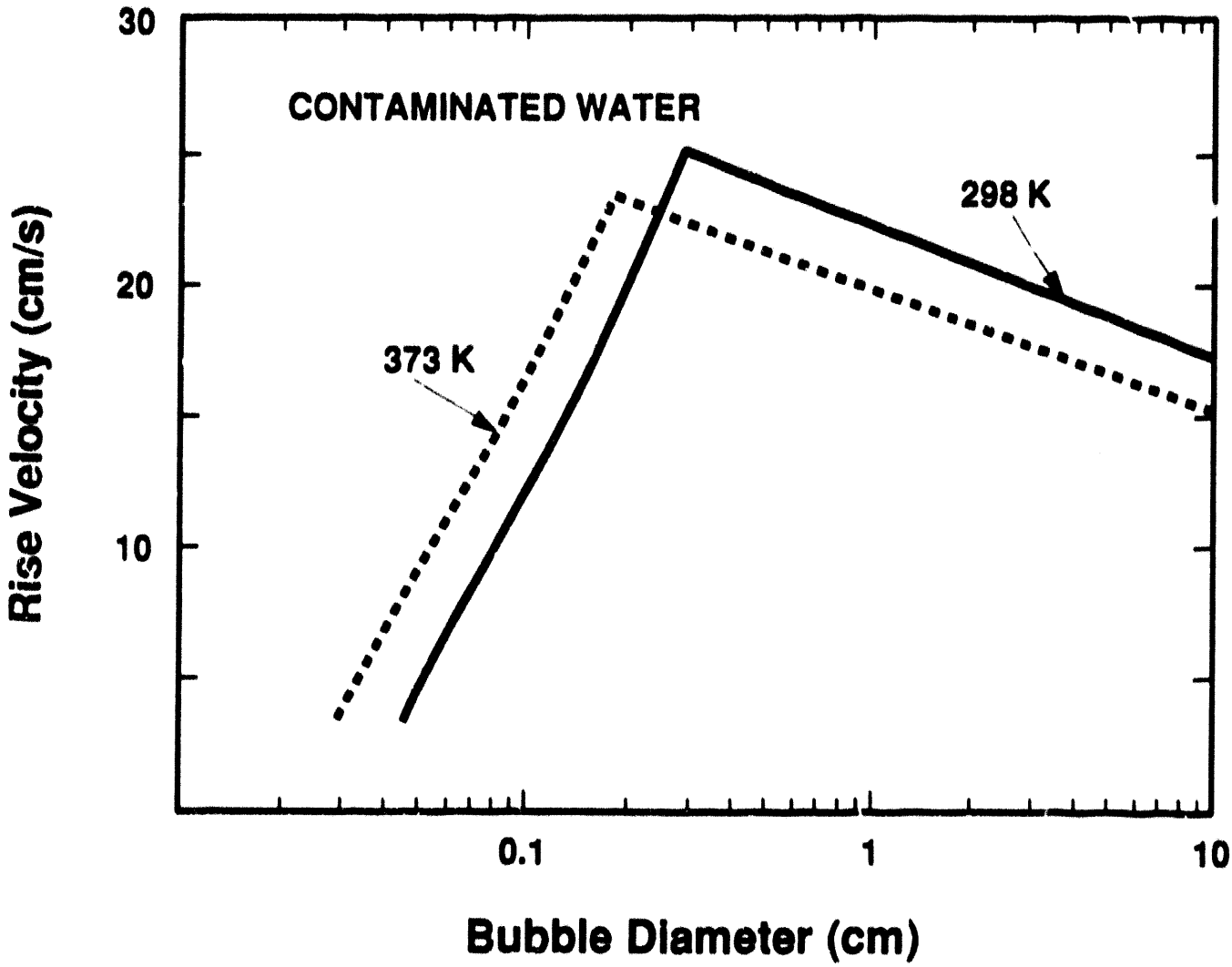

Figure 8 Terminal rise velocity of bubbles in water as a function of bubble size

$$\frac{D_b^3(0)}{D_b^3(x)} = \frac{P_{atms} + g\rho_l\,(H - x) / 1033.3}{P_{atms} + g\rho_l\,H / 1033.3}$$

where

$D_b(0)$ = initial bubble diameter

$D_b(x)$ = bubble diameter at a distance x above the point of bubble formation

H = depth of the water pool

P_{atms} = pressure in the gas phase above the water pool

Bubble growth is not unlimited. The envelope defining a bubble is not rigid. Disturbances in this envelope form, grow and are swept away as the bubble rises. If a bubble grows too large, disturbance in the bubble envelope can grow to bubble dimensions before being swept away. When this happens, the bubble splits ("calves"). Levich [34] has formulated a simple criterion for the maximum stable bubble size:

$$D_b^c = 1.8\ \sigma_l / U_T^2 \left[\rho_g \rho_l^2\right]^{1/3}$$

This is the criterion adopted here to define the maximum bubble size. More detailed stability analyses indicate somewhat smaller values for the maximum stable bubble size [25]. It takes time for the instability of bubbles to cause calving. The time necessary for instabilities to grow to produce "calving" increases as the bubble size approaches the maximum stable bubble size. Since pools of interest here are shallow and the residence times of bubbles in the pools are short, metastable bubbles can rise through the pool. The larger maximum size defined by the Levich criterion may, then, be a more realistic description of the largest bubble to be expected for the processes of interest here.

D. Characteristics of the Aerosol Particles

There have been many measurements of the size distributions of aerosols produced when high temperature melts interact with concrete. Brockmann [35] has reviewed much of this data. In the VANESA model of aerosol generation during core debris interactions with concrete, the aerosols are considered to have lognormal size distributions with mean sizes given by [25]:

$$d_p(\text{mean}) = 0.266 \left[\frac{A}{\rho_p}\right] \mu m$$

Source Term

where

A = mass concentration of aerosols in the gas (g/m^3)

ρ_p = material density of the aerosol particles [g/cm^3]

The geometric standard deviation of the distribution is taken to be 2.3 which is a weighted average of geometric standard deviations of 1.6 to 3.2 measured in experiments.

Mean sizes of the aerosols predicted [8] to form during core debris-concrete interaction in a Mark I containment are shown in Figure 9. During the periods of intense aerosol generation, aerosol sizes become quite large. As the aerosol generation rates fall, mean aerosol particle sizes fall to 0.2 to 0.3 μm. The trends shown in this figure are certainly in qualitative accord with experimental observations from tests of high temperature melt interactions with concrete without water present.

There have been no measurements of the size distributions of aerosols that emerge from water pools overlying core debris interacting with concrete. Certainly there have been no measurements of the size distributions of aerosols that emerge from the core debris and enter the water pool. In the absence of any actual data, it is certainly convenient to assume that the size distribution of aerosols that enter an overlying water pool is the same as the aerosol distribution that would be produced were no water pool present. Unfortunately, there is no reason to believe this is true.

Aerosols are produced in melt/concrete interactions by a combination of nucleation of particles from supersaturated vapor and the condensation of vapor on particles. Nucleation, of course, generates fine, so-called "embryonic," particles whereas condensation of vapor leads to particle growth. The relative contributions of nucleation and condensation affect the number and size of the so-called "primary" aerosol particles, that is, aerosol particles that exist prior to any agglomeration of particles. The relative contributions of these two processes depend on the nature of the thermal gradient the vapors pass through as they emerge from molten core debris. Though no detailed analyses have been done, it would certainly appear that the thermal gradient above molten core debris when a water pool is present would be different than when a water pool is not present. Whether the differences are enough to alter significantly the initial aerosol size distribution is, of course, not known.

As the primary particles are generated, they begin to coagulate. In tests of melt interactions with concrete, aerosols are collected at points some substantial distance away from the region of aerosol formation. There is, then, a substantial opportunity for aerosol coagulation. When a water pool is present, the time available for aerosol coagulation is much shorter. At first examination, it would appear that the aerosol that enters a water pool would not have as coarse a size distribution as have aerosols sampled in tests without a water pool present.

The elemental composition of vapors emerging from molten core debris is complex. The aerosol formation process is rapid. Consequently, it would be expected that aerosol formation would involve simultaneous nucleation and condensation of vapors so that there would be little variation in the composition of particles across the size spectrum of the aerosol. The exception would arise when particles produced by mechanical processes are compared to particles produced from vapors. Test data have not definitively proven that the compositions of aerosol particles are not size dependent. This

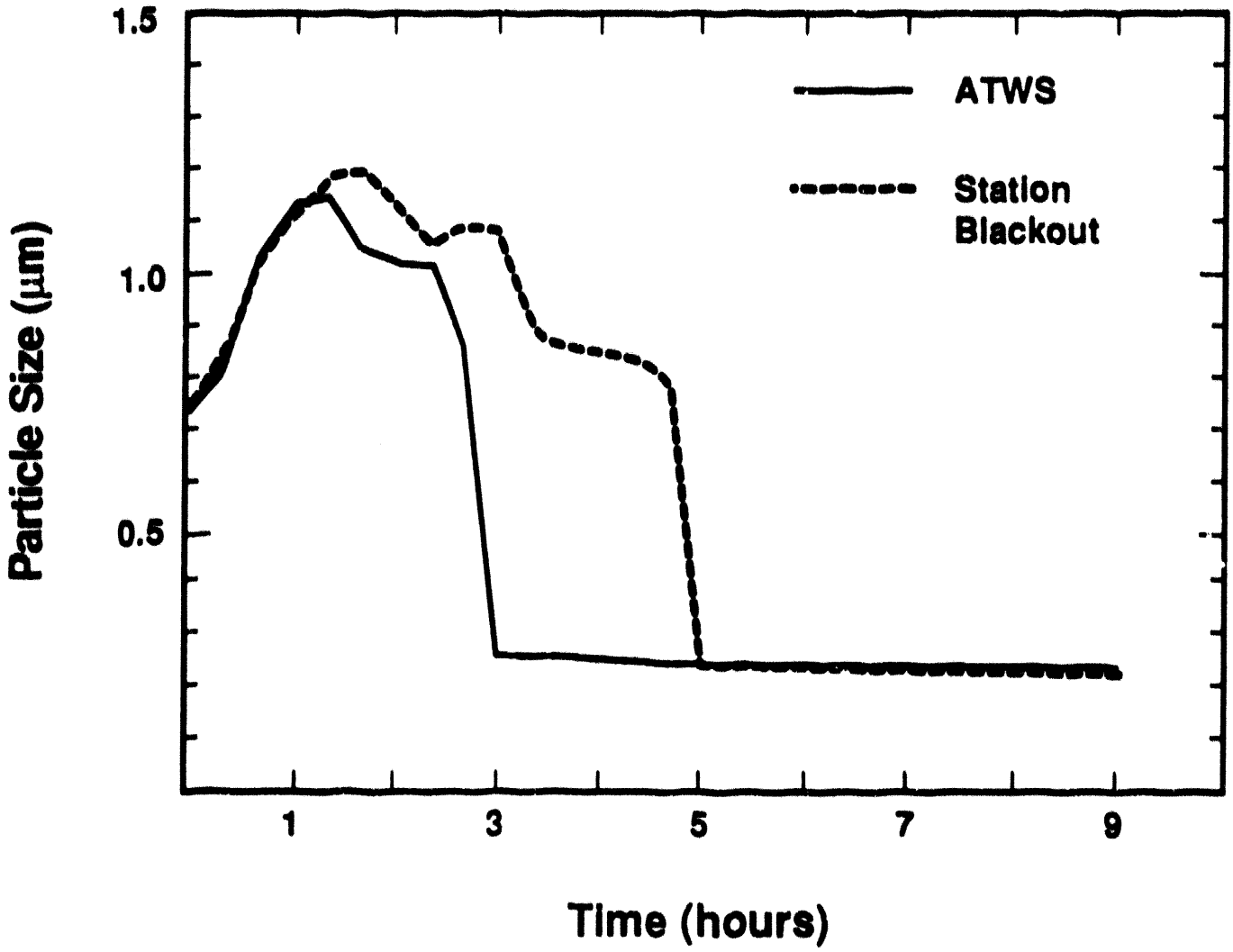

Figure 9 Predicted mean aerosol particle sizes during core debris interactions with concrete in severe reactor accidents at a Mark I boiling water reactor

independence is still assumed here. That is, decontamination factors found here for the overall aerosol can be used also as the decontamination factors for individual elements.

E. Properties of the Liquid Phase

The physical properties of the liquid phase enter into most of the correlations of bubble behavior and aerosol capture described above. The pertinent physical properties of pure water are shown in Table 1. These properties of pure water are quite accurately known relative to many other aspects of decontamination by overlying water pools. The water making up the pools will, however, not be pure for long during core debris interactions with concrete. Water collected during the SWISS-2 test [16] was found to contain 0.2 to 0.05 grams of suspended solids per kilogram of water and an undetermined amount of dissolved solids.

Suspended and dissolved solids will affect the thermophysical properties of the water. The density of the liquid phase is altered to be:

$$\rho_l = \left[\rho(w) + \frac{S}{V}\right](1 - \phi_s) + \rho(s)\,\phi_s$$

where

ρ_l = liquid density

$\rho(w)$ = density of pure water

S/V = mass of dissolved solute per unit volume

ϕ_s = volume fraction of suspended solids

$\rho(s)$ = density of solids suspended in the liquid

Dissolved solids will alter the viscosity of water:

$$\frac{\mu\,(\text{sol'n})}{\mu(w)} = 1 + 2.5\phi$$

where

μ(sol'n) = viscosity of the solution

$\mu(w)$ = viscosity of pure water

ϕ = ratio of ions and neutral molecules produced by the solute to the number of water molecules in the liquid

Table 1 Properties of pure water

Density (g/cm^3)

$$\rho(w) = 0.849397 + 1.29812 \times 10^{-3} T - 2.69233 \times 10^{-6} T^2$$

Viscosity (Poises)

$$\log_{10} \mu(w) = \log_{10}(0.01002) + \frac{\left[1.3272(293 - T) - 1.52 \times 10^{-3}(T - 293)^2\right]}{(T - 168)}$$

Surface Tension (dyne/cm)

$$\sigma(w) = 34.6 \, (T / 704)^{-0.8373}$$

Vapor Pressure (atms)

$$\ln P = -7938.16 / T + 88.912 - 12.1215 \ln (T) + 0.011079T$$

Source Term

There are several models in the literature that describe the effects of suspended solids on the viscosity of a liquid [36]. These models all yield rather similar results for concentrations of solids amounting to less than 30 volume percent. The model adopted here is:

$$\frac{\mu(\text{slurry})}{\mu_l} = \frac{0.403}{0.403 - \phi_s}$$

where

μ(slurry) = viscosity of the mixture of liquid and suspended solids

μ_l = viscosity of the liquid including the effects of dissolved materials

ϕ_s = volume fraction of suspended solids

None of the material thought likely to enter a water pool overlying core debris is an especially strong surface active agent. The effects of some inorganic solutes on the surface tension of water [37] are shown in Figure 10. Solutes may either increase or decrease the surface tension and the effect increases with concentration. The effects of mixtures of solutes is not known nor is the surface tension of water with prototypic solutes known. It seems likely, however, from the data shown in Figure 10 that solutes at concentrations expected to develop in water overlying core debris will alter the surface tension by no more than about ± 10 percent.

F. Properties of the Gas Phase

The major constituents of the gas phase that make up bubbles rising through a water pool overlying core debris in the drywell of a Mark I containment will be hydrogen, steam, carbon monoxide and carbon dioxide. Hydrogen, carbon monoxide and carbon dioxide come from the attack by core debris on concrete. A small fraction of steam will also come from the attack on concrete. Most of the steam comes from the boiling of water at the interfacial crust between core debris and the water pool.

Concrete, when heated to sufficiently high temperatures [38, 39], evolves steam and carbon dioxide. Steam that evolves from the concrete comes primarily from the cement phase of concrete. It is present in the cement phase as "gel" water and water of hydration. This type of water evolves at temperatures between 378 and 420 K. Water is also present as hydroxide groups notably as $Ca(OH)_2$, in the cement phase. This $Ca(OH)_2$ decomposes at around 680 K to produce water vapor. All concretes used in nuclear reactors have about the same type of cement and thus about the same amount of water bound as hydroxide groups. Consequently, the major differences in the water content in various concretes come from the relative humidity of air around the concrete during service. Concretes typically contain between 5 and 8 weight percent water.

Carbon dioxide evolved from concrete comes from the decomposition of calcareous material in the concrete which occurs at temperatures of about 960 K. All concretes contain some calcareous material. At the very minimum, calcium carbonate forms by reaction of atmospheric carbon dioxide with calcium hydroxide:

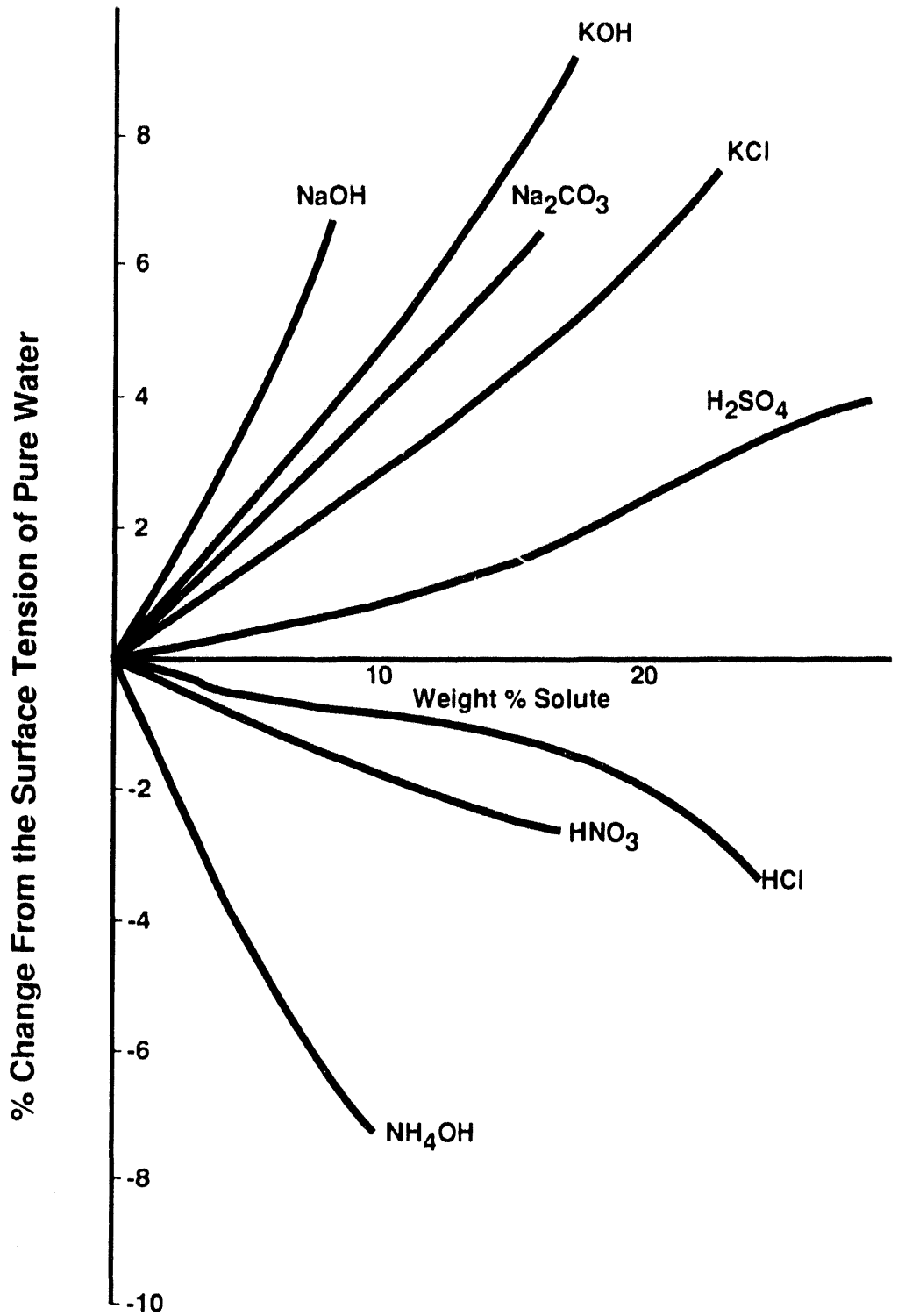

Figure 10 Effects of inorganic solutes on the surface tension of water at 293 K

$$CO_2(g) + Ca(OH)_2 = CaCO_3 + H_2O$$

This reaction begins when the concrete is first placed and continues throughout the service life of the concrete. Because of this reaction, all concretes have at least 1 weight percent CO_2 bound up as a carbonate.

Some concretes contain very much more carbon dioxide. These concretes use calcareous material as an aggregate. Usually, the aggregates are calcite ($CaCO_3$) or dolomite ($CaMg(CO_3)_2$). When crushed calcareous aggregate is also used as the fine aggregate, the concretes may contain over 36 weight percent carbon dioxide as carbonates. When silicon dioxide is used as the fine aggregate, and calcareous material is used as the coarse aggregate (so-called limestone-common sand concrete) the concrete contains over 20 weight percent carbon dioxide.

Carbon dioxide and steam are evolved from the concrete at temperatures well below the ablation temperature of the concrete. When molten core debris interacts with the concrete, steady-state temperature profiles develop ahead of the ablation front after a brief transient period (see for example References 16, 38, and 40). As a result, the isotherms that define the temperatures of the various concrete decomposition processes advance into the concrete at very nearly the same rate as the ablation front. Gas generation during the interaction of core debris with concrete is proportional to the concrete ablation with a proportionality constant determined by the concrete composition.*

Concrete erosion rates vary over the course of core debris interactions with concrete. The initial transient interaction of high temperature melts with concrete can produce erosion rates in excess of 100 cm/hr [41]. These initial rates decline quickly. Vigorous attack on concrete during the quasi-steady state when the melt is rich in zirconium will produce erosion rates as high as 35 cm/hr [42]. Once zirconium is consumed from the melt, erosion rates can be as low as about 3 cm/hr [43].

Gases evolved from the concrete react with the core debris. The reactions of carbon dioxide and steam yield carbon monoxide and hydrogen:

$$Fe(l) + CO_2 = FeO(l) + CO$$

$$Fe(l) + H_2O = FeO(l) + H_2$$

$$2Cr(l) + 3CO_2 = Cr_2O_3(l) + 3CO$$

$$2Cr(l) + 3H_2O = Cr_2O_3(l) + 3H_2$$

$$Zr(l) + 2CO_2 = ZrO_2(l) + 2CO$$

$$Zr(l) + 2H_2O = ZrO_2(l) + 2H_2$$

---

*Some experiments involving high temperature melt interactions with concrete may not show this proportionality. This is nearly always because the small concrete test fixtures develop cracks that would not form in the massive concrete structures of a nuclear reactor. Cracks provide low-resistance flow paths for gas that permit the gases to flow away from rather than through the high temperature melt.

There is some thermodynamic evidence that highly reactive metals such as Zr and possibly Cr can reduce carbon dioxide completely to elemental carbon:

$$Zr + CO_2 \rightarrow ZrO_2 + [C]_{melt}$$

Evidence of this complete reduction has not yet been obtained in tests of melt interactions with concrete [44, 45].

The extent of reaction depends on the composition of the melt. When there is metallic zirconium in the melt, reduction can be very extensive. The hydrogen to steam partial pressure ratio in gases emerging from the melt is about 10^5. When zirconium and chromium have been oxidized from the melt, the hydrogen-to-steam partial pressure ratio in gases emerging from the melt is only about 2.

The partial pressures of carbon monoxide and carbon dioxide in the gases emerging from the melt are related to the hydrogen-to-steam partial pressure ratio by the "shift gas" reaction:

$$CO_2 + H_2 \rightarrow CO + H_2O$$

$$K(T) = \frac{P(CO)\ P(H_2O)}{P(CO_2)\ P(H_2)} = \exp\left[\frac{-4078.3}{T} + 3.705\right]$$

where

K(T) = equilibrium constant

P(i) = partial pressure of gas species i = CO, CO_2, H_2, H_2O

As gases cool after emerging from the core debris, this equilibrium is maintained until a temperature is reached below which the kinetics of gas reactions are slow in comparison to the time scale of interest. If temperatures fall quickly below that so-called "quench" temperature, the gas composition is "frozen" at the equilibrium composition for the quench temperature. Cooling rates for gases emerging from melts interacting with concrete without a water pool present are sufficient to produce this quenching behavior. Quench temperatures are usually found to be between 1000 and 1300 K [46-48]. Quenching behavior at similar temperatures would, then, be expected to definitely occur when a water pool overlies the core debris.

With specification of the concrete erosion rate, hydrogen-to-steam partial pressure ratio and the "quench" temperature, the carbon dioxide, carbon monoxide and hydrogen contents of the gas sparging through the water pool can be determined. To specify the steam concentration, if is necessary to consider boiling at the crust-water interface. The boiling of water on the crust is complicated by the "barbotage" effect of gases generated by the attack on concrete [49]. For a long time, it was thought that water would be in film boiling on the crusts of debris and that the heat flux from the crust to the water would be enhanced by the barbotage effect as well as subcooling of the water [50]. Experimental data seem to indicate, however, that water is in nucleate boiling on the crusts. Heat fluxes to the water observed in

the SWISS-2 test were 70 to 80 W/cm^2 [16]. The recent MACE test indicated similar overall heat fluxes with periodic excursions as high as 160 W/cm^2 [50].

The recent WETCOR-1 test [22] suggests heat fluxes can be as low as 30 W/cm^2. Heat flux, and consequently steam production, during boiling on core debris must be considered quite uncertain. Recent uncertainty analyses by Theofanous et al. [15] consider the uncertainty range to be 50 to 100 W/cm^2. A requirement for advanced reactor designs suggested by the Electric Power Research Institute [12] demands that the heat flux be at least 50 W/cm^2. Once the heat flux is selected, the steam flux can be estimated and the gas composition of the aerosol-laden gas bubbles that enter the water pool overlying core debris can be specified.

Gas phase properties are sensitive to gas composition. The gas density is probably specified adequately by the ideal gas law:

$$\rho_g = \frac{P(H_2)\ 2.016}{RT} + \frac{P(H_2O)\ 18.015}{RT} + \frac{P(CO)\ 28.00}{RT} + \frac{P(CO_2)\ 44.001}{RT}$$

where R is the universal gas constant.

The viscosity of the gas mixture can be estimated from the Herning-Zipperer equation [52]:

$$\mu_g = \frac{\sum_{i=1}^{N} P(i)\ \mu(i)\ M(i)^{1/2}}{\sum_{i=1}^{N} P(i)\ M(i)^{1/2}}$$

where

N = number of gas species

P(i) = partial pressure of the i^{th} gas species

M(i) = molecular weight of the i^{th} gas species

μ(i) = viscosity of the i^{th} gas species when pure and at the same temperature as the mixture.

The pure gas viscosities are [25]:

$$\mu(H_2) = \frac{1.5769 \times 10^{-6}\ T^{0.705712}}{(1 - 3.378 / T)} \quad \text{Poises}$$

$$\mu(H_2O) = \frac{0.950 \times 10^{-6}\ T^{0.892912}}{(1 + 207.219 / T)} \quad \text{Poises}$$

$$\mu(CO) = \frac{14.151 \times 10^{-6}\ T^{0.502012}}{(1 + 117.178 / T)} \quad \text{Poises}$$

$$\mu(CO_2) = \frac{15.957 \times 10^{-6}\ T^{0.457212}}{(1 + 246.744 / T)} \quad \text{Poises}$$

Predictions obtained with the Herning-Zipperer equation agree with data for CO-H_2 mixtures at 298 K to within about 2 percent [25]. Predictions for steam-air mixtures agree with data to within about 4 percent [18].

III. Analysis of Source Term Attenuation by Overlying Water Pools in Mark I Reactors

A. Quantitative Analysis of Uncertainty

The previous chapter described the physical phenomena that affect aerosol scrubbing by a water pool overlying core debris interacting with concrete. In this chapter, predictions are made of the source term attenuation that can be achieved by such pools in severe accidents in Mark I boiling water reactors. The discussion of the pertinent physical phenomena in Chapter II identified several areas of phenomenological uncertainty. Other uncertainties arise, of course, in the application of the models described in Chapter II to specific situations. Many of the additional uncertainties arise because of variations in the boundary conditions and initial conditions among the various severe reactor accidents hypothesized to occur in Mark I boiling water reactors [2]. Understanding of the details of the progression of severe reactor accidents up to the point core debris is expelled into the Mark I containment is imperfect. This, too, can add uncertainty to the predicted performance of overlying water pools. All of these uncertainties need to be taken into account in the prediction of source term attenuation by the overlying water pool.

A number of approaches to the estimation of uncertainty have been used in the analysis of severe reactor accidents. Theofanous has categorized and criticized these approaches [53, 54]. Frequently "expert opinion" or "engineering judgment" is used as the basis for estimating the uncertainty in predictions made for high level issues such as decontamination by overlying water pools. The expert opinions or engineering judgments concerning these major issues of accident analysis may be obtained informally by the analysts [55] or in a highly structured polling of internal and external authorities selected to represent the range of views within the technical community.

This approach to uncertainty, no matter how elaborately conducted, does not provoke a great deal of confidence. There have not been enough severe reactor accidents to support anyone's claim to have expertise in the evaluation of such high level questions as the decontamination performance of water pools under severe reactor accident conditions. Engineering judgment is suspected because of the all too human tendency to underestimate the magnitude of uncertainty in areas of great uncertainty. But, the greatest flaw in past approaches to uncertainty is that they are difficult to reproduce. Almost never is a scrutable account of the expert opinion or engineering judgment set down so that a knowledgeable individual who accepts the basic assumptions can follow the logic and the arithmetic to arrive at the same conclusions reached by the "expert" or the engineer.

An alternate approach to the estimation of uncertainty is adopted here. This approach, first articulated by Theofanous [54], attempts to avoid the failings of the past uses of expert opinion and engineering judgment though both expert opinion and engineering judgment are still used. The essential step in the analysis of uncertainty is to decompose a high level question into its component phenomenological parts. This decomposition is done until each part is an area where there are or could be data and true expertise could exist. Uncertainties within these individual phenomenological areas can be identified. Furthermore, defensible ranges for the values of uncertain quantities can be prescribed. The definitions of uncertain quantities and the prescription of ranges for the values of these uncertain quantities are where expert opinion and engineering judgment are heavily used. More confidence can be had in this use of expert opinion and engineering judgment because there are, or at the very least could be, data bases and

theoretical bases for the expertise or judgment. Furthermore, it is convenient, if not mandatory, that the bases for the opinions and judgments in individual phenomenological areas be described in a way that is scrutable by other knowledgeable individuals. Conclusions reached by the experts can be reproduced by others if the articulated assumptions are accepted.

Once the decomposition of an issue has been done, uncertainties identified and ranges for uncertain quantities prescribed, the overall uncertainty in the high level issue can be defined. The mechanics adopted here involve Monte Carlo sampling of the predictions for an issue derived from the component phenomenological parts. The sampling is done by randomly selecting values for the uncertain quantities as prescribed by the probability distributions of values within the prescribed ranges. These sampled values of the uncertain quantities are then used in the calculation of the phenomena of interest.

Definition of probability distributions for uncertain quantities is, unfortunately, a subjective task. Though there have been some studies of the definition of these distributions [55], the author of this work knows of no mechanical or non-controversial method for defining these distributions. All that can be done is to clearly indicate what distributions are used. For the work described here, the probability density functions for values of uncertain quantities within prescribed ranges are defined by rules:

- Where significant values of an uncertain quantity span less than an order of magnitude, the probability density function for values of the uncertain quantity is taken to be a constant over the prescribed range and zero outside the range. This is called a "uniform" distribution.

- When significant values of an uncertain quantity span a range that is more than an order of magnitude, the probability density function for the logarithm of the value of the quantity is taken to be a constant over the prescribed range. This is called a "log-uniform" distribution.

- In those few cases in which a significant data base exists for an uncertain quantity, the probability distribution is taken to be lognormal. The limits of the prescribed range for values of the quantity are assumed to define the 1st and the 99th percentile of the cumulative distribution.

The predictions obtained with the Monte Carlo sampling constitute a sample of the true uncertainty distribution in the extent of decontamination by the pool. For the issue at hand here, the predictions constitute a sample of the distribution in values of the decontamination that can be achieved by a water pool overlying core debris in the drywell of a Mark I containment. This sample can be used to construct an estimate of the true distribution of values of the decontamination. Because the sample is finite, the estimate of the true distribution can be made only to a limited level of confidence. The mathematics and statistical analysis used to construct the estimate of the true distribution and to characterize the confidence level of the estimates are presented in Appendix A of this report.

B. Specific Uncertainties Considered

The specific uncertainties considered here in the analysis of aerosol scrubbing by an overlying water pool are summarized in Table 2. Ranges for many of the uncertain quantities listed in the table have been selected based on the discussions of physical phenomena presented in Chapter II. Probability density functions for values within the ranges are specified by the "rules" listed above. Other features of the various uncertain quantities are discussed below:

Table 2 Uncertain parameters and properties

Parameter or property	Range	Probability density
Ambient Pressure	1-9 atms	uniform
Concrete Erosion Rate	3-35 cm/hr	log-uniform
Carbon Dioxide Weight Fraction in Concrete	0.01-0.36	log-uniform
Water Weight Fraction in Concrete	0.05-0.08	uniform
Hydrogen-to-Steam Partial Pressure Ratio	$2\text{-}10^5$	log-uniform
CO/CO_2 Quench Temperature	1000-1300 K	uniform
Solute Mass	0.05-100 g/kg H_2O	uniform
Volume Fraction Suspended Solid	0-0.1	uniform
Density of Suspended Solids	1-6 g/cm^3	uniform
Sign Indicator for Uncertainty in Water Surface Tension	0-1	uniform
Mean Aerosol Particle Size	0.25-2.5 μm	log-uniform
Geometric Standard Deviation	1.6-3.2	uniform
Aerosol Material Density	1.5-10.0 g/cm^3	uniform
Coefficient in Davidson-Schular Model for Initial Bubble Size	1-1.54	uniform
Contact Angle in Fritz Formula	20-120°	uniform
Coefficient in the Taylor Instability Model for Bubble Size	1.9-4	uniform
Multiplier for Inertial Impaction	0-1	uniform
Boiling Heat Flux	0.16-1.6 MW/m^2	log normal μ = 0.5 = mean σ = 1.645 = std. dev.

1. Uncertainty in Drywell Pressure

The atmospheric pressure in the drywell of a Mark I containment during core debris interactions with concrete and water is one of the boundary conditions that varies among the many, hypothetical, core melting accidents that have been defined for Mark I boiling water reactors. The pressure affects both aerosol trapping and steam production by boiling. It is only possible for generic analyses to assume pressure in the drywell is between atmospheric pressure and the estimated failure pressure of the containment. Mark I containments, though small, are quite strong. Estimates [6] of the failure pressures of these containments range to over 10 atmospheres absolute pressure. The estimates have been made for reactor containments as designed. Fabrication errors and corrosion of the steel liners since installation undoubtably reduce the failure pressure for the containments though the failure pressure will still be well above the design pressure which takes into account fabrication errors and corrosion. A range of 1 to 9 atmospheres for the drywell pressure was selected here to capture, at least, the effect of pressure on the predictions of performance.

2. Uncertainty in Concrete Erosion Rate

Based on the discussions in Chapter II the concrete erosion rate has been selected to vary over the range of 3 to 35 cm/hr. The erosion rate does of course vary with time during a specific accident. Time resolved decontamination factors are not sought in the analyses presented here, so time variations in the concrete erosion rates are not considered. In principle, the concrete erosion rate is correlated with the composition of the concrete since the heat that must be imparted to a calcareous concrete to ablate a given volume of the concrete is greater than the heat needed to ablate siliceous concretes [38]. Inspection of a variety of published analyses of core debris interactions with concrete [7, 24] does not reveal a clear correlation in the erosion rates with concrete type. There are enough variations in the initial and boundary conditions for core debris/concrete interactions that the sensitivity of erosion rate to concrete type is overwhelmed.

3. Uncertainty in Concrete Composition

As discussed in Chapter II, the carbon dioxide contents of structural concretes vary between weight fractions of 0.01 in concretes with siliceous aggregates to 0.36 in concretes made using calcareous materials as both the coarse and the fine aggregate. A survey of what little information is available for Mark I containments revealed only that there are reactors that use siliceous, calcareous, and limestone-common sand concretes. Consequently, a distribution of the weight fractions of CO_2 was used in the analyses below. Clearly, there is no distribution in this quantity for a specific plant.

As discussed in Chapter II, the weight fraction of water in the concrete was taken to be uncertain over the range of 0.05 to 0.08.

4. Uncertainty in the Gas Composition

The ratio of the partial pressures of hydrogen and steam in gases that emerge from the core debris depends on the composition of the core debris. When the core debris is rich in metallic zirconium the ratio is quite large, on the order of 10^5. When reactive metals in the core debris have been oxidized the ratio is only about 2. The initial composition of the core debris is determined by the rather uncertain predictions of reactor accident progression prior to the onset of core debris interactions with concrete in the Mark I drywell. Whatever the initial composition, the core debris composition, and consequently the hydrogen-to-steam partial pressure ratio in gases emerging from the core debris, varies during the

interactions with concrete. For a specific set of initial conditions this variation can be predicted with acceptable accuracy. When averaged over a broad range of initial and boundary conditions the hydrogen-to-steam ratio becomes an uncertain quantity.

The temperature at which gas kinetics significantly affect the evolution in the gas composition is an important factor in the prediction of the gas composition. The range for this quench temperature selected here, 1000-1300 K, is the range inferred from various tests of high temperature melt interactions with concrete [38, 46, 47].

5. Uncertainty in Water Properties

Solids dissolved in the water affect water properties. There is little information available on how much material will be able to dissolve in the water pool. It is possible that water supplied to the drywell may contain additives such as boric acid and sodium hydroxide. An especially likely source of additional solute mass is the concrete. At high temperatures involved in the ablation of concrete alkali metals (Na and K) are vaporized from the concrete. These alkali metals are, of course, quite soluble in water. The concentrations of dissolved species of this type will increase in the water pool if water is recirculated from the steam suppression pool. The range for the concentrations of dissolved mass was selected somewhat arbitrarily to capture the uncertainty that exists as the water becomes contaminated with dissolved materials.

Much of the material in the water pool will not dissolve. Rather, it will be present as suspended solids. Aside from the fact that suspended solids are present in the water, there is little information on how much suspended material can be present. To some extent the volume fraction of suspended solids will depend on whether water supplied to the drywell is recirculated. The range of the volume fraction of solids selected here was limited to an upper bound of 0.1. Above a volume fraction of suspended solids of 0.1 the liquid phase begins to behave significantly differently than water.

Solid species found suspended in water during tests of the simultaneous interactions of high temperature melts with concrete and with water [16] include ZrO_2 (ρ = 5.9 g/cm^3) SiO_2 (ρ = 2.2 g/cm^3), $CaMg(CO_3)_2$ (ρ = 2.87 g/cm^3) $NaAlSiO_4$ (ρ = 2.6 g/cm^3), $Al_2Si_2O_5(OH)$ (ρ = 3.1 g/cm^3) and $CaCO_3$ (ρ = 2.7 g/cm^3). Were uranium dioxide used in the tests, hydrates of uranium oxide presumably would also be suspended in the water. Hydration will reduce the effective densities of the suspended solids. A lower bound on the density of the suspended solids was therefore set to be 1 g/cm^3. The upper bound on the density is determined by the ability of gas sparging to keep the solids suspended. Without a surface active agent present it is difficult for simple gas sparging to keep solids of densities greater than about 6 grams/cm^3 suspended in water [36].

Data presented in Chapter II show that solutes can either increase or decrease the surface tension of water and that the effect varies linearly with solute mass. Consequently the surface tension of the liquid phase is taken to be:

$$\sigma_l = \begin{cases} \sigma(w)(1-S) & \text{for } \epsilon < 0.5 \\ \sigma(w)(1+S) & \text{for } \epsilon \geq 0.5 \end{cases}$$

where

$\sigma(w)$ = surface tension of pure water

S = weight fraction of dissolved solids

ϵ = uncertain parameter with values uniformly distributed over the range of 0 to 1.

6. Uncertainty in Aerosol Size Distribution

The size distribution of aerosols being injected into an overlying water pool is quite uncertain largely because there are no data to indicate if the aerosol formation process is affected by the water pool. Here, the aerosol size distribution is taken to be a lognormal distribution characterized by a mean and a geometric standard deviation. Microscopic examinations of aerosol collected in tests of melt interactions with concrete show that the aerosols are agglomerates with primary particles about 0.1 μm in diameter. It would seem unlikely, then, that aerosols entering the water pool would be smaller than these primary particles. The mean size would, in fact, be somewhat larger since some particle agglomeration would be expected even over the short transport distances available in cases with a water pool present. Consequently, the lower bound on the mean aerosol size was selected to be 0.25 μm. The upper bound on the mean size was selected to be 2.5 μm based on the larger sizes predicted to occur during the most intense phases of aerosol generation by core debris-concrete interactions as discussed in Chapter II.

The geometric standard deviation of the aerosol size distribution was selected to be uncertain between 1.6 to 3.2 based on the observations from tests with no water pool present. Arguments can be made to suggest that the water pool could affect the geometric standard deviation. There are, however, no data to support contentions that the size distribution of aerosols being injected into the water pool is either narrowed or broadened because a water pool is present. Nor are there data to support or refute contentions that the geometric standard deviation is correlated with the mean size of the aerosol. Consequently, the mean size and the geometric standard deviation are taken to be independent.

Aerosols are all assumed to have shape factors of 1. This was done in the belief that water would condense in the interstices of agglomerates of primary aerosol particles. Surface tension forces exerted by the condensed water will tend to pull chain agglomerates of aerosols into spheres [56].

7. Uncertainty in Bubble Size

The initial sizes of bubbles entering the water pool are calculated from the Davidson-Schular equation for low viscosity fluids:

$$D_b = \epsilon \left(\frac{6}{\pi}\right)^{1/3} \frac{V_s^{0.4}}{g^{0.2}} \quad \text{cm}$$

as described in Chapter II. The leading coefficient ϵ has a nominal value of 1.1. Various experimental studies have shown this value to vary at least over the range of 1 to 1.54 depending on the details of the geometry of orifices at which bubbles are formed [26]. It was assumed then that ϵ was uniformly distributed over this range.

Analysis

A lower bound on the initial bubble size is defined by the Fritz equation:

$$D_b = 0.0105\ \psi \left[\sigma_l / g(\rho_l - \rho_g)\right]^{1/2}$$

The contact angle ψ in this equation depends on whether water can "wet" the interfacial crust that separates water from molten core debris. If water cannot "wet" this surface $\psi = 120°$. If water can "wet" the surface ψ approaches zero. Here a lower limit on ψ is taken to be 20°.

An upper bound on the initial bubble size is taken to be defined by Taylor instability:

$$D_b = 2C \left[\sigma_l / g(\rho_l - \rho_g)\right]^{1/2}$$

As discussed in Chapter II, the leading coefficient is taken to be uncertain and uniformly distributed over the range of 1.9 to 4. The Levich criterion is applied also to define an upper bound on the initial bubble size and a bound on the bubble growth that can occur as bubbles rise through the water pool.

8. Uncertainty in Inertial Impaction

Inertial impaction of aerosols with the bubble walls is a factor in aerosol scrubbing only if gases within rising bubbles circulate. In highly contaminated systems like water pools overlying core debris that is interacting with concrete, it is by no means certain that gases will circulate or at what rate gases will circulate within rising bubbles. Consequently, the coefficient for inertial impaction of aerosol particles described in Chapter II has been multiplied by an uncertain parameter with values uniformly distributed over the range 0 to 1.

9. Uncertainty in Boiling Heat Flux

The boiling heat flux from the interfacial crust to the water is controversial. The hope [23] that a progressive fragmentation of the crust will result in very high heat fluxes to the water has not been rewarded in experiments done to date. Progressive fragmentation and very high heat fluxes are neglected here. There is some evidence [23] that when melt first begins to spread out of the pedestal region across the drywell floor in a Mark I containment, high heat fluxes do develop. This is, however, a very transient period of time. This transient may be quite important for the analysis of attack on the containment liner. For source term considerations, the quasi-steady state heat flux to the water pool that develops after the molten core debris has spread is of more interest. Based on the experimental data that have been accumulated to date, this quasi-steady heat flux is assumed here to be lognormally distributed with a mean of 50 W/cm^2 and a geometric standard deviation of 1.645.

C. Predictions of the Decontamination Factors

A model of aerosol scrubbing by a water pool based on the phenomena described in Chapter II has been formulated. Details of the model are described elsewhere [18, 27]. In summary, the model uses a fourth order Runga-Kutta algorithm to solve the differential equation for aerosol scrubbing by sedimentation, diffusion and inertial impaction. Scrubbing due to the collapse of bubbles in a subcooled water pool is assumed to occur instantaneously. Step sizes are controlled in the algorithm so that no

more than 10 percent of the aerosol is removed during bubble rise in a given computation cycle. The initial size of all bubbles entering the overlying water pool is taken to be the same. If bubbles grow to exceed the Levich criterion (see Chapter II), they are instantaneously divided into bubbles with half the volume dictated by the Levich criterion.

Aerosols are assumed to be lognormally distributed in size. The cumulative, mass-weighted, size distribution is taken to be:

$$\Pr(d < D) = 0.5(1 + \text{erf}(z))$$

where

$\Pr(d_p < D)$ = cumulative probability of the particle size being less than D

$z = \ln(D/\mu) / \sqrt{2} \ln \sigma$

μ = mean size

σ = geometric standard deviation

$\text{erf}(x)$ = error function of x

Calculations are conducted by dividing the initial aerosol size distribution into 20 equal mass "bins." The necessary inversion of the error function is done with a Newton-Raphson method. The behaviors of aerosol particles in each bin are assumed to be well represented by a particle with the diameter of the mass median particle diameter in the bin.

Calculations are done by randomly selecting values of the uncertain parameters according to their respective probability density functions. This is easily done for the uniform and log-uniform distributions. The inversion of the error function necessary for lognormally distributed parameters is, again, done with the Newton-Rapson method for locating roots of non-linear equations. Random numbers needed for the selection of values of the uncertain parameters are obtained from a congruent sequential generator algorithm. Such algorithms are known to have a cyclical behavior. To avoid this, the random numbers were randomly "shuffled" using an algorithm by Knuth [57].

Results of the calculation are cast in terms of a decontamination factor (DF) defined by:

$$\text{DF} = \frac{\text{Mass of aerosol entering the water pool}}{\text{Mass of aerosol emerging from the water pool}}$$

This method of presentation eliminates some of the sensitivity of results to the uncertain initial and boundary conditions such as the mass of core melt on the drywell floor. Calculations were done using methods described in Reference 17 to generate uncertainty distributions for the decontamination factor. Typically about 500 calculations were done for each set of conditions. As is discussed in Appendix A, this number of calculations assures to at least a 95 percent confidence that 99 percent of the range of values of the decontamination factor has been sampled.

Analysis

The purpose of this work is to show that provision of water to the drywell of a Mark I boiling water reactor will reduce the magnitudes of the radionuclide releases from the plant even if the water fails to prevent containment failure. Details on the way water is to be provided to the drywell have not been specified. Possible variations in the supply of water include variations in the depth and the temperature of the water to be maintained over the core debris that is interacting with the drywell concrete. Therefore, calculations were done for water pool depths of 30 and 50 cm, and for water subcooling of 0, 2, 5, 10, 20, 30, 50, and 70°C. The calculated values of the decontamination factors for each of the sixteen sets of conditions were analyzed to construct at confidence levels of 50, 90, and 95 percent the cumulative probability distribution functions for the decontamination factor. The detailed results are presented in tabular form in Appendix B. Cumulative probability distributions for two typical results are shown in Figure 11. These results are shown in the figure as plots of the natural logarithm of the decontamination factor as a function of the quantile of the cumulative distribution. Confidence bands of 95 and 50 percent are shown in the figure.

One of the most useful features of this type of analysis is that it permits separation of the phenomenological uncertainty from the stochastic uncertainty associated with the finite size of the samples taken of the distribution. It is apparent from the results shown in Figure 11 that the stochastic uncertainties in the results obtained here are small in comparison to the phenomenological uncertainties in the vicinity of the mean. At the 95 percentile level and above the stochastic uncertainties are, in some cases, quite large. The confidence intervals to account for stochastic uncertainties could be narrowed by taking larger samples in the Monte Carlo sampling process.

Results obtained in the calculations for the median, the 10 percent quantile and the 90 percent quantile are summarized in Table 3 for specific confidence levels. Each entry in the table is a range of values whose width is determined by the specified confidence level.

The median decontamination factors (at 50 percent confidence level) for water pools 30 and 50 cm deep are shown as functions of pool subcooling in Figure 12. It is evident from this figure that subcooling greatly enhances the amount of decontamination that can be achieved by a water pool. Even for very shallow water pools with proper subcooling, median values of the decontamination factor in excess of 100 are achieved. That is, even with only a 30 cm deep water pool the radionuclide release from core debris interacting with concrete can be reduced by a factor 100.

Very conservative views of the state of phenomenological uncertainty might be based on the 10 percent quantile of the uncertainty distribution. Even in this pessimistic case, factor of 10 reductions in the radionuclide release can be achieved with well-subcooled, shallow water pools (see Figure 13).

The calculations presented here are for water pools overlying core debris within the drywell. Should core debris penetrate the steel liner and flow into the reactor torus room, water would follow. Water maintained over core debris in the torus room would achieve similar reductions of the aerosol and radionuclide emissions as have been calculated here. The results described in this chapter are used in Chapter VI to analyze aerosol concentration in the Mark I drywell for a particular accident.

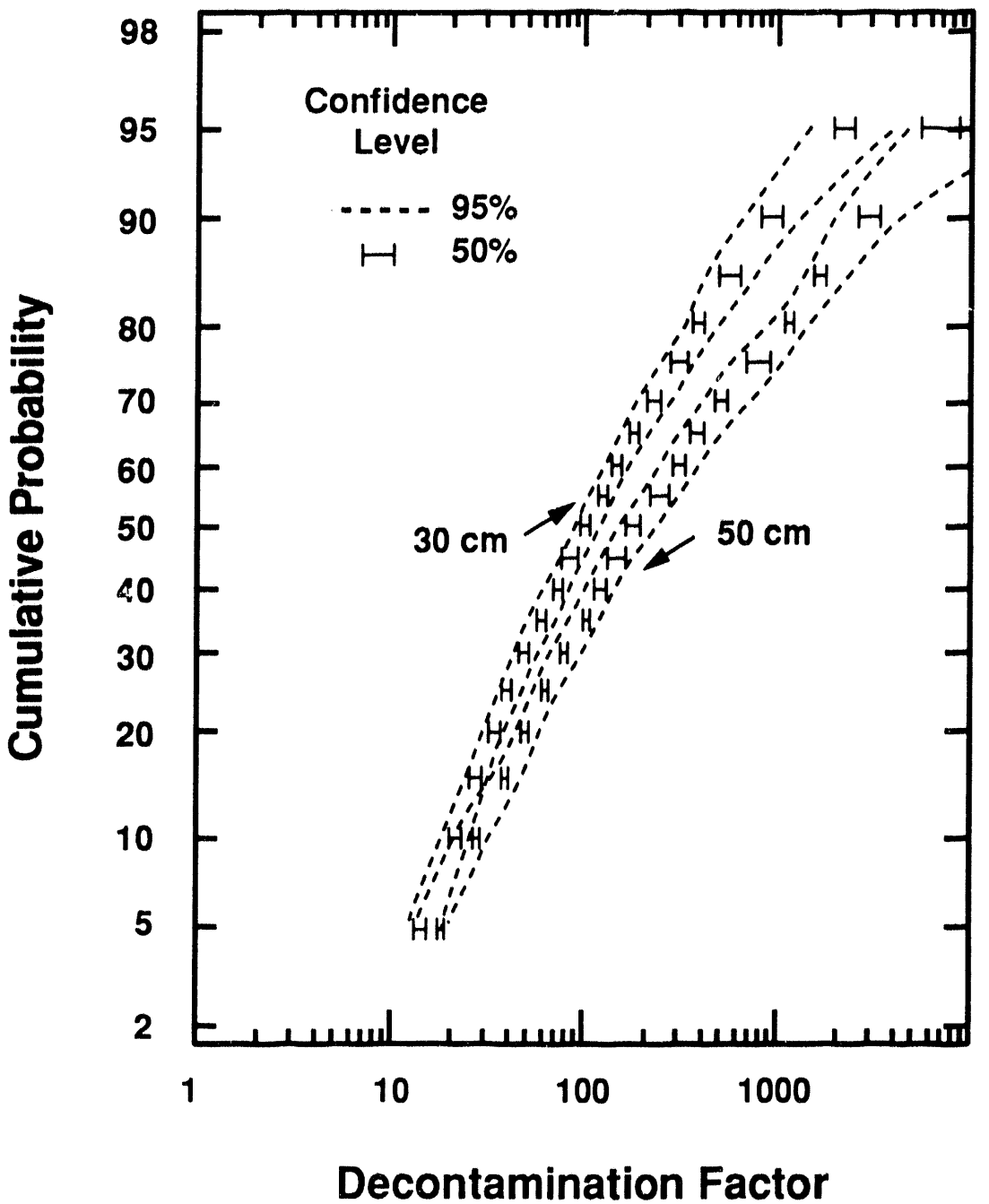

Figure 11 Cumulative probability distributions for the decontamination factors by water pools 30 and 50 cm deep and 20 degrees subcooled

Table 3 Summary of the results for decontamination by a water pool

Pool depth (cm)	Subcooling (K)	Median of ln (DF) at 50% confidence	90% quantile of ln (DF) at 90% confidence	10% quantile of ln (DF) at 90% confidence
30	0	0.7854-0.8158	1.6267-1.8245	0.2915-0.3348
30	2	2.3629-2.4250	3.6861-3.9945	1.2111-1.3854
30	5	3.0708-3.1175	4.7041-5.1801	1.7941-2.0150
30	10	3.7884-3.8978	5.5885-5.9541	2.2236-2.4091
30	20	4.5743-4.6779	6.6050-7.1592	2.9425-3.1907
30	30	5.0977-5.2478	7.2795-7.9798	3.3269-3.5749
30	50	5.7907-5.8814	8.3760-8.7992	3.8181-4.0992
30	70	5.7892-5.9429	8.5337-9.3989	3.5725-3.9342
50	0	1.0511-1.0763	2.1050-2.3269	0.4419-0.4885
50	2	2.7048-2.7805	4.2535-4.5795	1.4652-1.6618
50	5	3.5281-3.6559	5.4022-5.8733	1.9907-2.2740
50	10	4.3825-4.4949	6.4378-6.9502	2.6093-2.9217
50	20	5.0951-5.2448	7.7528-8.2354	3.0929-3.4076
50	30	5.6469-5.7914	8.0362-8.5868	3.4996-3.9106
50	50	6.4307-6.5659	9.3374-10.4523	3.9620-4.2385
50	70	7.1014-7.2417	10.0721-12.4243	4.3884-4.9852

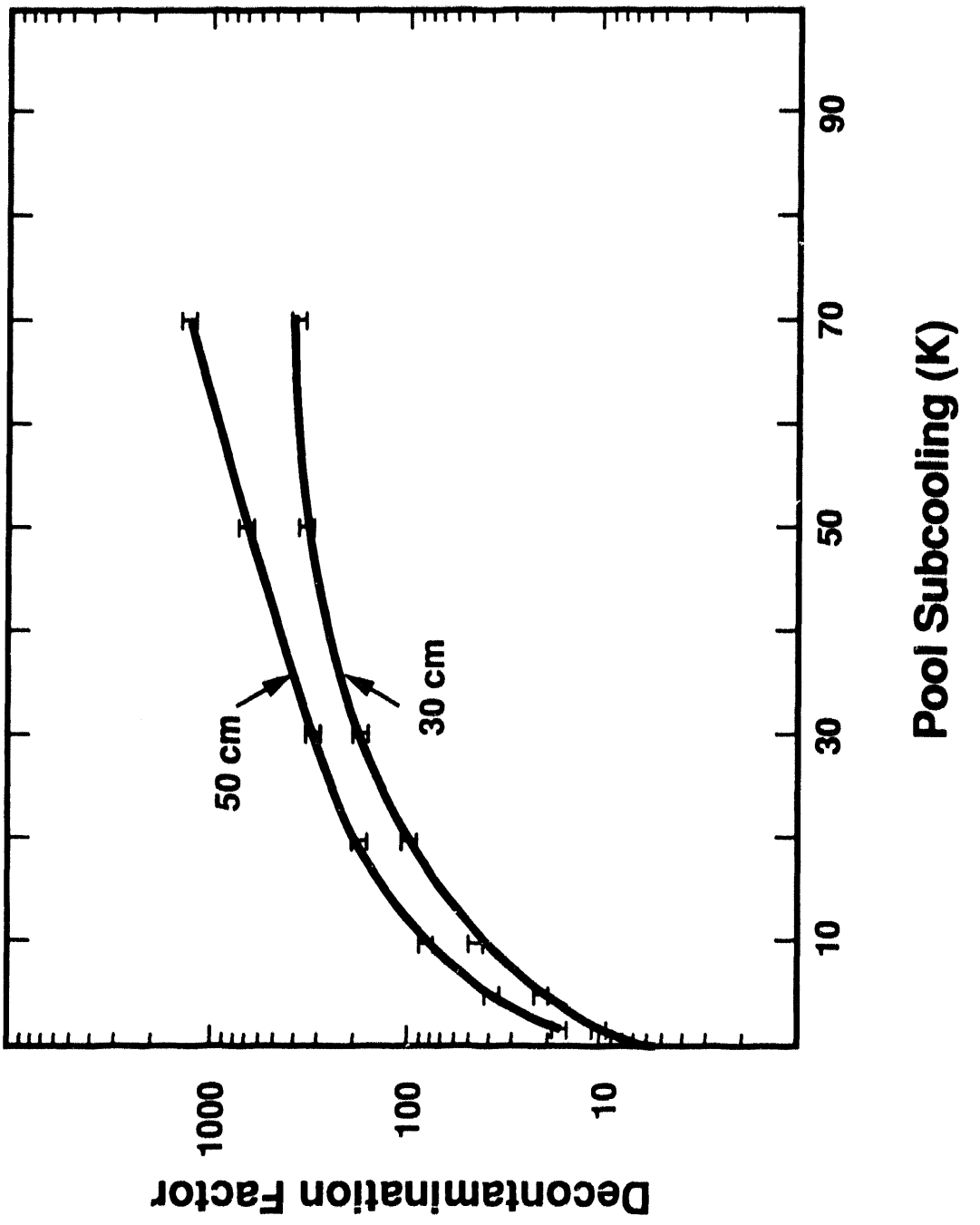

Figure 12 Median values of the decontamination factor at 50 percent confidence level for water pools 30 and 50 cm deep as functions of subcooling

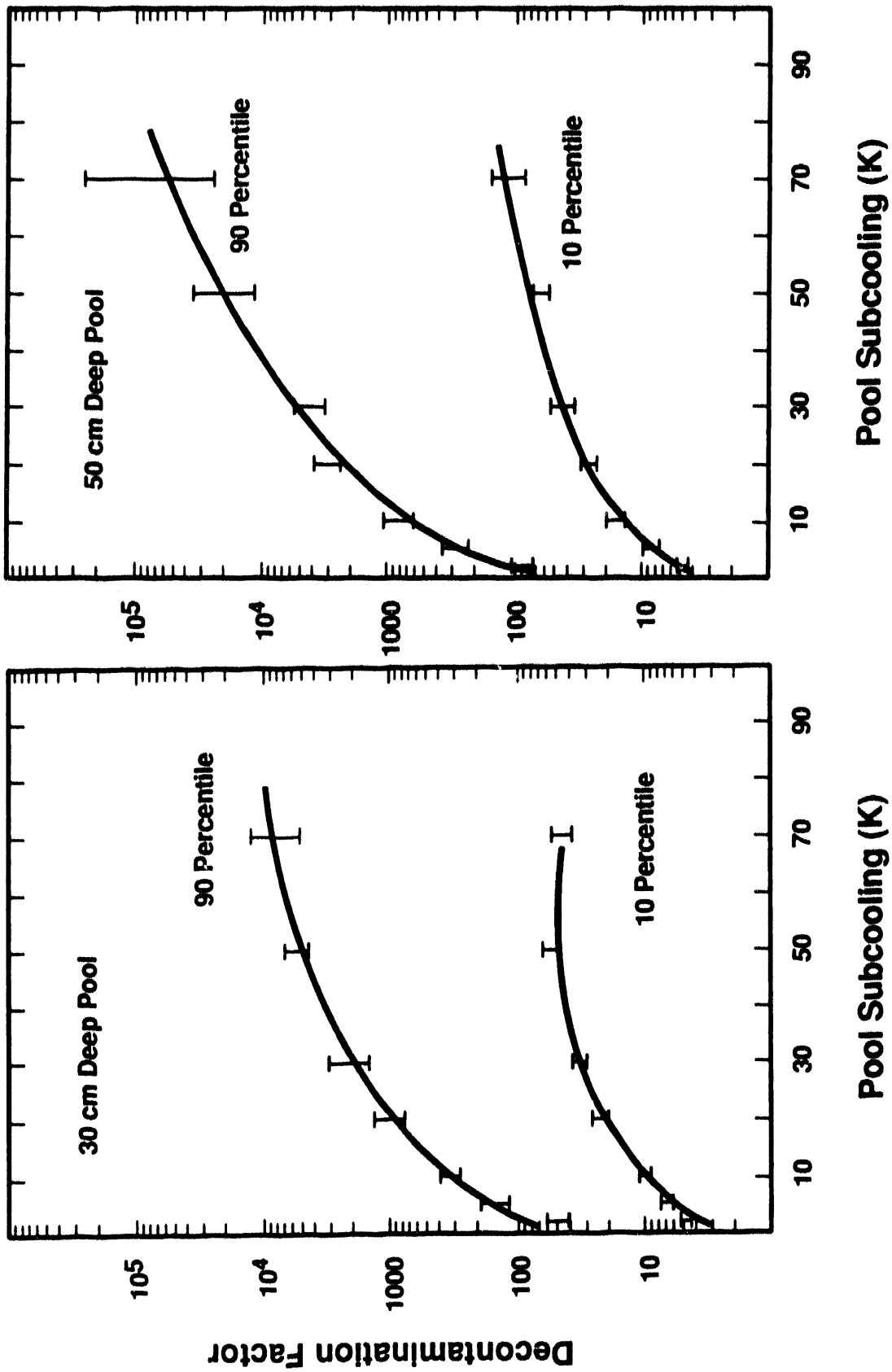

Figure 13 10 percentile and 90 percentile values of the decontamination factors at 90 percent confidence level for water pools 30 and 50 cm deep as functions of water subcooling

IV. Source Term Attenuation by Drywell Sprays

A. Background

In the previous chapter, it was shown that water pools overlying core debris could reduce the aerosol production and radionuclide release from core debris interactions with concrete. Release of radioactive materials during core debris/concrete interactions is but one of the processes that can contaminate the atmosphere of the Mark I drywell and contribute to the inventory of radioactive materials that could escape the plant should the containment fail. Release of radioactive materials from the reactor coolant system when core debris penetrates the reactor vessel, revaporization of radionuclides deposited in the reactor coolant system and release of radionuclides from residual fuel in the reactor coolant system after vessel failure are other ways the atmosphere of the drywell becomes contaminated with radioactive materials. Water pools overlying core debris on the drywell floor will little affect these sources of radioactivity to the drywell atmosphere.

The drywells of Mark I containments are equipped with sprays. The sprays are intended primarily to be used to condense steam in design-basis loss of coolant accidents. The sprays might, however, be used to supply the water needed to maintain a water pool over core debris deposited in the drywell during severe reactor accidents. Falling water drops produced by the spray will trap aerosols suspended in the drywell atmosphere. The sprays could, then, be used to attenuate the source term of radioactive material injected into the drywell atmosphere by processes other than core debris interactions with concrete as well as scavenge aerosols produced by core debris/concrete interactions and not trapped in the water pool.

In this and the next chapter, a quantitative analysis of the decontamination of the drywell atmosphere by drywell sprays is presented. The presentation is, in outline, rather similar to that used to present analyses of the decontamination by an overlying water pool. Phenomena that affect spray performance are discussed in the balance of this chapter. In Chapter V a detailed, quantitative analysis of spray performance is presented.

There is an important difference in the analyses of spray performance from the analyses of the decontamination by overlying water pools. Sprays can be operated for an indeterminant period of time. The decontamination that can be achieved by sprays is, then, unbounded whereas the decontamination by water pools is inherently limited by the depth of the pool and the rise velocities of aerosol-laden bubbles through the pool. That is, aerosols rising through an overlying water pool are exposed to the actions of the water pool for a fixed, predictable time. Aerosols in the drywell atmosphere can be exposed to the actions of spray droplets for times that can be known only if the schedule for spray operation is known. It would be presumptuous to assign a particular decontamination factor to the sprays if some mandated schedule for their operation does not exist.

The formal differential equation that describes aerosol mass in the containment atmosphere is:

$$\frac{dM}{dt} = - \lambda M + \dot{S} + \dot{R}$$

where

M = aerosol mass suspended in the containment atmosphere

λ = a coefficient for decontamination by sprays

$\dot{R}$ = rate of aerosol removal by mechanisms other than spray decontamination of the atmosphere

$\dot{S}$ = rate at which aerosol mass is injected into the containment atmosphere

A more convenient method for the analysis of spray performance is to determine λ, the coefficient for decontamination by sprays.* Specification of λ provides a much more generically useful result than does specification of a decontamination factor obtained by assuming some arbitrary operation of the sprays. In the subsections below, it will be shown that λ is not a constant. Rather, it has complicated functional dependencies on the aerosol trapping processes, the characteristics of the spray and the conditions under which the sprays operate.

---

*Regulatory descriptions of λ use the definition [84]:

$$\lambda = \frac{1.5HF}{V}\left(\frac{E}{D}\right)$$

where

H = fall distance
V = containment volume
F = water flow rate
$\frac{E}{D}$ = aerosol capture efficiency divided by droplet diameter

For 1000 μm diameter droplets a recommended value [84] for $\left(\frac{E}{D}\right)$ is 10 meters^{-1} until a decontamination factor of 50 (98 percent of the aerosol initially present has been removed) is reached. Then, the recommended value of $\left(\frac{E}{D}\right)$ is reduced to 1 meter^{-1}. Values of λ given in this report in units of hr^{-1} may be converted into values of $\left(\frac{E}{D}\right)$ in units of meters by:

$$\left(\frac{E}{D}\right)(\text{meters}^{-1}) = \frac{\lambda(\text{hr}^{-1})\ 0.01852}{Q}$$

where Q is the water flux into the containment atmosphere in units of cm^3 H_2O / cm^2-s. The reciprocal of λ is the time in hours for sprays to reduce the aerosol concentration in the atmosphere by a factor of e = 2.7 if there is no unsprayed volume.

B. Trapping of Aerosol Particles by Water Droplets

Activation of drywell sprays in a Mark I boiling water reactor must be done manually. If the drywell sprays are activated during a severe reactor accident the sprays will affect the pressure, temperature and composition of the containment atmosphere. Sprays will cool the atmosphere and condense steam in the atmosphere. Stefan forces on aerosol particles during the condensation of steam will drive aerosol particles into falling water droplets. There will also be some modest thermophoretic forces on aerosol particles that will drive the particles into the water droplets.

The dynamic conditions immediately following spray actuation will be of short duration. Rather quickly a quasi-steady state will be established in which the pressure, temperature and composition of the containment atmosphere are nearly in equilibrium with the falling spray droplets. It is the source term reduction that can be achieved during this quasi-steady operation of the sprays that is of interest here. Though a significant amount of decontamination of the drywell can be anticipated during the initial phase of spray operation, this early decontamination driven by steam condensation is neglected here. Neglect of decontamination during the early period of spray operation is not a serious omission if containment failure is not coincident with actuation of the sprays.

Under the essentially steady-state conditions assumed here, falling water droplets still sweep aerosol particles from the containment atmosphere. The predominant modes by which falling water droplets trap aerosol particles are:

- impaction
- interception, and
- diffusion.

Impaction refers to the collision of water droplets with aerosol particles. As a droplet falls through the drywell atmosphere, a flow field develops around the droplet. This flow field will carry aerosol particles. Some aerosol particles will be too massive to respond to the sudden accelerations of gas flow in the vicinity of the falling droplet. Inertia will allow these particles to cross the streamlines of the flow field and to contact the water droplet. It is assumed here that contact between a water droplet and an aerosol particle is sufficient to cause the capture of the aerosol particle whether or not the aerosol material is soluble in the droplet. Surface tension and van der Waals forces are sufficient to hold even insoluble particles to the droplet.

Particles of an intermediate size may be able to respond to the accelerations in the gas flow field near the droplet. The centers of mass of these droplets will follow trajectories around the droplet. But, because the droplets are of finite size, they may still be intercepted by the droplet.

Very small particles will be able to follow the flow field around a falling droplet easily. These small particles also respond to impulses provided by collisions with gas molecules. Because of the stochastic nature of these collisions, there is an apparent diffusion of small aerosol particles. This diffusive motion can carry the particles across streamlines into the droplet surface. Again, surface tension and van der Waals forces assure the diffusing particles are trapped by the falling drop once contact is made.

Attenuation

It is possible for aerosol particles and falling drops to be electrostatically charged. Coulombic forces between charged aerosols and charged droplets could attract or repel particles and drops depending on the relative signs of the charges. Radiation fields are, however, often used to discharge aerosol particles. Certainly under severe accident conditions both the drops and the aerosol particles in the Mark I drywell would be exposed to an intense radiation field. Electrostatic interactions are neglected here. No entirely satisfactory proof has been formulated to defend the decision to neglect electrostatic effects (but, see References 59, 60).

The quantitative descriptions of aerosol collection by falling drops are based on the assumption that the drops are spheres. This seems to be an acceptable assumption for droplets formed by sprays in nuclear power plants. Water droplets falling through air needed to be larger than 0.1 cm to distort significantly from spherical [26, 61]. The distortion of larger droplets and models for these distortions are described elsewhere [18].

Consider a sphere of diameter D_d falling through space. After falling a distance x, the sphere will have swept out a volume of gas given by:

$$\text{Volume} = \frac{\pi}{4} D_d^2 \, x$$

If the gas contains a concentration of n(i) aerosol particles of diameter $d_p(i)$, then the falling sphere would have encountered:

$$\frac{\pi}{4} D_d^2 \, n(i) x$$

of these aerosol particles in the absence of hydrodynamic forces on the particles. A convenient definition of the efficiency with which falling drops capture aerosol particles is the ratio of the actual number of particles captured to the number of particles in the volume swept by the falling sphere:

$$\epsilon (D_d \, , \, d_p(i)) = 4\Delta N(i) \, / \, \pi D_d^2 \, n(i) x$$

where

$\epsilon(D_d, d_p(i))$ = droplet capture efficiency for aerosol particles of diameter $d_p(i)$

$\Delta N(i)$ = actual number of particles of diameter $d_p(i)$ captured during a fall of distance x.

Hydrodynamic effects cannot be neglected in the analysis of aerosol capture by falling water drops. The efficiency with which droplets capture particles should depend on the nature of the gas flow around the droplet. Analytic results are available only for the limiting flow regimes of viscous flow (Reynolds number = Re → 0) and of potential flow (Re → ∞). Pemberton [62] has argued that in view of the substantial size differences between aerosols of interest ($d_p(i) < 10$ μm) and water droplets

(D_d > 100 μm), flows around falling water droplets can be satisfactorily treated as potential flows. Others [63], however, have felt it necessary to consider some means for interpolating between viscous and potential flow to predict real decontamination rates. Not everyone has agreed with the interpolation methods that have been proposed in the literature [64].

Widely used expressions for the efficiency of aerosol capture as a result of impaction are:

a. Potential Flow Regime

$\epsilon(\text{imp, pot}) = 0$ for $\text{Stk} \leq 0.0833$

$\epsilon(\text{imp, pot}) = [\text{Stk} / (\text{Stk} + \delta)]^2$ for $\text{Stk} \geq 0.2$

$\epsilon(\text{imp, pot}) = 8.57\,[\text{Stk} / (\text{Stk} + \delta)]^2\,(\text{Stk} - 0.08333)$ for $0.08333 < \text{Stk} < 0.2$

where δ has been given values between 0.25 and 0.75.

b. Viscous Flow Regime

$\epsilon(\text{imp, visc}) = 0$ for $\text{Stk} \leq 1.214$

$$\epsilon(\text{imp, visc}) = \left[1 + \frac{0.75\,\ln(2\,\text{Stk})}{(\text{Stk} - 1.214)}\right]^{-2} \quad \text{for Stk} > 1.214$$

c. Transition Flow Regime

$$\epsilon(\text{imp, trans}) = \frac{\epsilon(\text{imp, visc}) + \text{Re}_d\,\epsilon(\text{imp, pot}) / 60}{1 + \text{Re}_d / 60}$$

where

$$\text{Stk} = d_p^2\,\rho_p\,U_T / 9\,\mu_g\,D_d\,\chi$$

$$\text{Re}_d = U_T\,\rho_g\,D_d / \mu_g$$

ρ_g = density of the gas phase

U_T = terminal velocity of the droplet

μ_g = viscosity of the gas phase

χ = dynamic shape factor for the aerosol particle.

Note that two models of particle capture by impaction are presented above. All real flows are in the transition regime between the viscous and potential flow limits. One model follows the argument by

Pemberton [62] that real flows of interest here are adequately approximated by potential flow and the impaction efficiency is given by ϵ(imp, pot). The other model is based on an interpolation between potential and viscous flow. The efficiency of aerosol capture by impaction is then given by ϵ(imp, trans). Plots of ϵ(imp, pot) and ϵ(imp, trans) are shown in Figure 14 for water droplets falling through air at 1 atmosphere pressure and 298 K. Properties used for these calculations are shown in Table 4. The dynamic shape factor of the aerosol was taken to be 1 for the calculations used to prepare this figure.

Expressions for the efficiency of aerosol capture by interception are:

a. Potential Flow Regime

$$\epsilon(\text{int, pot}) = 3\gamma\, d_p / D_d$$

b. Viscous Fow Regime

$$\epsilon(\text{int, visc}) = 1.5\, (\gamma\, d_p / D_d)^2 / (1 + \gamma d_p / D_d)^{1/3}$$

c. Transition Flow Regime

$$\epsilon(\text{int, trans}) = \frac{\epsilon(\text{int, visc}) + Re_d\, \epsilon(\text{int, pot}) / 60}{1 + Re_d / 60}$$

where γ is the collision shape factor for the aerosol particles.

The capture efficiency for the viscous flow regime is that recommended by Lee and Gieseke [65] and differs somewhat from that often quoted $\epsilon(\text{int, visc}) = 1.5\, (\gamma d_p / D_d)^2$.

Again, note there are two models of interception efficiency presented above. These efficiencies--ϵ(int, pot) and ϵ(int, trans)--are shown as functions of aerosol particle size and droplet diameter in Figure 15. Also shown in the figure is the efficiency of aerosol capture in the viscous flow limit.

Expressions available for the description of the efficiency of aerosol capture by diffusion include:

$$\epsilon(\text{dif}) = 3.18\, Pe^{-2/3}$$

$$\epsilon(\text{dif}) = (4/Pe)\, (2 + 0.557\, Re_d^{1/2}\, Sc^{3/8})$$

where

Pe = Peclet number = Re_d Sc

Sc = Schmidt number = $\mu_g / \rho_g \mathcal{A}_p$

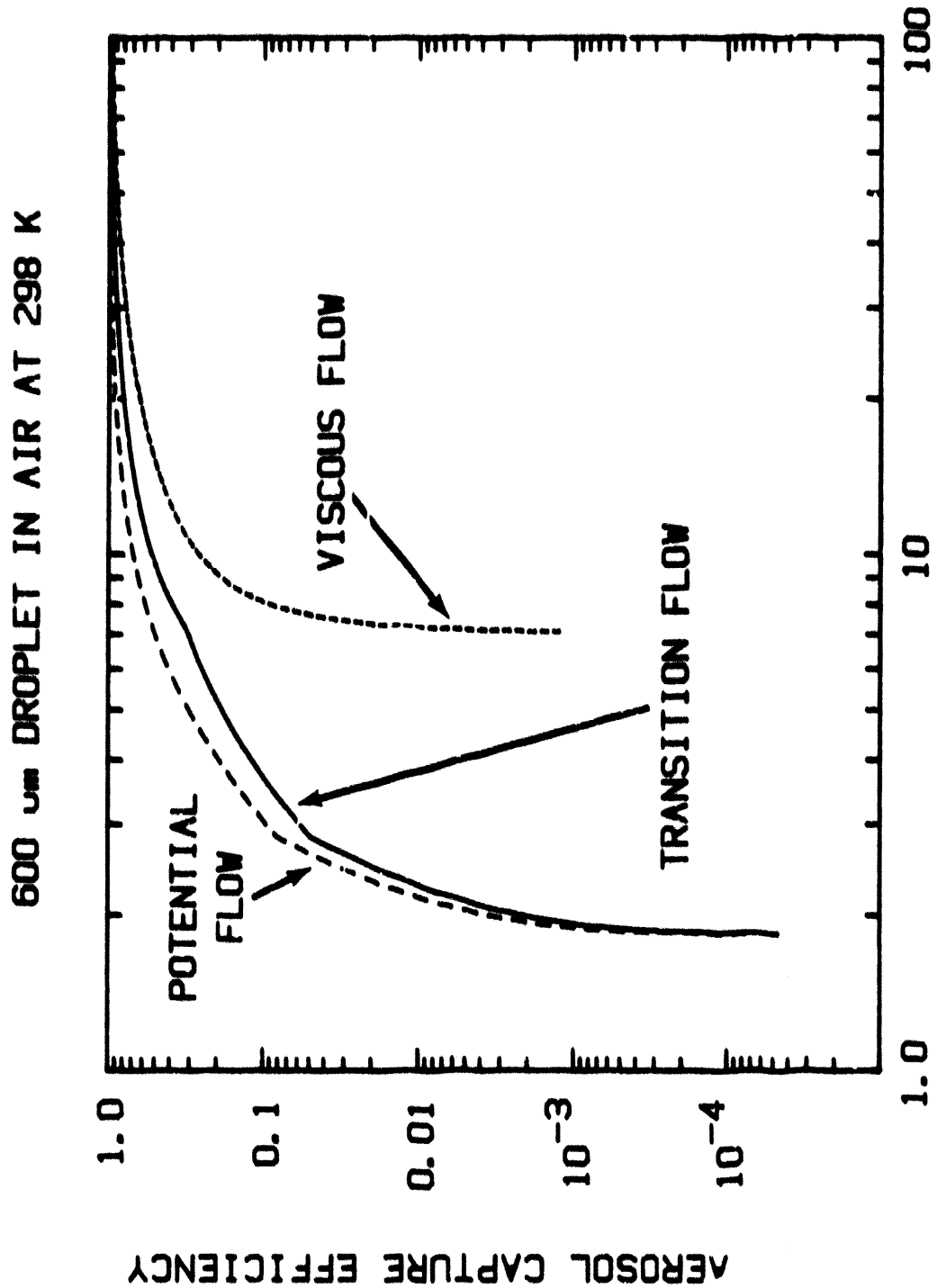

Figure 14 ϵ(imp, pot) and ϵ(imp, trans) as functions of aerosol particle size

Table 4 Properties of water and air

Water Density (g/cm^3)

$$\rho_l = 0.849397 + 1.29812 \times 10^{-3} T - 2.69223 \times 10^{-6} T^2$$

Water Viscosity (Poises)

$$\log_{10} \mu_l = \log_{10} (0.01002) + \frac{\left[1.3272\ (293 - T) - 1.52 \times 10^{-3}\ (T - 293)^2\right]}{(T - 168)}$$

Water Surface Tension (dyne/cm)

$$\sigma_l = 34.6\ (T/704)^{-0.8373}$$

Air Density (g/cm^3)

$$\rho_g(\text{air}) = 0.352\ P(\text{atms})/T$$

Air Viscosity (Poises)

$$\mu_g(\text{air}) = 2.3013 \times 10^{-6}\ T^{0.768}$$

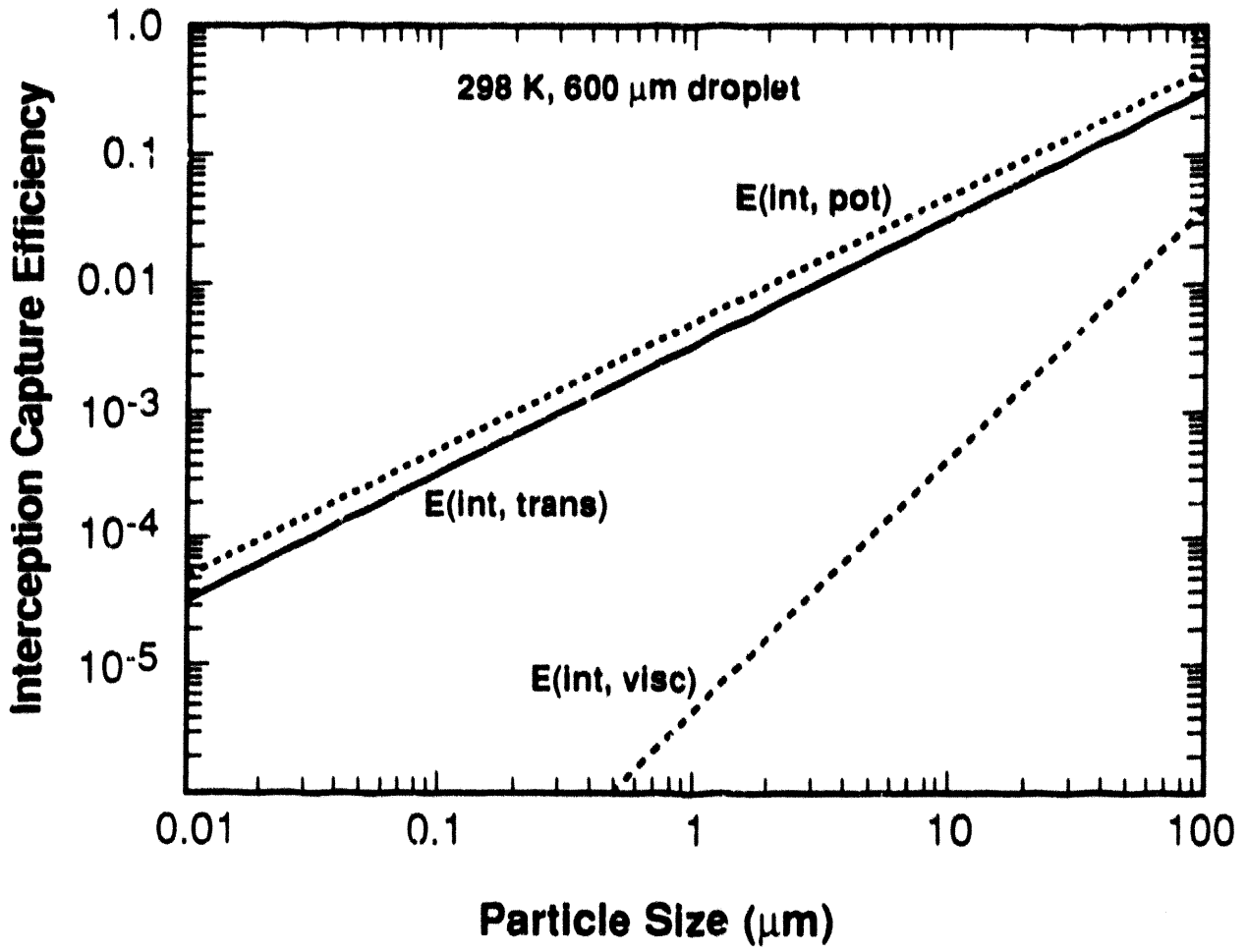

Figure 15 ϵ(int, pot) and ϵ(int, trans) as a function of aerosol particle size for droplets in air at 298 K and 1 atm

Attenuation

$\mathcal{D}_p$ = diffusion coefficient for aerosol particles

$= \bar{c}\ kT/3\pi\ \mu_g\ d_p$

k = Boltzmann's constant = 1.38×10^{-16} ergs/K

$\bar{c}$ = Cunningham slip correction

$$\bar{c} = 1 + \left(\frac{2\bar{l}}{d_p}\right)\left[1.257 + 0.4\ \exp\left(-0.55 d_p/\bar{l}\right)\right]$$

$\bar{l}$ = mean free path in the gas phase

$\bar{l}$ (cm) = 2.3×10^{-8} T(K) / P(atm)

Great confidence cannot be placed in any of these expressions for aerosol capture by diffusion. The expressions are based on isolated spherical collectors for aerosol particles. Spray droplets in the drywell atmosphere of a Mark I containment will not be isolated. There is substantial evidence that in arrays of spheres mass transport to a sphere is less than mass transport to an isolated sphere [65-66]. Detailed results are available only for cases involving two equal size spheres [66-68]. At the limit of Pe → 0 where the Sherwood number for an isolated sphere is 2, the Sherwood number for a sphere in a pair as a function of the septation between spheres is [68]:

Separation divided by the radius of the sphere	Sherwood number (Sh)
∞	2.00
20.14	1.9056
8.288	1.7852
3.0862	1.5232
2.0402	1.3920

Thus, the deviation increases as the spheres become closer. The obvious limit is Sh = 1.0 when the spheres coalesce. The presence of a second sphere drastically affects the angular distribution of local Sherwood numbers around a sphere.

Useful results for randomly dispersed spheres with varying diameters do not appear to be available. It is apparent, however, that the wake behind a large, fast moving drop could affect diffusive collection of aerosol particles by smaller droplets. Small droplets, it will be seen, are quite important in the decontamination of containment atmospheres by sprays.

Often the various mechanisms of aerosol capture by spray droplets are considered to operate independently. The overall efficiency of the spray is then given by (additive model):

$$\epsilon(\text{total}) = \epsilon(\text{imp}) + \epsilon(\text{int}) + \epsilon(\text{dif})$$

An alternate expression for the overall efficiency of decontamination by spray droplets is [69] (compound model):

$$\epsilon'(\text{total}) = 1-(1 - \epsilon(\text{imp}))\ (1 - \epsilon(\text{int}))\ (1 - \epsilon(\text{dif}))$$

This expression differs markedly from the previous expression only for capture of aerosols by large particles.

The overall efficiency of aerosol capture by water droplets is shown as a function of aerosol size and droplet size in Figure 16. Note that there is a minimum in the capture efficiency when is plotted against aerosol particle size. At this minimum, aerosols are too big to be significantly affected by Brownian motion responsible for aerosol capture by diffusion. Yet, the particles are still small enough that they have a high probability of avoiding capture by impaction or interception.

A great deal of significance has been attached to the existence of this minimum. Though sprays may be effective agents for cleansing the atmosphere of general aerosols, they may be quite inefficient at removing aerosols with sizes in the vicinity of the minimum. This size, not coincidently, is the aerosol size likely to be injected into containment by sources subjected to other decontamination processes such as overlying water pools or transport through the reactor coolant system. It is also the aerosol particle size to be expected when vapors are released from the reactor coolant system are suddenly condensed in the cooler drywell. The concern is, of course, that these particles might be substantially resistant to scrubbing by sprays.

Note, however, that the location of the minimum is dependent on the droplet size. Droplets having diameters of about 200 μm produce a minimum at a substantially different location than do droplets 600 μm in diameter and larger. At least some of the concern over the minimum in the overall decontamination factor arises because models used to predict decontamination by sprays [70] use a single monodisperse droplet size. Modeling sprays with a range of droplet sizes would reduce, but not eliminate, the concern over aerosol particles resistant to capture by droplets.

C. Characteristics of Sprays

A comprehensive examination of spray systems in the drywells of Mark I boiling water reactors has not been attempted. A brief description of features of these spray systems pertinent to the analysis of aerosol removal is presented here. At least for the plants that were examined, the spray system consists of at least two headers. One header is located near the waist of the so-called inverted lightbulb containment about 8.5 meters above the drywell floor. The other header may be variously located. At the Brown's Ferry plants, the second header is located 15.8 meters above the drywell. At other plants there may be a header even higher in the drywell.

In all cases examined, the spray system must be manually actuated. In the case of the Brown's Ferry plants, interlocks prevent actuation of the spray unless the drywell is pressurized and the core is 2/3 covered with water. Other characteristics of drywell sprays are listed in Table 5.

At the Brown's Ferry Units 1 and 2 sprays can provide 517 liters/second of water to the drywell. At Unit 3 sprays can provide 577 liters per second. Such high flow rates from drywell sprays may not be typical of all Mark I boiling water reactors. The containments of these reactors are designed for internal

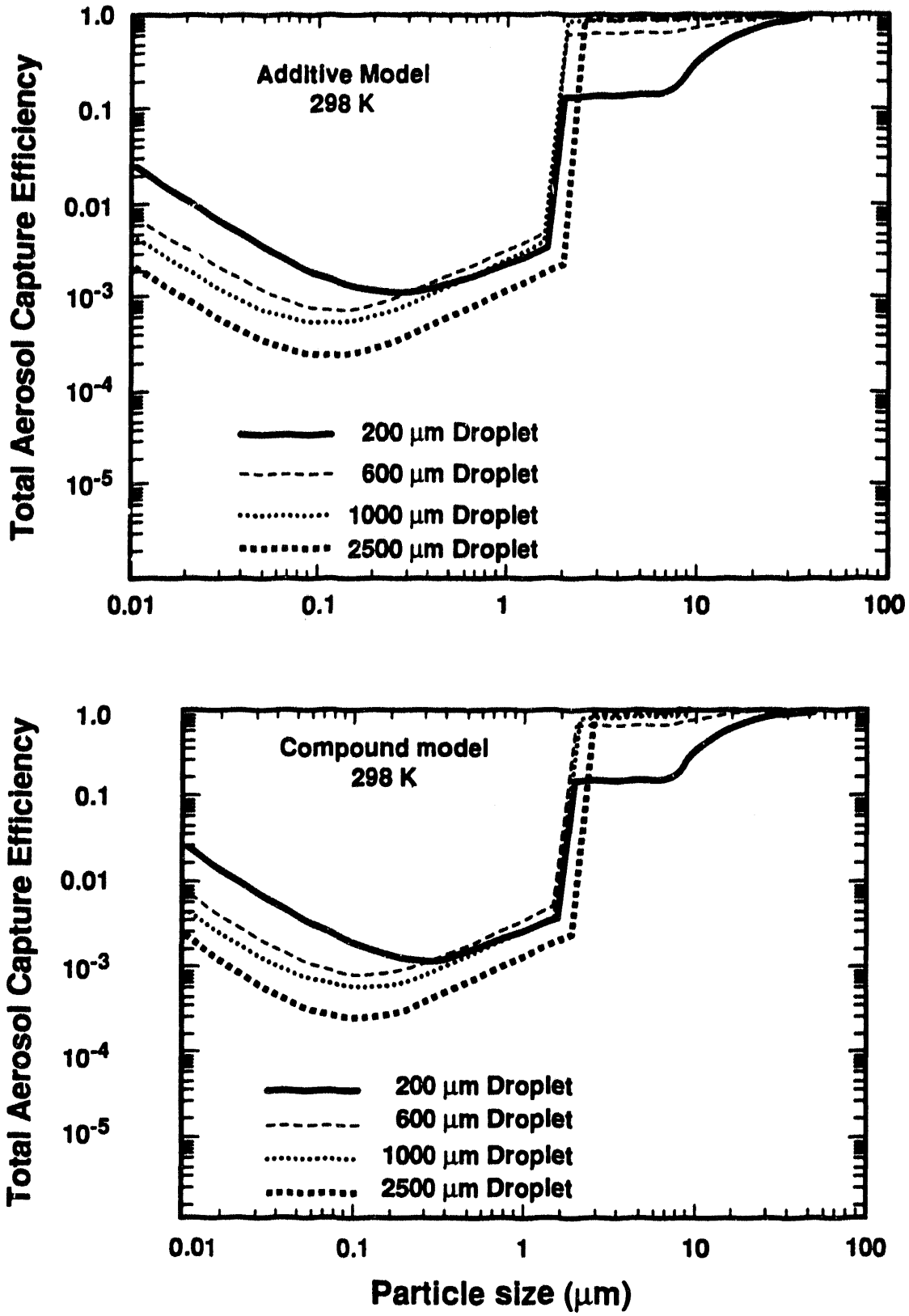

Figure 16 Overall capture efficiency as a function of aerosol particle size for various water drop sizes according to the additive and compound models described in the text

Table 5 Characteristics of drywell sprays in some Mark I boiling water reactors

Plant	MW_{th}	Drywell volume (m^3)	Wellwell volume (m^3)	Spray system description
Pilgrim 1	1998	4162	3398	Part of RHR; interlocks to prevent actuation unless water level 2/3 of core height and drywell pressure > 0.27 atms-gauge
Oyster Creek	1930	5097	3596	Two independent systems. Automatic initiation of one system on high drywell pressure and low water level in core. Power from emergency buses.
Nine Mile Point 1	1850	5037	3398	Independent system. One system automatically initiated on high drywell pressure and low water level. Second system connected to emergency diesel generators and manually initated.
Millstone 1	2011	4162	3540	Part of RHR. Manual initiation after core is flooded.
Fitzpatrick	2436	4248	3398	Part of RHR. System can be manually initiated after low pressure injection requirements are met.
Hope Creek 1 & 2	3436	4786	3879	Part of RHR. Manually initiated.
Vermont Yankee	1593	3794	3058	Part of RHR.
Dresden 2 & 3	2527	4474	3313	Part of RHR.
Quad Cities 1 & 2	2511	4474	3313	Part of RHR. Manual initiation permissible after water level 2/3 of core height.
Fermi 2	3430	4644	3681	Part of RHR. Manual initiation permissible after low pressure injection requirements are met.
Duane Arnold	1658	3086	2662	Part of RHR. Manual initiation after low pressure injection requirements are met.
Cooper	2381	3738	3115	Part of RHR. Manual initiation possible once water level > 2/3 of core height and drywell pressure > 0.27 atms-gauge.
Monticello	1670	3794	3058	Part of RHR. Manual initiation once low pressure injection requirements are met.

Table 5 Characteristics of drywell sprays in some Mark I boiling water reactors (Concluded)

Plant	MW_{th}	Drywell volume (m^3)	Wetwell volume (m^3)	Spray system description
Edwin Hatch 1 & 2	2436	4134	3143	Part of RHR. Manual initiation possible after low pressure injection requirements are met.
Brown's Ferry 1, 2, & 3	3293	4502	3370	Part of RHR. Manual initiation after low pressure injection requirements are met.
Brunswick 1 & 2	2436	4644	3511	Part of RHR. Manual initiation after low pressure injection requirements are met.

pressurization and are poorly suited to withstand pressurization by the external atmosphere. A concern has arisen that actuation of the sprays in the drywell may cool the drywell so much that it becomes externally pressurized. Some Mark I plants have been modified so that the drywell sprays can provide only about 50 liters of water per second.

Based on the examinations done for this work, two types of spray nozzles are used in the drywell sprays of Mark I boiling water reactors--Model 1-7G25 and 1-7G3 made by Spray Systems Co. A schematic diagram of the Model 1-7G25 spray nozzle is shown in Figure 17. The Model 1-7G3 is quite similar. Also shown in this figure is the spray pattern produced by the nozzle. About 65 percent of the water flow is within a central core region. The remaining 35 percent of the flow is within a coaxial annulus.

Flow rates through the nozzles as functions of water pressure are shown in Figure 18. The volume-weighted mean droplet sizes produced by the nozzles as a function of water pressure are shown in Figure 19.

More detailed droplet size data are not available for the Model 1-7G25 spray nozzle. Droplet size data have been obtained for the Model 1-7G3 nozzle [71]. These data were obtained by allowing droplets to fall into pools of liquid nitrogen and sieving the frozen particles. Some results are shown in Table 6. In comparison to photographic techniques, this method typically yields higher concentrations of fine droplets. This may be because it is able to measure droplets that cannot be resolved well by photographic methods. On the other hand, sieving may break particles and lead to erroneously high indications of fine droplet contributions to the distribution [72].

A surprising finding of the droplet size distribution measurements is that droplets obtained with "tap water" are somewhat smaller than droplets obtained with a sodium hydroxide-boric acid solution (see Figure 20). The concentrations of solutes (3000 ppm boron and pH 9.5) used in the experiments seem to be too low to produce changes in liquid properties that would account for the changes in droplet size distribution. Of course, it may be that solutes make frozen droplets less susceptible to breakage during sieving.

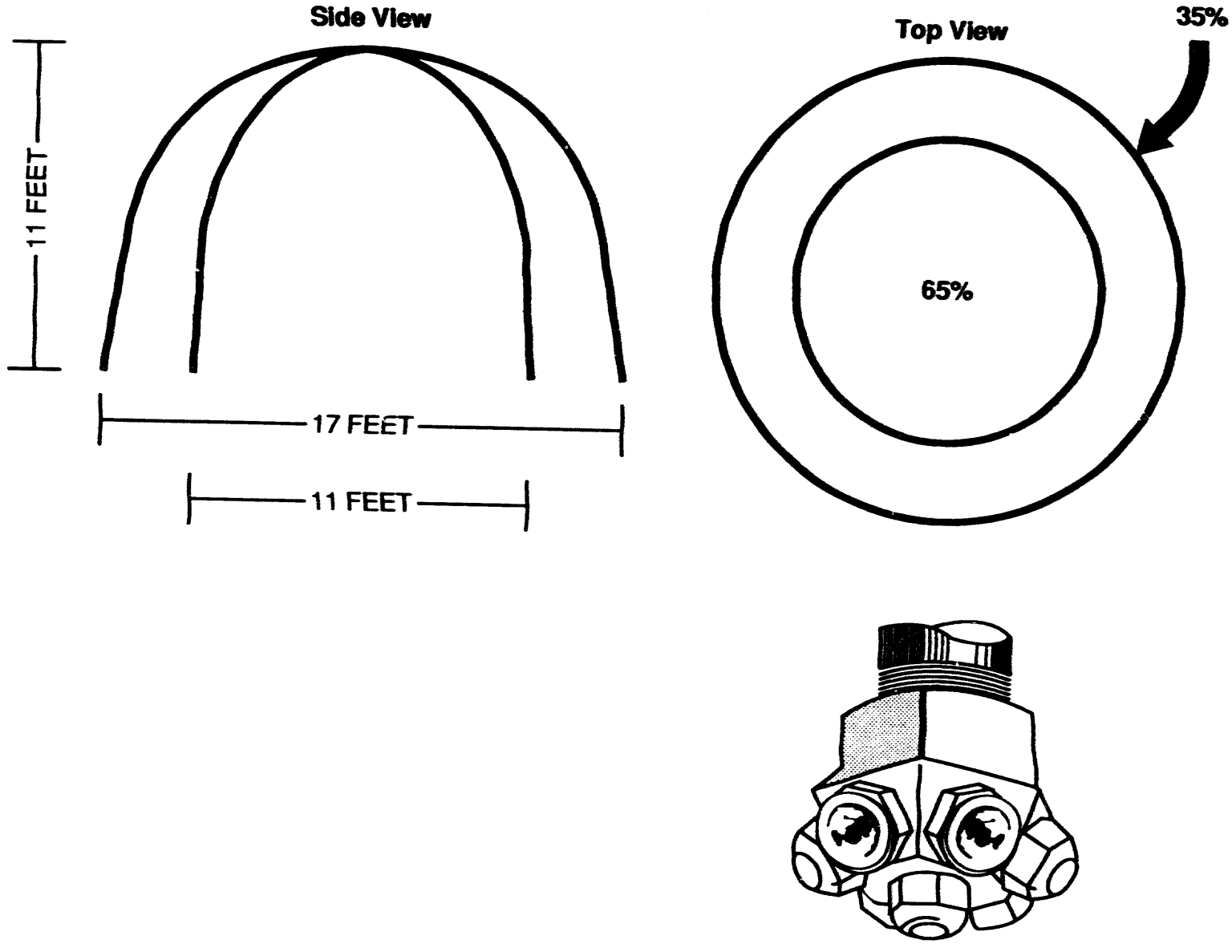

Figure 17 Schematic diagram of the spray nozzle and spray patterns. Note 11 feet ≅ 335 cm and 17 feet ≅ 518 cm

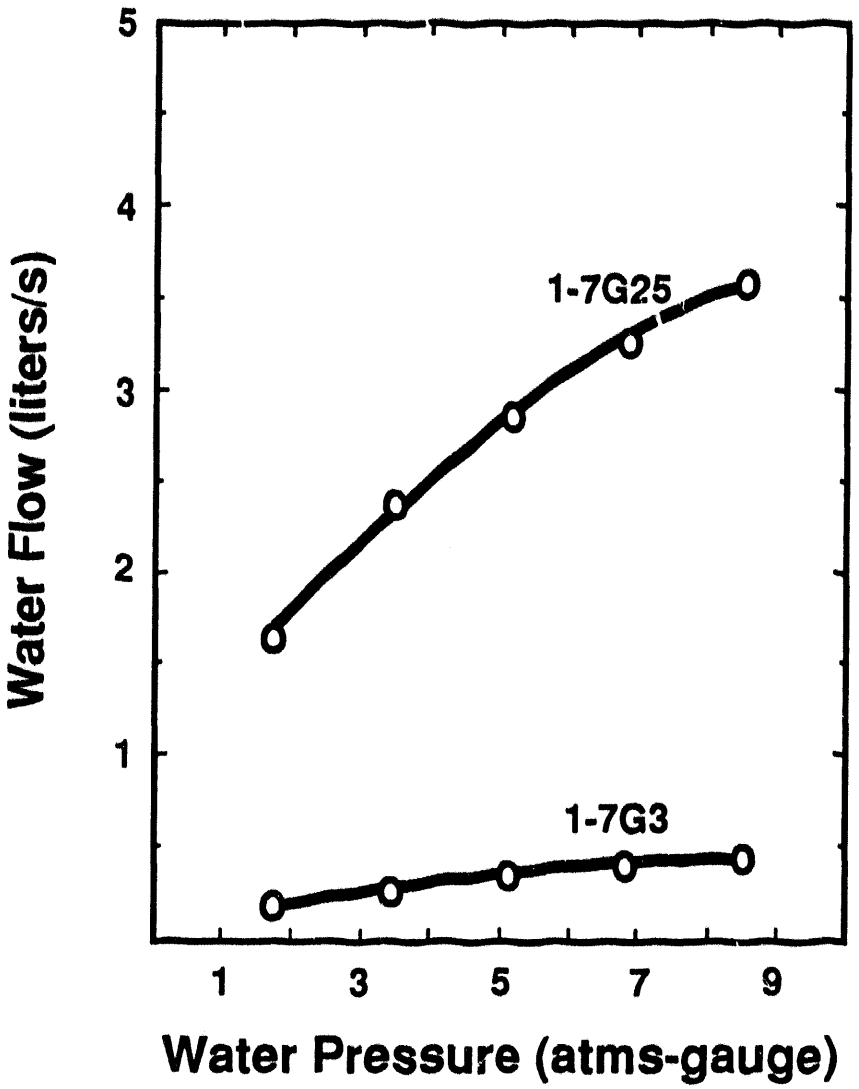

Figure 18 Volumetric flow rates through the Model 1-7G25 and Model 1-7G3 spray nozzles as functions of water pressure

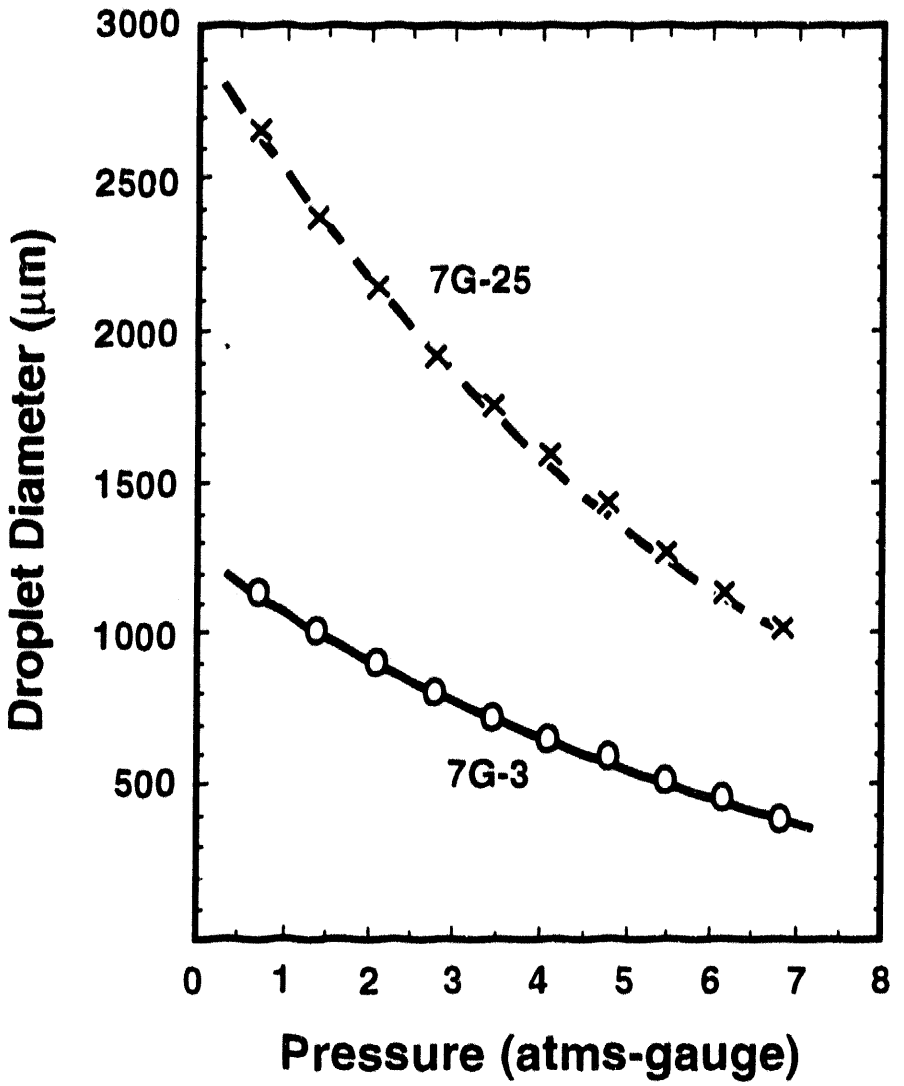

Figure 19 Volume-weighted mean droplet sizes produced by the Model 1-7G25 and Model 1-7G3 spray nozzles as functions of water pressure

Table 6 Droplet size data for the Model 1-7G3 spray nozzle [71]

Screen opening (μm)	Mass on screen (g) in			
	Test 3a (Tap water)	Test 3b	Test 4a (boric acid-sodium hydroxide solution)	Test 4b
2360				
1700			154.3	0
1400			154.3	77.2
1180	77.2		231.5	77.2
1000	77.2	77.2	77.2	77.2
850	231.5	154.3	231.5	231.5
710	231.5	77.2	540.1	540.1
600	385.8	231.5	925.8	848.7
500	540.1	462.9	1311.6	1388.7
355	1080.1	1234.4	2468.8	3008.9
300	462.9	617.2	1080.1	1234.4
250	462.9	462.9	462.9	462.9
125	231.5	154.3	462.9	771.5
pan	308.6	231.5	231.5	308.6

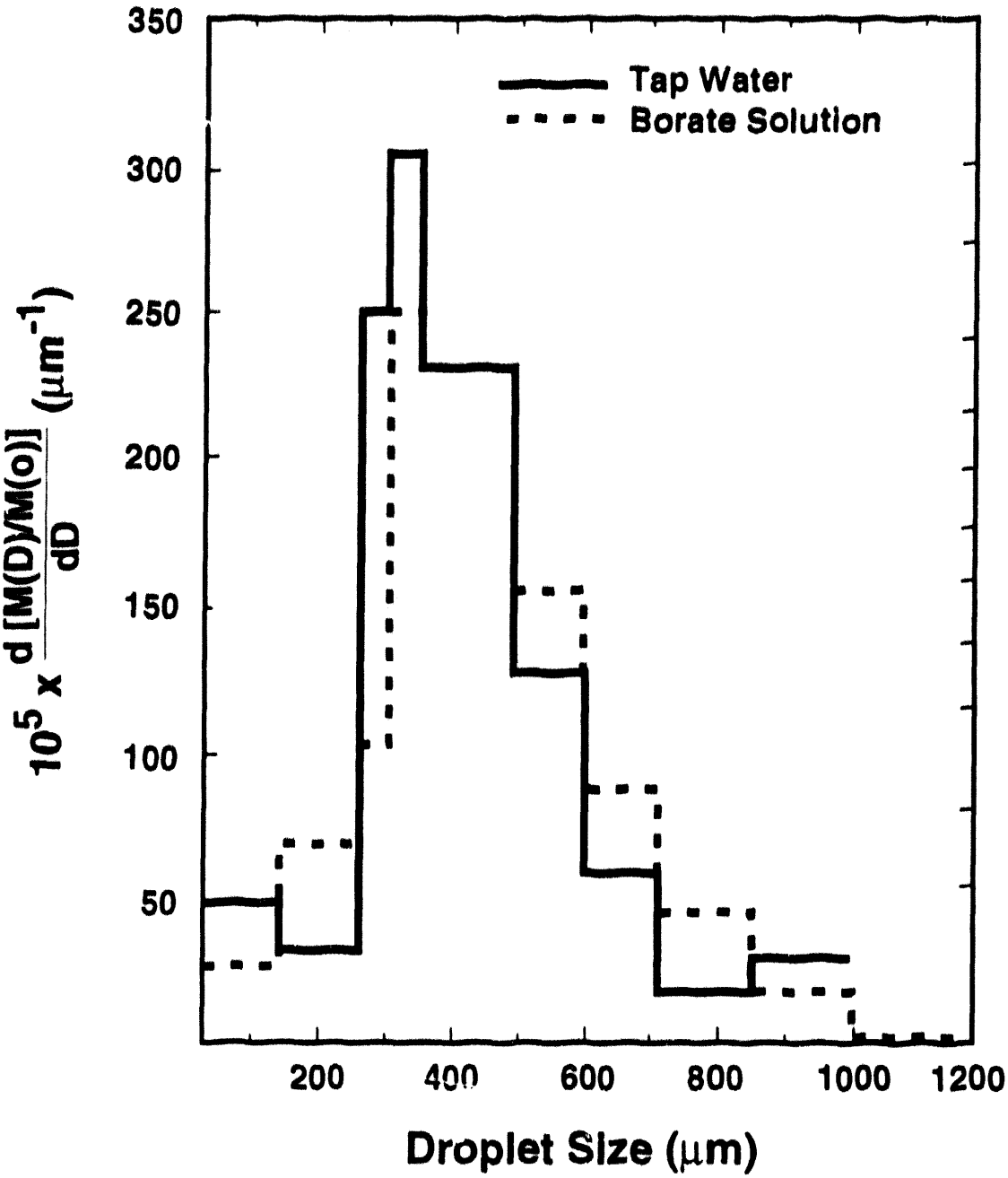

Figure 20 Droplet size distribution data for the Model 1-7G3 spray nozzle

D. Droplet Terminal Velocities

The database available for the terminal velocities of water droplets is not large [26]. Most data are for the terminal velocities of raindrops in air. Far fewer data have been obtained for the much finer drops produced by containment sprays. Most data are for terminal velocities in air at normal conditions. There appear to be no data for terminal velocities of water droplets in drywell atmospheres under severe reactor accident conditions.

Three correlations for the terminal velocities of water droplets are:

- Model A [14]

$$Re_T = \exp\left[-3.126 + 1.01 \ln N_D - 0.01912 (\ln N_D)^2\right]$$

$$\text{for } 2.4 < N_D < 10^7 \; ; \; 0.1 < Re_T < 3550$$

where

Re_T = terminal Reynolds number = $U_T \rho_g D_d / \mu_g$

N_D = Best number = $4\rho_g (\rho_l - \rho_g) g D_d^3 / 3 \mu_g^2$

C_D = drag coefficient = N_D / Re_T^2

- Model B [26]

$$Re_T = \begin{cases} 1.62 E_o^{0.755} M^{-0.25} & \text{for } 0.5 < E_o \le 1.84 \\ 1.83 E_o^{0.555} M^{-0.25} & \text{for } 1.84 < E_o \le 5.0 \\ 2.00 E_o^{0.5} M^{-0.25} & \text{for } E_o > 5.0 \end{cases}$$

and for $E_o < 0.5$,

$$Re_T = N_D / 24 - 1.7569 \times 10^{-4} N_D^2 + 6.9252 \times 10^{-7} N_D^3$$

$$+ -2.3027 \times 10^{-10} N_D^4$$

$$N_D < 73 \text{ and } Re_T < 2.37$$

$$\log_{10} Re_T = -1.7095 + 1.33438 \log_{10} N_D - 0.11591 (\log_{10} N_D)^2$$

$$73 < N_D < 580$$

$$\log_{10} Re_T = -1.81391 + 1.34671 \log_{10} N_D - 0.12427 (\log_{10} N_D)^2$$

$$+ 0.006344(\log_{10} N_d)^3 \qquad N_D > 580$$

where

M = Morton number = $g \mu_g^4 (\rho_l - \rho_g) / \rho_g^2 \sigma_l^3$

E_o = Eotvos number = $g (\rho_l - \rho_g) D_d / \sigma_l$

- Model C [26]

$$Re_T = \begin{cases} 0.766 E_o^{0.66} M^{-0.28} & \text{for } E_o \le 164M^{1/6} \\ 1.37 E_o^{0.55} M^{-0.26} & \text{for } E_o > 164M^{1/6} \end{cases}$$

Model C appears to be appropriate only for droplets much larger than those of interest here. Predictions of the terminal velocities of water drops falling through air at 1 atms and 298 K obtained with Models A, B, and C are compared in Figure 21. Clearly, predictions of terminal velocities obtained with Model C are quite different than predictions obtained with Models A and B. Model C is not used in analyses described below.

The essential result shown in Figure 21 is that larger droplets fall through the atmosphere at higher velocities than smaller droplets. Thus, the larger droplets will sweep out not just aerosols but also the smaller water drops. From the discussion of the mechanisms of aerosol capture by water drops, it is

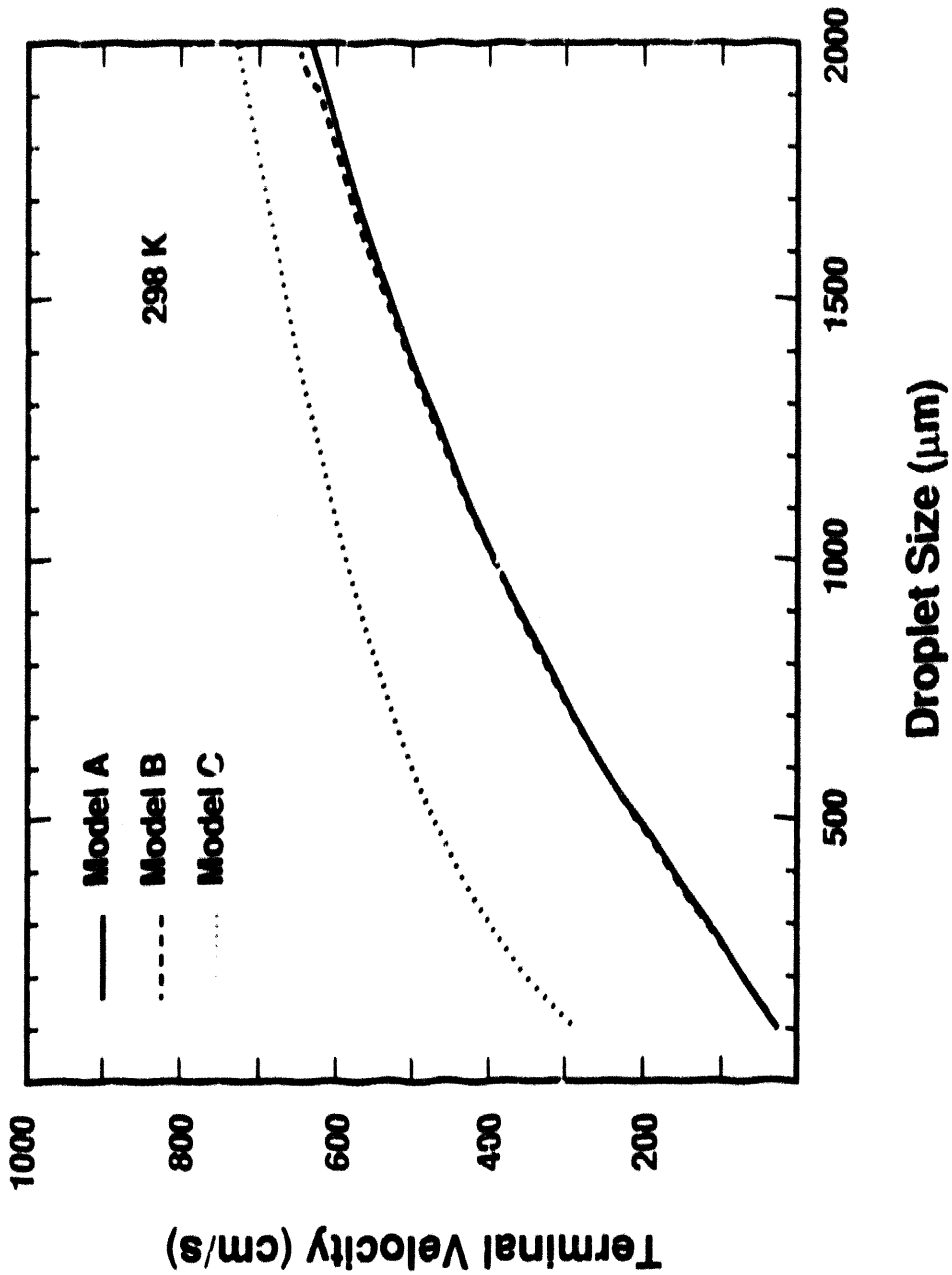

Figure 21 Comparison of the terminal velocities of water droplets in air at 298 K and 1 atm predicted by Models A and B

evident that the small droplets play a very important role in the decontamination of an atmosphere by sprays.

E. Droplet Trajectories

Droplet trajectories in the immediate vicinity of the spray nozzle are complicated. Directional orifices of the Model 1-7G25 and the Model 1-7G3 spray nozzles greatly complicate analysis of these trajectories. Small droplets emerging from these orifices quickly lose their horizontal components of motion. They fall downward through streams of larger droplets that still have significant components of horizontal motion. There are then opportunities for droplets to collide and for small droplets to coalesce. Were each spray nozzle well isolated there would not be a critical need to analyze the trajectories of water droplets and possible collisions of droplets. The droplet size data discussed above were obtained for the drops about 3 meters below the nozzle where all drops had reached steady, downward motion. The drop size data reflect collisions and the loss of small droplets from the spray distribution. But, nozzles are not isolated. There is a deliberate effort made in the spray systems to overlap the spray patterns from adjacent nozzles to achieve complete coverage of the drywell annulus cross section. Overlap creates additional opportunities for droplet-droplet collisions and the loss of small droplets. Collisions among droplets from different spray nozzles are not reflected in the droplet size data cited above. It would be expected that the contributions of small droplets to the spray are certainly no larger than is indicated by the data obtained for the isolated nozzle. The matter is, however, not entirely obvious. As discussed below, particularly energetic collisions of droplets possible near the nozzles will not result in coalescence of the droplets. The drops may bounce or even splatter into smaller droplets.

A detailed analysis of droplet trajectories and the possibilities of droplet collisions is not attempted here. There do not appear to be data needed for such an analysis. The analysis would be complicated by the coupling of atmospheric and liquid motions near the nozzle where the volume fraction of droplets is high. Instead, analyses of aerosol capture are restricted to the region of droplet motion where horizontal movement of the drops at least on some suitable time average basis has ceased. Certainly, this is "conservative" in the sense that aerosol trapping does occur in the region where droplets have horizontal motion. Some compensation for this conservatism can be achieved by considering the fall distance of the droplets to be uncertain by the length of the curvilinear arc they traverse when they have horizontal components of motion. The treatment adopted here is non-conservative in that the initial concentrations of small droplets may be too high. Some compensation for this is achieved by recognizing that the droplet size distributions are uncertain, especially with regard to the fraction of fine droplets.

F. Droplet Agglomeration

Because of drag, there is relative motion among droplets of different sizes falling through the drywell atmosphere. Large droplets falling faster than small droplets can sweep out the small droplets. Consider N_0 droplets with a distribution of sizes such that initially there are $f(i)N_0$ droplets with diameters between $D_d(i)$ and $D_d(i + 1)$. For calculational purposes, it is convenient to assume that all droplets in the i^{th} size class, that is droplets with diameters between $D_d(i)$ and $D_d(i + 1)$, have the same diameter. As the droplets fall and droplet-droplet collisions occur a real distribution of sizes will develop within a size class. Assume the aerodynamic properties of a size class i are well represented by a droplet with radius R(i). In general, the volumetric properties of the i^{th} size class will not be well represented by this droplet. Let the volumetric properties of the size class be represented by a droplet

of radius S(i). As droplets fall and strike or are struck by other droplets these representative droplet radii change.

Since all horizontal motions have been postulated to have ceased, the drywell can be treated as one dimensional. Mass balance requires that at any horizontal plane in the drywell:

$$\sum_{i=1}^{N} n(i, x)\ V(i)\ \frac{4}{3}\ \pi\ S(i)^3 = Q$$

where

$n(i, x)$ = number of concentration of droplets of size class i at a position x below the spray nozzle

$V(i)$ = terminal velocity of a droplet of radius R(i)

$S(i)$ = volume characteristic radius of droplets in size class i

Q = volume flux of water into the drywell produced by sprays

N = number of size classes

Consider a subvolume of the drywell defined by planes at x and x + dx. A number balance of droplets of size class j in this region is:

Number of j class droplets that enter the volume in time dt	-	Number of j class droplets that leave the volume in time dt	=	number of j class droplets removed by agglomeration in time dt in the volume	-	number of j class droplets created by agglomeration in time dt in the volume

or

$$[n(j,x) - n(j,x + dx)]\ V(j)\ A\ dt = \Delta N(j) - \psi(j)$$

where

$\Delta N(j)$ = number of j class droplets removed by agglomeration in the volume in time dt

$\psi(j)$ = number of j class droplets created by agglomeration in the volume in time dt

A = cross-sectional area of drywell that is sprayed

A single droplet of size class i such that R(i) > R(j), falling a distance dx, will encounter

$$\Delta n(i,j) = \pi(R(i) + R(j))^2 \, n(j,x) \, \frac{[V(i) - V(j)]}{V(i)} \, dx$$

droplets of size class j. During the period dt, the number of i class droplets that enter the volume is given by:

$$n(i,x) \; V(i) \; A \; dt$$

If the efficiency with which a collision of i and j class droplets results in agglomeration is $\epsilon(i, j)$, then the number of j class droplets lost by sweepout by larger i class droplets is:

$$\Delta N(i > j) = \sum_{i=j+1}^{N} \epsilon(i,j) \; \pi \, [R(i) + R(j)]^2 \; n(j,x) \; n(i,x) \; [V(i) - V(j)] \; A \; dt \; dx$$

By analogous arguments the number j class droplets lost by collisions with smaller droplets is:

$$\Delta N(j > k) = \sum_{k=1}^{j-1} \epsilon'(j,k) \; \pi \, [R(j) + R(k)]^2 \; n(j,x) \; n(k,x) \; [V(j) - V(k)] \; A \; dt \; dx$$

where $\epsilon'(j, k)$ includes an additional term that indicates whether the agglomeration of an i class droplet and a k-class droplet creates a droplet that is outside the size range of the j class.

Were all the droplets within a size class to have exactly the same diameter, then, under the idealized assumptions made here, there would be no collisions of droplets from the same size class. Because droplets within a size class are not all the same size, and because rather large size ranges are used to define a class, there can be collisions of droplets within the same size class. Coalescence of two droplets within a size class may yield a droplet with a diameter outside the boundaries of the size class. Such a collision and coalescence reduces the population of the size class by two. On the other hand, collision and coalescence of two droplets within a size class may yield a slightly larger droplet whose diameter leaves it within the size class. The population of the size class is only reduced by one.

Considering the limits for a size class, the expression for the loss of j-class droplets by collision with other j-class droplets can be constructed by analogy with expressions for collisions of droplets from different size classes. Recognizing that a collision can remove two droplets from the size class, rather than just one droplet as in other terms of the equation, yields:

Attenuation

$$\Delta N(j = j) = \epsilon''(j, j)\ \frac{\pi}{2}\left[D_d(j + 1) + D_d(j)\right]^2\ n(j,x)^2\ \Delta V(j)\ A\ dx\ dt$$

where

$$\Delta V = V(D_d(j + 1)) - V(D_d(j))$$

$$V(D_d(j)) = \text{terminal velocity of a droplet of diameter } D_d(j)$$

The efficiency term, $\epsilon''(j, j)$, includes an expression for the probability that a collision results in coalescence and a term that indicates if the droplet produced by coalescence is outside the size limits for the j-size class.

The total number of j-class droplets lost by collisions in the spatial interval from x to x + dx is:

$$\Delta N(j) = \Delta N(i > j) + \Delta N(j > k) + \Delta N(j, j)$$

Formation of j-class droplet by collisions of droplets in size classes k and ℓ such that $j > k > \ell$ can be analyzed in a similar fashion to yield:

$$\psi(j) = \sum_{k=2}^{j-1}\sum_{\ell=1}^{k-1} \epsilon'(k, \ell)\pi\left[R(k) + R(\ell)\right]^2 n(k,x)\ n(\ell,x)\left[V(k) - V(\ell)\right]\ A\ dt\ dx$$

$$+ \sum_{k=1}^{j-1} \epsilon'(k, k)\ \frac{\pi}{4}\left[D_d(k + 1) + D_d(k)\right]^2\ n(k,x)^2\ \Delta V(k)\ A\ dt\ dx$$

Then, from a number balance on droplets of size class j:

$$\frac{-dn(j,x)}{dt} = \sum_{i=j+1}^{N} \epsilon(i,j)\ \pi\ [R(i) + R(j)]^2\ n(j,x)\ n(i,x)\ \frac{[V(i) - V(j)]}{V(j)}$$

$$+ \sum_{k=1}^{j-1} \epsilon'(j,k)\ \pi\ [R(j) + R(k)]^2\ n(k,x)\ n(j,x)\ \frac{[V(j) - V(k)]}{V(j)}$$

$$+ \epsilon''(j,j)\ \frac{\pi}{2}\ [D_d(j+1) + D_d(j)]^2\ n(j,x)^2\ \frac{\Delta V(j)}{V(j)}$$

$$- \sum_{k=2}^{j-1} \sum_{\ell=1}^{k-1} \epsilon'(k,\ell)\ \pi\ [R(k) + R(\ell)]^2\ n(\ell,x)\ n(k,x)\ \frac{[V(k) - V(\ell)]}{V(j)}$$

$$- \sum_{k=1}^{j-1} \epsilon'(k,k)\ \frac{\pi}{4}\ [D_d(k+1) + D_d(k)]^2\ n(k,x)^2\ \frac{\Delta V(k)}{V(j)}$$

Differential equations of this type for j = 1 to N were solved by an explicit, Eulerian method to obtain the steady-state spatial distribution of droplet sizes. Term-by-term examinations were necessary to account for the changes in the water volume and droplet cross-sectional area within each size class. Values of R(j) and S(j) for each size class were adjusted at the end of each spatial step to reflect these changes in the population of the size class. Mass conservation was enforced by adjusting N_0 such that:

$$\frac{N_0 \sum_{i=1}^{N} n(i,x)\ V(i)\ \frac{4}{3}\pi\ S(i)^3}{\Omega} = Q$$

where

$$\Omega = \sum_{i=1}^{N} n(i,x)$$

G. Droplet-Droplet Interaction Efficiency

Collision of water droplets, even at low, terminal, velocities, does not ensure that the droplets will coalesce. This is especially true for droplet-droplet collisions that are not "head-on" [73-78]. A commonly cited expression for the efficiency of collisions at terminal velocities to result in coalescence is [73]:

$$\epsilon(i,\ j) = \frac{R(i)^2}{[R(i) + R(j)]^2} \qquad \text{for } R(i) > R(j)$$

The minimum efficiency according to this description is 0.25. Experimental evidence indicates that lower efficiencies can occur [74]. Collision efficiencies calculated based on various theoretical arguments for a 500 μm droplet are shown in Figure 22. As the small droplet involved in the collisions is increased in size, the above expression becomes an upperbound for the theoretically calculated efficiencies. An approximate lower bound for these efficiencies is taken to be:

$$\epsilon(i, j) = \begin{cases} 1 - 8R(j) / R(i) & \text{for } R(j) / R(i) < 0.125 \\ 0 & \text{otherwise} \end{cases}$$

H. Droplet-Structure Interactions

The drywells of Mark I boiling water reactors are notorious for their congestion. An obvious issue, then, in predicting the performance of drywell sprays is the effectiveness of droplets when they hit structures and equipment within the drywell. Droplets can be imagined to bounce off structures and continue to be effective as agents for cleansing the drywell atmosphere of aerosols. Droplets might coalesce with liquid films on surfaces and thereby be removed from the drywell atmosphere. Droplets may drip off surfaces, and droplets may splatter when they strike surfaces. Baker et al. [79] have reviewed the literature concerning the possible behaviors of droplets impacting surfaces. They conclude that regimes of behavior can be defined based on the droplet Weber number, We:

$$We = D_d \rho_l U_T^2 / \sigma_l$$

At Weber numbers of 5 and less, droplets striking a surface bounce [80]. The recoiled droplet retains only about 6 percent of its initial kinetic energy [81]. At Weber numbers between about 5 and about 65 water droplets spread over surfaces they impact or coalesce with a pre-existing water film. At higher Weber numbers the droplets that hit a wetted surface begin to splash [81-83]. The amount of material splashed back into the atmosphere increases with Weber number. About 50 percent of the incident water mass for droplets with median diameters of 1000 to 500 μm is splashed at a Weber number of about 1500. At a Weber number of about 3000, essentially 100 percent of the incident water mass is splashed back into the atmosphere.

Based on these correlations in terms of the Weber number, larger drops in the spray distribution would be expected to coalesce with water films on structure surfaces. Droplets smaller than about 400 μm could bounce off the surfaces.

As water films collect on a surface, drips will form. Baker et al. [79] predicted that the major droplet formed by dripping from a surface would have a diameter determined by Taylor instability to be:

$$D_d(\text{drip}) = 3 \sqrt{\frac{\sigma}{\rho_l g}}$$

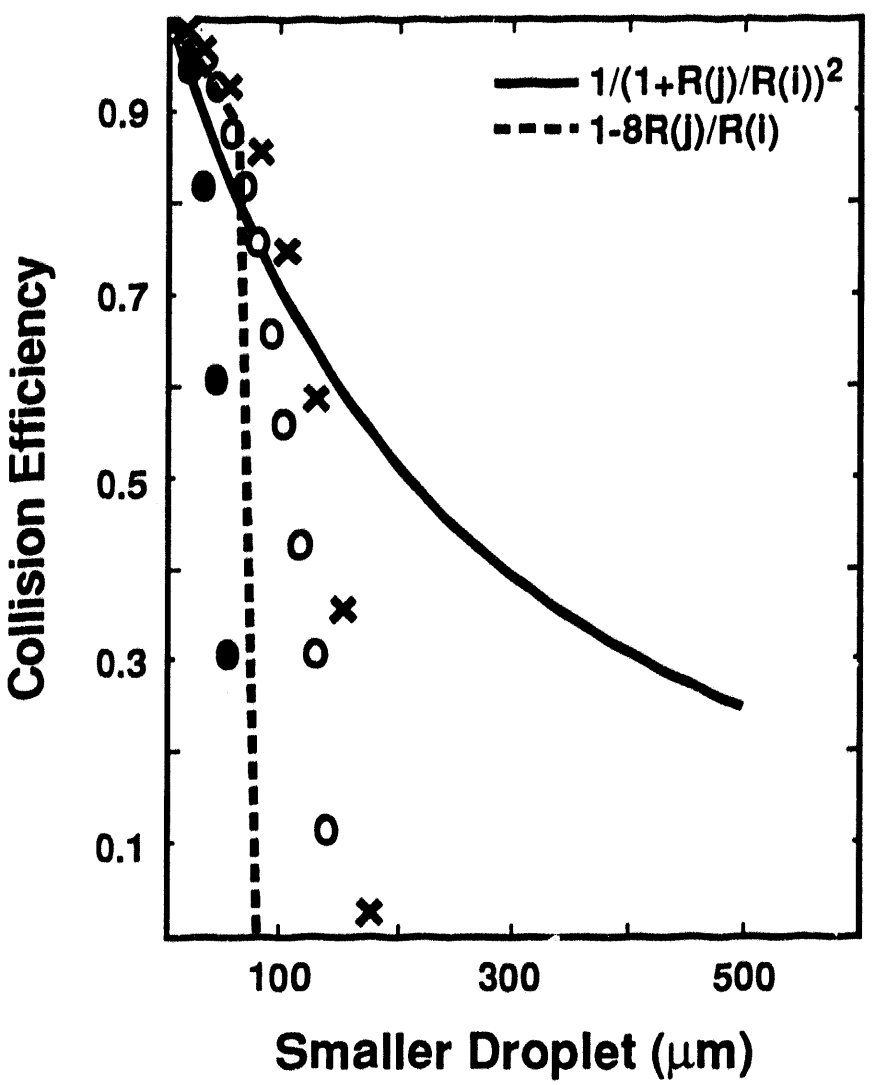

Figure 22 Comparison of the usual collision efficiency (bold line) to theoretical analyses [73] of the collision efficiency of a 500 μm droplet (symbols) and an alternate model (dashed line) described in the text

Such drops (D_d ~ 8500 μm) are huge in comparison to spray drops and would be expected to be largely ineffective at sweeping aerosols from drywell atmosphere. Baker et al. indicated, however, that when the major drop detached from the surface, filaments of liquid ruptured and 4 or 5 smaller droplets were formed. These smaller droplets should be more effective at aerosol removal from the drywell atmosphere than the major drop. On a volumetric basis, however, their contribution to the spray flow is small. At steady state, assuming the smaller droplets were 1000 μm in diameter, these small drops would replace only about 4 percent of the water flow through the containment atmosphere lost by interactions with structures. This, of course, is well within the uncertainty in the estimate of water lost by droplet interactions with surfaces.

It appears at this juncture that water droplets striking surfaces should be considered to be lost from the spray. The uncertainty in this position with respect to small droplets that bounce off surfaces may be adequately reflected in the uncertainty in the size distribution of droplets.

V. Analysis of Source Term Attenuation by Drywell Sprays

A Monte Carlo uncertainty analysis of the performance of drywell sprays is described in this chapter. The approach to uncertainty and its quantification as well as the mathematical methods used in this analysis are entirely similar to those described in Chapter III concerning the analysis of decontamination by an overlying waterpool. Here, however, the rate constant for spray decontamination, λ, rather than the total decontamination is taken as the uncertain quantity. Values of the rate constant are sampled from its uncertainty distribution using a model of the phenomena and processes described above and Monte Carlo sampling of uncertain quantities in the models. The set of sampled values of the rate constant is analyzed using the non-parametric statistics described in Appendix A. This analysis is used to construct an estimate of the uncertainty distribution of λ. Again, because only a finite sample is taken, the estimated uncertainty distribution is known only to a specified confidence level. As in the uncertainty analysis of decontamination by an overlying pool, stochastic uncertainty associated with the finite sample sizes and phenomenological uncertainty are distinguished and separately quantified.

A key step in the uncertainty analysis is the identification of uncertain aspects of the prediction of spray performance obtained with models of phenomena and processes described in the previous chapter. These uncertainties are summarized in Table 7. They are individually discussed in the subsection below. Ranges assigned to each of the uncertain quantities are described and probability density functions for values within the ranges are defined. The model of spray performance and its predictions are described in a subsequent subsection of this chapter.

A. Specific Uncertainties Considered

The principle objective of this section is to discuss uncertain quantities that arise in the description of spray performance in terms of the phenomena and processes presented in Chapter IV. These uncertain quantities are summarized in Table 7. For each of the uncertain quantities a range is specified for values this quantity can adopt. The bases for these ranges are presented, in many cases, in Chapter IV as part of the discussion of phenomena and processes. Only when some elaboration is thought necessary is further justification or description of the ranges presented here. Probability density functions for values of the uncertain quantities within their specified ranges are assigned here following the same set of rules described in Chapter III in connection with the uncertainty analysis of decontamination by an overlying water pool.

1. Uncertainty in Drywell Pressure and Temperature

Pressures and temperatures in the drywell atmosphere can affect the performance of sprays as a mechanism for removal of aerosols. Actions of the sprays also affect pressures and temperatures in the drywell. Certainly, sprays can condense steam from the atmosphere and cool structures within the drywell. How much pressure reduction can be achieved by the sprays depends on the details of the accident in question. The extent to which non-condensible gases such as CO, CO_2 and H_2 are produced during the accident and the temperature of water used to feed the sprays will greatly affect pressures and temperatures in the drywell. Pressure and temperature conditions in the drywell vary widely among the many varieties of severe accidents hypothesized to be possible in a Mark I boiling water reactor. These conditions also vary in the course of a given hypothetical accident sequence.

Table 7 Uncertain quantities considered in the analysis of spray decontamination

Symbol	Description	Range	Probability density function
1a. P(atms)	Pressure in drywell	1.1 - 9	uniform
1b. δ(H)	$[P(CO) + P(CO_2)]/P(H_2)$ in the drywell atmosphere	0.02 - 3	log-uniform
1c. δ(C)	$P(CO)/P(CO_2)$ in the drywell atmosphere	10^{-4} - 1	log-uniform
1d. $P(H_2O)$ (atms)	Steam partial pressure in the drywell atmosphere	0.1 - 7.8	uniform
2. $\delta\mu_g$(%)	Uncertainty in the viscosity of gas mixtures	± 4%	uniform
3. $\delta\sigma_\ell$	Uncertainty in the surface tension of water	+0.1 to -0.1	uniform
4. $\delta\rho_\ell$(g/cm^3)	Uncertainty in the density of water	0 - 0.05	uniform
5a. σ_g	Uncertainty in the geometric standard deviation of the initial water droplet size distribution	1.5 - 1.7	uniform
5b. P_w (atms)	Uncertainty in the water pressure for the spray nozzles	2 - 7	uniform
6. ϵ(1)	Parameter for selection between models for droplet shape	0 - 1	uniform
7. ϵ(2)	Parameter for the determination of the terminal velocities of water droplets	0 - 1	uniform

Table 7 Uncertain quantities considered in the analysis of spray decontamination (Concluded)

Symbol	Description	Range	Probability density function
8. δ(drop)	Parameter for the selection of models for droplet-droplet collision efficiencies	0 - 1	uniform
9. μ(μm)	Mean size of aerosol particles initially present in the dry well atmosphere	0.15 - 0.6	uniform
10. δ(s)	Uncertainty in the aerosol shape factors	-	log normal $\mu = 0.3$ $\sigma_g = 3.04$
11. δ(i)	Parameter to select between potential flow and transition flow models of aerosol collection by impaction and interception	0 - 1	uniform
12. δ	Uncertain parameter in the correlation for the efficiency of aerosol collection by impaction in the potential flow regime	0.25 - 0.75	uniform
13. δ(t)	Parameter for the interpolation between viscous and potential flow correlations	-	log normal $\mu = 60$ $\sigma_g = 4$
14. δ(dif)	Parameter for selection among models for aerosol collection by diffusion	0 - 1	uniform
15. δ(sum)	Parameter for the selection of the method to sum efficiencies	0 - 1	uniform

Sprays

A detailed analysis of the ranges of pressure and temperature in the drywell is beyond the scope of this work. A more bounding analysis is undertaken here.

It is clear that pressures in excess of the containment failure pressure are not of interest. The pressure boundary of a Mark I containment is very strong. Based on "as-designed" analyses, containment failure pressure may be in excess of 10 atmospheres. There may have been, however, some degradation of the strength of the containment structures over the years (for example corrosion of the liner in the sand buffer) and there is the omnipresent difficulty of flaws in construction. Consequently, 9 atmospheres is taken to be the limiting pressure of interest for the analysis of spray performance. The lower bound on the pressure in the drywell is taken to be 1.1 atmospheres.

With sprays in operation, the atmospheric temperature will be such that the partial pressure of water is in equilibrium with liquid water. The temperature can be found from:

$$\ln P(H_2O) = \frac{-7938.16}{T} + 88.912 - 12.1215 \ln T + 0.011079\ T$$

where $P(H_2O)$ is the partial pressure of steam in atmospheres and T is the Kelvin scale temperature. Again, temperatures are not allowed to exceed the temperature of containment failure which is here taken to be 533 K [8] which is significantly above the typical design temperature of 411 K.

The partial pressure of steam in the atmosphere is estimated to be between 0.1 and 7.8 atmospheres. The partial pressure of nitrogen in the atmosphere is taken to always be T/298 atmospheres. The sum of this partial pressure and the partial pressure of steam is constrained to be less than the total pressure.

The remaining source of pressure within the drywell is taken to be the non-condensible gases H_2, CO, and CO_2 produced during core degradation and core debris interactions with concrete.

The relative contributions H_2, CO, and CO_2 make to the atmospheric composition depend on the extent to which hydrogen is produced in the course of core degradation and the type of concrete used in the construction of the drywell floor. Concretes composed of siliceous aggregates may contain as little as 1 weight percent carbon dioxide. Concrete composed of calcareous aggregates (dolomite or limestone) may contain as much as 36 weight percent CO_2. All concretes contain 5 to 8 weight percent water. Then, the gases evolved during core debris-concrete interactions may have the partial pressure ratio

$$\left[P(CO) + P(CO_2)\right] / P(H_2) = \delta(H)$$

as high as 3 in the case of concretes with calcareous aggregate or as low as 0.05 in the case of siliceous aggregates. The same partial pressure ratio in the drywell atmosphere may be even lower if the production of hydrogen during core degradation is included.

Carbon monoxide and hydrogen are produced during core debris interactions with concrete when carbon dioxide and steam from the concrete react with the metallic constituents remaining in the core debris.

The extent to which carbon dioxide is reduced chemically to carbon monoxide (and steam is reduced to hydrogen) depends on the chemistry of the metallic phase of core debris. When zirconium is present in the core debris, chemical reduction of the carbon dioxide is very nearly complete. The ratio of the partial pressure of carbon monoxide to the partial pressure of carbon dioxide in the drywell atmosphere evolves to quite high values:

$$\frac{1}{\delta(C)} = \frac{P(CO)}{P(CO_2)} = 10^4$$

Once the highly electronegative elements in the debris such as zirconium are consumed by chemical reactions, iron becomes the most reactive constituent remaining in the core debris. The ratio of the partial pressure of carbon monoxide to the partial pressure of carbon dioxide in the drywell atmosphere will evolve toward one:

$$\frac{1}{\delta(C)} = \frac{P(CO)}{P(CO_2)} = 1$$

Classic analyses of core degradation in Mark I boiling water reactors, such as those analyses done with the Source Term Code Package [85], often indicate that core debris interacting with concrete initially contains large amounts of metallic core debris--certainly larger amounts of zirconium than in core debris than in core meltdown accidents in pressurized water reactors. The larger amounts of metallic zirconium occur, if for no other reason, because boiling water reactors use significant amounts of zirconium for the channel boxes in the core as well as cladding on the fuel.

Recently, alternative depictions of the core degradation process in boiling water reactors have been hypothesized. Ott and coworkers at the Oak Ridge National Laboratory [86] have suggest that core debris is expelled from the reactor coolant system in a segregated manner. The first molten materials expelled are metals which may be rich in molten zirconium. This expulsion is followed by the slow draining of molten reactor fuel. Like the more classic analysis, this scenario would initially involve very extensive carbon dioxide and steam reduction. Later in time, once all the highly reactive metals were consumed, the reduction of carbon dioxide and steam would be small.

A third hypothesis is that molten metals are not major contributors to the molten core debris expelled into the drywell. The metals including unoxidized cladding on the fuel are assumed to melt early in the accident, drain out of the core region and freeze on structures. Because of the low decay heating rates in these metals, they do not remelt unless they come in contact with molten fuel. Molten fuel is assumed to pour from the core region much as it did at Three Mile Island, penetrate the reactor vessel and interact with the concrete in the drywell floor. Except for a brief period during the first contact of molten fuel with concrete, the extent to which this oxidic core debris can chemically reduce carbon dioxide and steam liberated from the concrete is small throughout the ex-vessel phase of the accident.

At this juncture, it is by no means clear which of the above core degradation scenarios is correct. Consequently, the parameter $\delta(C)$ is taken to be uncertain and to be log-uniformly distributed over the range of 1 to 10^{-4}. Then, the composition of the gas phase can be defined to be:

Sprays

$$P(N_2) = T/298 \text{ atms}$$

$$P(H_2) = \Delta/(1+\delta(H))$$

$$P(CO) = \delta(H)\Delta/(1+\delta(H))\ (1+\delta(c))$$

$$P(CO_2) = \delta(C)\delta(H)\Delta/(1+\delta(H)\ (1+\delta(C))$$

where

Δ = P - T/298 - $P(H_2O)$

P = total pressure

$P(H_2O)$ = partial pressure of steam

$\delta(H)$ = $[P(CO) + P(CO_2)] / P(H_2)$

$\delta(C)$ = $P(CO_2) / P(CO)$

2. Uncertainty in the Viscosity of Gas Mixtures

The viscosity of the ambient gas phase has a pervasive effect of the behavior of water droplets in free fall and the ability of water droplets to trap aerosols. The gas phase in the drywell of a Mark I containment will have a fairly complicated composition during the course of a severe accident. Initially, the drywell is inserted with nitrogen (<5 percent oxygen). As the severe accident begins, the steam concentration in the atmosphere will increase. When core debris is expelled into the drywell, gases, products of concrete decomposition (H_2O and CO_2) and the products of reaction of these gases with core debris (H_2 and CO, respectively), will be added to the atmosphere. Hot steel in the atmosphere can catalyze reactions of hydrogen and carbon monoxide to form hydrocarbons such as methane, ethane, ethylene and acetylene. It is likely, however, that hydrocarbons will not reach concentrations high-enough to affect significantly the viscosity of the gas phase. Here, the gas phase in the drywell is taken to be a mixture of N_2, H_2O, CO_2, H_2, and H_2O. The viscosity of this gas mixture is calculated from the Herning-Zipperer formula [53]:

$$\mu_g = \frac{\sum_i \left(\frac{P(i)}{P}\right) \mu_g(i) \sqrt{Mw(i)}}{\sum_i \left(\frac{P(i)}{P}\right) \sqrt{Mw(i)}}$$

where the summation are over the major constituents of the gas phase and

$P(i)$ = partial pressure of the i^{th} gas phase constituent,

$\mu_g(i)$ = temperature-dependent viscosity of the i^{th} gas phase constituent when pure, and

$Mw(i)$ = molecular weight of the i^{th} gas phase constituent.

The viscosities of pure gaseous species used in connection with the Herning-Zipperer formula are:

$$\mu_g(N_2) = 11.674 \times 10^{-6}\, T^{0.522602}/(1 + 87.143/T) \text{ Poise}$$

$$\mu_g(H_2O) = 0.950 \times 10^{-6}\, T^{0.892912}/(1 + 207.219/T) \text{ Poise}$$

$$\mu_g(H_2) = 1.5765 \times 10^{-6}\, T^{0.705712}/(1 - 3.378/T) \text{ Poise}$$

$$\mu_g(CO_2) = 15.957 \times 10^{-6}\, T^{0.457212}/(1 + 246.744/T) \text{ Poise}$$

$$\mu_g(CO) = 14.151 \times 10^{-6}\, T^{0.502012}/(1 + 117.178/T) \text{ Poise}$$

The Herning-Zipperer formula has been shown to predict within about 2 percent the viscosities of H_2-CO gas mixtures at 298 K [25]. It has been shown to predict within about 4 percent the viscosities of air-steam mixtures [18]. For these two cases, the predictions of the Herning-Zipperer formula were biased toward higher values than were observed, but there is no assurance that this would be the case either for other binary gas mixtures or more complicated mixtures. Here the gas viscosity predictions of the Herning-Zipperer formula are taken to be uncertain to ± 4 percent and to be uniformly distributed over this range

3. Uncertainty in the Surface Tension of Water

The surface tension of pure water is not particularly uncertain. Solutes in the water can change the water's surface tension. Changes in the surface tension of water caused by solutes can affect the distortion of the water droplets and the terminal velocities of the droplets. Sprays may contain solutes such as sodium hydroxide and boric acid deliberately added to affect iodine chemistry in the containment. When sprays operate in the recirculation model, the spray water will accumulate both dissolved and suspended material.

As discussed above in Chapter II, dissolved species may increase or decrease the surface tension of water (see Figure 10, above). For solute concentrations likely to develop in severe accidents there ought not be more than a 10 percent increase or decrease in the surface tension caused by solutes. The surface tension of water used in the sprays is then taken to be

$$\sigma_\ell = \sigma(w)(1 + \delta\sigma_\ell)$$

where

σ_ℓ = liquid surface tension

$\sigma(w)$ = temperature-dependent surface tension of pure water (see Table 4)

and $\delta\sigma_\ell$ is an uncertain parameter uniformly distributed over the range of -0.1 to $+0.1$.

4. Uncertainty in the Density of Water

The density of pure water is also not particularly uncertain. Materials dissolved and suspended in the water will affect the liquid density used in the calculations of spray performance. The density of the liquid is taken to be:

$$\rho_\ell = \rho(w)(1 + \delta\rho_\ell)$$

where $\rho(w)$ is the temperature dependent density of pure water and $\delta\rho_\ell$ is an uncertain parameter uniformly distributed over the range of 0 to 0.05.

5. Uncertainty in the Initial Droplet Size

The complexities of spray trajectories near the spray nozzles as well as some overlap of spray patterns from adjacent nozzles forces the introduction of some artificiality in the analysis of spray performance. The scrubbing of the drywell atmosphere is considered to begin only after droplets have traversed an arc and lost all horizontal components of motion. During this travel there is, in reality, opportunity for droplets to contact aerosol particles. There are also opportunities for droplets to coalesce and to distort the size distribution of droplets that emerges from individual nozzles. Even the size distribution of droplets emerging from the nozzles is uncertain. One cannot be absolutely confident in the distributions determined by the freeze-and-sieve technique since particle breaking during the sieving process may lead to over-emphasis of the contributors made by very fine droplets. Furthermore, it was found that solutions containing modest concentrations of boric acid and sodium hydroxide produce different droplet size distributions than does tap water. As spray operation continues during severe reactor accidents, it is quite likely that water drawn into the spray system will become much more heavily contaminated with both solutes and suspended particles than the boric acid-sodium hydroxide solutions used in the tests. It is, of course, unknown if these solutes and suspended particles will cause further changes in the size distribution of droplets produced by individual nozzles.

Under reactor accident conditions, it is by no means obvious that it will be possible to operate the sprays at their design flow rates. Or, it may be that in the heat of the moment that a severe nuclear reactor accident is likely to cause, that drywell sprays may be operated at beyond design flow rates. The spray nozzles here are known to produce droplets with volume mean diameter that vary with the flow rate.

At a given flow rate, it appears that the principle uncertainty in the droplet size distribution is in the contribution to this distribution made by droplets with diameters less than the mean size. The experimentally determined droplet-size distributions only approximately fit log normal distributions. This may be because the data are not sufficiently abundant or precise. It is convenient here to assume

the distributions do fit a log normal distribution. It is further assumed that the effects of the processes that might affect the droplet size distribution produced by a nozzle are to narrow the spread in the distribution by sweeping out the finer droplets without greatly affecting the volume weighted mean size. Thus, for this work, the volume weighted mean droplet size is taken to be known precisely in terms of its dependence on water flow (see Figures 18 and 19). Fitting the mass fraction data obtained by freeze-and-sieve technique to a log normal distribution yields geometric standard deviation values of 1.60 ± 0.10. This same range of geometric standard deviation values is assumed to apply to the number distribution of the droplets. The mean size of the number distribution is, then, given by:

$$\mu(\text{number}) = \mu(\text{volume}) \exp [-3 \ln^2 \sigma_g]$$

6. Uncertainty in the Droplet Shape

Only the largest water droplets of interest here distort significantly from spherical during fall through the drywell atmosphere. Typically, only droplets larger than 0.1 cm (1000 μm) distort significantly. The Pruppacher and Board model [61] considers distortion only of droplets larger than 0.1 cm. This model is designated model A here. A more complicated model that considers distortion of droplets when the Eotvos number, E_0, is greater than 0.4 is designated model B [18]. An uncertain parameter, $\epsilon(1)$, which is uniformly distributed over the interval 0 to 1 is used to select between these models. Model A from Pruppacher and Board is used when $\epsilon(1)$ is less than 0.5. Model B is used otherwise. Note, that the distorted geometry is involved only in the calculations of impaction and interception of aerosols by water drops and the sweepout of water droplets. The distorted geometry is not used for calculations of the terminal velocity of droplets. Correlations used here to calculate terminal velocities implicitly include the effects of droplet distortion.

7. Uncertainty in the Droplet Terminal Velocities

The limited data base on the terminal velocities of water droplets does not extend into the extreme conditions of temperature, pressure, and atmospheric composition likely to develop in the Mark I drywell under severe accident conditions. Two applicable correlations of droplet terminal velocities were described in the previous chapter. It is assumed that these correlations can be extrapolated to predict terminal velocities in drywell atmospheres. The correlations considered here are:

Correlation A: A best fit to droplet terminal velocities in air.

$$Re_T(A) = \exp\left[-3.126 + 1.013 \ln N_D - 0.01912(\ln N_D)^2\right]$$

where

$$N_D = 4\rho_g(\rho_\ell - \rho_g)g D_d^3/3 \mu_g^3$$

$$Re_T = U_T \rho_g D_d/\mu_g$$

Correlation B: Used by others to extrapolate data [26].

$$Re_T(B) = \begin{cases} 1.62\ E_o^{0.755} M^{-0.25} & \text{for } 0.5 < E_o \le 1.84 \\ 1.83\ E_o^{0.555} M^{-0.25} & \text{for } 1.84 < E_o \le 5.0 \\ 2.0\ E_o^{0.5} M^{-0.25} & \text{for } E_o > 5.0 \end{cases}$$

$$Re_T(B) = N_D/24 - 1.769 \times 10^{-4} N_D^2 + 6.952 \times 10^{-7} N_D^3 - 2.3027 \times 10^{-10} N_D^4$$

$$\text{for } N_D < 73;\ E_o \le 0.5;\ Re_T \le 2.37$$

$$\log_{10} Re_T(B) = -1.7095 + 1.33438 \log_{10} N_D - 0.11591(\log_{10} N_D)^2$$

$$\text{for } 73 < N_D \le 580;\ E_o \le 0.5;\ 2.37 < Re_T(B) \le 12.2$$

$$\log_{10} Re_T(B) = -1.81391 + 1.34671 \log_{10} N_D - 0.12427(\log_{10} N_D)^2 + 0.006344(\log_{10} N_D)^3$$

$$\text{for } N_D > 580;\ E_o \le 0.5;\ 12.2 < Re_T(B) < 6350$$

To account for the uncertainty in the extrapolation of these two correlations, an uncertain parameter $\epsilon(2)$, which is uniformly distributed over the range of 0 to 1, is defined. The terminal Reynolds numbers of droplets in a calculation are found from:

$$Re_T = Re_T(A)\epsilon(2) + [1 - \epsilon(2)]Re_T(B)$$

8. Uncertainty in Droplet-Droplet Interactions

Sweepout of small spray droplets by larger spray droplets is an important phenomenon in the prediction of spray removal of aerosol particles. Small droplets can be more efficient at the capture of aerosol particles than larger droplets. Simple contact between two spray droplets does not necessarily result in the coalescence of the droplets into a larger droplet. Two limiting models for the efficiency with which collisions of water droplets lead to coalescence are described in Chapter IV:

Model A:

$$\epsilon(A) = \frac{R(i)^2}{[R(i) + R(j)]^2} \qquad \text{for } R(j) < R(i)$$

Model B:

$$\epsilon(B) = \begin{cases} 1 - 8R(j)/R(i) & \text{for } R(j)/R(i) < 0.125 \\ 0 & \text{for } R(j)/R(i) \geq 0.125 \end{cases}$$

An uncertain parameter, δ(drop), is defined here to have values uniformly distributed over the range from 0 to 1. This parameter is used to evaluate the efficiency of droplet-droplet collisions from

$$\epsilon = \begin{cases} \epsilon(A) & \text{for } \delta(\text{drop}) < 0.5 \\ \epsilon(B) & \text{for } \delta(\text{drop}) \geq 0.5 \end{cases}$$

9. Uncertainty in the Aerosol Size Distribution

The size distribution of the aerosols suspended in the drywell atmosphere will have an important bearing on the efficiency with which sprays can decontaminate the drywell atmosphere. Shown in Figure 23 are size distributions for aerosols in a Mark I drywell predicted with the Source Term Code Package [85] to arise in various, hypothetical severe reactor accidents. The size distributions are complicated. Mean sizes vary from fractions of a micrometer to nearly 10 μm. The size distributions predicted with the Source Term Code Package [85] do not reflect decontamination by a water pool overlying the core debris. The principle interest in this work is, in fact, to ascertain the additional decontamination that sprays can achieve on aerosols that have been subjected to the action of water pools overlying core debris. As discussed in Chapter III of this document, aerosols that emerge from water pools have narrow size distributions centered around the minimum in the decontamination efficiency size for the water pool. Therefore, size distributions for the aerosols to be considered for the analysis of spray effectiveness, while still uncertain, are quite different than the size distribution of aerosols found in past accident analyses. Based on the analyses of decontamination by a water pool described above, the mean aerosol diameter is taken to be uniformly distributed over the range of 0.15 to 0.65 μm. The geometric standard deviation of the distribution is taken to be closely correlated with the mean size:

$$\sigma_g = 0.860 + 3.6\ \mu$$

where

σ_g = geometric standard deviation

μ = mean of the aerosol size distribution in micrometers.

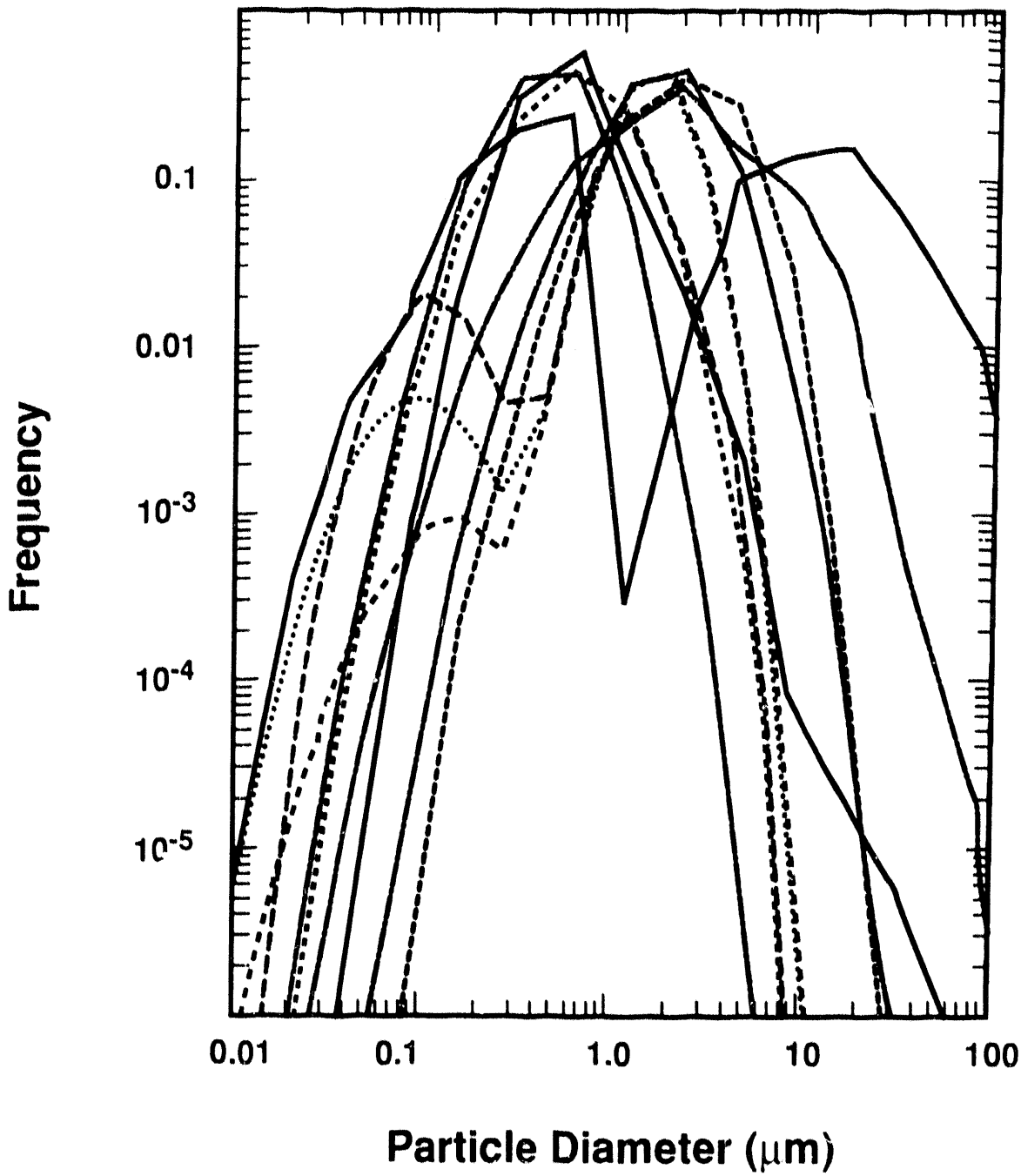

Figure 23 Size distributions of aerosols in the drywell of a Mark I boiling water reactor during various accidents as predicted with the Source Term Code Package [85]

10. Uncertainty in the Aerosol Shape Factors

Models for the efficiency of aerosol capture by falling water droplets discussed in Chapter IV have been derived assuming the aerosol particles to be spheres. It is likely in the water vapor saturated environment that will exist once the sprays are activated that the aerosol particles will not deviate markedly from spherical. Water will condense within the concave interstices of particles composed of agglomerates of smaller particles. Surface tension forces generated by the condensed water will tend to draw particles making up any agglomerate into a spherical shape. The two shape factors of interest here, the dynamic shape factor, χ, and the collision shape factor, γ, will be equal under these conditions [57]:

$$\chi = \gamma$$

But, because the spheridized agglomerates are not uniformly dense, their shape factors need not be equal to 1. Based on experiments with U_3O_8 and Fe_2O_3 aerosols [87], Kress has suggested that under high humidity conditions the shape factors will not exceed 3 [88]. The agglomerates of particles are, in fact, likely to have shape factors that approach the theoretical packaging limit of 1.1.

For this work, the dynamic shape factor and the collision shape factor are taken to be equal. Values are uncertain and given by

$$\chi = \gamma = 1 + \delta(s)$$

where $\delta(s)$ is log-normally distributed with mean equal to 0.3 and a geometric standard deviation of 3.04. This uncertain distribution assures that shape factors are never selected to be less than 1 and that about 80 percent of the distribution lies between 1.1 and 1.9.

11. Uncertainty in Collection Efficiency by Impaction and Interception

It was noted in the description of aerosol capture by impaction and interception that correlations are known only for the viscous and potential flow limits. Some have argued that because of the size disparity between aerosol particles of interest and droplets of interest that correlations for potential flow conditions are adequate for the description of impaction and interception under real flow conditions. Others have argued that some interpolation between correlations for viscous and potential flows is needed to describe impaction and interception under realistic flow conditions.

To account for the uncertainty reflected in the debate over the need to interpolate, a parameter $\delta(i)$ is defined and taken to be uniformly distributed over the range of 0 to 1. Efficiencies of impaction and interception are then found from:

$$\epsilon(\text{imp}) = \begin{cases} \epsilon(\text{imp,pot}) & \text{for } \delta(i) \le 0.5 \\ \epsilon(\text{imp,trans}) & \text{for } \delta(i) > 0.5 \end{cases}$$

$$\epsilon(\text{int}) = \begin{cases} \epsilon(\text{int,pot}) & \text{for } \delta(i) \le 0.5 \\ \epsilon(\text{int,trans}) & \text{for } \delta(i) > 0.5 \end{cases}$$

Note that the selections of the models for impaction and interception are completely correlated. The uncertainty being addressed with the parameter $\delta(i)$ is an uncertainty in the flow field. Once this value of $\delta(i)$ is selected to define the nature of the flow field, the correlations to be used for both impaction and interception are defined.

12. Uncertainty in ϵ(imp,pot)

The correlation given above for impaction efficiency under potential flow conditions involves an uncertain parameter δ:

$$\epsilon(\text{imp,pot}) = \begin{cases} 0 & \text{for Stk} \le 0.08333 \\ \left[\dfrac{\text{Stk}}{\text{Stk} + \delta}\right]^2 & \text{for Stk} \ge 0.2 \\ 8.57\left[\dfrac{\text{Stk}}{\text{Stk} + \delta}\right]^2 (\text{Stk} - 0.08333) & \text{for } 0.08333 < \text{Stk} < 0.2 \end{cases}$$

This parameter, δ, was taken to be uncertain and to have values uniformly distributed over the range of 0.25 and 0.75.

13. Uncertainty in the Collection Efficiencies in the Transition Flow Regime

The Langmuir interpolation [63] between the viscous and potential flow regimes is used in many models of aerosol collection by interception or impaction with water droplets. Fuchs [64] has criticized this interpolation, but has offered no better alternative. Here the Langmuir interpolation is generalized to be:

$$\epsilon(\text{transition}) = \frac{\epsilon(\text{viscous}) + \epsilon(\text{potential})\ \text{Re}/\delta(t)}{1 + \text{Re}/\delta(t)}$$

where

$$\epsilon(\text{transition}) = \epsilon(\text{imp, trans}) \text{ or } \epsilon(\text{int, trans})$$

$$\epsilon(\text{viscous}) = \epsilon(\text{imp, visc}) \text{ or } \epsilon(\text{int, visc})$$

$$\epsilon(\text{potential}) = \epsilon(\text{imp, pot}) \text{ or } \epsilon(\text{int, pot})$$

$$\text{Re} = \text{Reynolds number} = U_T D_d \rho_g / \mu_g$$

In the Langmuir interpolation $\delta(t) = 60$. Here $\delta(t)$ is taken to be uncertain with values log-normally distributed with mean 60 and geometric standard deviation of 4. Thus, the interpolation parameter has an uncertainty distribution centered around the Langmuir value, but has significant densities for somewhat higher and somewhat lower values.

14. Uncertainty is Aerosol Collection by Diffusion

Several possible models of aerosol collection by diffusion of particles across stream lines into water droplets. Diffusion is by far the most uncertain of the aerosol collection processes. Yet, for the particles of interest here, as it will be shown, diffusion is as important a collection mechanism as interception and more important than impaction. To account for the uncertainty in the description of the diffusion mechanism of aerosol capture a parameter, $\delta(\text{dif})$, is defined and taken to have values uniformly distributed over the range of 0 to 1. The efficiency of aerosol capture by diffusion is then taken to be:

$$\epsilon(\text{dif}) = \begin{cases} 3.18\ \text{Pe}^{-2/3} & \text{for } 0 < \delta(\text{dif}) \leq 0.5 \\ \left(\frac{4}{\text{Pe}}\right)\left[2 + \text{Re}_d^{1/2}\ \text{Sc}^{3/8}\right] & \text{for } 0.5 < \delta(\text{dif}) \leq 1.0 \end{cases}$$

Note that the term $0.557\ \text{Re}_d^{1/2}\ \text{Sc}^{3/8}$ is the convective enhancement term in the third of these models. This term is itself uncertain both because of the flow regime and because of wake effects caused by adjacent droplets. Here, these uncertainties were thought to be adequately treated by consideration of other models with empirical coefficients.

15. Uncertainty in the Summation of Efficiencies

Two methods for summing collection efficiencies due to impaction, interception and diffusion are considered here. Selection of the method to be used in a particular calculation is based on the value of the uncertain parameter $\delta(\text{sum})$ which is taken to have values uniformly distributed over the range of 0 to 1. Then,

Sprays

$$\epsilon(\text{total}) = \begin{cases} \epsilon(\text{dif}) + \epsilon(\text{imp}) + \epsilon(\text{int}) & \text{for } 0 < \delta(\text{sum}) \le 0.5 \\ 1 - [1 - \epsilon(\text{dif})][1 - \epsilon(\text{imp})][1 - \epsilon(\text{int})] & \text{for } 0.5 < \delta(\text{sum}) \le 1 \end{cases}$$

16. Other Uncertainties

The formulation of the spray decontamination process adopted here yields results in terms of the fractional removal of aerosols. Consequently, the predictions are not especially sensitive to either the amount of core debris expelled into the drywell or its initial temperature. There is some sensitivity to the composition of the metallic phase of the core debris since this composition affects the composition of the drywell atmosphere as discussed above.

The water flux provided by sprays to the drywell atmosphere has a first order effect on spray performance. The water flux has not been defined. This water flux is treated here as a design variable rather than an uncertain quantity. Results presented here may be of some use in specifying the need for drywell sprays and the minimum useful levels of spray performance.

B. Model Description

The final steps in the uncertainty analysis of predictions of spray removal of aerosols involve the repeated evaluation of spray performance while sampling from the uncertain quantities that affect spray performance. The model used here for the evaluation of spray performance is based on the phenomena described in the previous chapter. Predictions obtained in the repeated evaluations with the model are accumulated and used to formulate estimates of the uncertainty distributions of the spray decontamination coefficient, λ.

Major steps in the calculation of spray performance are:

- select randomly the values of uncertain quantities,
- define the steady-state population and size distribution of water droplets in the drywell atmosphere,
- evaluate the rates at which droplets of various sizes capture particles of various sizes, and
- accumulate the results in terms of an overall rate of aerosol capture.

Uncertain parameters are selected using the same procedure as that involved in the uncertainty analysis of decontamination by a water pool. That is, for each uncertain quantity a random number is selected. The value of the uncertain quantity is found by solution of the equation:

$$\text{rnd } \# = \Pr(x < X_0)$$

where

rnd # = random number

x = value of the uncertain quantity

X_o = selected value of the uncertain quantity

$Pr(x < X_o)$ = cumulative probability that x is less than or equal to X_o.

This equation is readily solved for all the probability density functions used here by a simple Newton-Raphson method. Again, random numbers used here were "shuffled" to avoid any periodicity in the congruent, sequential random number generator [58].

The method by which water will be supplied to the drywell has not been specified. The most likely method is to use the existing drywell sprays. In the case of the Brown's Ferry plant, there are two spray headers located 15.84 meters and 8.53 meters above the drywell floor. For the analyses done here, this was assumed to be the spray configuration. It was further assumed that half the available flux of water was supplied by each header. Thus, in defining the water droplet population density in the drywell atmosphere, there is half the total water flux between elevations 15.84 meters and 8.53 meters. Droplets in free fall between these elevations were allowed to coalesce. At 8.53 meters the remaining half of the water flux was injected. The injected droplets and the droplets from the upper header were allowed to coalesce during free fall to the drywell floor. The water injected at 8.53 meters had the same droplet size distribution as that injected at 15.84 meters.

The water flux that would be employed with the sprays is not defined. Here it was assumed that any of the spray water that hit the vessel or the drywell liner was not able to remove aerosols from the drywell atmosphere. (This water would, still, be able to contribute to the water pool overlying core debris on the drywell floor.) The existing spray system at Brown's Ferry is then able to supply a water flux of about 0.25 cm^3/cm^2-s (0.125 cm^3/cm^2-s from each header). In other plants, such intense water fluxes may not be provided by the unmodified spray system. Further, accident management efforts may restrict the amounts of water supplied to the drywell. Consequently, calculations were done for water fluxes of:

$$Q = 0.25,\ 0.01,\ \text{and } 0.002\ cm^3\ H_2O/cm^2\text{-s}$$

Again, half of the water flux was assumed to come from each header. Results presented below can be fit to simple polynomial expressions to interpolate or extrapolate to other values of the water flux.

The steady-state, spatial, size distributions of droplets in the drywell atmosphere were calculated using an explicit, Eulerian differential equation solver for the droplet growth equations described in Chapter IV. The initial size distribution of droplets was divided into 18 "bins." The size boundaries on these "bins" are listed in Table 8. The volumetric properties of droplets within a given bin were assumed to be represented initially by a droplet whose diameter is given by:

Table 8 Droplet size bins

Bin #	Size range (μm)
1	2000-3000
2	1587-2000
3	1260-1587
4	1000-1260
5	794-1000
6	630-794
7	500-630
8	397-500
9	315-397
10	250-315
11	198-250
12	157-198
13	125-157
14	99-125
15	79-99
16	62-79
17	50-62
18	39-50

$$D_v(i) = \left\{[D(i)^3 + D(i+1)]^3/2\right\}^{1/3}$$

where D(i) and D(i + 1) are the upper and lower limits defining the i^{th} bin. The hydrodynamic and aerosol capture properties of droplets in the i^{th} bin were taken to be represented initially by a droplet whose diameter is given by:

$$D_h(i) = \left\{[D(i)^2 + D(i+1)^2]/2\right\}^{1/2}$$

Values of $D_v(i)$ and $D_h(i)$ were adjusted as the average volume and average surface area of droplets in a bin changed during free fall through the atmosphere.

Calculations of the spatial size distribution of droplets were done at spatial intervals such that the population of a given bin did not change by more than 25 percent. Spatial intervals were, then, much denser near the start of droplet fall than near the drywell floor. Spatial intervals were limited also to be larger than 1 cm and smaller than 20 cm.

Capture of aerosol particles by falling droplets was also done using an explicit, Eulerian solver. The calculations of aerosol capture were done at the same spatial intervals used for the calculation of the droplet size distribution. Droplet size distributions at the end of an interval were assumed to exist over the entire interval. Calculations done, instead, with the droplet size distribution present at the top of an interval yielded very similar results.

For the calculation of aerosol capture, the aerosol size distribution was divided into 20 size bins. The size limits on these bins were selected so that initially each bin contained 5 percent of the aerosol mass. The dynamic properties of aerosols within a size bin were assumed to be well represented by a particle with the mass median diameter of particles in the size bin.

The capture rates were computed for aerosols in each size bin by droplets of each size class. That is, the decontamination coefficient for aerosols in the j^{th} size bin is defined by:

$$-\frac{1}{M(j)}\frac{dM(j)}{dt} = \lambda(j)$$

where M(j) is the mass concentration of aerosol in the j^{th} size bin. The value of $\lambda(j)$ is determined by the capture efficiencies of droplets in all size classes and the fall distance:

$$\lambda(j) = \sum_{i=1}^{18}\sum_{k}\frac{\Delta x(k)}{H}\pi R(i)^2\, n(i,x)\, V(i,x)\, \epsilon(i,j)$$

where

$\Delta x(k)$ = length of the kth spatial interval

$n(i,x)$ = number concentration of droplets in the i^{th} size class at the bottom of the k^{th} spatial interval

$V(i,x)$ = terminal velocity of droplets in the i^{th} size class

$$x = \sum_{j=1}^{k} \Delta x(j)$$

$$H = \text{total fall distance} = 1584 \text{ cm} = \sum_{k} \Delta x(k)$$

Note, that droplets are assumed to be at their terminal velocities at the moment they start free fall through the drywell atmosphere. Aerosols are assumed to be well mixed in the drywell so the terminal velocities of the droplets are not adjusted in the above equation to be velocities relative to the settling velocities of the aerosol particles.

Results of the calculations were then summed to yield an overall aerosol decontamination coefficient:

$$\frac{dM}{dt} = -\lambda(\text{overall})\ M = -\sum_{j=1}^{20} \lambda(j)\ M(j)$$

where

$$M = \sum_{j=1}^{20} M(j).$$

The calculations of the overall spray decontamination coefficient were done for fixed amounts of aerosol in the drywell atmosphere and assuming that any unsprayed volume in the atmosphere was negligible. Neglect of the unsprayed volumes in a Mark I drywell may, at first, be surprising. In the last section of this chapter it will be shown that the decontamination coefficients calculated here are readily corrected to account for unsprayed volumes if, as seems likely, the atmospheres in these volumes mix rapidly with the volumes subjected to the spray.

C. Results of the Uncertainty Analysis

The repeated evaluations of the spray performance model while sampling from the distributions of uncertain quantities yield a sample of the uncertainty distribution for the spray decontamination coefficient, λ. The samples obtained here were analyzed using the distribution-independent order

statistics described in Appendix A. These analyses produced cumulative probability distributions for the spray decontamination coefficients. Because only a finite sample of an uncertainty distribution is available for the analyses, an estimate of the uncertainty distribution can be done only to a prescribed confidence level. Here, as for the analysis of the decontamination by overlying water pools, confidence levels of 95, 90, and 50 percent are used. Thus, percentiles of the cumulative probability distribution are defined by ranges of values. The range can be interpreted for a confidence level of C percent (here C = 95, 90 or 50 percent) that there is a C percent probability that the true value of λ corresponding to the percentile of the distribution in question actually lies somewhere within the indicated range of values. There is a 100-C percent probability that the true value of λ corresponding to the percentile of the distribution lies outside (either above or below) the indicated range.

An example of the tabulated probability distribution for λ is shown in Table 9. This particular example is for a case in which the total water flux is 0.25 cm^3/cm^2-s and the mass fraction of aerosol remaining in the drywell atmosphere is 0.9. Percentile levels from 5 to 95 percent at 5 percent intervals for confidence levels of 95, 90 and 50 percent are listed in the table. Note that the range of values of λ that define a percentile level decreases in width as the level of confidence being demanded decreases. The width of the range at a given confidence level is a measure of the stochastic uncertainty that exists because only a finite sample of the uncertainty distribution was taken. The width of the range can be decreased by taking a larger sample. Unfortunately, the width of the range varies with about the square root of the sample size, so quite a large sample must be taken to dramatically reduce the range of values defining the percentile levels.

Example probability distributions are shown graphically in Figure 24. The sample size chosen here (400 samples) was selected so there was a 95 percent confidence that 99 percent of the range of the uncertainty distribution of λ was sampled. Ranges of values of λ that define the percentile levels of the distribution are shown for 50 and 95 percent confidence. (That is, one can be 50 or 95 percent confident that the true value of λ defining the percentile of the distribution in question lies within the range indicated.) It is evident from the figure that the stochastic uncertainty associated with this sample size is indeed quite small in comparison to the uncertainties in phenomenology, boundary conditions and initial conditions that dictate the range of the distribution for λ. It is also evident from results shown in Figure 24 that the decontamination coefficient does depend on the mass fraction of aerosol remaining in the atmosphere, m_f. That is, λ decreases as decontamination progresses.

Tables showing the cumulative probability distributions for λ in other cases are collected in Appendix C. Summaries of these results are shown in Tables 10-12. This summary indicates the 90 percentile and 10 percentile of the distribution at 90 percent confidence as well as the median or 50 percentile at 50 percent confidence for each calculated case. The rationale for focusing on these particular percentiles of the distributions is the same as the rationale described in connection with the distributions of decontamination factors for overlying water pools. Median values of λ are representative of the spray performance, but analyses using median values are not likely to demand high confidence levels. The 90 and 10 percentile values of the distributions are reasonable upper and lower bounds on the distributions for many purposes. Analyses using such upper and lower bounds are likely to also demand high confidence levels.

Table 9 Example cumulative probability distributions for the spray decontamination coefficient for a water flux of 0.25 cm^3/cm^2-s and the mass fraction of aerosol remaining in the drywell atmosphere equal to 0.9

Aerosol mass fraction remaining	Total water flux (cm/s)	Quantile (%)	Range for λ(total) at a confidence level of 95%	90%	50%	
0.9	0.25	5	3.717 - 5.285	3.904 - 5.145	4.373 - 5.010	MEAN =
		10	5.264 - 7.126	5.372 - 7.050	5.988 - 6.567	= 32.974 hr^{-1}
		15	6.787 - 8.739	6.917 - 8.454	7.326 - 7.902	
		20	7.881 - 10.301	8.182 - 10.118	8.768 - 9.424	
		25	9.288 - 11.486	9.440 - 11.320	10.175 - 11.115	
		30	10.678 - 14.248	11.018 - 14.114	11.310 - 13.071	STD. DEV. =
		35	12.107 - 15.409	12.643 - 15.256	14.024 - 14.724	= 45.312
		40	14.415 - 16.429	14.604 - 16.177	15.154 - 15.577	
		45	15.454 - 18.589	15.532 - 18.510	16.058 - 17.150	
		50	16.512 - 20.130	16.964 - 20.004	18.023 - 19.221	
		55	18.811 - 22.388	19.153 - 22.037	19.778 - 20.924	SAMPLE SIZE =
		60	20.225 - 24.766	20.582 - 24.313	21.655 - 23.344	= 400
		65	22.423 - 28.617	22.850 - 28.110	24.131 - 26.313	
		70	25.067 - 32.834	25.429 - 32.157	27.705 - 30.148	
		75	29.182 - 39.510	30.052 - 37.414	32.048 - 34.866	
		80	34.679 - 49.994	34.982 - 48.893	37.663 - 46.056	
		85	46.180 - 66.140	47.483 - 64.951	49.924 - 54.568	
		90	59.025 - 89.060	63.239 - 82.164	67.231 - 73.509	
		95	87.961 -166.701	93.885 -156.147	104.554 -138.851	

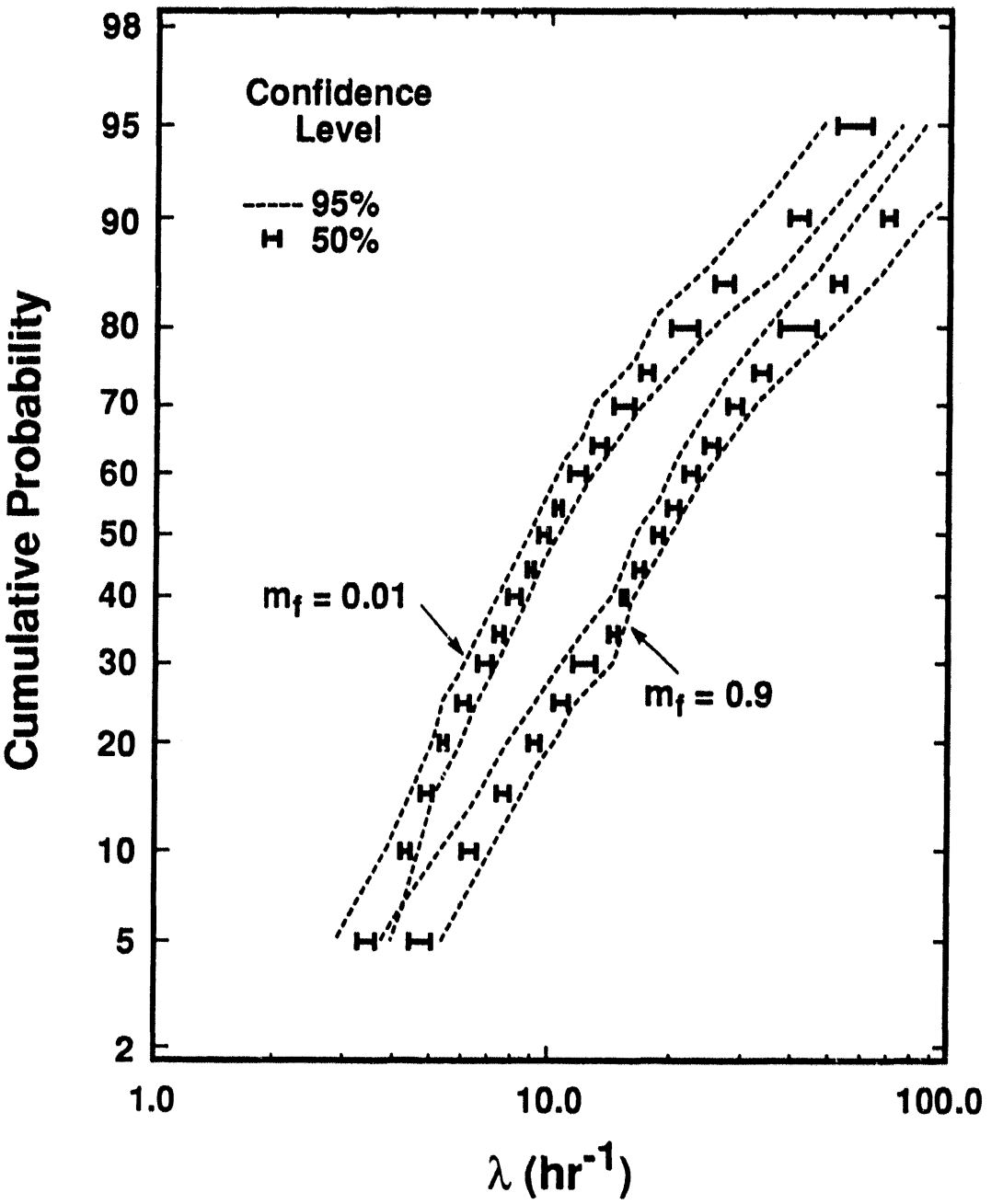

Figure 24 Cumulative probability distribution for λ in the cases Q = 0.25 cm^3/cm^2-s, m_f = 0.9 and m_f = 0.01

Table 10 Summary of uncertainty analyses for Q = 0.25 cm^3/cm^2-s

Total water flux (cm^3/cm^2-s)	Mass fraction of aerosol remaining in atmosphere	90 percentile at 90 percent confidence	10 percentile at 90 percent confidence	50 percentile at 50 percent confidence
0.25	0.9	63.239 - 82.164	5.372 - 7.050	18.023 - 19.221
	0.5	50.098 - 73.841	5.218 - 6.444	14.846 - 15.862
	0.3	45.028 - 66.335	5.047 - 5.984	13.297 - 14.136
	0.1	38.817 - 55.199	4.628 - 5.364	11.030 - 11.690
	0.01	36.621 - 46.118	3.981 - 4.627	9.328 - 9.883
	0.001	31.005 - 44.006	3.654 - 4.175	8.516 - 9.182

Table 11 Summary of uncertainty analyses for Q = 0.01 cm^3/cm^2-s

Total water flux (cm^3/cm^2-s)	Mass fraction of aerosol remaining in atmosphere	90 percentile at 90 percent confidence	10 percentile at 90 percent confidence	50 percentile at 50 percent confidence
0.01	0.9	3.044 - 4.046	0.374 - 0.443	1.020 - 1.108
	0.5	2.579 - 3.284	0.355 - 0.406	0.877 - 0.925
	0.3	2.290 - 2.979	0.332 - 0.379	0.797 - 0.853
	0.1	1.944 - 2.563	0.274 - 0.335	0.689 - 0.742
	0.01	1.733 - 2.227	0.210 - 0.276	0.575 - 0.622
	0.001	1.609 - 2.116	0.196 - 0.239	0.532 - 0.562

Table 12 Summary of uncertainty analyses for Q = 0.002 cm^3/cm^2-s

Total water flux (cm^3/cm^2-s)	Mass fraction of aerosol remaining in atmosphere	90 percentile at 90 percent confidence	10 percentile at 90 percent confidence	50 percentile at 50 percent confidence
0.002	0.9	0.440 - 0.547	0.039 - 0.050	0.119 - 0.131
	0.5	0.362 - 0.462	0.038 - 0.046	0.100 - 0.113
	0.3	0.307 - 0.423	0.036 - 0.042	0.092 - 0.099
	0.1	0.253 - 0.359	0.032 - 0.036	0.082 - 0.088
	0.01	0.223 - 0.310	0.025 - 0.031	0.071 - 0.074
	0.001	0.212 - 0.284	0.023 - 0.029	0.063 - 0.068

These spray decontamination coefficients derived here are not especially large. They may be compared, for instance, to values of 135 hr^{-1} for Q = 0.25 cm^3/cm^2-s, 5.4 hr^{-1} for Q = 0.01 cm^3/cm^2-s and 1.08 hr^{-1} for Q = 0.002 cm^3/cm^2-s derived from recommendations for analyses of spray performance [89]. The values of λ found here are smaller because:

a. the aerosol particles that will pass through a water pool will be of a size that is inefficiently trapped by falling droplets, and

b. the water droplet size is not constant throughout the entire sprayed volume as was assumed when previous recommendations were developed.

Sprays will be far more efficient at scrubbing relatively large aerosol particles released into the containment without passing through a water pool. For further discussions of spray effectiveness at removing more general aerosol particles see Reference 18.

The median values of λ are shown in Figure 25 as functions of the mass fraction of aerosol remaining in the containment atmosphere. The curves in this figure show that the spray decontamination coefficient decreases as decontamination of the atmosphere progresses. This occurs because spray droplets remove aerosol particles in a size-selective manner. That is, the spray not only attenuates the amount of aerosol present in the atmosphere, it also changes the size distribution of the aerosol that is remaining in the atmosphere. As decontamination progresses the remaining aerosol has a size distribution that evolves toward the size of minimum decontamination efficiency. The distribution is progressively narrowed around this size of minimum efficiency. As decontamination progresses, the remaining aerosol becomes less efficiently trapped by the spray droplets.

The variations in λ with the mass fraction of aerosol remaining in the atmosphere, m_f, shown in Figure 25 and listed in Tables 10-12, must be carefully used. There is a strong correlation among values of λ at various values of m_f. That is, sets of vales of uncertain quantities that produce large values of λ at m_f = 0.9 are also likely to produce relatively large values of λ at smaller values of m_f. This correlation among values of λ is readily seen in the plot of samples of $\lambda(m_f = 0.01)$ against values of $\lambda(m_f = 0.9)$ shown in Figure 26.

Some of the correlation can be eliminated by considering $\lambda(m_f = 0.9)$ and $\lambda(m_f)/\lambda(m_f = 0.9)$ as the quantities of interest. The plot of $\lambda(m_f = 0.01)/\lambda(m_f = 0.9)$ against $\lambda(m_f = 0.9)$ shown in Figure 27 reveals that much of the correlation has, indeed, been removed.

Samples of the spray decontamination coefficient were reanalyzed to obtain probability distribution functions for $\lambda(m_f)/\lambda(m_f = 0.9)$ for m_f = 0.5, 0.3, 0.1, 0.01, and 0.001 (these values of m_f correspond to decontamination factors of 2, 3.3, 10, 100, and 1000, respectively). The detailed distributions are collected in Appendix D. The results are summarized in Table 13.

Plots of $\lambda(m_f)/\lambda(m_f = 0.9)$ against m_f for various values of the water flux, Q, are shown in Figure 28. It is evident that the dependence of the spray decontamination ratio on m_f is quite uncertain. The 90 percentile values show very little variation with m_f. The 50 percentile and 10 percentile values show an initially sharp variation as m_f goes from 0.9 to 0.1. Thereafter, the ratio changes little with m_f. This behavior comes about because the initial size distributions for aerosols emerging from water pools into the drywell atmosphere can have mean sizes rather close to the size that is trapped with minimal

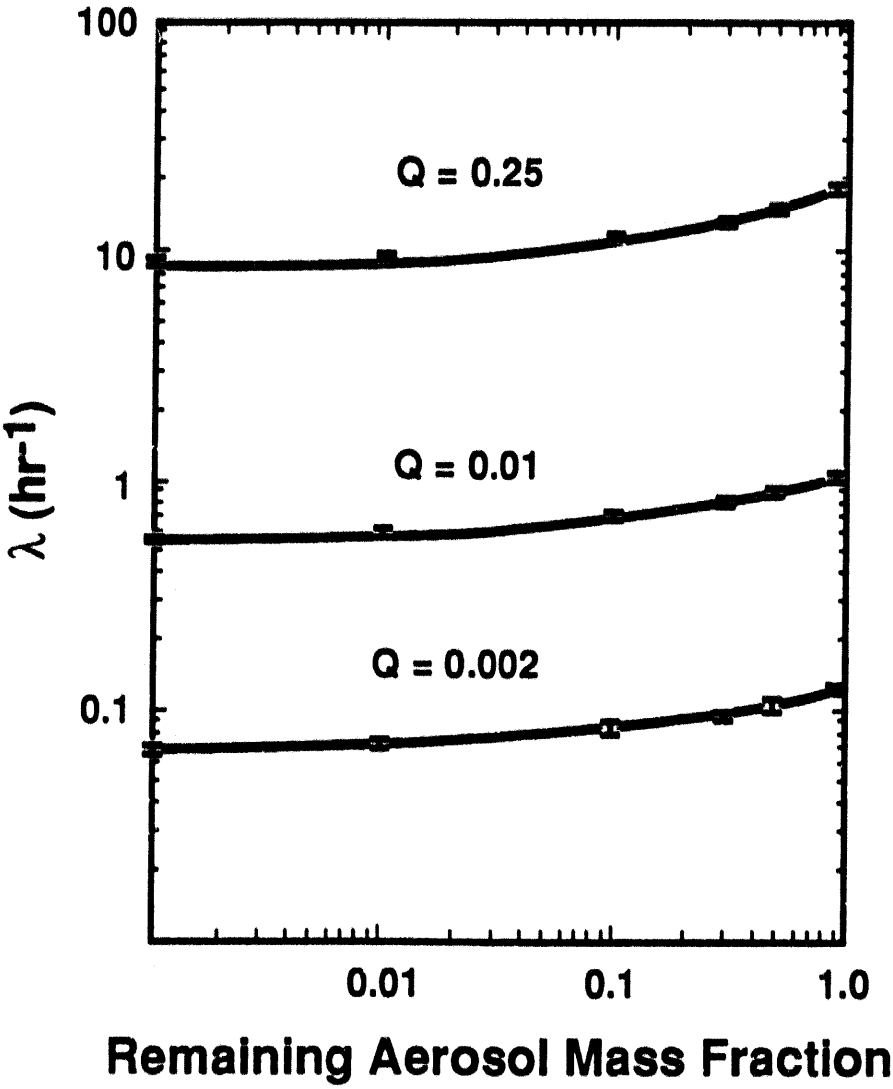

Figure 25 Median values of $\lambda(m_f = 0.9)$ for Q = 0.25, 0.01 and 0.002 cm^3/cm^2-s as functions of m_f

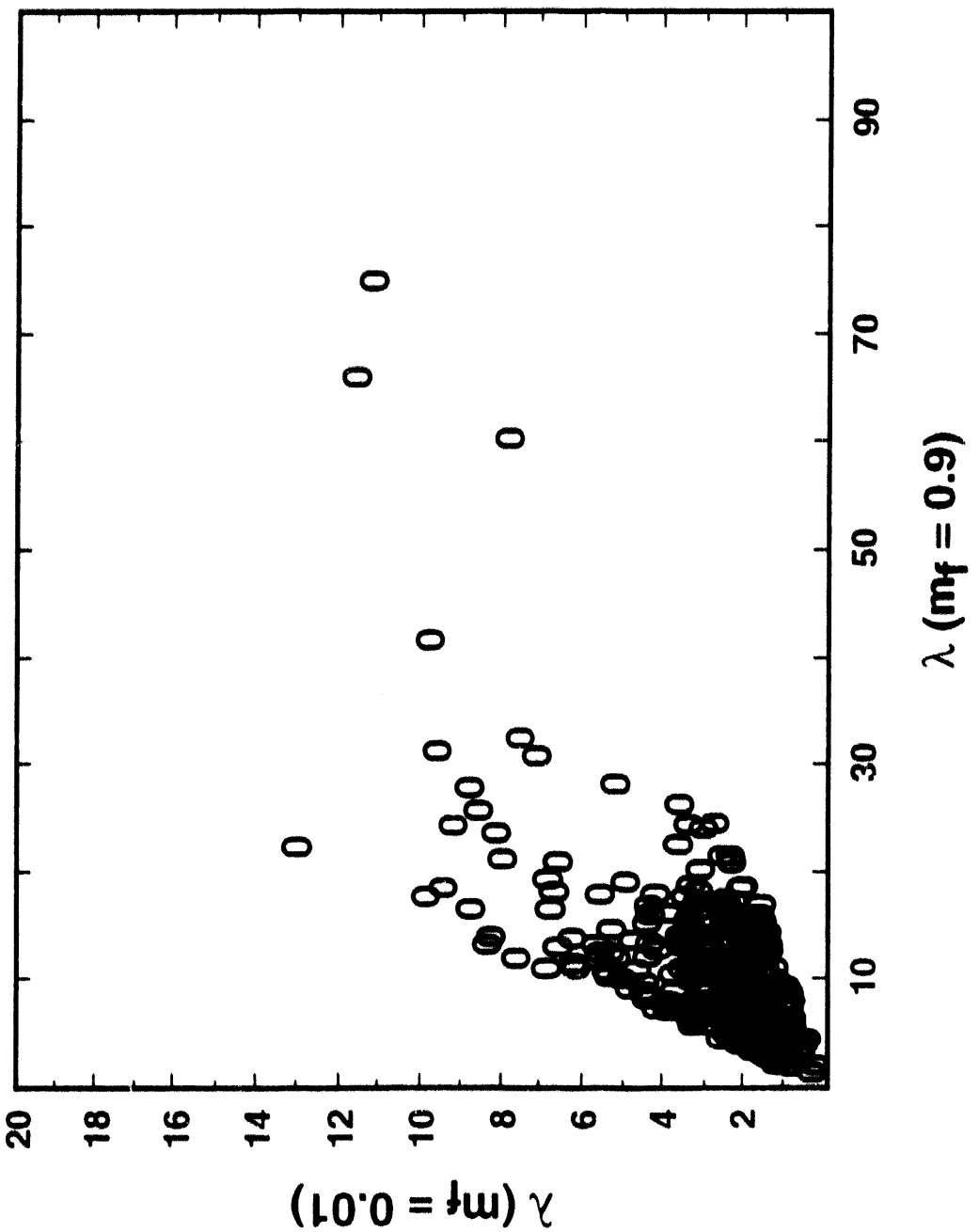

Figure 26 Sampled values of $\lambda(m_f = 0.01)$ plotted against sampled values of $\lambda(m_f = 0.9)$ for Q = 0.25 cm^3/cm^2-s

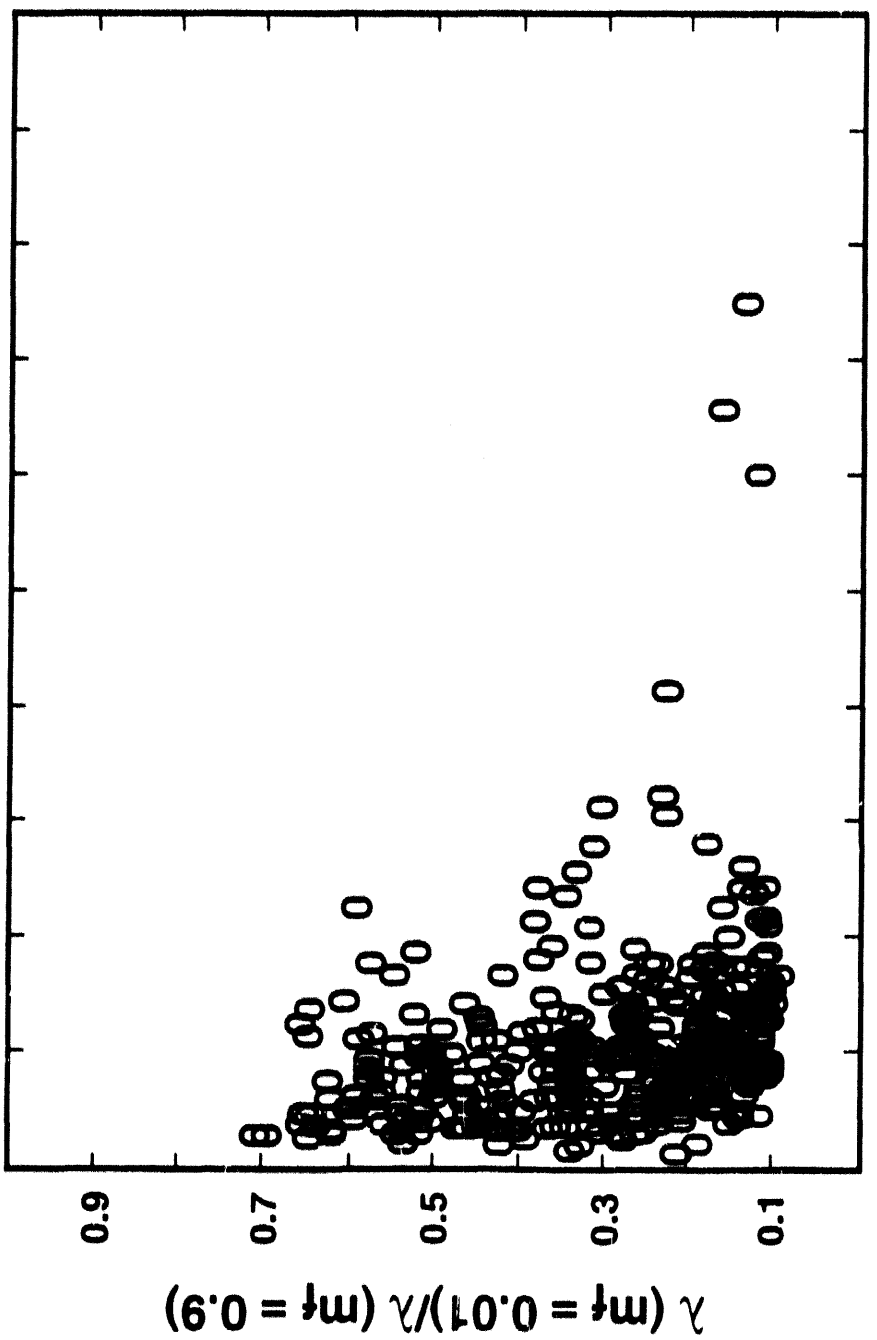

Figure 27 Sampled values of $\lambda(m_f = 0.01)/\lambda(m_f = 0.9)$ plotted against sampled values of $\lambda(m_f = 0.9)$ for Q = 0.25 cm^3/cm^2-s

Table 13 Summary of probability distributions for $\lambda(m_f)/\lambda(m_f = 0.9)$

Total water flux Q	m_f	$\lambda(m_f)/\lambda(m_f = 0.9)$		
		90 percentile at 90 percent confidence	10 percentile at 90 percent confidence	50 percentile at 50 percent confidence
0.25	0.5	0.983 - 0.991	0.715 - 0.737	0.864 - 0.876
	0.3	0.970 - 0.985	0.574 - 0.607	0.787 - 0.799
	0.1	0.949 - 0.975	0.423 - 0.460	0.681 - 0.706
	0.01	0.912 - 0.955	0.305 - 0.333	0.571 - 0.601
	0.001	0.896 - 0.943	0.247 - 0.280	0.518 - 0.548
0.01	0.5	0.986 - 0.994	0.710 - 0.736	0.874 - 0.882
	0.3	0.975 - 0.990	0.574 - 0.600	0.791 - 0.810
	0.1	0.957 - 0.981	0.415 - 0.453	0.691 - 0.703
	0.01	0.932 - 0.967	0.288 - 0.331	0.585 - 0.606
	0.001	0.915 - 0.957	0.242 - 0.283	0.532 - 0.554
0.002	0.5	0.979 - 0.990	0.721 - 0.744	0.884 - 0.892
	0.3	0.966 - 0.981	0.584 - 0.615	0.814 - 0.826
	0.1	0.940 - 0.967	0.434 - 0.465	0.711 - 0.731
	0.01	0.899 - 0.941	0.303 - 0.338	0.609 - 0.638
	0.001	0.880 - 0.923	0.256 - 0.294	0.570 - 0.593

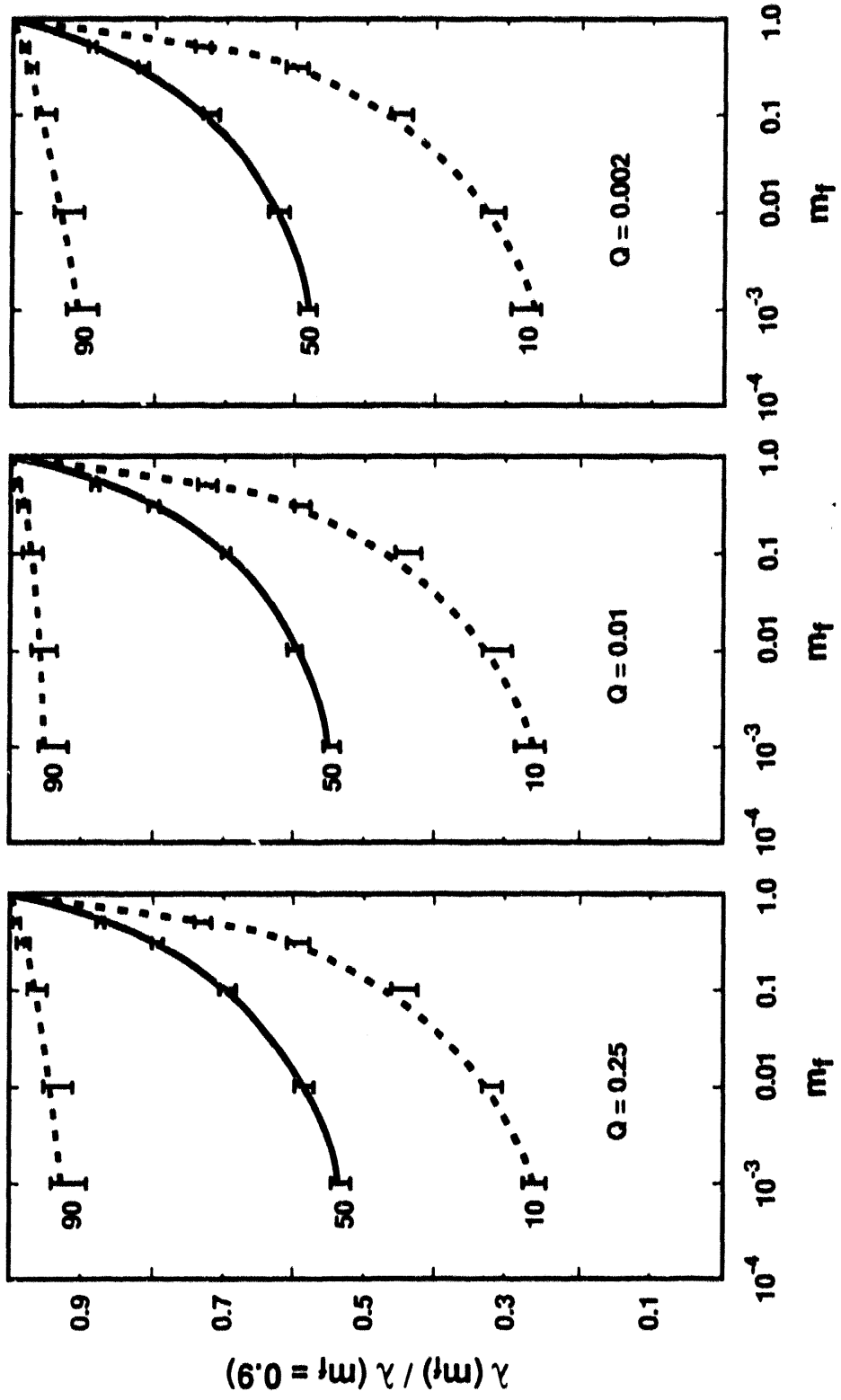

Figure 28 Median values of $\lambda(m_f = 0.9)$ as functions of m_f for Q = 0.25, 0.01, and 0.002 cm^3/cm^2-s. Curves are shown for the 90 and 10 percentiles at 90 percent confidence and for the mean (50 percentile) at 50 percent confidence.

efficiency by spray droplets. Also, relative to aerosols injected into the drywell without passing through the water pool, the aerosols hypothesized here to be in the drywell initially have narrow size distributions. After some small amount of decontamination, an aerosol remaining in the drywell atmosphere is very narrowly distributed around the size of minimum trapping efficiency by the spray. Thereafter, there is only a small variation in the efficiency of aerosol trapping as decontamination progresses.

The values of the ratio $\lambda(m_f)/\lambda(m_f = 0.9)$ may be compared to the recommendation [84] that the decontamination coefficient attributed to sprays be reduced by a factor of 10 once the decontamination factor exceeds 50 ($m_f \leq 0.02$). It is evident from the results shown in Figure 28 that such a sharp reduction in the decontamination coefficient would be quite a conservative estimate of the rate of atmosphere dcontamination. Even at the 10 percentile level, the decontamination coeficient has fallen by only about a factor of 3 from its initial value once the decontamination factor exceeds 50 ($m_f \leq 0.02$).

A plot of $\lambda(m_f = 0.9)$ against the water flux to the drywell atmosphere, Q, is shown in Figure 29. $\lambda(m_f = 0.9)$ is not just linearly dependent on the water flux. As Q increases the rate of water droplet coalescence to form larger water droplets that less efficiently trap aerosols increases more rapidly than the rate of droplet-particle interactions. It is also evident from results shown in this figure that spray decontamination of the small aerosol particles considered here is not very efficient. A principle interest of analyses done here is the rapid decontamination of the drywell atmosphere even if the drywell has been ruptured. At the highest water fluxes considered here, spray decontamination factors are large-enough to provide significant decontamination of the atmosphere over short periods of time (< 15 minutes). At water fluxes less than about 0.08 cm^3/cm^2-s, spray decontamination coefficients become so small that significant additional decontamination of the atmosphere (DF ~ 10) could be achieved only if drywell liner penetration were delayed or the rupture of the drywell were small so the contaminated atmosphere is exposed to the spray for protracted periods.

Median values of $\lambda(m_f)/\lambda(m_f = 0.9)$ are plotted in Figure 30 against the water flux to the drywell atmosphere. This ratio has only a very weak dependence on the magnitude of the water flux to the atmosphere.

D. Effects of Unsprayed Volumes

All of the discussions to this point have assumed implicitly that the entire aerosol-laden gas phase is exposed to the direct actions of spray droplets. This is certainly not the case in the Mark I boiling water reactor. Certainly, the volume within the pedestal support wall is not subjected to the spray. Also, spray headers are not at the top of drywell. In the case of the Brown's Ferry plant, spray headers are located at elevations 15.84 and 8.53 meters above the floor. The top of the drywell is 32.03 m above the floor.

It is likely that there will be very rapid mixing of the unsprayed volumes in the drywell with the volumes that are exposed to the actions of the spray. Displacement of gas by the falling spray as well as temperature differences between sprayed and unsprayed volumes will assure this mixing. If it is assumed that this mixing is rapid in comparison to the rate of decontamination, the spray decontamination coefficients are readily adjusted to account for the unsprayed volumes:

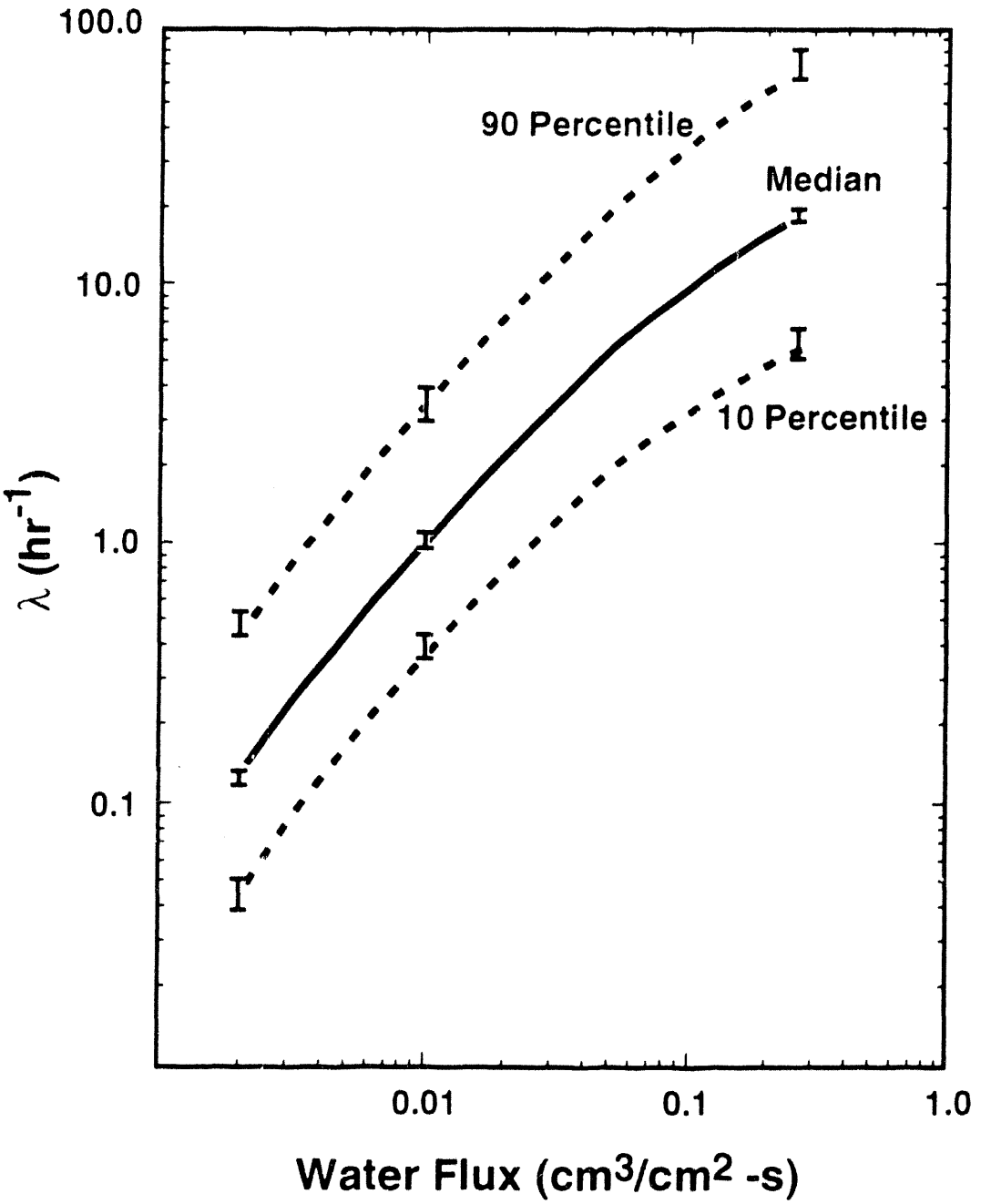

Figure 29 $\lambda(m_f = 0.9)$ as a function of water flux, Q

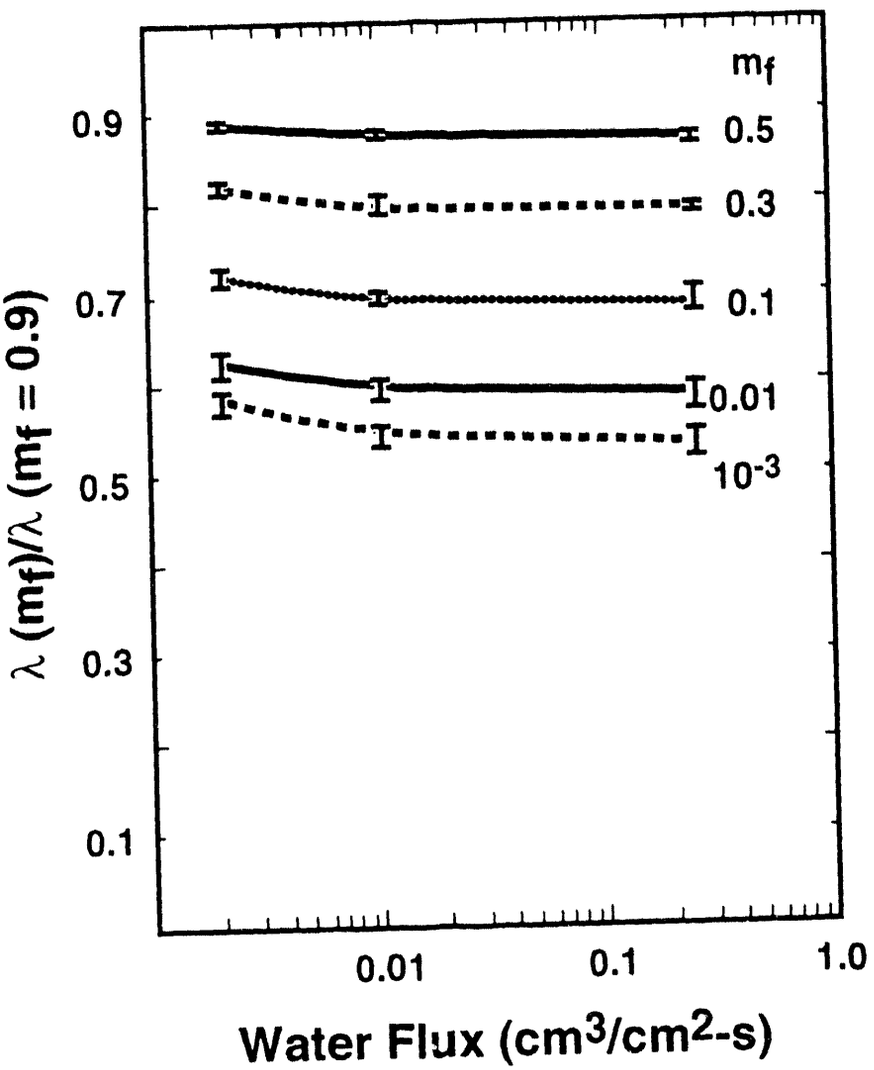

Figure 30 Median values of $\lambda(m_f)/\lambda(m_f = 0.9)$ as functions of water flux, Q, for m_f = 0.5, 0.3, 0.1, 0.01, and 0.001

Sprays

$$\lambda(\text{real}) = \lambda(Q,m_f)/(1 + \alpha)$$

where

$\lambda(\text{real})$ = the apparent decontamination coefficient for the drywell spray including the effects of unsprayed volumes

$\lambda(Q,m_f)$ = decontamination coefficient calculated here for the sprayed volume

α = V(unsprayed)/V(sprayed)

The ratio of sprayed to unsprayed volume is not easily calculated with confidence. For the Brown's Ferry plant the ratio of unsprayed volume to sprayed volume is about 2.6. Other values of this value might be found for other plants. The ratio is large-enough that the quantitative estimates of spray capabilities are affected. Qualitative conclusions that have been drawn above are not greatly affected.

E. Simple Correlation of the Results

The detailed, mechanistic analyses presented above and in the previous chapter provide quantitative predictions of the decontamination of the drywell atmosphere that can be achieved by sprays and the uncertainties that ought to be ascribed to these predictions. From these results, a reader can easily derive a qualitative indication of the effects sprays in the drywell might have on severe accident source terms. More quantitative insight could be obtained from simple correlations of the results in a form suitable for routine calculations. The results obtained above for $\lambda(m_f = 0.9)$ may be correlated with a polynomial expression in the water flux to the drywell atmosphere, Q. The results for $\lambda(m_f)/\lambda(m_f = 0.9)$ may be correlated in terms of Q and the mass fraction of aerosol remaining in the drywell atmosphere, m_f. Such correlations, derived by least-squares analyses, are developed here for the median values at 50 percent confidence, the 90 percentile values at 90 percent confidence, and the 10 percentile values at 90 percent confidence. The correlations are:

- Median (50 Percentile) Values at 50 Percent Confidence

$$\lambda(m_f = 0.9) = Q[51.073 + 5759.2\ Q - 22662\ Q^2]$$

$$\lambda(m_f)/\lambda(m_f = 0.9) = (0.50730 - 0.02055 \log_{10} Q)(1 - z) + z$$

where $z = (m_f/0.9)^{0.491736}$

- 90 Percentile Values at 90 Percent Confidence

$$\lambda(m_f = 0.9) = Q[218.705 + 14133.3\ Q - 55379.6\ Q^2]$$

$$\lambda(m_f)/\lambda(m_f = 0.9) = (0.90531 + 0.00708 \log_{10} Q)(1 - z) + z$$

where $z = (m_f/0.9)^{0.207615}$

- 10 Percentile Values at 10 Percent Confidence

$$\lambda(m_f = 0.9) = Q[17.446 + 2434.05\ Q - 9617.81\ Q^2]$$

$$\lambda(m_f)/\lambda(m_f = 0.9) = (0.27608 - 0.00284 \log_{10} Q)(1 - z) + z$$

where $z = (m_f/0.9)^{0.73410}$

Note that values of the decontamination coefficient derived from correlation should be corrected for the effects of unsprayed volumes in the drywell. If rapid mixing of the atmospheres of the sprayed and unsprayed volumes occurs, the correction is given by:

$$\lambda = \lambda(\text{correlation}) / (1 + \alpha)$$

where

λ = corrected value of the spray decontamination coefficient

λ(correlation) = value of the spray decontamination coefficient derived from any of the above correlations

α = V(unsprayed) / V(sprayed)

V(unsprayed) = volume of the drywell that is not directly affected by the spray

V(sprayed) = volume of the drywell through which spray droplets fall.

These correlations will be utilized in an example accident analyses in Chapter VI of this report.

VI. Accident Analyses

The analyses of decontamination by an overlying water pool and the analyses of the decontamination coefficient of sprays presented above certainly indicate that some substantial source term reduction can be achieved if water is present in the Mark I boiling water drywell during a severe reactor accident. It is useful to have a quantitative indication of the magnitude of source term reduction by applying the results presented above to a specific reactor accident. Recent probablistic risk assessments [2] have shown that the risk dominant accidents in a particular Mark I boiling water reactor are anticipated transients without scram (ATWS) and station blackout accidents in which off-site and on-site AC power fails. The ex-vessel phases of these two classes of hypothetical accidents are rather similar (see for instance Figure 4). Analyses here focus, then, on the ATWS type accident.

The predicted rates of aerosol generation by core debris interactions with concrete during an ATWS accident with no water in the drywell are shown in Figure 4. Aerosol generation is very intense for the first 2 to 3 hours of ex-vessel core debris interactions. At the maximum shown in Figure 4, aerosol generation rates reach nearly 1000 g/s. Once reactive zirconium metal in the core debris has been consumed by chemical reactions, the core debris temperature falls rapidly and the rate of aerosol production drops to 1 to 2 g/s.

Were the aerosols produced by the core debris interactions with concrete unable to settle or deposit in the Mark I drywell, aerosol concentrations shown by the curve marked "no mitigation" in Figure 31 would develop during the accident. Ten hours after the onset of core debris interactions with concrete aerosol, concentrations reach about 457 g/m^3. Most of the particulate materials suspended in the drywell atmosphere are products of concrete vaporization or are constituents of steel. Mixed with these materials can be a substantial amount of radionuclides from the core debris.

Aerosols lofted into the drywell atmosphere will, of course, agglomerate, deposit, and settle within the drywell. Barring some resuspension process,* settled and deposited particles are removed from the inventory of aerosol that could escape into reactor building in the event the drywell integrity is lost by any mechanism (overpressurization, overheating or direct attack by the melt on the drywell liner). Some indication of the magnitude of the effects of settling and deposition on aerosol concentrations is shown in Figure 31 by the curve marked "natural mitigation." Natural mitigation processes reduce the peak aerosol concentration in the drywell from about 460 g/m^3 to about 46 g/m^3. At 10 hours after the start of core debris/concrete interactions, aerosol concentration in the drywell is only 0.75 g/m^3. The safety advantages of delaying drywell failure so that there is time for the natural mitigation processes to operate are apparent from these results.

Even when natural mitigation processes are considered, it is evident that substantial masses of radioactive material may be available for release if the drywell fails. It is of interest, then, to see what additional attenuation of the potential source term might be produced by water in the drywell. Both the effects of a water pool overlying the core debris and the effects of sprays are demonstrated below. For these demonstrations, aerosol concentrations are compared to the concentrations that would be present were

*Aerosols that settle onto the core debris could, presumably, revaporize. There has been no attempt to take this into account in preparing Figure 31.

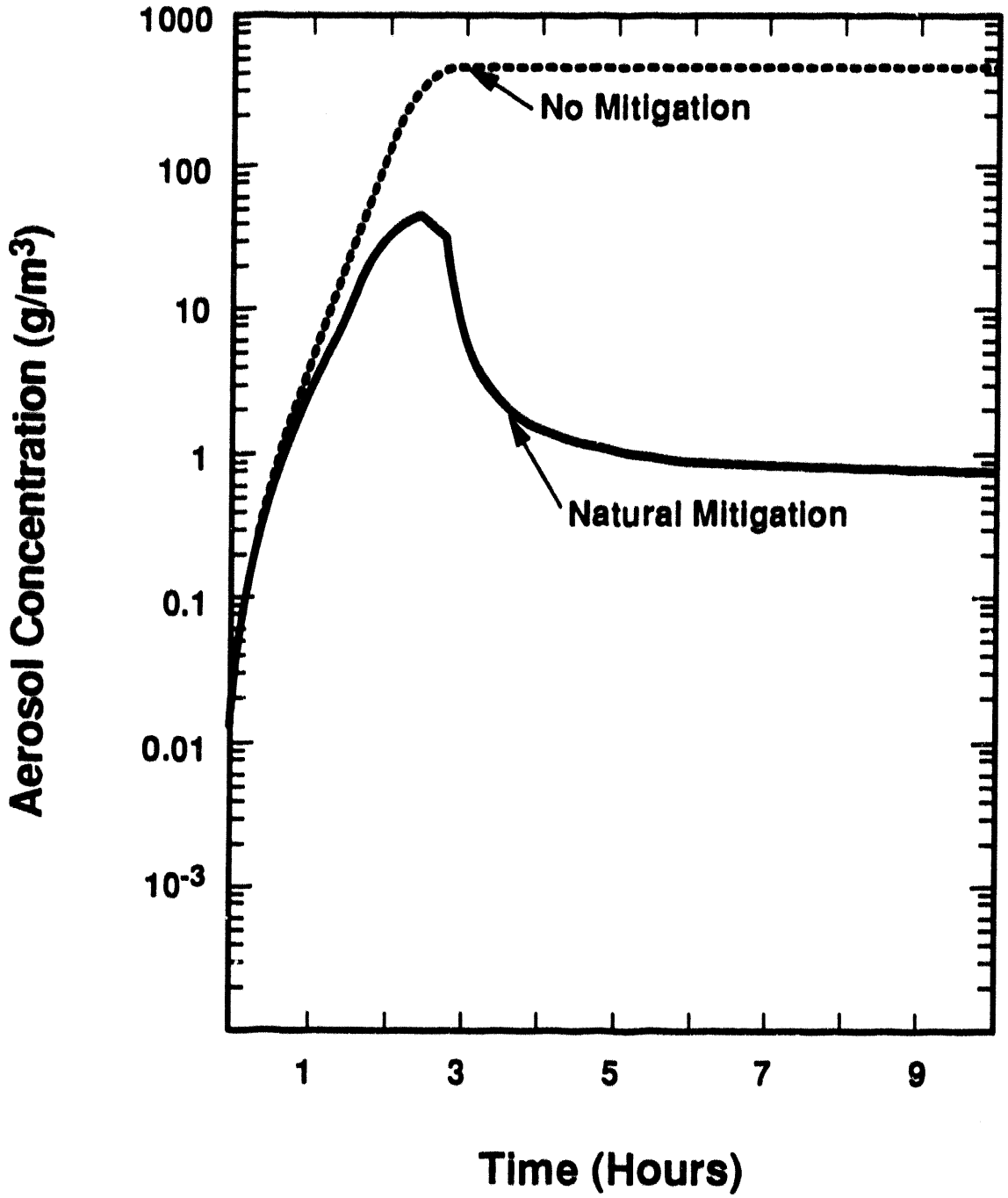

Figure 31 Aerosol concentrations in the drywell during an ATWS accident with no water present. The dashed curve marked "no mitigation" indicates concentrations that would exist if natural processes such as settling and deposition are neglected. The solid curve marked "natural mitigation" was calculated including these natural deposition processes.

there no natural mitigation by settling and deposition of aerosols. This type of comparison makes it more apparent how much aerosol mass is prevented from being available for release irrespective of the time at which a rupture in the drywell occurs.

First, the effect of an overlying water pool on the mass of aerosol available for release is considered. Only the decontamination effects of the water pool are considered here. Any effects an overlying water pool might have on reducing temperatures of the core debris, and consequently reducing the rates of aerosol generation, have been neglected here. The case of a 50 cm deep water pool subcooled by 20°C is shown in Figure 32. The 90 percentile, median and 10 percentile aerosol concentrations are shown in this figure. (These aerosol concentrations correspond, of course, to the 10, 50, and 90 percentile pool decontamination factors, respectively.) The median decontamination factor produced by the 50 cm deep pool is about 180. Even in the very pessimistic case represented by the 90 percentile aerosol concentration, the water pool provides a decontamination factor of about 26. The 10 percentile aerosol concentration corresponds to a decontamination factor produced by the overlying water pool of almost 3000.

Subcooling of the water pool is important in achieving high levels of decontamination. Results are shown in Figure 33 for the case of a 50 cm deep water pool with only 2°C subcooling. The median decontamination factor in this case is only about 16. The 10 and 90 percentile aerosol concentrations correspond to decontamination factors by the water pool of about 83 and about 4.8, respectively.

Increasing the depth of the water pool will, of course, increase the extent of decontamination. The effect is not, however, especially large until depths in excess of about 1 meter are reached. Such water pool depths could be produced in the Mark I drywell only by filling the wetwell with water.

It might be argued that subcooling, even by only 20 degrees, necessary to achieve large decontamination coefficients by water pools might be difficult to maintain early in the ex-vessel phase of an accident when most of the aerosol release occurs. Or, it might be contended that the violence of the early stages of core debris interactions with concrete could disrupt the water pool so that evolved streams of aerosol-laden gas are not efficiently scrubbed. Evidence from tests of combined core debris-concrete-coolant interactions done to date [16, 22, 46, 51, 52] indicate that any violent disruption of the water pool takes place only for a brief period. Extrapolation of these results to reactor accident conditions is, of course, uncertain. Furthermore, recent tests [51, 52] suggest that there can be episodic eruptions of melt into a well-established water pool that might, in extreme cases, result in, at least, localized disruption of the water pool. For these reasons the incremental decontamination of the drywell by sprays is of interest. Spray would, of course, also scrub from the atmosphere aerosols that were not exposed to the overlying water pool.

To illustrate the effects of sprays, it is assumed that a 50 cm deep water pool, subcooled by only 2°C, is maintained over the core debris and that the decontamination efficiency of this pool is at the pessimistic 10 percentile level. Aerosol concentrations in the drywell atmosphere with sprays operating at a water flux of 0.25 cm^3/cm^2-s are shown in Figure 34. The spray was assumed to contact only 28 percent of the containment volume. (Note that the drywell volume during the ex-vessel stage of the accident includes the volume of the reactor coolant system and the reactor vessel). The median aerosol concentration curve shown in this figure has a maximum aerosol concentration of 3.4 g/m^3. This corresponds to an overall decontamination factor of about 134. After 10 hours of core debris interactions with concrete, the aerosol concentration is reduced to about 5.3×10^{-3} g/m^3. The overall

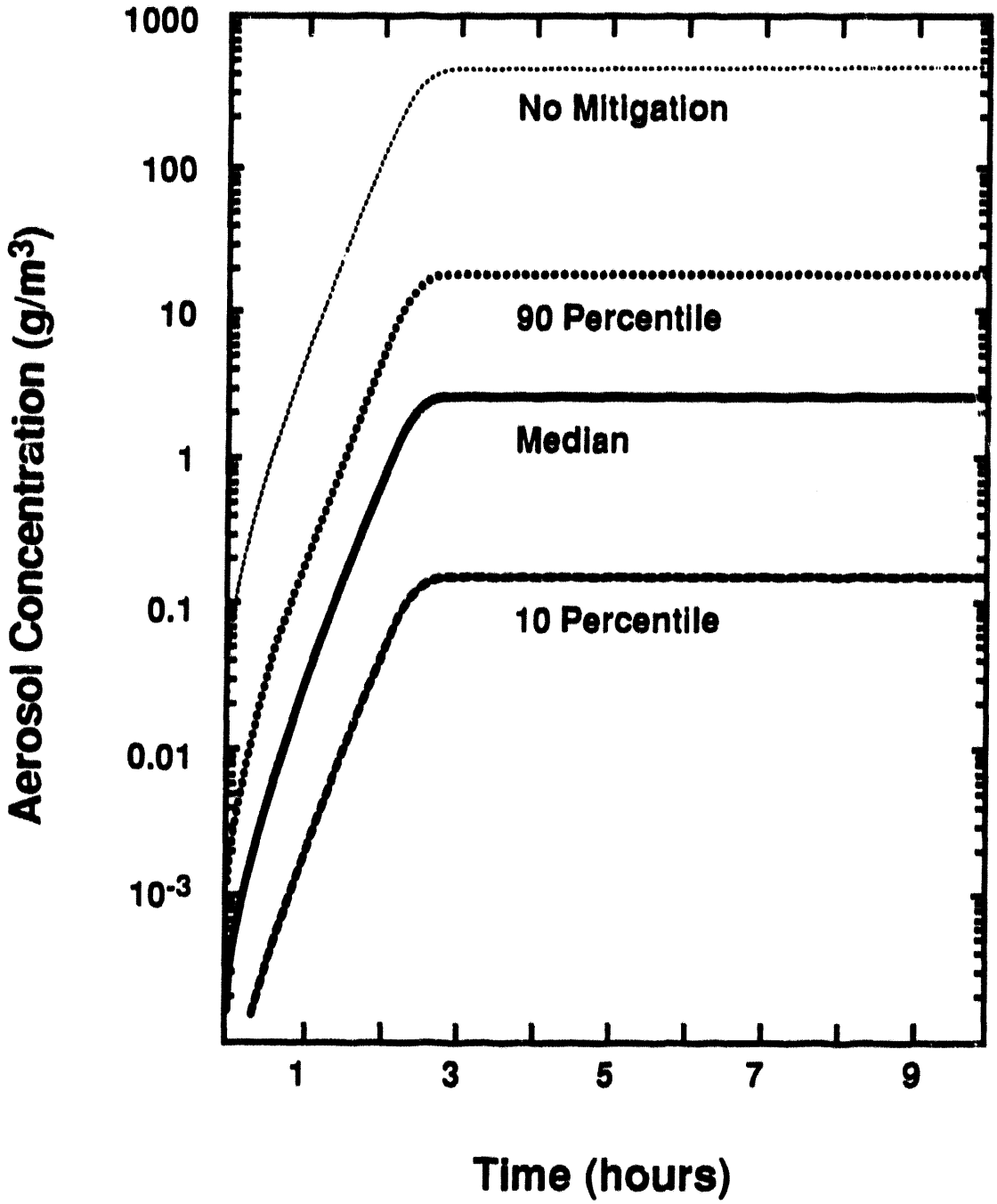

Figure 32 Aerosol concentrations in the drywell when a 50 cm deep water pool subcooled by 20°C is maintained over the core debris. The median (solid line), 90 percentile (dashed line) and 10 percentile (dotted line) concentrations are compared to concentrations for the case when no water pool is present.

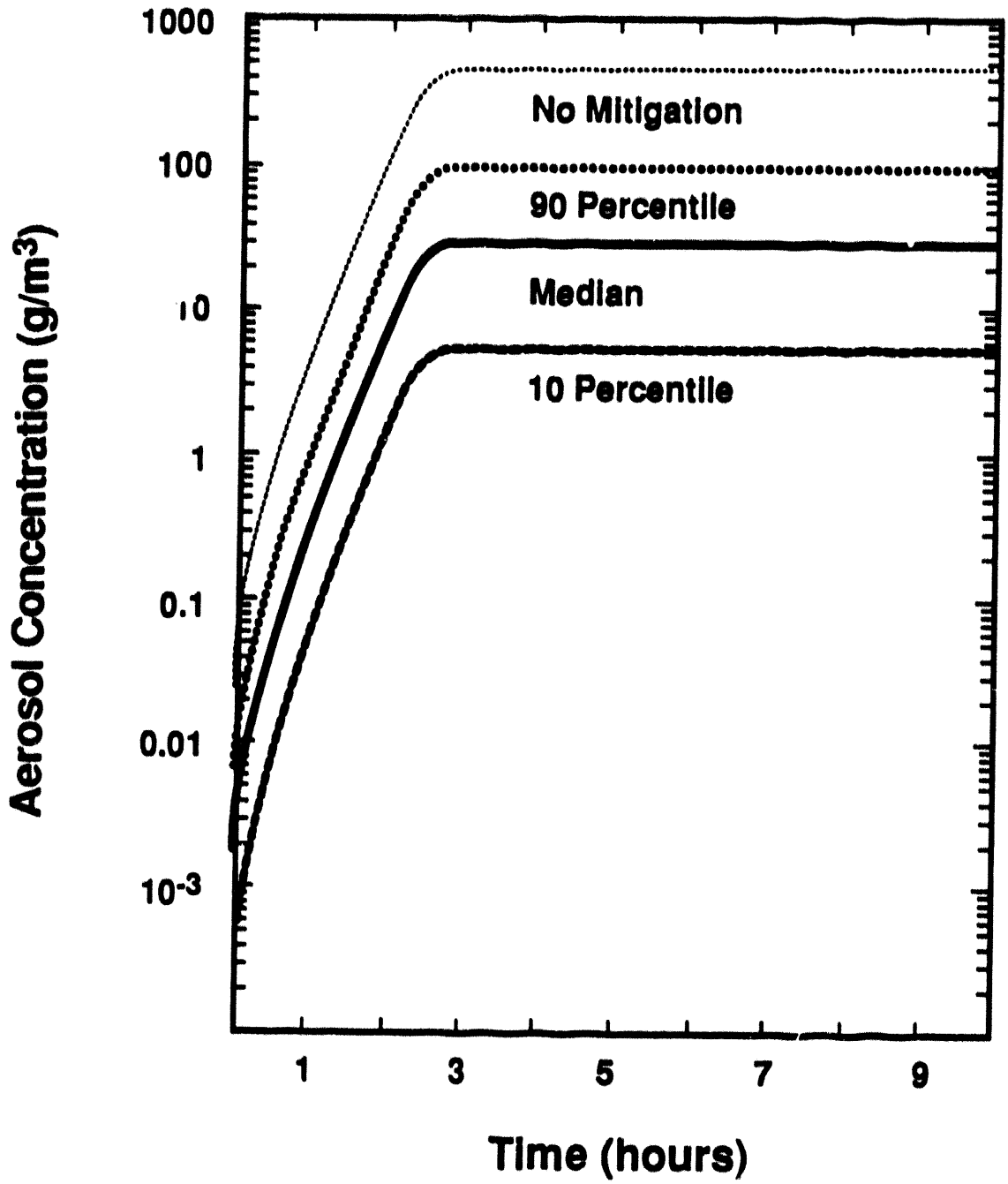

Figure 33 Aerosol concentrations in the drywell when a 50 cm deep water pool subcooled by only 2°C is maintained over the core debris. The median (solid line), 90 percentile (dashed line) and 10 percentile (dotted line) concentrations are compared to concentrations for the case of no water pool present.

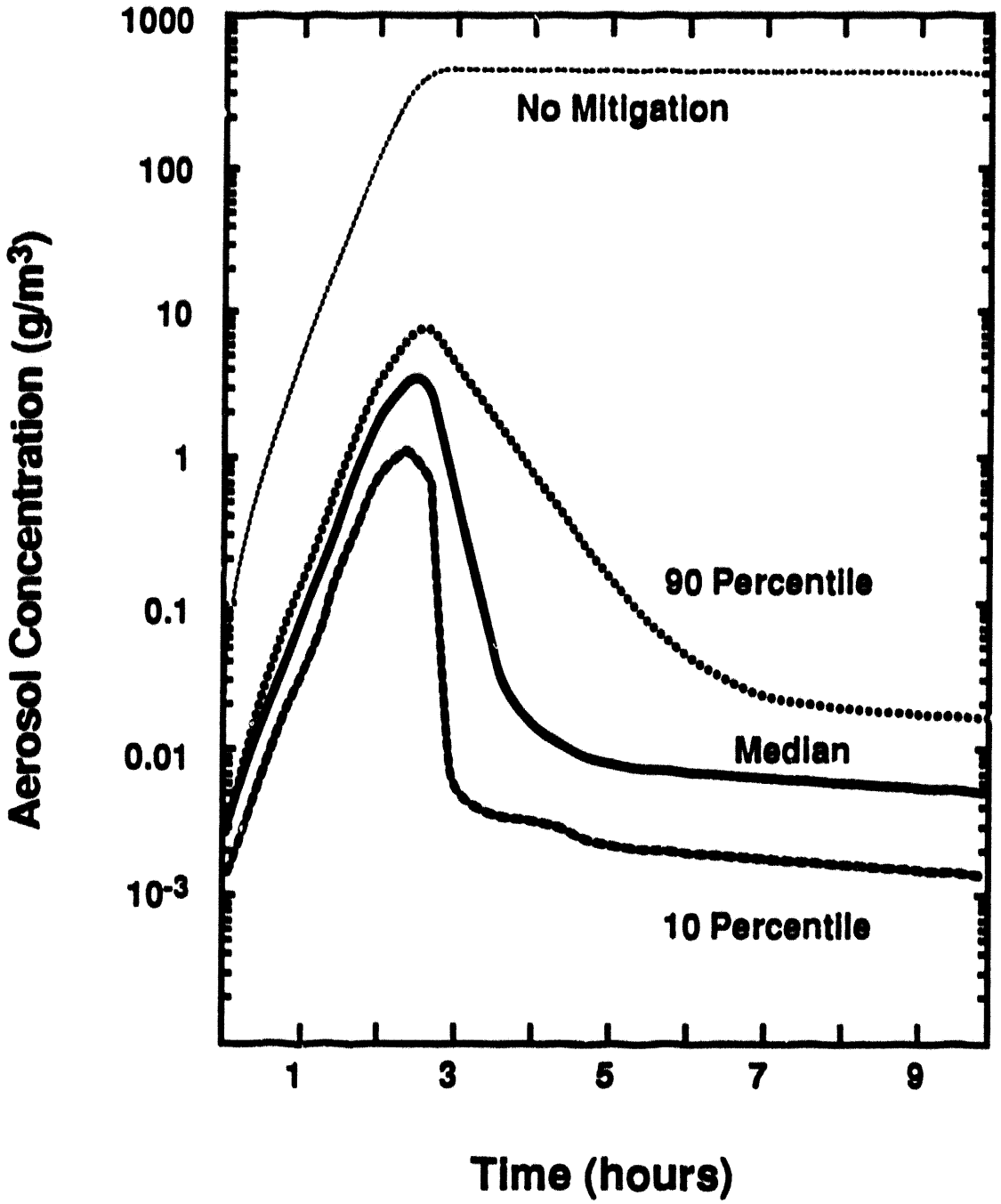

Figure 34 Effects of sprays on aerosol concentrations in the drywell atmosphere. A 50 cm deep water pool, subcooled by 2°C was assumed to be present. Sprays were assumed to supply a water flux of 0.25 cm^3/cm^2-s.

decontamination factor at this time is about 8.6×10^4. The apparent, overall, decontamination factor increases with time because aerosols suspended in the drywell atmosphere continue to be exposed to the spray. Though sprays do not have as immediate effect on aerosol concentrations as water pools, the effects of sprays accumulate with time. Delaying drywell failure or limiting drywell failure to a small leak greatly improves the effectiveness of sprays at source term mitigation.

Reduction in the spray flow rate, of course, reduces spray effectiveness. Results are shown in Figure 35 for a spray operating at a water flux of only 0.01 cm^3/cm^2-s and other conditions the same as they were for calculations used to prepare Figure 34. The median aerosol concentration curve has a maximum at about 13.5 g/m^3. The 10 and 90 percentile concentrations reach maxima of about 9.8 and 14.9 g/m^3. Late in the course of the core debris interactions with concrete the 90, 50 and 10 percentile aerosol concentrations are calculated to be about 7.4, 1.6, and 0.036 g/m^3, respectively.

The relatively high concentrations of aerosol that are calculated here to exist even with the spray operating (albeit at lower water fluxes) arise because aerosol particles are too small to be efficiently removed by spray droplets. At these higher concentrations, the aerosols would agglomerate. As this agglomeration progresses, the efficiency of particle removal by sprays would improve in comparison to what has been calculated here neglecting particle agglomeration. Nevertheless, it is evident that low water flux spray operations do not greatly augment the decontamination effect achieved by water pools overlying core debris. Certainly, low water flux spray operation does not produce a prompt decontamination that would be important for source term mitigation after drywell failure.

To summarize the findings of the accident analysis, a comparison of the effects of various mitigation processes is shown in Figure 36. Shown in this figure are aerosol concentrations in the drywell during an ATWS accident considering:

1. no mitigation processes,

2. mitigation by natural processes of settling and agglomeration,

3. natural processes supplemented by the effects of a 50 cm deep 20°C subcooled water pool (median value of the decontamination factor), and

4. natural processes supplemented by the effects of both the water pool and sprays operated at 0.25 cm^3/cm^2-s (median value of the decontamination factor).

By far the biggest reduction in the aerosol mass produced promptly in the first 1 or 2 hours is that provided by the water pool. The incremental effect of sprays in this early period is not espeically large. Sprays, and to a lesser extent the "natural" aerosol removal processes, have, however, an accumulating effect on aerosol concentrations. With continued operation sprays continue to decontaminate the atmosphere. Depending on when drywell failure occurs, these example calculations indicate that the combination of a subcooled water pool and high water flux sprays could reduce the amount of radioactivity released after drywell failure by factors of 4000 to over 10^5.

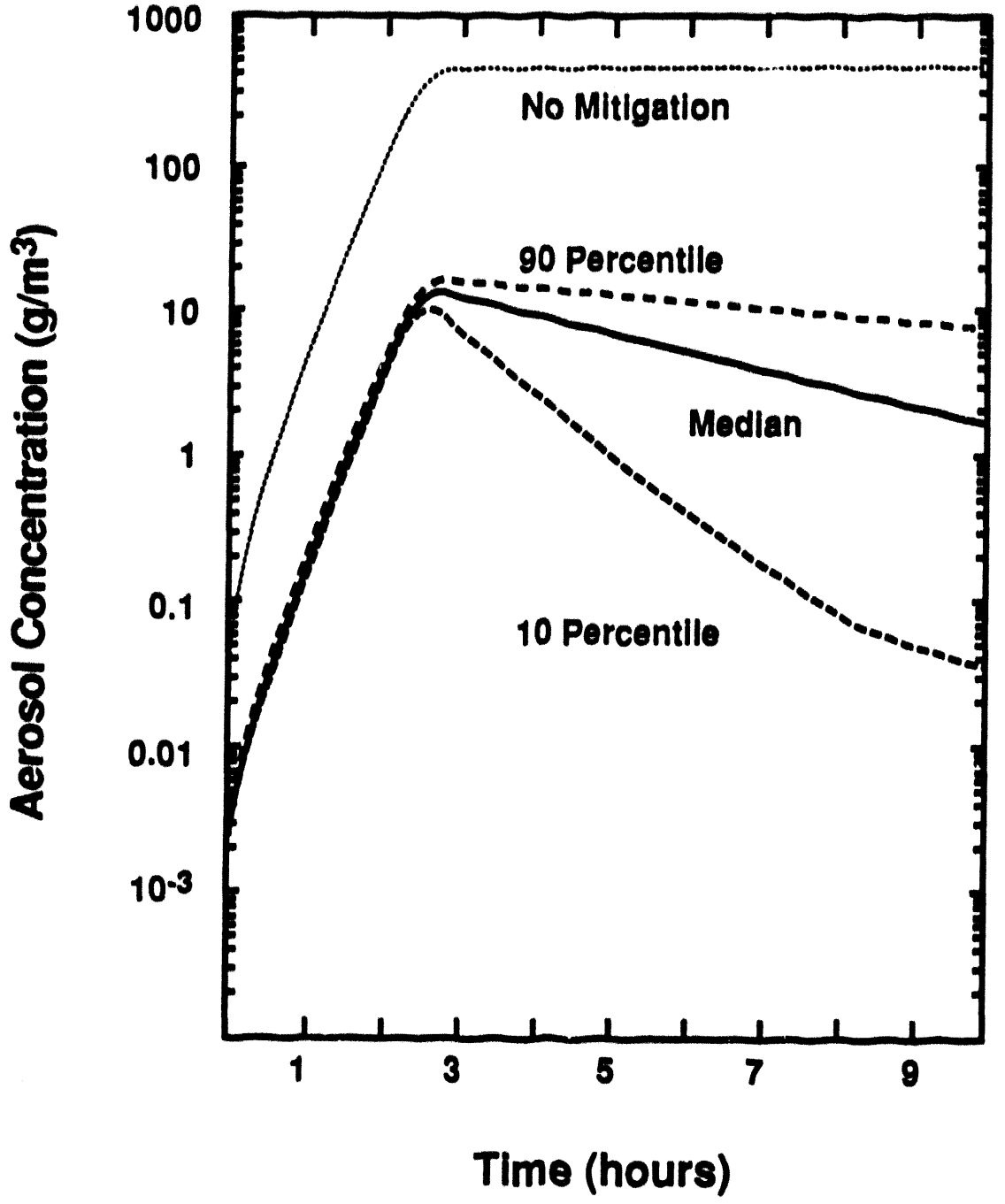

Figure 35 Effects of sprays operated at a water flux of 0.01 cm^3/cm^2-s on aerosol concentrations in the drywell. A water pool 50 cm deep and 2°C subcooled was assumed to be present.

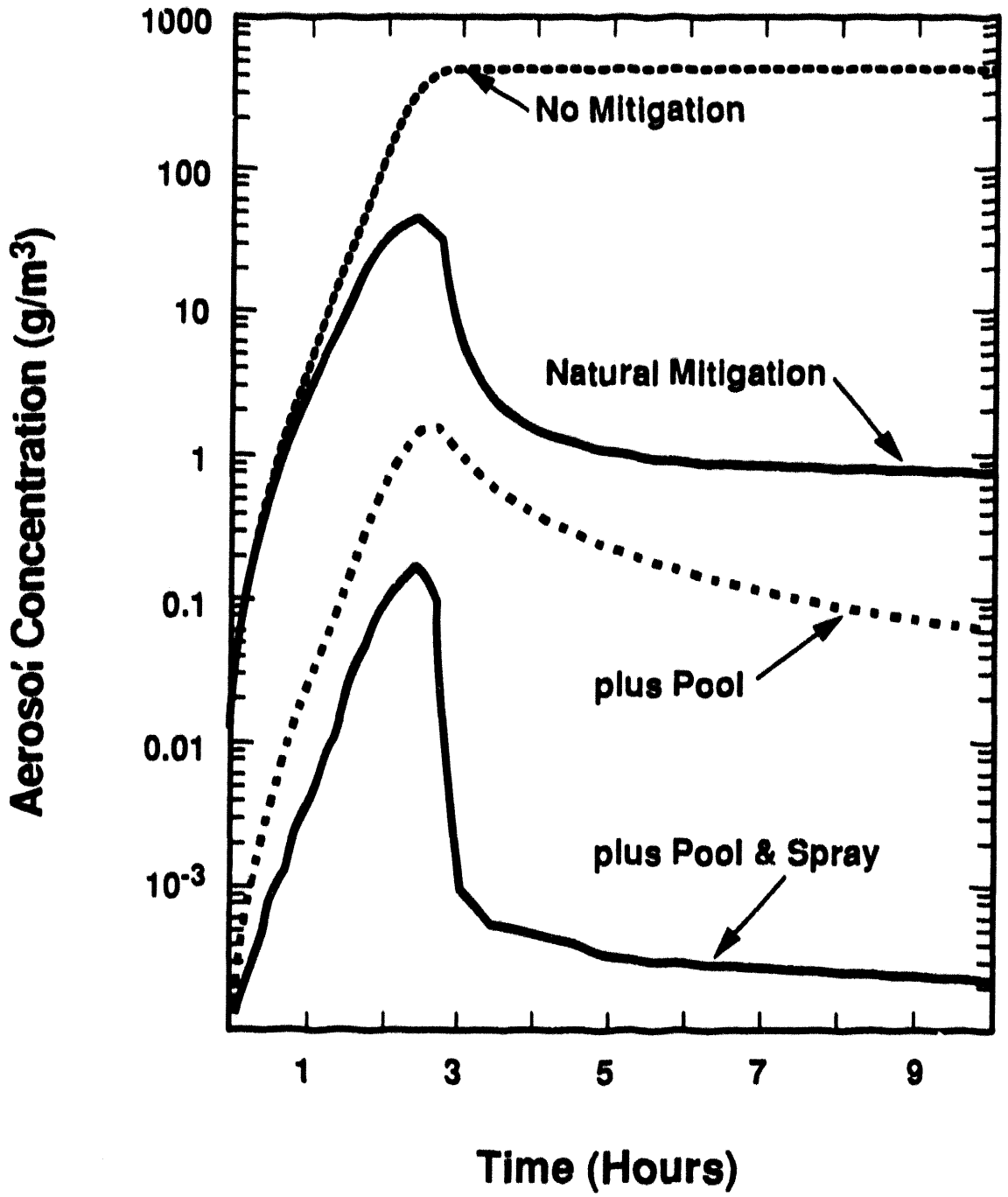

Figure 36 Comparison of aerosol concentrations considering various mitigation processes. The dotted curve was calculated neglecting any mitigation, the curve marked natural mitigation was calculated by aerosol settling and deposition. The other curves were calculated considering mitigation by a 50 cm deep 20°C subcooled water pool alone and in conjunction with a spray operated at 0.25 cm^3/cm^2-s.

VII. Conclusions

The principal conclusion that can be reached from the analyses presented in this report is that water in the Mark I drywell can reduce substantially the reactor accident source term in the event of drywell rupture. That is, water in the drywell can reduce the risks of severe reactor accidents even if the water cannot prevent or delay the rupture of the drywell. Water can reduce the amount of radioactive material suspended in the the drywell atmosphere and available for release should containment fail by direct melt attack, overpressurization or as result of excessive temperatures.

Attenuation of the releases of radioactive materials by an overlying water pool during core debris interactions with concrete is the most important process by which drywell water reduces the severe accident source term. The key to achieving high levels of decontamination by shallow water pools in the Mark I drywell is substantial subcooling of the water. If median values of the uncertain decontamination factors calculated for water pools are considered, then releases of radioactivity during core debris, concrete interactions can be reduced by a factor of about 180 with a 50 cm deep water pool that is kept subcooled by about 20°C. Allowing the pool to become saturated reduces the source term mitigation to about a factor of 16. More pessimistic views of the uncertainties in the predictions of decontamination by a water pool overlying core debris still indicates that a 50 cm deep pool with 20°C subcooling can reduce releases of radioactive materials during core debris interactions with concrete by factors of about 26.

Whereas water pools overlying core debris in the Mark I drywell only affect the radionuclide releases during core debris interactions with concrete, drywell sprays can attenuate radionuclide inventories in the drywell atmosphere from all sources. That is, drywell sprays can reduce the inventory of radionuclides suspended in the containment atmosphere as a result of core debris/concrete interactions, revaporization, and releases from residual fuel in the reactor coolant system. Drywell sprays lose effectiveness as aerosol particles become small. Only at high water fluxes do the sprays significantly augment the prompt attenuation by water pools of radionuclide releases during core debris/concrete interactions. Protracted exposure of aerosols to the action of sprays can produce very large reductions in the amounts of radioactive material available for release in the event of drywell rupture.

Simple correlations of the results obtained here can be used to prepare estimates of decontamination by water pools and sprays in the Mark I drywell at prescribed levels of conservatism and confidence.

A decision to assure water is present in the drywell during a severe reactor accident to protect the integrity of the drywell liner would have the derivative benefit of reducing the magnitude of radionuclide release to the reactor building should the drywell fail. Most of the potential attenuation of the severe accident source term comes from a water pool overlying the core debris interacting with concrete. Admission of water to the drywell by sprays could augment the source term attenuation. The augmentation provided by the sprays could be important if:

- the drywell water pool could not be kept subcooled,
- there was extensive, late, release of coarse aerosols from residual fuel in the reactor vessel directly to the drywell atmosphere, or
- there was extensive revaporization of deposited fission products from the reactor coolant system after reactor vessel failure.

VIII. References

1. U.S. Nuclear Regulatory Commission, Reactor Safety Study: An Assessment of Accident Risks in U.S. Commercial Nuclear Power Plants, WASH1400, NUREG-75/14, 1975.

2. Office of Nuclear Regulatory Research, Severe Accident Risks: An Assessment for Five U.S. Nuclear Power Plants, NUREG-1150, Vols. 1 and 2, U.S. Nuclear Regulatory Commission (Second Draft for Peer Review), Washington, D.C., June 1989.

3. A. T. Wassel, A. F. Mills, D. C. Bugby, and R. Oehlberg, Nuclear Engineering and Design, 90 (1985) 87.

4. P. C. Owczarski, A. K. Postma, and R. L. Schrek, Technical Bases and User's Manual for SPARC--A Suppression Pool Aerosol Removal Code, NUREG/CR-3317, PNL-4742, Pacific Northwest Laboratory, Richland, WA, 1983.

5. P. N. Clough, S. A. Ramsdale, and P. N. Smith, "Aerosol Decontamination Factors in Pools Overlying Molten Core-Concrete-Code Modeling," Proceedings OECD(NEA) CSNI Specialists' Meeting on Core Debris/Concrete Interactions, EPRI Electric Power Research Institute, Palo Alto, CA, February 1987.

6. L. G. Griemann, F. Famous, A. Wold-Tinsai, D. Ketalaar, T. Lin, and D. Bluhm, Reliability Analysis of Steel Containment Strength, NUREG/CR-2442, 1984.

7. R. S. Denning et al., Radionuclide Release Calculations for Selected Severe Accident Scenarios, NUREG/CR-4624, BMI-2139, Vol. 1, Battelle's Columbus Division, Columbus, Ohio, July 1986.

8. Office of Nuclear Reactor Regulation, Estimates of Early Containment Loads From Core Melt Accidents, NUREG-1079, U.S. Nuclear Regulatory Commission, Washington, D.C., December 1985.

9. D. H. Cook et al., Station Blackout at Brown's Ferry Unit One - Accident Sequence Analysis, NUREG/CR-2182, Oak Ridge National Laboratory, Oak Ridge, TN, November 1981.

10. D. H. Cook et al., Loss of DHR Sequence at Brown's Ferry Unit One - Accident Sequence Analysis, NUREG/CR-2973, Oak Ridge National Laboratory, Oak Ridge, TN, May 1983.

11. G. A. Greene, K. R. Perkins, and S. A. Hodge, "Mark I Containment Drywell - Impact at Core/Concrete Interactions on Containment Integrity and Failure of the Drywell Liner," IAEA-SM-281/36, pp. 429-442, Source Term Evaluation for Accident Conditions, International Atomic Energy Agency, 1986.

12. Approximate Source Term Methodology for Boiling Water Reactors, FAI/86-1, Fauske and Associates, Inc., Burr Ridge, IL, December 1986.

13. J. J. Weingardt and K. D. Bergeron, TAC2D Studies of Mark I Containment Drywell Shell Melt-Through, NUREG/CR-5126, SAND88-1407, Sandia National Laboratories, Albuquerque, NM, August 1988.

14. N. T. Pratt et al., Assessment of Severe Accident Prevention and Mitigation Features: BWR, Mark I Containment Design, NUREG/CR-4920, BNL-NUREG-52070, Vol. 1, Brookhaven National Laboratory, Upton, NY, March 1988.

15. T. G. Theofanous, W. H. Amarasooriya, H. Yan, and U. Ratman, The Probability of Liner Failure in a Mark I Containment, NUREG/CR-5423, University of California, Santa Barbara, CA, July 1989.

16. R. E. Blose et al., Swiss 1 and 2: Sustained Interaction of Molten Stainless Steel and Concrete in the Presence of Water, NUREG/CR-4727, SAND85-1546, Sandia National Laboratories, Albuquerque, NM, July 1987.

17. D. A. Powers and J. L. Sprung, A Simplified Model of Aerosol Scrubbing by a Water Pool Overlying Core Debris Interacting With Concrete, NUREG/CR-5901, SAND92-1422, Sandia National Laboratories, Albuquerque, NM, October 1992.

18. D. A. Powers and S. B. Burson, A Simplified Model of Aerosol Removal by Containment Sprays, NUREG/CR-5966, SAND92-2689, Sandia National Laboratories, Albuquerque, NM, December 1992.

19. D. A. Powers and R. C. Schmidt, "Analysis of Revaporization of Deposited Radionuclides," in Evaluation of Accident Risks Volume 2, Appendices, Part 5, Supporting Calculations, NUREG/CR-4551, Rev. 1, Sandia National Laboratories, Albuquerque, NM, draft available in NRC Public Document Room.

20. D. A. Powers and J. E. Brockmann, "An Analysis of Aerosol Transport Through a Ruptured Steam Generator Tube," in Evaluation of Accident Risks Volume 2, Appendices, Part 5, Supporting Calculations, NUREG/CR-4551, Rev. 1, Sandia National Laboratories, Albuquerque, NM, draft available in NRC Public Documents Room.

21. D. A. Powers, "A Probabilistic Method for the Evaluation of Severe Accident Source Term Uncertainties," pp. 1173-1178, Vol. 2, Probabilistic Safety Assessment and Management, G. Apostolakis, editor, Elsevier, 1991.

22. E. R. Copus, "Quick Look Data Report - WETCOR-1 Test," Sandia National Laboratories, Albuquerque, NM, October 1991.

23. DOE/ARSAP, Technical Support for the Debris Coolability Requirements for Advanced Light Water Reactors in the Utility/EPRI Light Water Reactor Requirements Document, DOE/ID-10278, Fauske and Associates, Inc., Burr Ridge, IL, June 1990.

References

24. R. J. Lipinski et al., Uncertainty in Radionuclide Release Under Specific LWR Accident Conditions, Vols. I-IV, SAND84-410, Sandia National Laboratories, Albuquerque, NM, May 1984.

25. D. A. Powers, J. E. Brockmann, and A. W. Shiver, VANESA: A Mechanistic Model of Radionuclide Release and Aerosol Generation During Core Debris Interactions With Concrete, NUREG/CR-4308, SAND85-1370, Sandia National Laboratories, Albuquerque, NM, July 1986.

26. R. Clift, J. R. Grace, and M. E. Weber, Bubbles, Drops, and Particles, Academic Press, 1978.

27. D. A. Powers, An Analysis of Radionuclide Behavior in Water Pools During Accidents at the Annular Core Research Reactor, SAND91-1222, Sandia National Laboratories, Albuquerque, NM, April 1992.

28. J. E. Brockmann, F. E. Arellano, and D. A. Lucero, Validation of Models of Gas Holdup in the CORCON Code, NUREG/CR-5433, SAND89-1951, Sandia National Laboratories, Albuquerque, NM, December 1989.

29. W. Fritz, Physik, 36(1965)379.

30. F. G. Blottner, Hydrodynamics and Heat Transfer Characteristics of Liquid Pools With Bubble Agitation, NUREG/CR-0944, SAND79-1132, Sandia National Laboratories, Albuquerque, NM, November 1979.

31. J. F. Davidson and B.O.G. Schuler, Trans. Inst. Chemical Eng., 38 (1960) 335.

32. I. A. Vaklirushev and G. I. Efremor, Chemical Technology Fuels Oils (USSR), 5/6 (1970) 376.

33. J. R. Grace, T. Wairegi, and T. H. Nguyen, Trans. Inst. Chemical Eng., 54 (1976) 167.

34. V. G. Levich, Physicochemical Hydrodynamics, Prentice Hall Publishing Co., 1962.

35. J. E. Brockmann, "Ex-Vessel Releases: Aerosol Source Terms in Reactor Accidents," Progress in Nuclear Energy, 19 (1987) 7.

36. Chemical Engineers' Handbook, 4th Edition, R. H. Perry, C. H. Chilton, and S. D. Kirkpatrick, editors, McGraw-Hill Book Co., 1963.

37. Handbook of Chemistry and Physics, 45th Edition, R. C. Weast, editor-in-chief, The Chemical Rubber Publishing Co., Cleveland, OH, 1964.

38. D. A. Powers and F. E. Arellano, Large-scale, Transient Tests of the Interactions of Molten Steel With Concrete, NUREG/CR-2282, SAND81-1753, Sandia National Laboratories, Albuquerque, NM, January 1982.

39. L. A. Kent, Water Release From Heated Concrete, NUREG/CR-2279, SAND81-1732, Sandia National Laboratories, Albuquerque, NM, March 1982.

40. J. F. Muir, Response of Concrete Exposed to a High Heat Flux on One Surface, SAND77-1467, Sandia National Laboratories, Albuquerque, NM, 1977.

41. H. J. Sutherland, Nuclear Technology, 46 (1979) 350.

42. E. R. Copus et al., Core-Concrete Interactions Using Molten Urania With Zirconium on a Limestone Concrete Basemat: The SURC-1 Experiment, NUREG/CR-5443, SAND90-0087, Sandia National Laboratories, Albuquerque, NM, April 1992.

43. E. R. Copus and D. R. Bradley, Interactions of Hot Solid Core Debris With Concrete, NUREG/CR-4558, SAND85-1789, Sandia National Laboratories, Albuquerque, NM, June 1986.

44. E. R. Copus et al., Experimental Results of Core-Concrete Interactions Using Molten Steel With Zirconium, NUREG/CR-4794, SAND86-2638, Sandia National Laboratories, Albuquerque, NM, July 1990.

45 E. R. Copus et al., Core-Concrete Interactions Using Molten Steel With Zirconium on a Basaltic Basemat: The SURC-4 Experiment, NUREG/CR-4994, SAND87-2008, Sandia National Laboratories, Albuquerque, NM, April 1989.

46. W W. Tarbell et al., Sustained Concrete Attack by Low-Temperature, Fragmented Core-Debris, NUREG/CR-3024, SAND82-2476, Sandia National Laboratories, Albuquerque, NM, July 1987.

47. D. A. Powers and F. E. Arellano, Direct Observation of Melt Behavior During High Temperature Melt/Concrete Interactions, NUREG/CR-2283, SAND81-1754, Sandia National Laboratories, Albuquerque, NM, January 1982.

48. D. A. Powers et al., Exploratory Study of Molten Core Material/Concrete Interactions, SAND77-2042, Sandia National Laboratories, Albuquerque, NM, February 1978.

49. S. S. Kutateladze and I.G. Malenkov, High Temperature, 14 (1976) 703.

50. D. R. Bradley et al., CORCON-Mod3: An Integrated Computer Model for Analysis of Molten Core-Concrete Interactions: User's Manual, NUREG/CR-5843, SAND92-0167, Sandia National Laboratories, Albuquerque, NM, April 1993.

51. M. Fischer et al., "MACE Scoping Test Data Report," ACE-TR-D3, Argonne National Laboratory, Argonne, IL, March 1991.

52. R. E. Blose, D. A. Powers, E. R. Copus, J. E. Brockmann, R. B. Simpson, and D. A. Lucero, Core-Concrete Interactions with Overlying Water Pool: WETCOR-1, NUREG/CR-5907, SAND92-1563, Sandia National Laboratories, Albuquerque, NM, March 1993.

53. F. Herning and L. Zipperer, Gas Wasserfach, 79 (1936) 49-73. See also P. K. Tondon and S. C. Saxena, Indian J. Pure Appl. Phys., 6 (1968) 475.

References

54. T. G. Theofanous, "Dealing With Phenomenological Uncertainties in Severe Accident Assessments and Probabilistic Risk Analyses," Proceedings 3rd International Topical Meeting on Nuclear Power Plant Thermal Hydraulics and Operations, November 14-17, 1988, Seoul, South Korea, 1989.

55. W. E. Kastenberg et al., Findings of the Peer Review Panel on the Draft Reactor Risk Reference Document, NUREG-1150, NUREG/CR-5113, UCID-21345, Lawrence Livermore National Laboratory, Livermore, CA, May 1988.

56. I. Cook and S. Unwin, Nuclear Science and Engineering, 94 (1986) 107.

57. J. E. Brockmann, "Range of Possible Dynamic and Collision Shape Factors," Appendix F in R. J. Lipinski et al., Uncertainty in Radionuclide Release Under Specific LWR Accident Conditions Volume II, TMLB' Analysis, SAND84-410, Vol. 2, Sandia National Laboratories, Albuquerque, NM, February 1985.

58. D. E. Knuth, Seminumerical Algorithms, Second Edition, Addison-Wesley Publishing Co., 1981.

59. L. D. Reed, H. Jordan, and J. A. Gieseke, J. Aerosol Science 8 (1977) 457.

60. W. C. Hinds, Aerosol Technology - Properties Behavior and Measurement of Airborne Particle, John Wiley and Sons, 1982.

61. H. R. Proppacher and R. V. Beard, Quarterly J.R. Meteorological Society, 96 (1970) 247.

62. C. S. Pemberton, J. Air Pollution, 3 (1960) 168.

63. I. Langmuir, J. Meteorology, 5 (1948) 175.

64. N. A. Fuchs, The Mechanics of Aerosols, Pergamon Press, 1964.

65. K. W. Lee and J. A. Gieseke, J. Aerosol Science, 11 (1980) 335.

66. R. Tal, D. N. Lee, and W. A. Sirigano, Int'l J. Heat Mass Transfer, 27 (1984) 1953.

67. K. Aminzadeh, T. R. Altaha, A. R. H. Cornish, M. S. Kolansky, and R. Pfeffer, Int'l J. Heat Mass Transfer, 17 (1974) 1425.

68. A. R. N. Cornish, Trans. Instn. Chem. Engrs., 43 (1965) 332.

69. D. Rimberg and Y-M. Peng, "Aerosol Collection by Falling Droplets," Air Pollution Control and Design Handbook, Part 2, Chapter 27, P. N. Cheremisinoff and R. A. Young, editors, Marcell Dekker, Inc., 1977.

70. K. E. Washington et al., Reference Manual for CONTAIN 1.1 Code for Containment Severe Accident Analysis, NUREG/CR-5715, SAND91-0835, Sandia National Laboratories, Albuquerque, NM, July 1991.

71. T. B. Powers and D. L. Reid, Size Distribution of Drops from Containment Spray Nozzles, NUREG/CR-0608, PNL-2840, Pacific Northwest Laboratory, Richland WA, 1979.

72. G. Herdan, Small Particle Statistics, Butterworths, 1960.

73. D. M. Whelpdale and R. List, J. Geophysics Research, 76 (1971) 2836.

74. N. Arbel and Z. Levin, Pure and Applied Geophysics, 115 (1977) 869.

75. A. M. Podrystosky and A. A. Shraiber, Fluid Mechanics - Soviet Research, 7 (1978) 152.

76. A. M. Podrystosky and A. A. Shraiber, Int'l J. Multiphase Flow, 10 (1984) 195.

77. S. G. Bradley and C. D. Stow, J. Atmospheric Science, 36 (1979) 494.

78. V. A. Arkhipor, J. Appl. Mech. and Tech. Phys., 24 (1983) 371.

79. L. Baker, Jr., M. Pilch, and W. W. Tarbell, "Droplet Structure Interactions in Direct Containment Heating," Transactions ANS, 57 (1988) 323.

80. R. M. Schotland, Disc. Faraday Society, 30 (1960) 72.

81. L. S. Christensen, Bounce, Coalescence, and Splash of Water Drops, Master's thesis, University of Nevada, Reno, Nevada, 1960.

82. C. K. Mutchler, Water Resources Research, 7 (1971) 1024.

83. C. D. Stow and R. D. Stainer, J. Metr. Soc. Japan, 55 (1977) 518.

84. U.S. Nuclear Regulatory Commission, Standard Review Plan for the Review of Safety Analysis Reports for Nuclear Power Plants, NUREG-800, Section 6.5.2, December 1988.

85. J. A. Gieseke et al., Source Term Code Package: A User's Guide, NUREG/CR-4587, Battelle Columbus Laboratory, Columbus, Ohio, July 1986.

86. L. J. Ott, "Advanced Severe Accident Models for BWR Applications," Proc. 15th Light Water Reactor Safety Research Information Meeting, Gaithersburg, MD, 1988.

87. R. Adams, "Behavior of U_3O_8, Fe_2O_3 and Concrete Aerosols in a Condensing Steam Environment," Proc. Eleventh Water Reactor Safety Research Meeting, Volume 3, page 129, NUREG/CR-0048, U.S. Nuclear Regulatory Commission, Washington, D.C., January 1984.

88. T. S. Kress as cited in Reference 57.

Appendix A: Statistics of Order Distributions

The statistical methods used to develop the probability distributions described in the text are derived in this appendix. The derivations used here follow directly from derivations presented by Hogg and Craig [1].

Consider a random variable X. Assume this random variable to have a continuous, positive probability density function f(x) over the interval from a to b such that a < b. The cumulative probability distribution function for X is F(X) and is given by:

$$F(X) = \int_{-\infty}^{X} f(x)dx = \int_{a}^{X} f(x)dx$$

such that

$$\int_{-\infty}^{+\infty} f(x)dx = 1 = \int_{a}^{b} f(x)dx$$

The probability density function, f(x) or equivalently the cumulative probability distribution function F(x), are unknown for the problems posed in the text of this report. The objective of the Monte Carlo sampling is to obtain a sample of the random variable X from which some estimate of f(x) or F(X) can be made.

At the conclusion of the Monte Carlo sampling for a given problem, a set of n possible values of the random variable X is available:

$$\{X_1, X_2, X_3 \cdots X_{n-1}, X_n\}$$

These sampled values can be arranged in increasing order--say, for example, $X_1, X_{n-1}, X_2 \ldots X_n, X_3$. The values can then be relabelled Y_i such that $Y_i < Y_{i+1}$:

$$\{Y_1, Y_2, Y_3 \cdots Y_{n-1}, Y_n\}$$

This ordered set of the sampled values of the random variable is the "order statistic" for the sample of size n. The joint probability density function for this order statistic is labelled $g(Y_1, Y_2, Y_3 \ldots Y_{n-1}, Y_n)$ and is given by:

$$g(Y_1, Y_2, Y_3, \ldots Y_{n-1}, Y_n) = \begin{cases} n! f(y_1) f(Y_2) f(Y_3) \ldots f(Y_{n-1}) f(Y_n) \\ \text{for} \quad Y_i < Y_{i+1} \quad \text{for } i = 1 \text{ to } n-1 \\ 0 \quad \text{otherwise} \end{cases}$$

This follows directly because there are n! ways that it might have been necessary to arrange the sampled values of X in order to formulate the statistic.

A new statistic Z can be formulated from:

$$Z_i = F(Y_i)$$

where $F(Y_i)$ is the cumulative probability distribution function for the random variable X. The Jacobian for this transformation of Y into Z is:

$$J = \begin{vmatrix} \frac{dY_1}{dZ_1} & 0 \ldots\ldots\ldots\ldots 0 \\ 0 & \frac{dY_2}{dZ_2} \ldots\ldots\ldots\ldots 0 \\ 0 & 0 \quad \frac{dY_3}{dZ_3} \ldots\ldots 0 \\ 0 & 0 \quad 0 \ldots\ldots \frac{dY_n}{dZ_n} \end{vmatrix} = \frac{dY_1}{dZ_1}\frac{dY_2}{dZ_2}\frac{dY_3}{dZ_3}\cdots\frac{dY_n}{dZ_n}$$

$$= \frac{1}{\frac{dZ_1}{dY_1}\frac{dZ_2}{dY_2}\frac{dZ_3}{dY_3}\cdots\frac{dZ_n}{dY_N}}$$

Since $Z = F(Y)$ and $dZ_i/dY_i = f(Y_i)$:

$$J = \frac{1}{f(Y_1) f(Y_2) f(Y_3) \cdots f(Y_n)}$$

Then, the joint probability density function for the Z statistic is:

$$h(Z_1, Z_2, Z_3 \cdots Z_n) = Jg(Y_1, Y_2, Y_3 \cdots y_n)$$

$$= n!$$

The probability density function of a particular Z_K is:

$$h(Z_K) =$$

$$= \int_0^{Z_2} \cdots \int_0^{Z_K} \left[\int_{Z_K}^{1} \cdots \left[\int_{Z_{n-2}}^{1} \left[\int_{Z_{n-1}}^{1} h(Z_1, Z_2, Z_3, \ldots Z_n) dZ_n \right] dZ_{n-1} \right] \ldots dZ_{K+1} \right] dZ_{K-1} \ldots dZ_1$$

$$= \int_0^{Z_2} \cdots \int_0^{Z_K} \left[\int_{Z_K}^{1} \cdots \left[\int_{Z_{n-2}}^{1} n!(1 - Z_{n-1}) dZ_{n-1} \right] \ldots dZ_{K+1} \right] dZ_{K-1} \ldots dZ_1$$

$$= \int_0^{Z^2} \cdots \int_0^{Z_K} \frac{n!}{(n-K)!} (1 - Z_K)^{n-K} dZ_{K-1} \ldots dZ_1$$

$$= \frac{n!}{(K-1)!(n-K)!} Z_K^K (1 - Z_K)^{n-K}$$

Now, for some probability p such that $0 < p < 1$, the solution for

$$F(x) = p$$

is $\xi_p = x$. ξ_p is the p^{th} quantile of the cumulative distribution function. The order statistic for the sample of size n of the random variable X can be characterized by the probability that $Y_K < \xi_p$ or

$$Pr(Y_K < \xi_p) = Pr(Z_K < p)$$

Appendix A

From the probability density function of Z_K:

$$\Pr(Z_K < p) = \int_0^p h(Z_K)dZ_K = \int_0^p \frac{n!}{(K-1)!(n-K)!} Z_K^K(1-Z_K)^{n-K}dZ_K$$

$$= \frac{n!}{K!(n-K)!} p^K(1-p)^{n-K} + \frac{n!}{(K+1)!(n-K-1)!} p^{K+1}(1-p)^{n-K-1} + \ldots + p^n$$

$$= \sum_{i=K}^{n} \frac{n!}{i!(n-i)!} p^i(1-p)^{n-i} = \Pr(Y_K < \xi_p)$$

This result is sufficient to provide a basis to bracket critical values of the unknown distribution function F(X) from the order statistic Y [2]. Note that

$$\Pr(Y_i < \xi_p) = \Pr(Y_j < \xi_p) + \Pr(Y_i < \xi_p < Y_j)$$

and that

$$\Pr(Y_i < \xi_p < Y_j) = \Pr(Y_i < \xi_p) - \Pr(Y_j < \xi_p)$$

The joint probability density function of $Z_i = F(Y_i)$ and $Z_j = F(Y_j)$ for $i < j$ is:

$$h_{ij}(Z_i, Z_j) =$$

$$= \int_0^{Z_i} \ldots \int_0^{Z_i} \int_{Z_i}^{Z_j} \ldots \int_{Z_{j-2}}^{Z_j} \int_{Z_j}^{1} \ldots \int_{Z_{n-1}}^{1} n!dZ_n \ldots dZ_{j+1}dZ_{j-1} \ldots dZ_{i+1}dZ_1 \ldots dZ_{i-1}$$

$$= \frac{n!}{(i-1)!(j-i-1)!(n-j)!} Z_i^{i-1}(Z_j - Z_i)^{j-i-1}(1-Z_j)^{n-j}$$

$$\text{for } 0 < Z_i < Z_j < 1$$

The most interesting of the joint probabilities is that of Z_1 and Z_n. Then,

$$h_{1n}(Z_1, Z_n) = n(9n-1)\,(Z_n - Z_1)^{n-2} \text{ for } 0 < Z_1 < Z_n < 1$$

Then, the probability that the sample of X exceeds some fraction p of the range of values of X is given by:

$$\Pr[F(Y_n) - F(Y_1) \geq p] = \Pr[Z_n - Z_1 \geq p]$$

$$= \int_0^{1-p} \int_{p+Z_1}^{1} n(n-1)(Z_n - Z_1)^{n-2} dZ_n dZ_1$$

$$= 1 - np^{n-1} + (n-1)p^n = C$$

C is then the confidence level that a sample of n values spans a fraction p of the distribution.

Some values of the confidence level C for various values of n and p are shown in Table A-1.

Table A-1 Sample size necessary to span a fraction of the uncertainty distribution, p, at a confidence Level C

Confidence level (%)	Sample size to span p =			
	0.9	0.95	0.99	0.999
90	37	76	388	3888
95	46	93	473	4742
99	64	130	661	6635
99.9	88	180	919	9228

An example is used to illustrate how the characterization of the distribution improves with the sample size. For this example, samples of 100, 500, 1000, and 3000 values were taken from a lognormal distribution with a mean of 1.48 and a geometric standard deviation of 2.546. The samples were ordered and subjected to the non-parametric statistical analyses described above. Cumulative probability distributions derived from the samples at the 95 percent confidence level are shown in Figures A-1 to A-4. These are conventional cumulative probability plots. The known distribution is shown as a solid line in the figures for comparison purposes. These results show that median values are derived fairly accurately from samples of just 100 values if the distribution is not too complicated. Samples of about 1000 values are needed to get accurate values at the 5 percent and 95 percent quantiles.

The principal advantage of the Monte Carlo method and the non-parametric order statistic analysis adopted here is that the number of samples that must be taken to characterize a distribution is independent of the number of uncertain quantities that arise in calculations of the type described in the

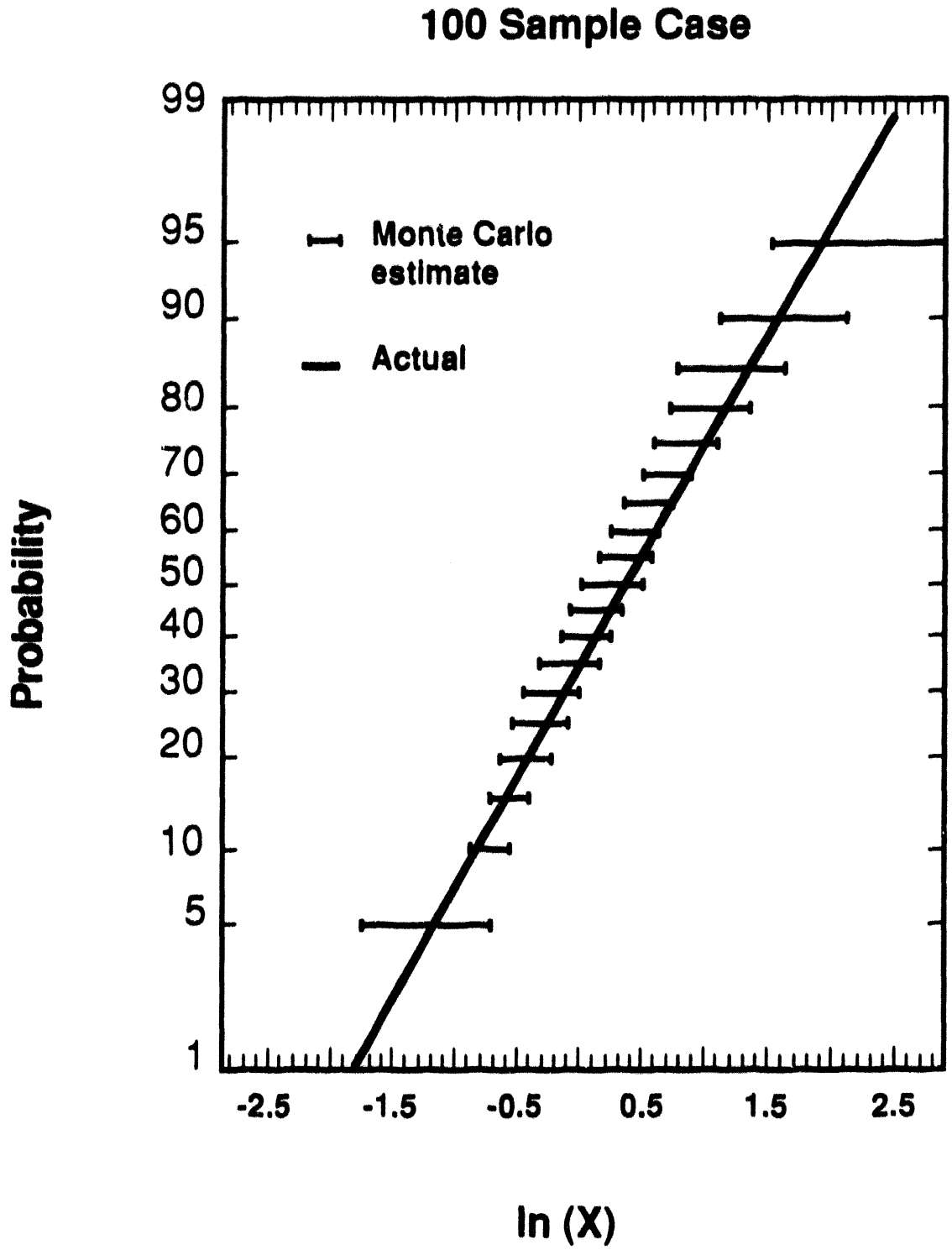

Figure A-1 95 percent confidence intervals for quantiles of the example distribution derived from a 100 value sample. The actual underlying distribution is shown by the continuous line.

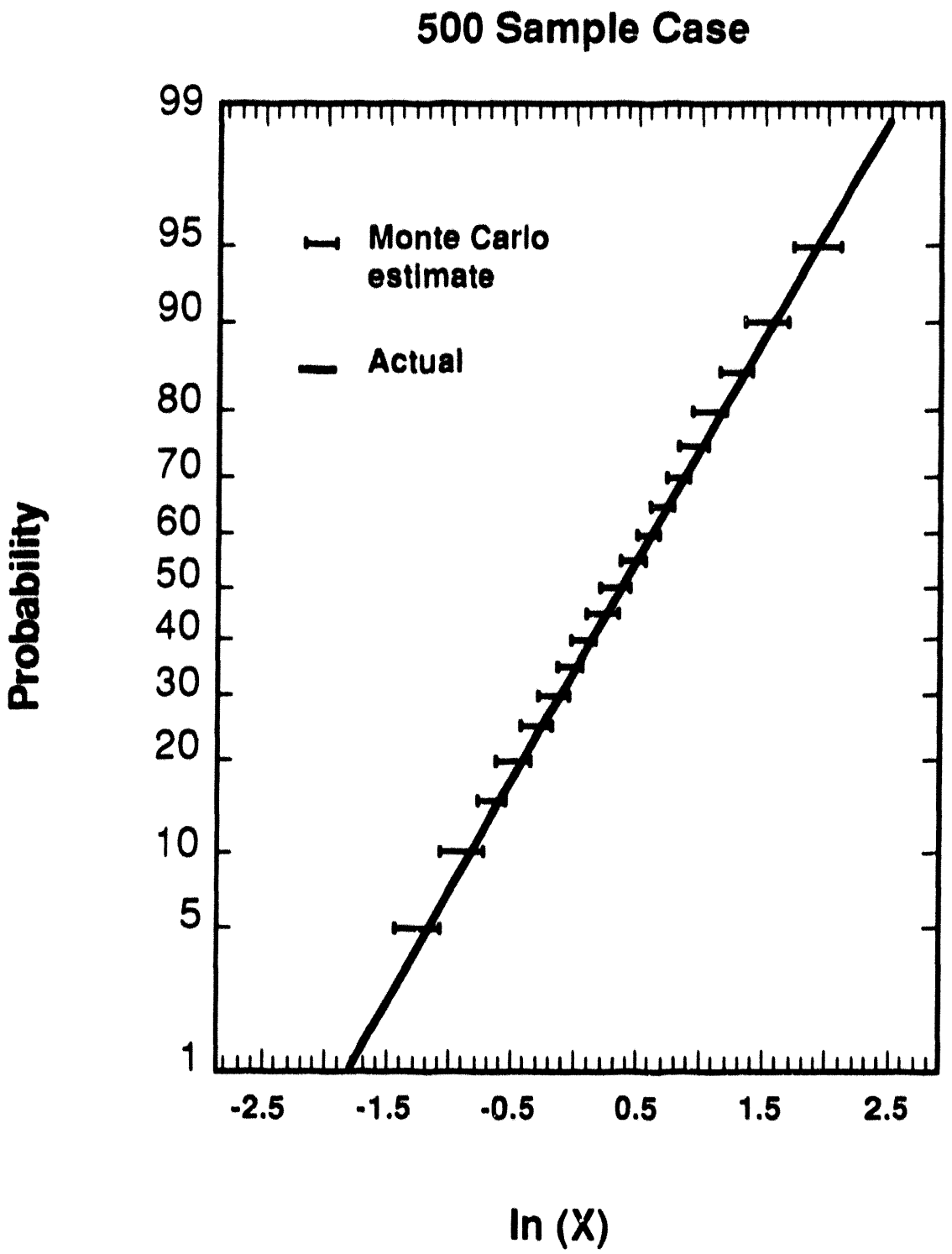

Figure A-2 95 percent confidence intervals for quantiles of the example distribution derived from a 500 value sample. The actual underlying distribution is shown by the continuous curve.

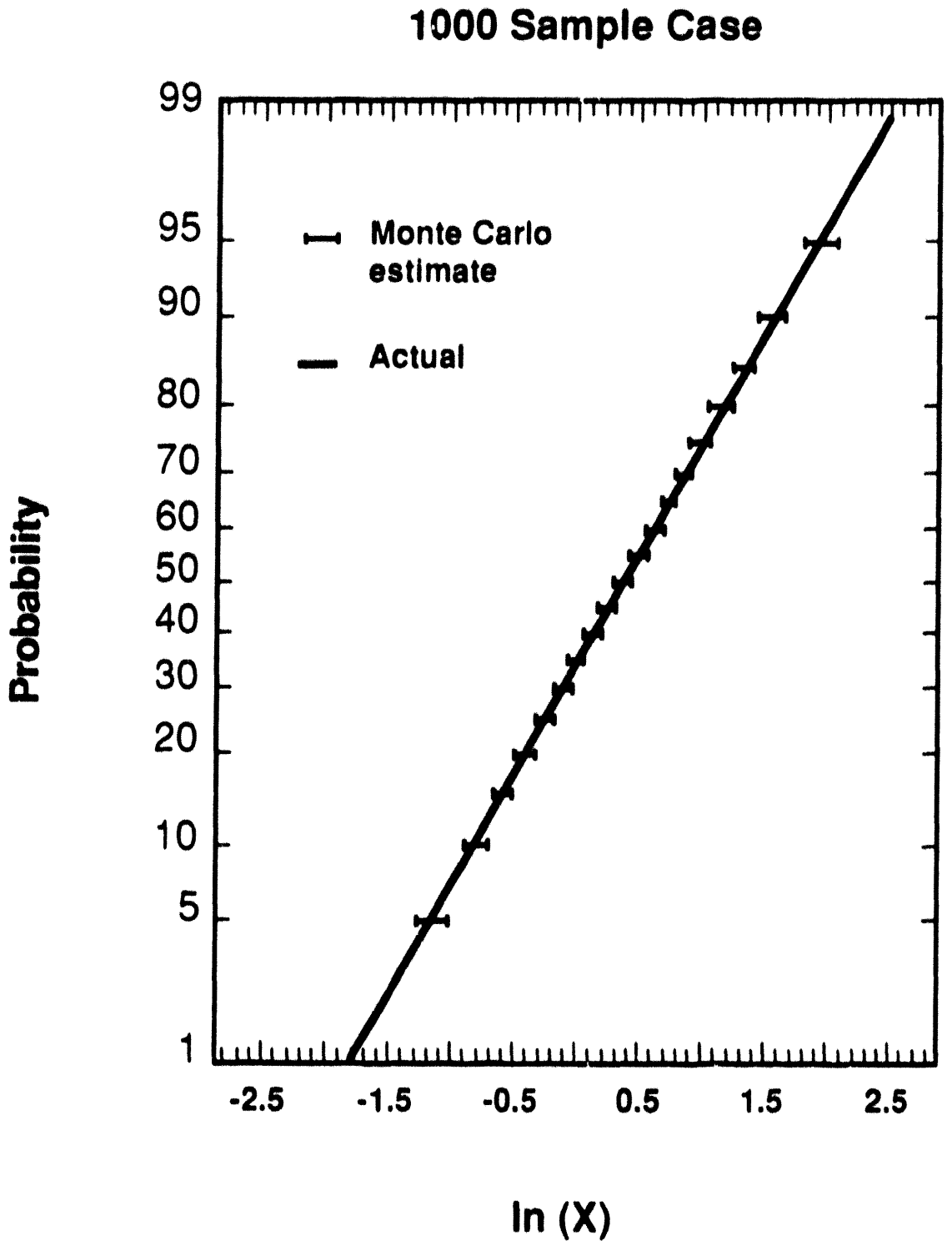

Figure A-3 95 percent confidence intervals for quantiles of the example distribution derived from a 1000 value sample. The actual underlying distribution is shown by the continuous curve.

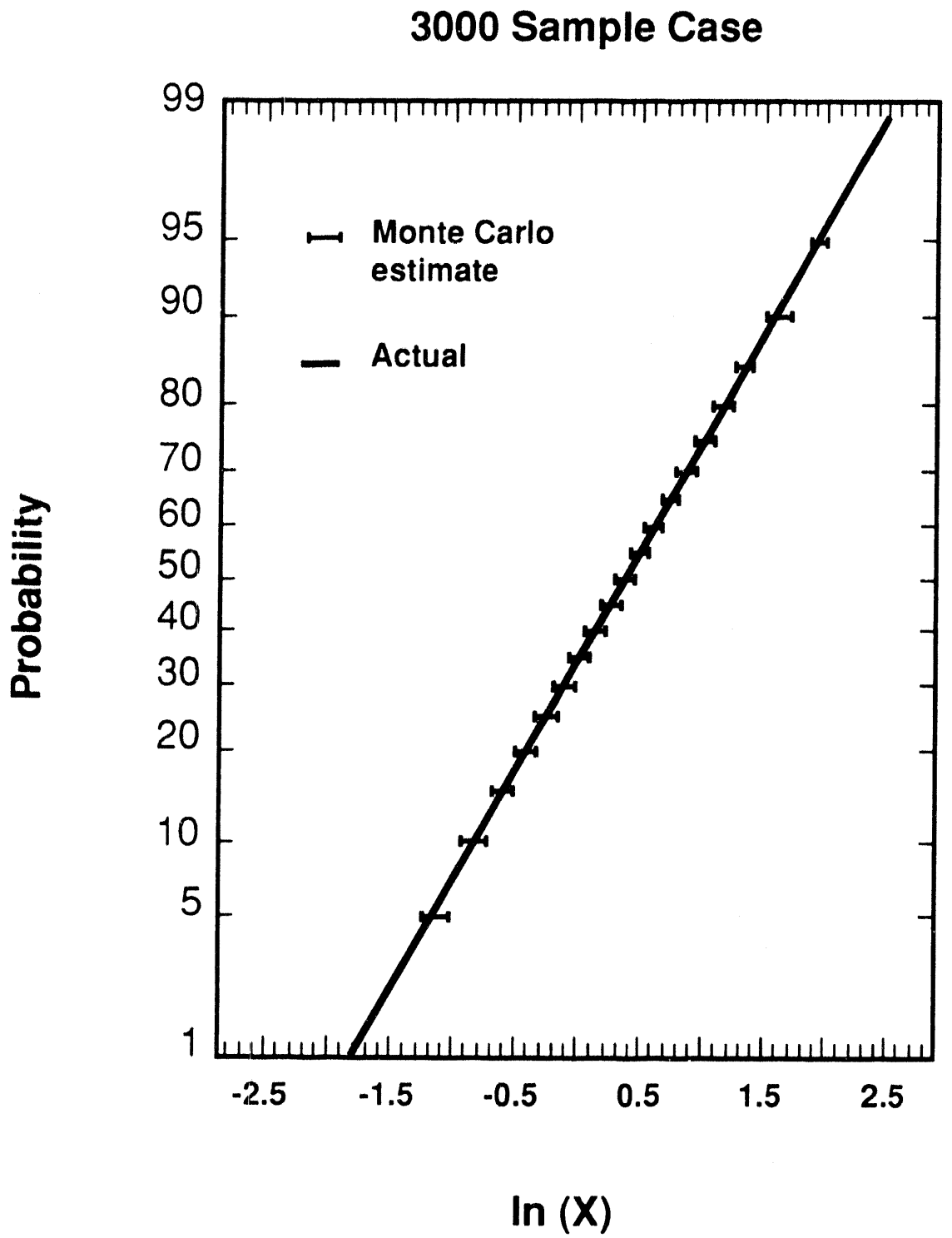

Figure A-4 95 percent confidence intervals for quantiles of the example distribution derived from a 3000 value sample. The actual underlying distribution is shown by the continuous curve.

text. The values listed in Table A-1 can be compared to the number of calculations of values that would be required in a deterministic analysis. For instance, a simple two-level factorial analysis of a problem with 16 uncertain variables would require

$$2^{16} = 65536$$

calculations. A far more complete characterization of the distribution is obtained at fairly high confidence levels with only a few hundred calculations following the Monte Carlo method.

References:

1. R. V. Hogg and A. T. Craig, Introduction to Mathematical Statistics, MacMillan Co.

2. The factorials found in these equations can be accurately calculated for values greater than 10 from:

$$\ln n! = \left[n+\frac{1}{2}\right] \ln(n+1) - n - 1 + \frac{1}{2}\ln(2\pi) + \frac{1}{12(n+1)} - \frac{1}{360(n+)^3} + \frac{1}{1260(n+1)^5} - \frac{1}{1680(n+1)^7}$$

See

M. Abramowitz and I. A. Stegan, Handbook of Mathematical Functions, Dover Publications, 1970.

Appendix B: Detailed Results of the Uncertainty Analyses of Decontamination by an Overlying Water Pool

Results of the Monte Carlo uncertainty analyses for decontamination by an overlying water pool are collected in this appendix. Results are for water pools 30 and 50 cm deep subcooled by 0, 2, 5, 10, 20, 30, 50, and 70°C. The results are shown as cumulative probability distributions at confidence levels of 50, 90, and 95 percent as defined in Appendix A. Tabulated results are shown in the enclosed tables for quantiles of the distribution from 5 to 95 percent at 5 percent intervals. Mean values and standard deviaitons are also shown in the tables.

Table B-1 Summary of results for a saturated pool 30 cm deep

Pool depth (cm)	Pool temp (K)	Quantile (%)	Range for ln DF at a confidence level (%) of		
			50	90	95
30	sat'd	5	0.2264-0.2354	0.2144-0.2482	0.2123-0.2539
		10	0.3032-0.3217	0.2915-0.3348	0.2890-0.3361
		15	0.3668-0.3891	0.3516-0.3966	0.3474-0.3995
		20	0.4201-0.4465	0.4070-0.4583	0.4043-0.4603
		25	0.4830-0.5169	0.4628-0.5332	0.4589-0.5370
		30	0.5518-0.5781	0.5368-0.5929	0.5307-0.5990
		35	0.6110-0.6280	0.5948-0.6416	0.5902-0.6485
Mean =		40	0.6596-0.6861	0.6409-0.7079	0.6391-0.7166
0.928		45	0.7229-0.7478	0.7044-0.7673	0.6997-0.7732
		50	0.7854-0.8158	0.7645-0.8295	0.7600-0.8382
Std. Dev.		55	0.8504-0.8805	0.8267-0.9119	0.8225-0.9255
= 0.586		60	0.9329-0.9689	0.9100-0.9927	0.9051-1.0066
		65	1.0203-1.0476	0.9918-1.0661	0.9843-1.0727
		70	1.0891-1.1254	1.0685-1.1575	1.0617-1.1642
		75	1.1928-1.2400	1.1615-1.2659	1.1555-1.2685
Sample Size		80	1.3188-1.3741	1.2702-1.4104	1.2666-1.4138
= 1000		85	1.4738-1.5207	1.4322-1.5449	1.4202-1.5628
		90	1.7042-1.7496	1.6267-1.8245	1.6159-1.8534
		95	1.9797-2.0714	1.9566-2.1116	1.9486-2.1177

Table B-2 Results for a 30 cm pool with 2 degrees subcooling

Pool depth (cm)	Sub-cooling (K)	Quantile (%)	Range for ln(DF) at a confidence level (%) of		
			50	90	95
30	2	5	1.0257-1.0852	0.9941-1.1612	0.9738-1.1811
		10	1.2581-1.3275	1.2111-1.3854	1.1994-1.3880
		15	1.4488-1.5122	1.3868-1.5770	1.3759-1.5992
		20	1.6158-1.6934	1.5693-1.7319	1.5505-1.7655
		25	1.7675-1.8252	1.7056-1.8673	1.6979-1.8712
Mean =		30	1.8689-1.9311	1.8302-2.0025	1.8185-2.0153
= 2.5024		35	2.0101-2.0562	1.9448-2.0994	1.9139-2.1102
		40	2.0992-2.1741	2.0555-2.2308	2.0426-2.2446
		45	2.2293-2.3129	2.1709-2.3715	2.1478-2.3918
		50	2.3629-2.4250	2.3093-2.4797	2.2841-2.5127
Std. Dev. =		55	2.4779-2.5960	2.4233-2.6368	2.4109-2.6471
= 0.9867		60	2.6315-2.6881	2.5940-2.7510	2.5615-2.7663
		65	2.7510-2.8230	2.6881-2.8827	2.6765-2.9000
		70	2.8852-2.9622	2.8255-3.0398	2.8125-3.0450
		75	3.0407-3.1082	2.9686-3.1780	2.9570-3.2204
Sample Size=		80	3.2251-3.3533	3.1482-3.4288	3.1115-3.4364
= 500		85	3.4903-3.5975	3.4207-3.6856	3.4014-3.6873
		90	3.7549-3.8952	3.6861-3.9945	3.6817-4.0237
		95	4.1755-4.4744	4.0739-4.5574	4.0475-4.6018

Table B-3 Results for a 30 cm deep pool with 5 degrees subcooling

Pool depth (cm)	Sub-cooling (K)	Quantile (%)	Range for ln(DF) at a confidence level (%) of		
			50	90	95
30	2	5	1.5373-1.6335	1.5210-1.6783	1.5129-1.7439
		10	1.8902-1.9810	1.7941-2.0150	1.7893-2.0250
		15	2.0492-2.1081	2.0168-2.1921	2.0050-2.2105
		20	2.2275-2.2749	2.1630-2.3547	2.1221-2.3657
		25	2.3753-2.4100	2.3141-2.4644	2.2766-2.4715
Mean =		30	2.4659-2.6034	2.4257-2.6611	2.4097-2.6723
= 3.2797		35	2.6636-2.7146	2.6071-2.7760	2.5490-2.7970
		40	2.7760-2.8648	2.7138-2.8991	2.6977-2.9266
		45	2.8928-3.0120	2.8637-3.0733	2.8463-3.0904
		50	3.0708-3.1175	3.0027-3.1798	2.9705-3.2119
Std. Dev. =		55	3.1757-3.2879	3.1147-3.3649	3.1071-3.3809
= 1.2323		60	3.3628-3.5007	3.2853-3.5632	3.2622-3.5739
		65	3.5622-3.6447	3.5006-3.7297	3.4503-3.7477
		70	3.7322-3.8668	3.6515-3.9180	3.6215-3.9511
		75	3.9321-4.0614	3.8796-4.0905	3.8620-4.0963
Sample Size =		80	4.0981-4.1963	4.0774-4.2568	4.0630-4.2976
= 500		85	4.3174-4.4735	4.2341-4.6745	4.2134-4.7341
		90	4.7935-4.9239	4.7041-5.1801	4.6312-5.1901
		95	5.3264-5.5741	5.2359-5.8275	5.2254-6.0112

Table B-4 Results for a 30 cm deep pool with 10 degrees subcooling

Pool depth (cm)	Sub-cooling (K)	Quantile (%)	Range for ln(DF) at a confidence level (%) of		
			50	90	95
30	10	5	2.0850-2.1362	2.0321-2.1696	1.9847-2.1887
		10	2.2844-2.3495	2.2236-2.4091	2.2033-2.4176
		15	2.4945-2.5830	2.4148-2.6741	2.3983-2.7137
		20	2.7177-2.8447	2.6495-2.8957	2.6253-2.9217
		25	2.9361-3.0377	2.8550-3.1085	2.8450-3.1215
Mean =		30	3.1168-3.1989	3.0591-3.2653	3.0329-3.2954
= 3.9776		35	3.2725-3.3724	3.2042-3.4207	3.1825-3.4521
		40	3.4195-3.5316	3.3711-3.6125	3.3416-3.6351
		45	3.6106-3.7186	3.5313-3.7957	3.5109-3.8224
		50	3.7884-3.8978	3.7083-3.9601	3.6953-3.9794
Std. Dev. =		55	3.9584-4.0543	3.8955-4.1354	3.8724-4.1496
= 1.3552		60	4.1300-4.2265	4.0504-4.2868	4.0364-4.3196
		65	4.2867-4.4153	4.2265-4.5534	4.2030-4.5801
		70	4.5607-4.6504	4.4380-4.7227	4.3733-4.7329
		75	4.7287-4.8177	4.6656-4.9203	4.6402-4.9981
Sample Size =		80	5.0109-5.1016	4.8387-5.2624	4.8182-5.3399
= 500		85	5.3728-5.5039	5.2001-5.5840	5.1462-5.5996
		90	5.6705-5.7915	5.5855-5.9541	5.5803-5.9787
		95	6.2587-6.5598	6.0905-6.7729	6.0132-6.9426

Table B-5 Results for a 30 cm deep pool with 20 degrees subcooling

Pool depth (cm)	Sub-cooling (K)	Quantile (%)	Range for ln(DF) at a confidence level (%) of		
			50	90	95
30	20	5	2.6347-2.7398	2.5383-2.8428	2.5068-2.8864
		10	3.0192-3.1206	2.9425-3.1907	2.9079-3.2034
		15	3.2568-3.3255	3.1940-3.4021	3.1721-3.4175
		20	3.4377-3.5874	3.3814-3.6365	3.3616-3.6514
		25	3.6521-3.7318	3.6013-3.7989	3.5886-3.8236
Mean =		30	3.8150-3.9267	3.7420-4.0208	3.7262-4.0315
= 4.8443		35	4.0269-4.0907	3.9364-4.2127	3.9109-4.2594
		40	4.2111-4.3187	4.0902-4.3639	4.0748-4.4023
		45	4.3575-4.5125	4.3180-4.5771	4.3083-4.5968
		50	4.5743-4.6779	4.5122-4.7774	4.4785-4.7851
Std. Dev. =		55	4.7740-4.8883	4.6670-4.9425	4.6285-4.9676
= 1.6431		60	4.9380-5.0416	4.8878-5.1318	4.8458-5.1495
		65	5.1313-5.2527	5.0408-5.3464	5.0133-5.3869
		70	5.3521-5.5278	5.2551-5.6537	5.2234-5.6630
		75	5.6575-5.8328	5.5420-5.9024	5.5237-5.9127
Sample Size =		80	5.9134-6.0184	5.8602-6.1186	5.8349-6.1902
= 500		85	6.2049-6.4617	6.0880-6.5898	6.0502-6.6331
		90	6.7291-6.9697	6.6050-7.1592	6.5446-7.1919
		95	7.5790-7.8508	7.3273-8.0699	7.2758-8.2959

Table B-6 Results for a 30 cm deep pool with 30 degrees subcooling

Pool depth (cm)	Sub-cooling (K)	Quantile (%)	Range for ln(DF) at a confidence level (%) of		
			50	90	95
30	30	5	2.9779-3.0352	2.9381-3.1484	2.9058-3.2035
		10	3.3771-3.5028	3.3269-3.5749	3.2715-3.6555
		15	3.7332-3.8961	3.5874-3.9572	3.5662-3.9717
		20	3.9941-4.0576	3.9275-4.1629	3.9069-4.1906
		25	4.1940-4.3134	4.0981-4.3932	4.0600-4.4062
Mean = = 5.4376		30	4.4022-4.5314	4.3306-4.6116	4.2922-4.6335
		35	4.6208-4.7124	4.5345-4.7563	4.5223-4.7851
		40	4.7560-4.8752	4.7106-4.9577	4.6914-4.9632
		45	4.9575-5.0272	4.8566-5.0995	4.8321-5.1384
		50	5.0977-5.2478	5.0240-5.3400	5.0062-5.3761
Std. Dev. = = 1.7468		55	5.3385-5.4562	5.2467-5.5309	5.2222-5.5743
		60	5.5298-5.6807	5.4524-5.7874	5.4064-5.8436
		65	5.7863-5.9235	5.6802-6.0494	5.6519-6.0771
		70	6.0515-6.1883	5.9298-6.2800	5.8964-6.3282
		75	6.3195-6.4185	6.1971-6.5623	6.1774-6.6045
Sample Size = = 500		80	6.6173-6.8605	6.4811-6.9937	6.4407-7.0165
		85	7.0453-7.1639	6.9697-7.2634	6.9370-7.3101
		90	7.4124-7.7175	7.2795-7.9798	7.2528-8.0105
		95	8.3130-8.6026	8.1195-8.7214	8.0512-8.7538

Table B-7 Results for a 30 cm deep pool with 50 degrees subcooling

Pool depth (cm)	Sub-cooling (K)	Quantile (%)	Range for ln(DF) at a confidence level (%) of		
			50	90	95
30	50	5	3.3845-3.4949	3.2113-3.7281	3.2023-3.7483
		10	3.9292-4.0371	3.8181-4.0992	3.8012-4.1233
		15	4.1895-4.3306	4.1074-4.4489	4.0898-4.4806
		20	4.5394-4.6987	4.4248-4.7990	4.3415-4.8269
		25	4.8318-4.9420	4.7443-5.0172	4.6994-5.0422
Mean =		30	5.0392-5.0979	4.9508-5.1337	4.9272-5.1559
= 6.1298		35	5.1356-5.2794	5.0983-5.3743	5.0942-5.3849
		40	5.3743-5.4952	5.2770-5.6030	5.2416-5.6413
		45	5.6009-5.7182	5.4912-5.7921	5.4563-5.8056
		50	5.7907-5.8814	5.7123-5.9605	5.6871-5.9889
Std. Dev. =		55	5.9489-6.0682	5.8780-6.1986	5.8580-6.2536
= 1.9380		60	6.1882-6.3343	6.0673-6.4419	6.0200-6.4851
		65	6.4392-6.6593	6.3341-6.7734	6.2758-6.8136
		70	6.7872-6.9641	6.6663-7.1096	6.6220-7.1250
		75	7.1219-7.1979	6.9931-7.3482	6.9330-7.4932
Sample Size =		80	7.4948-7.6300	7.2440-7.7231	7.2004-7.7953
= 500		85	7.8153-8.0135	7.6916-8.3703	7.6536-8.4072
		90	8.4943-8.6151	8.3760-8.7992	8.1916-8.9859
		95	9.3548-9.?350	9.1332-10.5710	9.0560-10.6971

Table B-8 Results for a 30 cm deep pool with 70 degrees subcooling

Pool depth (cm)	Sub-cooling (K)	Quantile (%)	Range for ln(DF) at a confidence level (%) of		
			50	90	95
30	70	5	3.3027-3.3830	3.2045-3.4768	3.1998-3.5083
		10	3.7114-3.8132	3.5725-3.9342	3.5353-3.9765
		15	4.0950-4.2563	3.9511-4.3468	3.9168-4.3890
		20	4.4233-4.5492	4.3352-4.6987	4.2830-4.7625
		25	4.7825-4.9973	4.6032-5.0504	4.5548-5.0754
Mean =		30	5.0548-5.1541	5.0050-5.2112	4.9818-5.2349
= 6.2685		35	5.2204-5.3896	5.1570-5.4512	5.1443-5.4702
		40	5.4511-5.5326	5.3889-5.6179	5.3721-5.6452
		45	5.6156-5.7374	5.5279-5.7946	5.4959-5.8645
		50	5.7892-5.9429	5.7356-6.0294	5.7062-6.0547
Std. Dev. =		55	6.0133-6.1635	5.9331-6.2253	5.9184-6.2597
= 2.3913		60	6.2221-6.3566	6.1630-6.5356	6.1396-6.5709
		65	6.5319-6.7318	6.3558-6.7987	6.3349-6.8278
		70	6.8022-6.9888	6.7390-7.1184	6.6929-7.1428
		75	7.1308-7.3062	7.0013-7.5420	6.9848-7.6333
Sample Size =		80	7.6359-7.9165	7.4235-8.0845	7.3269-8.1274
= 500		85	8.1484-8.3169	8.0539-8.5225	7.9710-8.5505
		90	8.7262-9.0258	8.5337-9.3989	8.5010-9.5258
		95	9.8988-10.2119	9.7265-10.6287	9.6539-10.7503

Table B-9 Summary of results for a saturated pool 50 cm deep

Pool depth (cm)	Pool temp. (K)	Quantile (%)	Range for ln DF at a confidence level (%) of		
			50	90	95
50	sat'd	5	0.3525-0.3712	0.3402-0.3805	0.3393-0.3823
		10	0.4629-0.4754	0.4419-0.4885	0.4362-0.4909
		15	0.5382-0.5614	0.5223-0.5749	0.5177-0.5815
		20	0.6141-0.6416	0.6031-0.6587	0.6004-0.6623
		25	0.7012-0.7202	0.6767-0.7348	0.6707-0.7450
Mean		30	0.7699-0.7928	0.7357-0.8086	0.7484-0.8143
=		35	0.8361-0.8626	0.8203-0.8804	0.8176-0.8855
		40	0.9068-0.9270	0.8932-0.9437	0.8855-0.9536
		45	0.9802-1.0038	0.9578-1.0227	0.9508-1.0316
		50	1.0511-1.0763	1.0365-1.0925	1.0302-1.0979
Std. Dev. =		55	1.1281-1.1636	1.0994-1.1850	1.0974-1.2030
		60	1.2318-1.2660	1.2071-1.2921	1.2002-1.2990
		65	1.3272-1.3633	1.3052-1.3810	1.2991-1.2906
		70	1.4194-1.4552	1.3987-1.4769	1.3918-1.4863
		75	1.5328-1.5750	1.5035-1.6030	1.4934-1.6063
Sample Size					
= 1455		80	1.7091-1.7659	1.6507-1.7918	1.6482-1.8010
		85	1.8747-1.9569	1.8427-1.9975	1.8306-2.0150
		90	2.1647-2.2469	2.1050-2.3269	2.0951-2.3399
		95	2.5977-2.7028	2.5281-2.7375	2.5156-2.7529

Table B-10 Results for a 50 cm deep pool with 2 degrees subcooling

Pool depth (cm)	Sub-cooling (K)	Quantile (%)	Range for ln(DF) at a confidence level (%) of		
			50	90	95
50	2	5	1.3659-1.3889	1.3350-1.4337	1.3156-1.4389
		10	1.5577-1.6100	1.4652-1.6618	1.4463-1.6838
		15	1.7519-1.8133	1.6671-1.8628	1.6551-1.8831
		20	1.8920-1.9600	1.8279-2.0160	1.8215-2.0690
		25	2.0819-2.1342	1.9909-2.1936	1.9610-2.2067
Mean = = 2.9413		30	2.2055-2.2676	2.1453-2.3246	2.1325-2.3464
		35	2.3333-2.3919	2.2695-2.4247	2.2553-2.4386
		40	2.4247-2.5097	2.3915-2.5814	2.3843-2.5955
		45	2.5801-2.6354	2.4905-2.7073	2.4784-2.7279
		50	2.7048-2.7805	2.6288-2.8377	2.6215-2.8508
Std. Dev. = = 1.2085		55	2.8341-2.8975	2.7781-2.9912	2.7565-3.0369
		60	2.9812-3.1059	2.8968-3.1549	2.8766-3.1750
		65	3.1521-3.2584	3.1056-3.3155	3.0919-3.3512
		70	3.3169-3.4360	3.2648-3.5164	3.2407-3.5517
		75	3.5341-3.6894	3.4660-3.7573	3.4216-3.7854
Sample Size = = 500		80	3.7871-3.8553	3.7066-4.0302	3.6921-4.0435
		85	4.0527-4.1490	3.9509-4.2475	3.8835-4.2826
		90	4.3327-4.4848	4.2535-4.5795	4.2347-4.6509
		95	4.9590-5.2124	4.8064-5.5113	4.7482-5.7450

Table B-11 Results for a 50 cm deep pool with 5 degrees subcooling

Pool depth (cm)	Sub-cooling (K)	Quantile (%)	Range for ln(DF) at a confidence level (%) of		
			50	90	95
50	5	5	1.8375-1.9170	1.7369-1.9426	1.7332-1.9566
		10	2.0554-2.1692	1.9907-2.2740	1.9766-2.2885
		15	2.3632-2.4497	2.2853-2.5103	2.2175-2.5417
		20	2.5760-2.6734	2.4896-2.7193	2.4705-2.7396
		25	2.7401-2.8545	2.6840-2.9037	2.6736-2.9320
Mean = = 3.7644		30	2.9206-2.9856	2.8619-3.0453	2.8301-3.0698
		35	3.0493-3.1560	2.9962-3.1970	2.9766-3.2210
		40	3.1967-3.2975	3.1552-3.3895	3.1214-3.4340
		45	3.3700-3.4962	3.2908-3.5328	3.2808-3.5466
		50	3.5281-3.6559	3.4957-3.7443	3.4758-3.7656
Std. Dev. = = 1.3447		55	3.7408-3.8356	3.6427-3.8898	3.6031-3.9090
		60	3.8883-3.9825	3.8271-4.0534	3.8070-4.0701
		65	4.0530-4.2045	3.9825-4.3215	3.9453-4.3732
		70	4.3366-4.4367	4.2088-4.5298	4.2000-4.5911
		75	4.5643-4.6775	4.4401-4.7370	4.4321-4.7553
Sample Size = = 500		80	4.7570-4.8597	4.6973-4.9217	4.6776-4.9328
		85	4.9969-5.2619	4.9088-5.3842	4.8810-5.4393
		90	5.5344-5.6614	5.4022-5.8733	5.3691-5.9016
		95	6.1494-6.3807	6.0455-6.5367	5.9789-6.5692

Table B-12 Results for a 50 cm deep pool with 10 degrees subcooling

Pool depth (cm)	Sub-cooling (K)	Quantile (%)	Range for ln(DF) at a confidence level (%) of		
			50	90	95
50	10	5	2.3539-2.4919	2.2108-2.5785	2.1557-2.5910
		10	2.7134-2.8351	2.6093-2.9217	2.5992-2.9428
		15	2.999-3.1200	2.9302-3.2129	2.9011-3.2471
		20	3.2612-3.3757	3.1588-3.4521	3.1350-3.4776
		25	3.4805-3.5738	3.4169-3.6180	3.3833-3.6368
Mean =		30	3.6246-3.7397	3.5852-3.8249	3.5698-3.8722
= 4.6346		35	3.8293-3.9660	3.7506-4.0281	3.7301-4.0439
		40	4.0277-4.1252	3.9658-4.1966	3.9530-4.2474
		45	4.1933-4.2944	4.1225-4.3839	4.1142-4.4087
		50	4.3825-4.4949	4.2929-4.5726	4.2769-4.5875
Std. Dev. =		55	4.5596-4.6625	4.4942-4.7690	4.4793-4.7944
= 1.6077		60	4.7619-4.8707	4.6603-4.9900	4.6321-5.0060
		65	4.9884-5.1080	4.8707-5.1621	4.8615-5.1812
		70	5.1674-5.2976	5.1193-5.4006	5.0810-5.4260
		75	5.4039-5.6399	5.3402-5.7857	5.2907-5.8469
Sample Size =		80	5.8566-5.9593	5.7161-5.9987	5.6463-6.0477
= 500		85	6.0748-6.2124	5.9880-6.4273	5.9769-6.4549
		90	6.5519-6.6764	6.4373-6.9502	6.3408-7.0046
		95	7.2270-7.6409	7.1663-7.9425	7.1024-7.9884

Table B-13 Results for a 50 cm deep pool with 20 degrees subcooling

Pool depth (cm)	Sub-cooling (K)	Quantile (%)	Range for ln(DF) at a confidence level (%) of		
			50	90	95
50	20	5	2.6821-2.8589	2.6265-2.9573	2.5903-2.9762
		10	3.1933-3.3115	3.0929-3.4076	3.0300-3.4445
		15	3.5537-3.7511	3.4235-3.7984	3.3922-3.8178
		20	3.8411-3.9427	3.7882-4.0153	3.7680-4.0374
		25	4.0414-4.1843	3.9727-4.2715	3.9466-4.2940
Mean =		30	4.2822-4.4249	4.2030-4.5547	4.1651-4.5951
= 5.5245		35	4.5746-4.6450	4.4293-4.7271	4.4026-4.7575
		40	4.7265-4.8574	4.6437-4.9356	4.6240-4.9627
		45	4.9339-5.0749	4.8548-5.0980	4.8386-5.1195
		50	5.0951-5.2448	5.0562-5.3978	5.0208-5.4725
Std. Dev. =		55	5.3887-5.6161	5.2430-5.6858	5.2255-5.7316
= 2.0147		60	5.6755-5.8010	5.5947-5.8801	5.5393-5.9264
		65	5.8781-6.0302	5.8002-6.1730	5.7762-6.1968
		70	6.1751-6.2983	6.0376-6.5530	6.0079-6.5842
		75	6.5445-6.8054	6.3185-6.9905	6.2830-7.0012
Sample Size =		80	7.0019-7.1165	6.8716-7.3138	6.8068-7.3186
= 500		85	7.3324-7.4754	7.2611-7.7264	7.2409-7.8019
		90	7.8994-8.1412	7.7528-8.2354	7.6376-8.3488
		95	8.6196-9.0436	8.5191-9.7546	8.4695-9.9856

Table B-14 Results for a 50 cm deep pool with 30 degrees subcooling

Pool depth (cm)	Sub-cooling (K)	Quantile (%)	Range for ln(DF) at a confidence level (%) of		
			50	90	95
50	30	5	3.1952-3.2875	3.1241-3.3776	3.1127-3.4077
		10	3.6486-3.8498	3.4996-3.9106	3.4312-3.9227
		15	4.0447-4.1304	3.9134-4.1723	3.9010-4.2068
		20	4.2683-4.3837	4.1526-4.4785	4.1472-4.5174
		25	4.5222-4.6568	4.4409-4.7591	4.3852-4.8221
Mean = = 5.9125		30	4.7933-4.9559	4.6929-5.0378	4.6531-5.0586
		35	5.0396-5.1507	4.9589-5.2356	4.9218-5.2615
		40	5.2354-5.3638	5.1501-5.4698	5.1388-5.4929
		45	5.4610-5.6025	5.3525-5.6575	5.3203-5.6845
		50	5.6469-5.7914	5.5588-5.8551	5.5321-5.8800
Std. Dev. = = 1.9181		55	5.8538-5.9509	5.7863-6.0039	5.7473-6.0389
		60	6.0034-6.1567	5.9475-6.2434	5.9263-6.2700
		65	6.2428-6.3659	6.1560-6.5450	6.0799-6.6080
		70	6.5482-6.7791	6.3736-6.8286	6.3497-6.8499
		75	6.8340-7.0403	6.7988-7.1326	6.7633-7.1757
Sample Size = = 500		80	7.1766-7.4141	7.0594-7.5486	7.0412-7.6113
		85	7.6568-7.8402	7.5167-8.0184	7.4584-8.0489
		90	8.1099-8.3041	8.0362-8.5868	8.0007-8.6305
		95	9.0330-9.4238	8.7304-9.5990	8.6665-9.6518

Table B-15 Results for a 50 cm deep pool with 50 degrees subcooling

Pool depth (cm)	Sub-cooling (K)	Quantile (%)	Range for ln(DF) at a confidence level (%) of		
			50	90	95
50	50	5	3.5955-3.7463	3.4620-3.8611	3.4008-3.8757
		10	4.0290-4.1873	3.9472-4.2385	3.8972-4.2506
		15	4.4203-4.5973	4.2452-4.7099	4.2263-4.7235
		20	4.7695-4.9482	4.6884-5.0877	4.6506-5.1087
		25	5.1095-5.2601	5.0145-5.3882	4.9486-5.4115
Mean =		30	5.4092-5.5023	5.2757-5.6100	5.2560-5.6615
= 6.9015		35	5.6308-5.7628	5.5115-5.8638	5.4880-5.9031
		40	5.8638-6.0270	5.7624-6.1575	5.7518-6.1873
		45	6.1561-6.2937	6.0159-6.4312	5.9820-6.4736
		50	6.4307-6.5659	6.2867-6.7004	6.2682-6.7163
Std. Dev. =		55	6.6930-6.7883	6.5609-6.9479	6.5370-7.0126
= 2.7161		60	6.9416-7.1590	6.7747-7.3125	6.7359-7.3266
		65	7.3114-7.4201	7.1566-7.5848	7.0955-7.6529
		70	7.5868-7.8314	7.4227-8.0317	7.4036-8.0648
		75	8.0500-8.2038	7.8774-8.3263	7.7748-8.3989
Sample Size =		80	8.4019-8.6177	8.2476-8.7365	8.2116-8.7603
= 500		85	8.8977-9.0595	8.7161-9.3008	8.6476-9.3544
		90	9.4390-10.1692	9.3374-10.4523	9.2363-10.6419
		95	11.1363-11.7915	10.7847-12.0537	10.7063-12.2857

Table B-16 Results for a 50 cm deep pool with 70 degrees subcooling

Pool depth (cm)	Sub-cooling (K)	Quantile (%)	Range for ln(DF) at a confidence level (%) of		
			50	90	95
50	70	5	3.8315-4.0895	3.6110-4.2238	3.5782-4.3633
		10	4.5572-4.8263	4.3884-4.9852	4.2368-5.0320
		15	5.0411-5.1829	4.9309-5.3146	4.8410-5.3832
		20	5.3427-5.5712	5.2240-5.6406	5.1558-5.6593
		25	5.6381-5.7291	5.5604-5.9033	5.5244-5.9209
Mean =		30	5.8943-6.1627	5.7250-6.2422	5.6955-6.3451
= 7.7924		35	6.2155-6.5148	6.0860-6.6834	5.9778-6.7047
		40	6.6387-6.7932	6.4203-6.9270	6.3663-6.9729
		45	6.8950-7.0522	6.7469-7.1433	6.7027-7.2037
		50	7.1014-7.2417	6.9867-7.3856	6.9395-7.4254
Std. Dev. =		55	7.3402-7.5045	7.2171-7.6119	7.1856-7.6659
= 3.5256		60	7.5512-7.8159	7.4665-8.0150	7.4155-8.0574
		65	7.9304-8.2269	7.6843-8.3344	7.6659-8.4080
		70	8.2603-8.6093	8.1902-8.7249	8.0720-8.7860
		75	8.7077-9.0308	8.5621-9.2267	8.4891-9.3086
Sample Size =		80	9.2093-9.4807	9.0217-9.6231	8.9516-9.7032
= 360		85	9.6563-9.9369	9.4994-10.2462	9.4567-10.2803
		90	10.2879-11.2271	10.0721-12.4243	10.0132-12.7523
		95	13.2847-14.1425	12.7569-15.6067	12.5553-16.6816

Appendix C: Uncertainty Distributions for the Spray Decontamination Coefficient

Detailed uncertainty distributions for the spray decontamination coefficient, $\lambda(hr^{-1})$, are presented in the tables of this appendix. Uncertainty distributions were calculated for total water fluxes of 0.002, 0.01, and 0.25 cm^3 H_2O/cm^2-s and fractions of the initial aerosol remaining in the atmosphere of 0.9, 0.5, 0.3, 0.1, 0.01, and 0.001. The distributions are calculated for confidence levels of 50, 90, and 95 percent. That is, percentiles of a cumulative probability distribution are defined by a range of values of λ. Ranges such that there is a 50, 90, or 95 percent confidence that the true value of λ characteristic of the specified percentile lies within the range are given. Percentiles of 5 to 95 percent at 5 percent intervals are tabulated. Means and standard deviations for the distributions are also given, though for these distributions neither of these quantities is especially useful.

Table C-1 Uncertainty distributions for λ(total) for Mark-1 drywell sprays

Aerosol mass fraction remaining	Total water flux (cm/s)	Quantile (%)	Range for λ(total) at a confidence level of 95%	90%	50%	
0.9	0.25	5	3.717 - 5.285	3.904 - 5.145	4.373 - 5.010	MEAN =
		10	5.264 - 7.126	5.372 - 7.050	5.988 - 6.567	= 32.974 hr^{-1}
		15	6.787 - 8.739	6.917 - 8.454	7.326 - 7.902	
		20	7.881 - 10.301	8.182 - 10.118	8.768 - 9.424	
		25	9.288 - 11.486	9.440 - 11.320	10.175 - 11.115	
		30	10.678 - 14.248	11.018 - 14.114	11.310 - 13.071	STD. DEV. =
		35	12.107 - 15.409	12.643 - 15.256	14.024 - 14.724	= 45.312
		40	14.415 - 16.429	14.604 - 16.177	15.154 - 15.577	
		45	15.454 - 18.589	15.532 - 18.510	16.058 - 17.150	
		50	16.512 - 20.130	16.964 - 20.004	18.023 - 19.221	
		55	18.811 - 22.388	19.153 - 22.037	19.778 - 20.924	SAMPLE SIZE =
		60	20.225 - 24.766	20.582 - 24.313	21.655 - 23.344	= 400
		65	22.423 - 28.617	22.850 - 28.110	24.131 - 26.313	
		70	25.067 - 32.834	25.429 - 32.157	27.705 - 30.148	
		75	29.182 - 39.510	30.052 - 37.414	32.048 - 34.866	
		80	34.679 - 49.994	34.982 - 48.893	37.663 - 46.056	
		85	46.180 - 66.140	47.483 - 64.951	49.924 - 54.568	
		90	59.025 - 89.060	63.239 - 82.164	67.231 - 73.509	
		95	87.961 - 136.701	93.885 - 156.147	104.554 - 138.851	

Table C-2 Uncertainty distributions for λ(total) for Mark-1 drywell sprays

Aerosol mass fraction remaining	Total water flux (cm/s)	Quantile (%)	Range for λ(total) at a confidence level of 95%	90%	50%	
0.5	0.25	5	3.653 - 5.106	3.845 - 4.968	4.110 - 4.679	MEAN =
		10	5.050 - 6.512	5.218 - 6.444	5.693 - 5.947	= 27.013 hr^{-1}
		15	6.134 - 7.745	6.392 - 7.547	6.716 - 7.117	
		20	7.116 - 9.085	7.255 - 8.839	7.780 - 8.568	
		25	8.409 - 10.669	8.578 - 10.256	8.885 - 10.026	
		30	9.757 - 11.895	9.971 - 11.807	10.242 - 11.158	STD. DEV. =
		35	10.946 - 13.144	11.065 - 13.066	11.798 - 12.207	= 34.606
		40	12.028 - 14.079	12.115 - 13.955	12.939 - 13.370	
		45	13.169 - 15.321	13.326 - 15.175	13.709 - 14.386	
		50	14.123 - 16.889	14.275 - 16.579	14.846 - 15.862	
		55	15.330 - 18.414	15.482 - 18.320	16.432 - 17.247	SAMPLE SIZE =
		60	16.991 - 20.276	17.070 - 19.985	18.065 - 18.843	= 400
		65	18.490 - 23.143	18.747 - 22.734	19.782 - 21.622	
		70	20.771 - 26.824	21.509 - 26.466	22.512 - 24.337	
		75	23.816 - 33.063	24.321 - 31.638	26.307 - 29.433	
		80	28.719 - 43.897	29.519 - 40.690	32.022 - 35.300	
		85	35.347 - 53.402	36.147 - 50.900	43.692 - 47.411	
		90	49.252 - 77.782	50.098 - 73.841	54.452 - 61.292	
		95	77.682 -135.057	79.399 -133.113	87.935 -109.815	

Table C-3 Uncertainty distributions for λ(total) for Mark-1 drywell sprays

Aerosol mass fraction remaining	Total water flux (cm/s)	Quantile (%)	Range for λ(total) at a confidence Level of 95%	90%	50%	
0.3	0.25	5	3.472 - 5.029	3.638 - 4.817	3.878 - 4.463	MEAN =
		10	5.026 - 6.039	5.047 - 5.984	5.293 - 5.670	= 24.003 hr^{-1}
		15	5.852 - 7.242	5.921 - 6.947	6.139 - 6.739	
		20	6.739 - 8.451	6.750 - 8.264	7.260 - 7.942	
		25	7.863 - 9.738	7.968 - 9.633	8.287 - 8.909	
		30	8.626 - 10.502	8.856 - 10.456	9.603 - 9.908	STD. DEV. =
		35	9.815 - 11.488	9.889 - 11.398	10.316 - 10.991	= 29.962
		40	10.835 - 12.496	10.928 - 12.362	11.354 - 11.968	
		45	11.561 - 13.577	11.706 - 13.443	12.170 - 12.916	
		50	12.678 - 14.845	12.804 - 14.688	13.297 - 14.136	
		55	13.604 - 16.295	13.790 - 15.959	14.640 - 15.242	SAMPLE SIZE =
		60	14.881 - 18.428	15.076 - 18.191	15.783 - 16.859	= 400
		65	16.357 - 20.337	16.608 - 19.970	17.830 - 19.367	
		70	18.821 - 23.997	19.168 - 23.499	19.888 - 21.529	
		75	21.165 - 28.811	21.501 - 28.411	23.457 - 25.996	
		80	25.772 - 37.061	26.105 - 36.235	28.443 - 30.243	
		85	30.317 - 46.776	31.616 - 45.461	37.034 - 44.050	
		90	44.799 - 69.293	45.028 - 66.335	47.981 - 56.768	
		95	69.135 -123.433	70.458 -120.289	80.067 - 93.519	

Table C-4 Uncertainty distributions for λ(total) for Mark-1 drywell sprays

Aerosol mass fraction remaining	Total water flux (cm/s)	Quantile (%)	Range for λ(total) at a confidence level of			
			95%	90%	50%	
0.1	0.25	5	3.279 - 4.484	3.373 - 4.398	3.780 - 4.052	MEAN =
		10	4.457 - 5.421	4.628 - 5.364	4.827 - 5.130	= 20.381 hr^{-1}
		15	5.213 - 6.450	5.334 - 6.276	5.544 - 5.928	
		20	5.921 - 7.308	6.106 - 7.226	6.455 - 6.841	
		25	6.785 - 8.186	6.913 - 7.960	7.240 - 7.723	
		30	7.558 - 8.848	7.717 - 8.732	7.958 - 8.461	STD. DEV. =
		35	8.269 - 9.763	8.276 - 9.642	8.691 - 9.320	= 25.015
		40	8.912 - 10.599	9.235 - 10.527	9.585 - 10.282	
		45	9.823 - 11.321	10.052 - 11.170	10.421 - 10.841	
		50	10.611 - 12.761	10.744 - 12.399	11.030 - 11.690	
		55	11.422 - 14.106	11.465 - 13.517	12.010 - 13.011	SAMPLE SIZE =
		60	12.800 - 15.572	12.946 - 15.166	13.417 - 14.621	= 400
		65	14.128 - 17.542	14.331 - 17.308	15.042 - 16.511	
		70	15.892 - 20.319	16.361 - 20.118	17.016 - 18.281	
		75	17.893 - 23.997	18.236 - 23.488	20.069 - 21.671	
		80	21.477 - 31.851	21.827 - 30.356	23.582 - 26.412	
		85	26.506 - 42.506	27.271 - 41.448	31.700 - 35.176	
		90	36.982 - 56.597	38.817 - 55.199	44.975 - 52.013	
		95	56.217 - 99.002	57.249 - 93.671	72.571 - 78.573	

Table C-5 Uncertainty distributions for λ(total) for Mark-1 drywell sprays

Aerosol mass fraction remaining	Total water flux (cm/s)	Quantile (%)	Range for λ(total) at a confidence level of			
			95%	90%	50%	
0.01	0.25	5	2.872 - 3.926	2.880 - 3.835	3.280 - 3.595	MEAN =
		10	3.896 - 4.671	3.981 - 4.627	4.194 - 4.420	= 17.181 hr^{-1}
		15	4.544 - 5.171	4.597 - 5.149	4.701 - 5.053	
		20	5.052 - 5.964	5.096 - 5.729	5.175 - 5.459	
		25	5.408 - 6.641	5.478 - 6.578	5.745 - 6.161	
		30	6.102 - 7.413	6.137 - 7.250	6.560 - 7.091	STD. DEV. =
		35	6.800 - 8.046	7.018 - 7.912	7.212 - 7.644	= 21.393
		40	7.534 - 8.814	7.600 - 8.774	7.796 - 8.364	
		45	8.137 - 9.645	8.268 - 9.449	8.662 - 9.150	
		50	8.872 - 10.395	9.101 - 10.308	9.328 - 9.883	
		55	9.645 - 11.733	9.714 - 11.428	10.200 - 10.662	SAMPLE SIZE =
		60	10.482 - 12.938	10.623 - 12.835	11.210 - 12.216	= 400
		65	11.941 - 15.079	12.087 - 14.602	12.685 - 13.762	
		70	13.172 - 17.129	13.630 - 16.871	14.343 - 16.169	
		75	15.813 - 21.110	16.150 - 19.962	16.760 - 18.131	
		80	17.878 - 25.562	18.329 - 25.251	20.054 - 23.173	
		85	23.228 - 36.800	23.844 - 35.180	25.536 - 28.700	
		90	32.079 - 50.010	36.621 - 46.118	39.840 - 44.110	
		95	48.580 - 78.193	51.188 - 74.809	54.510 - 64.720	

Table C-6 Uncertainty distributions for λ(total) for Mark-1 drywell sprays

Aerosol mass fraction remaining	Total water flux (cm/s)	Quantile (%)	Range for λ(total) at a confidence level of			
			95%	90%	50%	
0.001	0.25	5	2.583 - 3.623	2.700 - 3.547	2.957 - 3.280	MEAN =
		10	3.610 - 4.218	3.654 - 4.175	3.844 - 4.038	= 15.852 hr^{-1}
		15	4.101 - 4.690	4.125 - 4.678	4.260 - 4.528	
		20	4.527 - 5.211	4.563 - 5.148	4.692 - 4.948	
		25	4.905 - 5.945	4.960 - 5.887	5.168 - 5.736	
		30	5.573 - 6.644	5.705 - 6.600	5.883 - 6.331	STD. DEV. =
		35	6.194 - 7.178	6.275 - 7.135	6.537 - 6.907	= 20.078
		40	6.779 - 7.987	6.838 - 7.933	7.076 - 7.511	
		45	7.253 - 8.827	7.377 - 8.736	7.756 - 8.181	
		50	8.024 - 9.661	8.086 - 9.545	8.516 - 9.182	
		55	8.871 - 10.667	9.004 - 10.518	9.430 - 9.932	SAMPLE SIZE =
		60	9.676 - 11.876	9.738 - 11.823	10.390 - 11.249	= 400
		65	10.827 - 13.865	10.987 - 13.752	11.689 - 12.542	
		70	12.296 - 15.943	12.481 - 15.769	13.726 - 14.480	
		75	14.175 - 19.135	14.372 - 18.708	15.728 - 17.272	
		80	17.012 - 23.512	17.320 - 22.918	18.811 - 21.143	
		85	21.170 - 34.422	21.721 - 32.662	23.505 - 26.582	
		90	29.718 - 45.458	31.005 - 44.006	34.869 - 41.148	
		95	45.192 - 74.010	46.100 - 71.079	49.578 - 59.749	

Table C-7 Uncertainty distributions for λ(total) for Mark-I drywell sprays

Aerosol mass fraction remaining	Total water flux (cm/s)	Quantile (%)	Range for λ(total) at a confidence level of 95%	Range for λ(total) at a confidence level of 90%	Range for λ(total) at a confidence level of 50%	
0.9	0.01	5	0.259 - 0.370	0.262 - 0.365	0.312 - 0.357	MEAN =
		10	0.368 - 0.448	0.374 - 0.443	0.388 - 0.423	= 1.587 hr^{-1}
		15	0.436 - 0.536	0.440 - 0.533	0.452 - 0.488	
		20	0.487 - 0.589	0.514 - 0.585	0.537 - 0.560	
		25	0.560 - 0.682	0.560 - 0.656	0.586 - 0.623	
		30	0.610 - 0.772	0.619 - 0.770	0.655 - 0.713	STD. DEV. =
		35	0.697 - 0.863	0.702 - 0.860	0.754 - 0.805	= 1.568
		40	0.780 - 0.949	0.800 - 0.937	0.847 - 0.899	
		45	0.864 - 1.041	0.882 - 1.029	0.922 - 0.993	
		50	0.964 - 1.223	0.984 - 1.169	1.020 - 1.108	
		55	1.058 - 1.332	1.078 - 1.321	1.130 - 1.279	SAMPLE SIZE =
		60	1.226 - 1.471	1.251 - 1.456	1.311 - 1.396	= 400
		65	1.357 - 1.662	1.377 - 1.624	1.448 - 1.538	
		70	1.503 - 1.936	1.519 - 1.880	1.600 - 1.765	
		75	1.709 - 2.157	1.762 - 2.142	1.861 - 2.001	
		80	1.968 - 2.560	2.013 - 2.489	2.143 - 2.317	
		85	2.318 - 3.190	2.337 - 3.098	2.555 - 2.767	
		90	3.005 - 4.126	3.044 - 4.046	3.385 - 3.736	
		95	4.114 - 5.502	4.178 - 5.408	4.358 - 4.945	

Table C-8 Uncertainty distributions for λ(total) for Mark-1 drywell sprays

Aerosol mass fraction remaining	Total water flux (cm/s)	Quantile (%)	Range for λ(total) at a confidence level of			
			95%	90%	50%	
0.5	0.01	5	0.230 - 0.353	0.246 - 0.347	0.289 - 0.319	MEAN =
		10	0.353 - 0.412	0.355 - 0.406	0.366 - 0.388	= 1.344 hr^{-1}
		15	0.395 - 0.468	0.400 - 0.465	0.427 - 0.447	
		20	0.446 - 0.537	0.449 - 0.516	0.468 - 0.490	
		25	0.485 - 0.594	0.492 - 0.587	0.524 - 0.559	
		30	0.552 - 0.671	0.557 - 0.661	0.585 - 0.613	STD. DEV. =
		35	0.602 - 0.739	0.609 - 0.722	0.635 - 0.695	= 1.312
		40	0.684 - 0.809	0.690 - 0.799	0.714 - 0.776	
		45	0.742 - 0.893	0.766 - 0.887	0.797 - 0.859	
		50	0.827 - 0.999	0.850 - 0.982	0.877 - 0.925	
		55	0.897 - 1.081	0.916 - 1.142	0.975 - 1.071	SAMPLE SIZE =
		60	1.003 - 1.208	1.046 - 1.257	1.122 - 1.199	= 400
		65	1.161 - 1.365	1.188 - 1.356	1.226 - 1.289	
		70	1.273 - 1.567	1.280 - 1.532	1.342 - 1.465	
		75	1.414 - 1.777	1.465 - 1.752	1.518 - 1.637	
		80	1.606 - 2.128	1.647 - 2.066	1.755 - 1.956	
		85	1.959 - 2.630	1.982 - 2.585	2.128 - 2.446	
		90	2.538 - 3.419	2.579 - 3.284	2.698 - 3.035	
		95	3.379 - 5.054	3.553 - 4.641	3.653 - 4.249	

Table C-9 Uncertainty distributions for λ(total) for Mark-1 drywell sprays

Aerosol mass fraction remaining	Total water flux (cm/s)	Quantile (%)	Range for λ(total) at a confidence level of 95%	90%	50%	
0.3	0.01	5	0.219 - 0.316	0.234 - 0.305	0.246 - 0.293	MEAN =
		10	0.315 - 0.385	0.332 - 0.379	0.346 - 0.365	= 1.213 hr^{-1}
		15	0.367 - 0.433	0.372 - 0.432	0.391 - 0.409	
		20	0.407 - 0.479	0.424 - 0.472	0.433 - 0.447	
		25	0.444 - 0.546	0.448 - 0.540	0.474 - 0.509	
		30	0.496 - 0.597	0.507 - 0.588	0.540 - 0.562	STD. DEV. =
		35	0.556 - 0.664	0.561 - 0.645	0.572 - 0.619	= 1.189
		40	0.606 - 0.762	0.614 - 0.740	0.641 - 0.695	
		45	0.683 - 0.834	0.688 - 0.807	0.728 - 0.786	
		50	0.765 - 0.908	0.772 - 0.897	0.797 - 0.853	
		55	0.838 - 1.003	0.842 - 0.986	0.876 - 0.955	SAMPLE SIZE =
		60	0.915 - 1.114	0.935 - 1.087	0.975 - 1.050	= 400
		65	1.013 - 1.236	1.033 - 1.216	1.078 - 1.153	
		70	1.134 - 1.401	1.148 - 1.390	1.208 - 1.278	
		75	1.255 - 1.532	1.271 - 1.518	1.385 - 1.480	
		80	1.440 - 1.977	1.486 - 1.956	1.526 - 1.725	
		85	1.741 - 2.310	1.847 - 2.298	1.977 - 2.168	
		90	2.254 - 3.044	2.290 - 2.979	2.372 - 2.782	
		95	3.037 - 4.613	3.116 - 4.360	3.269 - 3.974	

Table C-10 Uncertainty distributions for λ(total) for Mark-1 drywell sprays

Aerosol mass fraction remaining	Total water flux (cm/s)	Quantile (%)	Range for λ(total) at a confidence level of 95%	90%	50%	
0.1	0.01	5	0.191 - 0.267	0.200 - 0.260	0.218 - 0.250	MEAN =
		10	0.263 - 0.337	0.274 - 0.335	0.305 - 0.324	= 1.052 hr^{-1}
		15	0.332 - 0.375	0.335 - 0.372	0.341 - 0.358	
		20	0.357 - 0.418	0.365 - 0.408	0.376 - 0.392	
		25	0.390 - 0.463	0.393 - 0.456	0.411 - 0.439	
		30	0.429 - 0.516	0.435 - 0.511	0.455 - 0.480	STD. DEV. =
		35	0.469 - 0.576	0.474 - 0.562	0.507 - 0.534	= 1.050
		40	0.523 - 0.662	0.528 - 0.656	0.551 - 0.618	
		45	0.587 - 0.711	0.598 - 0.695	0.644 - 0.677	
		50	0.666 - 0.782	0.672 - 0.771	0.689 - 0.742	
		55	0.715 - 0.841	0.733 - 0.832	0.764 - 0.802	SAMPLE SIZE =
		60	0.786 - 0.923	0.796 - 0.904	0.820 - 0.868	= 400
		65	0.854 - 1.072	0.864 - 1.007	0.896 - 0.962	
		70	0.940 - 1.213	0.959 - 1.179	0.987 - 1.131	
		75	1.108 - 1.377	1.129 - 1.325	1.170 - 1.244	
		80	1.234 - 1.685	1.248 - 1.650	1.345 - 1.479	
		85	1.482 - 2.106	1.504 - 1.973	1.685 - 1.849	
		90	1.909 - 2.620	1.944 - 2.563	2.155 - 2.338	
		95	2.602 - 3.903	2.666 - 3.798	3.003 - 3.429	

Table C-11 Uncertainty distributions for λ(total) for Mark-1 drywell sprays

Aerosol mass fraction remaining	Total water flux (cm/s)	Quantile (%)	Range for λ(total) at a confidence level of 95%	90%	50%	
0.01	0.01	5	0.165 - 0.209	0.167 - 0.208	0.177 - 0.190	MEAN =
		10	0.209 - 0.280	0.210 - 0.276	0.247 - 0.262	= 0.904 hr^{-1}
		15	0.267 - 0.314	0.273 - 0.305	0.283 - 0.292	
		20	0.292 - 0.347	0.296 - 0.340	0.314 - 0.331	
		25	0.326 - 0.394	0.332 - 0.392	0.341 - 0.368	
		30	0.365 - 0.435	0.367 - 0.430	0.391 - 0.405	STD. DEV. =
		35	0.396 - 0.486	0.401 - 0.479	0.427 - 0.460	= 0.936
		40	0.437 - 0.552	0.452 - 0.543	0.478 - 0.515	
		45	0.494 - 0.595	0.511 - 0.585	0.536 - 0.568	
		50	0.555 - 0.668	0.564 - 0.643	0.575 - 0.622	
		55	0.597 - 0.722	0.611 - 0.720	0.632 - 0.689	SAMPLE SIZE =
		60	0.670 - 0.776	0.678 - 0.762	0.712 - 0.740	= 400
		65	0.725 - 0.849	0.736 - 0.834	0.757 - 0.810	
		70	0.795 - 1.019	0.806 - 0.991	0.829 - 0.904	
		75	0.891 - 1.193	0.902 - 1.163	0.986 - 1.079	
		80	1.059 - 1.387	1.090 - 1.343	1.170 - 1.249	
		85	1.249 - 1.808	1.276 - 1.772	1.387 - 1.582	
		90	1.673 - 2.319	1.733 - 2.227	1.906 - 2.082	
		95	2.281 - 3.543	2.361 - 3.474	2.558 - 3.116	

Table C-12 Uncertainty distributions for λ(total) for Mark-1 drywell sprays

Aerosol mass fraction remaining	Total water flux (cm/s)	Quantile (%)	Range for λ(total) at a confidence level of 95%	90%	50%	
0.001	0.01	5	0.153 - 0.189	0.156 - 0.185	0.158 - 0.174	MEAN =
		10	0.189 - 0.241	0.196 - 0.239	0.209 - 0.230	= 0.840 hr^{-1}
		15	0.234 - 0.282	0.238 - 0.276	0.251 - 0.264	
		20	0.264 - 0.320	0.266 - 0.312	0.283 - 0.302	
		25	0.298 - 0.357	0.303 - 0.355	0.316 - 0.334	
		30	0.332 - 0.406	0.333 - 0.400	0.352 - 0.369	STD. DEV. =
		35	0.363 - 0.453	0.367 - 0.445	0.393 - 0.419	= 0.890
		40	0.418 - 0.505	0.418 - 0.503	0.442 - 0.473	
		45	0.457 - 0.551	0.460 - 0.544	0.498 - 0.515	
		50	0.505 - 0.607	0.510 - 0.595	0.532 - 0.562	
		55	0.552 - 0.670	0.556 - 0.665	0.584 - 0.632	SAMPLE SIZE =
		60	0.612 - 0.718	0.621 - 0.710	0.657 - 0.681	= 400
		65	0.674 - 0.779	0.678 - 0.768	0.708 - 0.747	
		70	0.735 - 0.926	0.743 - 0.906	0.764 - 0.841	
		75	0.795 - 1.097	0.834 - 1.085	0.900 - 0.991	
		80	0.981 - 1.282	0.994 - 1.256	1.090 - 1.186	
		85	1.190 - 1.706	1.209 - 1.652	1.282 - 1.494	
		90	1.570 - 2.138	1.609 - 2.116	1.798 - 1.988	
		95	2.136 - 3.357	2.205 - 3.299	2.383 - 2.983	

Table C-13 Uncertainty distributions for λ(total) for Mark-1 drywell sprays

Aerosol mass fraction remaining	Total water flux (cm/s)	Quantile (%)	Range for λ(total) at a confidence level of 95%	90%	50%	
0.9	0.002	5	0.027 - 0.038	0.029 - 0.038	0.031 - 0.035	MEAN =
		10	0.038 - 0.050	0.039 - 0.050	0.041 - 0.047	= 0.210 hr^{-1}
		15	0.048 - 0.058	0.049 - 0.057	0.050 - 0.054	
		20	0.054 - 0.066	0.055 - 0.066	0.058 - 0.063	
		25	0.062 - 0.076	0.063 - 0.074	0.066 - 0.070	
		30	0.068 - 0.090	0.070 - 0.089	0.074 - 0.084	STD. DEV. =
		35	0.079 - 0.096	0.081 - 0.096	0.088 - 0.092	= 0.252
		40	0.091 - 0.108	0.092 - 0.105	0.095 - 0.101	
		45	0.098 - 0.122	0.100 - 0.120	0.105 - 0.114	
		50	0.110 - 0.137	0.112 - 0.134	0.119 - 0.131	
		55	0.123 - 0.157	0.127 - 0.153	0.133 - 0.141	SAMPLE SIZE =
		60	0.137 - 0.174	0.140 - 0.169	0.149 - 0.162	= 400
		65	0.160 - 0.194	0.161 - 0.189	0.168 - 0.179	
		70	0.178 - 0.244	0.179 - 0.235	0.188 - 0.218	
		75	0.209 - 0.290	0.217 - 0.281	0.232 - 0.262	
		80	0.262 - 0.356	0.264 - 0.348	0.286 - 0.303	
		85	0.304 - 0.454	0.317 - 0.351	0.355 - 0.404	
		90	0.423 - 0.563	0.440 - 0.547	0.462 - 0.521	
		95	0.558 - 0.859	0.571 - 0.848	0.648 - 0.774	

Table C-14 Uncertainty distributions for λ(total) for Mark-1 drywell sprays

Aerosol mass fraction remaining	Total water flux (cm/s)	Quantile (%)	Range for λ(total) at a confidence level of 95%	90%	50%	
0.5	0.002	5	0.027 - 0.038	0.028 - 0.036	0.032 - 0.034	MEAN =
		10	0.037 - 0.046	0.038 - 0.046	0.039 - 0.042	= 0.175 hr^{-1}
		15	0.044 - 0.052	0.046 - 0.052	0.047 - 0.050	
		20	0.050 - 0.060	0.050 - 0.060	0.052 - 0.054	
		25	0.054 - 0.067	0.054 - 0.066	0.060 - 0.063	
		30	0.063 - 0.078	0.063 - 0.077	0.066 - 0.070	STD. DEV. =
		35	0.067 - 0.089	0.069 - 0.087	0.076 - 0.081	= 0.195
		40	0.078 - 0.097	0.080 - 0.094	0.083 - 0.090	
		45	0.089 - 0.106	0.090 - 0.104	0.093 - 0.098	
		50	0.097 - 0.120	0.098 - 0.119	0.100 - 0.113	
		55	0.108 - 0.130	0.109 - 0.128	0.116 - 0.123	SAMPLE SIZE =
		60	0.121 - 0.151	0.123 - 0.148	0.127 - 0.137	= 400
		65	0.130 - 0.171	0 134 - 0.169	0.145 - 0.158	
		70	0.154 - 0.203	0.157 - 0.201	0.166 - 0.185	
		75	0.176 - 0.245	0.184 - 0.237	0.200 - 0.218	
		80	0.214 - 0.289	0.221 - 0.282	0.238 - 0.264	
		85	0.264 - 0.368	0.272 - 0.365	0.288 - 0.333	
		90	0.343 - 0.467	0.362 - 0.462	0.374 - 0.434	
		95	0.466 - 0.687	0.484 - 0.665	0.548 - 0.609	

Table C-15 Uncertainty distributions for λ(total) for Mark-1 drywell sprays

Aerosol mass fraction remaining	Total water flux (cm/s)	Quantile (%)	Range for λ(total) at a confidence level of 95%	90%	50%	
0.3	0.002	5	0.025 - 0.034	0.027 - 0.034	0.028 - 0.033	MEAN =
		10	0.034 - 0.043	0.036 - 0.042	0.037 - 0.040	= 0.157 hr^{-1}
		15	0.041 - 0.048	0.041 - 0.048	0.043 - 0.045	
		20	0.045 - 0.053	0.046 - 0.052	0.048 - 0.051	
		25	0.050 - 0.062	0.051 - 0.062	0.052 - 0.056	
		30	0.055 - 0.069	0.056 - 0.068	0.062 - 0.065	STD. DEV. =
		35	0.063 - 0.078	0.065 - 0.075	0.067 - 0.074	= 0.168
		40	0.071 - 0.089	0.072 - 0.088	0.075 - 0.084	
		45	0.079 - 0.095	0.083 - 0.094	0.086 - 0.091	
		50	0.089 - 0.110	0.089 - 0.109	0.092 - 0.099	
		55	0.096 - 0.121	0.098 - 0.116	0.106 - 0.111	SAMPLE SIZE =
		60	0.110 - 0.134	0.110 - 0.131	0.115 - 0.126	= 400
		65	0.123 - 0.156	0.124 - 0.152	0.130 - 0.144	
		70	0.138 - 0.184	0.143 - 0.181	0.150 - 0.165	
		75	0.160 - 0.227	0.164 - 0.214	0.178 - 0.197	
		80	0.196 - 0.261	0.198 - 0.260	0.217 - 0.242	
		85	0.242 - 0.322	0.244 - 0.315	0.261 - 0.298	
		90	0.305 - 0.448	0.307 - 0.423	0.328 - 0.393	
		95	0.441 - 0.631	0.460 - 0.620	0.474 - 0.531	

Table C-16 Uncertainty distributions for λ(total) for Mark-1 drywell sprays

Aerosol mass fraction remaining	Total water flux (cm/s)	Quantile (%)	Range for λ(total) at a confidence level of			
			95%	90%	50%	
0.1	0.002	5	0.022 - 0.032	0.024 - 0.031	0.026 - 0.030	MEAN =
		10	0.031 - 0.036	0.032 - 0.036	0.033 - 0.035	= 0.134 hr^{-1}
		15	0.035 - 0.041	0.035 - 0.041	0.038 - 0.040	
		20	0.040 - 0.047	0.040 - 0.047	0.041 - 0.045	
		25	0.044 - 0.052	0.045 - 0.051	0.047 - 0.049	
		30	0.049 - 0.062	0.049 - 0.061	0.051 - 0.057	STD. DEV. =
		35	0.055 - 0.066	0.055 - 0.066	0.060 - 0.063	= 0.139
		40	0.062 - 0.077	0.062 - 0.076	0.065 - 0.072	
		45	0.067 - 0.084	0.067 - 0.083	0.075 - 0.078	
		50	0.077 - 0.094	0.077 - 0.092	0.082 - 0.088	
		55	0.084 - 0.106	0.085 - 0.103	0.091 - 0.097	SAMPLE SIZE =
		60	0.094 - 0.118	0.096 - 0.116	0.100 - 0.111	= 400
		65	0.107 - 0.133	0.109 - 0.130	0.114 - 0.121	
		70	0.118 - 0.161	0.120 - 0.154	0.129 - 0.148	
		75	0.140 - 0.189	0.147 - 0.180	0.153 - 0.170	
		80	0.168 - 0.227	0.170 - 0.222	0.181 - 0.210	
		85	0.210 - 0.373	0.212 - 0.258	0.227 - 0.243	
		90	0.248 - 0.368	0.253 - 0.359	0.278 - 0.331	
		95	0.368 - 0.522	0.369 - 0.507	0.430 - 0.453	

Table C-17 Uncertainty distributions for λ(total) for Mark-1 drywell sprays

Aerosol mass fraction remaining	Total water flux (cm/s)	Quantile (%)	Range for λ(total) at a confidence level of			
			95%	90%	50%	
0.01	0.002	5	0.018 - 0.025	0.019 - 0.025	0.021 - 0.024	MEAN =
		10	0.025 - 0.031	0.025 - 0.031	0.027 - 0.030	= 0.113 hr^{-1}
		15	0.030 - 0.037	0.031 - 0.036	0.032 - 0.034	
		20	0.034 - 0.040	0.036 - 0.039	0.037 - 0.038	
		25	0.038 - 0.045	0.038 - 0.044	0.039 - 0.042	
		30	0.040 - 0.050	0.042 - 0.049	0.043 - 0.047	STD. DEV. =
		35	0.045 - 0.058	0.047 - 0.057	0.048 - 0.054	= 0.117
		40	0.052 - 0.063	0.053 - 0.062	0.056 - 0.060	
		45	0.059 - 0.072	0.060 - 0.071	0.061 - 0.066	
		50	0.063 - 0.079	0.065 - 0.077	0.071 - 0.074	
		55	0.072 - 0.089	0.074 - 0.087	0.077 - 0.084	SAMPLE SIZE =
		60	0.080 - 0.103	0.082 - 0.100	0.086 - 0.094	= 400
		65	0.090 - 0.115	0.094 - 0.112	0.098 - 0.105	
		70	0.104 - 0.136	0.105 - 0.131	0.111 - 0.123	
		75	0.118 - 0.160	0.121 - 0.158	0.129 - 0.145	
		80	0.144 - 0.185	0.146 - 0.180	0.158 - 0.169	
		85	0.169 - 0.229	0.174 - 0.226	0.184 - 0.212	
		90	0.216 - 0.313	0.223 - 0.310	0.231 - 0.286	
		95	0.312 - 0.460	0.320 - 0.430	0.345 - 0.393	

Table C-18 Uncertainty distributions for λ(total) for Mark-1 drywell sprays

Aerosol mass fraction remaining	Total water flux (cm/s)	Quantile (%)	Range for λ(total) at a confidence level of			
			95%	90%	50%	
0.001	0.002	5	0.017 - 0.022	0.017 - 0.022	0.018 - 0.020	MEAN =
		10	0.022 - 0.029	0.023 - 0.029	0.024 - 0.027	= 0.105 hr^{-1}
		15	0.028 - 0.034	0.028 - 0.033	0.029 - 0.031	
		20	0.031 - 0.036	0.032 - 0.036	0.034 - 0.036	
		25	0.035 - 0.040	0.036 - 0.040	0.036 - 0.038	
		30	0.037 - 0.046	0.038 - 0.046	0.039 - 0.043	STD. DEV. =
		35	0.041 - 0.053	0.043 - 0.051	0.044 - 0.049	= 0.109
		40	0.047 - 0.059	0.048 - 0.059	0.051 - 0.055	
		45	0.053 - 0.066	0.054 - 0.063	0.057 - 0.061	
		50	0.059 - 0.074	0.060 - 0.072	0.063 - 0.068	
		55	0.066 - 0.083	0.067 - 0.081	0.071 - 0.076	SAMPLE SIZE =
		60	0.074 - 0.093	0.075 - 0.092	0.080 - 0.086	= 400
		65	0.084 - 0.108	0.085 - 0.105	0.090 - 0.098	
		70	0.095 - 0.124	0.097 - 0.122	0.104 - 0.111	
		75	0.109 - 0.144	0.110 - 0.143	0.121 - 0.132	
		80	0.131 - 0.171	0.132 - 0.167	0.143 - 0.160	
		85	0.160 - 0.217	0.161 - 0.214	0.171 - 0.198	
		90	0.206 - 0.294	0.212 - 0.284	0.223 - 0.255	
		95	0.292 - 0.421	0.298 - 0.407	0.317 - 0.366	

Appendix D: Cumulative Probability Distributions for $\lambda(m_f)/\lambda(m_f = 0.9)$

Correlations among the values of the spray decontamination coefficients for various values of the mass fraction of aerosol remaining in the containment, m_f, make results of the uncertainty analyses difficult to use. Much of this correlation can be eliminated by selecting as the uncertain variables for a given water flux $\lambda(m_f = 0.9)$ and $\lambda(m_f)/\lambda(m_f = 0.9)$ for $m_f = 0.5, 0.3, 0.1, 0.01$, and 0.001. Samples of the spray decontamination coefficient were reanalyzed in terms of these variables. Deatiled cumulative probability distributions for the variables $\lambda(m_f)/\lambda(m_f = 0.9)$ for $Q = 0.25, 0.01$, and 0.002 cm^3/cm^2-s are shown in the tables in this appendix. The form and the contents of these tables are rather similar to the tables in Appendix C, showing detailed probability distributions for the spray decontamination coefficients.

Table D-1 Probability distribution of $\lambda(m_f)/\lambda(m_f = 0.9)$ for Q = 0.25 cm^3/cm^2-s and $m_f = 0.5$

Total water flux cm^3/cm^2-s	Mass fraction aerosol remaining	Percentile	$\lambda(m_f)/\lambda(m_f = 0.9)$ 95% confidence	90% confidence	50% confidence	
0.25	0.5	5	0.688 - 0.713	0.690 - 0.710	0.697 - 0.703	MEAN =
		10	0.712 - 0.738	0.715 - 0.737	0.723 - 0.729	= 0.861 hr^{-1}
		15	0.733 - 0.762	0.735 - 0.760	0.740 - 0.753	
		20	0.753 - 0.775	0.754 - 0.773	0.762 - 0.768	
		25	0.766 - 0.791	0.769 - 0.790	0.773 - 0.782	
		30	0.779 - 0.807	0.781 - 0.806	0.787 - 0.795	STD. DEV. =
		35	0 793 - 0.823	0.793 - 0.820	0.803 - 0.812	= 0.097
		40	0.809 - 0.846	0.811 - 0.844	0.819 - 0.833	
		45	0.826 - 0.867	0.830 - 0.865	0.840 - 0.854	
		50	0.849 - 0.886	0.851 - 0.881	0.864 - 0.876	
		55	0.868 - 0.904	0.873 - 0.901	0.880 - 0.889	SAMPLE SIZE =
		60	0.886 - 0.917	0.888 - 0.916	0.900 - 0.906	= 400
		65	0.904 - 0.932	0.905 - 0.929	0.913 - 0.921	
		70	0.919 - 0.952	0.920 - 0.951	0.928 - 0.945	
		75	0.939 - 0.965	0.944 - 0.963	0.951 - 0.958	
		80	0.957 - 0.977	0.958 - 0.975	0.963 - 0.971	
		85	0.971 - 0.984	0.972 - 0.984	0.977 - 0.980	
		90	0.982 - 0.991	0.983 - 0.991	0.985 - 0.988	
		95	0.991 - 0.995	0.991 - 0.995	0.992 - 0.994	

Table D-2 Probability distribution of $\lambda(m_f)/\lambda(m_f = 0.9)$ for Q = 0.25 cm^3/cm^2-s and $m_f = 0.3$

Total water flux cm^3/cm^2-s	Mass fraction aerosol remaining	Percentile	$\lambda(m_f)/\lambda(m_f = 0.9)$ 95% confidence	90% confidence	50% confidence	
0.25	0.3	5	0.542 - 0.573	0.543 - 0.571	0.552 - 0.562	MEAN =
		10	0.573 - 0.608	0.574 - 0.607	0.587 - 0.599	= 0.786 hr^{-1}
		15	0.602 - 0.638	0.605 - 0.636	0.611 - 0.628	
		20	0.628 - 0.660	0.629 - 0.657	0.639 - 0.650	
		25	0.648 - 0.677	0.650 - 0.676	0.657 - 0.669	
		30	0.664 - 0.702	0.667 - 0.700	0.675 - 0.690	STD. DEV. =
		35	0.681 - 0.729	0.689 - 0.727	0.696 - 0.713	= 0.142
		40	0.708 - 0.761	0.710 - 0.757	0.726 - 0.742	
		45	0.730 - 0.794	0.738 - 0.792	0.751 - 0.769	
		50	0.762 - 0.817	0.765 - 0.812	0.787 - 0.799	
		55	0.796 - 0.837	0.796 - 0.836	0.811 - 0.821	SAMPLE SIZE =
		60	0.818 - 0.864	0.820 - 0.862	0.834 - 0.844	= 400
		65	0.839 - 0.891	0.841 - 0.886	0.859 - 0.873	
		70	0.867 - 0.919	0.870 - 0.918	0.883 - 0.908	
		75	0.897 - 0.940	0.907 - 0.937	0.917 - 0.926	
		80	0.925 - 0.959	0.926 - 0.957	0.938 - 0.950	
		85	0.950 - 0.972	0.953 - 0.970	0.959 - 0.964	
		90	0.968 - 0.985	0.970 - 0.985	0.973 - 0.978	
		95	0.985 - 0.992	0.986 - 0.991	0.986 - 0.990	

Table D-3 Probability distribution of $\lambda(m_f)/\lambda(m_f = 0.9)$ for Q = 0.25 cm^3/cm^2-s and $m_f = 0.1$

Total water flux cm^3/cm^2-s	Mass fraction aerosol remaining	Percentile	$\lambda(m_f)/\lambda(m_f = 0.9)$ 95% confidence	90% confidence	50% confidence	
0.25	0.1	5	0.376 - 0.421	0.377 - 0.414	0.393 - 0.402	MEAN =
		10	0.420 - 0.463	0.423 - 0.460	0.434 - 0.450	= 0.693 hr^{-1}
		15	0.453 - 0.489	0.458 - 0.487	0.466 - 0.477	
		20	0.477 - 0.522	0.480 - 0.519	0.490 - 0.508	
		25	0.500 - 0.549	0.508 - 0.543	0.521 - 0.530	
		30	0.526 - 0.581	0.529 - 0.578	0.542 - 0.565	STD. DEV. =
		35	0.559 - 0.613	0.561 - 0.610	0.575 - 0.591	= 0.194
		40	0.585 - 0.646	0.588 - 0.641	0.604 - 0.627	
		45	0.614 - 0.689	0.623 - 0.686	0.636 - 0.666	
		50	0.647 - 0.724	0.651 - 0.719	0.681 - 0.706	
		55	0.689 - 0.736	0.697 - 0.736	0.715 - 0.729	SAMPLE SIZE =
		60	0.726 - 0.792	0.728 - 0.787	0.732 - 0.763	= 400
		65	0.742 - 0.833	0.755 - 0.821	0.779 - 0.802	
		70	0.796 - 0.869	0.801 - 0.862	0.819 - 0.848	
		75	0.839 - 0.899	0.847 - 0.892	0.861 - 0.874	
		80	0.871 - 0.930	0.874 - 0.926	0.894 - 0.913	
		85	0.914 - 0.952	0.921 - 0.951	0.930 - 0.941	
		90	0.945 - 0.976	0.949 - 0.975	0.956 - 0.970	
		95	0.976 - 0.987	0.976 - 0.986	0.980 - 0.984	

Table D-4 Probability distribution of $\lambda(m_f)/\lambda(m_f = 0.9)$ for Q = 0.25 cm^3/cm^2-s and $m_f = 0.01$

Total water flux cm^3/cm^2-s	Mass fraction aerosol remaining	Percentile	$\lambda(m_f)/\lambda(m_f = 0.9)$ 95% confidence	90% confidence	50% confidence	
0.25	0.01	5	0.248 - 0.301	0.250 - 0.295	0.262 - 0.281	MEAN =
		10	0.298 - 0.337	0.305 0.333	0.310 - 0.326	= 0.604 hr^{-1}
		15	0.328 - 0.364	0.333 - 0.363	0.341 - 0.352	
		20	0.352 - 0.398	0.360 - 0.395	0.364 - 0.381	
		25	0.379 - 0.436	0.383 - 0.429	0.396 - 0.419	
		30	0.412 - 0.472	0.419 - 0.467	0.429 - 0.451	STD. DEV. =
		35	0.441 - 0.509	0.447 - 0.502	0.463 - 0.484	= 0.225
		40	0.473 - 0.541	0.476 - 0.538	0.496 - 0.519	
		45	0.511 - 0.585	0.513 - 0.572	0.535 - 0.555	
		50	0.545 - 0.620	0.550 - 0.612	0.571 - 0.601	
		55	0.591 - 0.655	0.596 - 0.650	0.608 - 0.631	SAMPLE SIZE =
		60	0.623 - 0.711	0.630 - 0.697	0.642 - 0.675	= 400
		65	0.658 - 0.765	0.665 - 0.748	0.693 - 0.730	
		70	0.724 - 0.796	0.729 - 0.795	0.741 - 0.783	
		75	0.775 - 0.841	0.782 - 0.834	0.793 - 0.810	
		80	0.806 - 0.887	0.811 - 0.884	0.837 - 0.864	
		85	0.864 - 0.921	0.869 - 0.919	0.886 - 0.904	
		90	0.908 - 0.956	0.912 - 0.955	0.922 - 0.940	
		95	0.956 - 0.976	0.960 - 0.975	0.965 - 0.971	

Table D-5 Probability distribution of $\lambda(m_f)/\lambda(m_f = 0.9)$ for Q = 0.25 cm^3/cm^2-s and m_f = 0.001

Total water flux cm^3/cm^2-s	Mass fraction aerosol remaining	Percentile	$\lambda(m_f)/\lambda(m_f = 0.9)$ 95% confidence	90% confidence	50% confidence	
0.25	0.001	5	0.206 - 0.246	0.208 - 0.244	0.216 - 0.232	MEAN =
		10	0.245 - 0.285	0.247 - 0.280	0.266 - 0.274	= 0.565 hr^{-1}
		15	0.277 - 0.322	0.279 - 0.319	0.288 - 0.304	
		20	0.304 - 0.351	0.309 - 0.343	0.322 - 0.332	
		25	0.326 - 0.389	0.332 - 0.386	0.344 - 0.363	
		30	0.361 - 0.424	0.362 - 0.416	0.385 - 0.406	STD. DEV. =
		35	0.398 - 0.466	0.401 - 0.460	0.416 - 0.434	= 0.237
		40	0.426 - 0.496	0.429 - 0.493	0.449 - 0.472	
		45	0.468 - 0.525	0.470 - 0.520	0.490 - 0.509	
		50	0.496 - 0.574	0.500 - 0.573	0.518 - 0.548	
		55	0.526 - 0.616	0.536 - 0.610	0.568 - 0.588	SAMPLE SIZE =
		60	0.575 - 0.668	0.579 - 0.653	0.608 - 0.631	= 400
		65	0.621 - 0.728	0.626 - 0.715	0.650 - 0.695	
		70	0.684 - 0.758	0.693 - 0.755	0.706 - 0.746	
		75	0.740 - 0.811	0.743 - 0.797	0.754 - 0.775	
		80	0.771 - 0.862	0.777 - 0.853	0.799 - 0.836	
		85	0.836 - 0.904	0.839 - 0.900	0.862 - 0.882	
		90	0.888 - 0.948	0.896 - 0.943	0.904 - 0.933	
		95	0.946 - 0.970	0.949 - 0.967	0.956 - 0.965	

Table D-6 Probability distribution of $\lambda(m_f)/\lambda(m_f = 0.9)$ for Q = 0.01 cm^3/cm^2-s and $m_f = 0.5$

Total water flux cm^3/cm^2-s	Mass fraction aerosol remaining	Percentile	$\lambda(m_f)/\lambda(m_f = 0.9)$ 95% confidence	90% confidence	50% confidence	
0.01	0.5	5	0.692 - 0.709	0.693 - 0.708	0.695 - 0.703	MEAN =
		10	0.709 - 0.737	0.710 - 0.736	0.721 - 0.727	= 0.868 hr^{-1}
		15	0.730 - 0.765	0.735 - 0.757	0.739 - 0.752	
		20	0.752 - 0.787	0.754 - 0.784	0.765 - 0.771	
		25	0.769 - 0.811	0.773 - 0.810	0.784 - 0.800	
		30	0.793 - 0.833	0.800 - 0.828	0.810 - 0.821	STD. DEV. =
		35	0.817 - 0.850	0.820 - 0.847	0.827 - 0.841	= 0.096
		40	0.837 - 0.862	0.839 - 0.860	0.844 - 0.854	
		45	0.851 - 0.876	0.852 - 0.875	0.858 - 0.867	
		50	0.862 - 0.894	0.866 - 0.890	0.874 - 0.882	
		55	0.877 - 0.912	0.881 - 0.908	0.888 - 0.903	SAMPLE SIZE =
		60	0.896 - 0.923	0.900 - 0.922	0.907 - 0.914	= 400
		65	0.913 - 0.937	0.913 - 0.935	0.919 - 0.928	
		70	0.925 - 0.952	0.928 - 0.951	0.934 - 0.940	
		75	0.938 - 0.967	0.940 - 0.966	0.950 - 0.957	
		80	0.955 - 0.979	0.958 - 0.978	0.966 - 0.975	
		85	0.975 - 0.989	0.975 - 0.987	0.979 - 0.984	
		90	0.985 - 0.994	0.986 - 0.994	0.990 - 0.993	
		95	0.994 - 0.997	0.995 - 0.997	0.995 - 0.996	

Table D-7 Probability distribution of $\lambda(m_f)/\lambda(m_f = 0.9)$ for Q = 0.01 cm^3/cm^2-s and $m_f = 0.3$

Total water flux cm^3/cm^2-s	Mass fraction aerosol remaining	Percentile	$\lambda(m_f)/\lambda(m_f = 0.9)$ 95% confidence	90% confidence	50% confidence	
0.01	0.3	5	0.545 - 0.570	0.546 - 0.567	0.551 - 0.563	MEAN =
		10	0.568 - 0.603	0.574 - 0.600	0.580 - 0.597	= 0.796 hr^{-1}
		15	0.598 - 0.641	0.599 - 0.637	0.609 - 0.625	
		20	0.625 - 0.668	0.627 - 0.666	0.642 - 0.660	
		25	0.656 - 0.714	0.661 - 0.710	0.667 - 0.694	
		30	0.685 - 0.738	0.693 - 0.733	0.709 - 0.718	STD. DEV. =
		35	0.716 - 0.764	0.717 - 0.761	0.726 - 0.747	= 0.141
		40	0.742 - 0.779	0.745 - 0.778	0.758 - 0.770	
		45	0.764 - 0.801	0.767 - 0.796	0.777 - 0.785	
		50	0.779 - 0.828	0.782 - 0.818	0.791 - 0.810	
		55	0.801 - 0.852	0.803 - 0.848	0.816 - 0.840	SAMPLE SIZE =
		60	0.829 - 0.873	0.835 - 0.871	0.847 - 0.862	= 400
		65	0.854 - 0.892	0.860 - 0.889	0.869 - 0.881	
		70	0.876 - 0.918	0.879 - 0.916	0.888 - 0.901	
		75	0.898 - 0.944	0.900 - 0.942	0.915 - 0.927	
		80	0.923 - 0.964	0.928 - 0.962	0.943 - 0.956	
		85	0.956 - 0.980	0.957 - 0.978	0.964 - 0.971	
		90	0.974 - 0.990	0.975 - 0.990	0.981 - 0.987	
		95	0.990 - 0.994	0.990 - 0.994	0.991 - 0.993	

Table D-8 Probability distribution of $\lambda(m_f)/\lambda(m_f = 0.9)$ for Q = 0.01 cm^3/cm^2-s and $m_f = 0.1$

Total water flux cm^3/cm^2-s	Mass fraction aerosol remaining	Percentile	$\lambda(m_f)/\lambda(m_f = 0.9)$ 95% confidence	90% confidence	50% confidence	
0.01	0.1	5	0.384 - 0.414	0.385 - 0.412	0.390 - 0.404	MEAN =
		10	0.413 - 0.457	0.415 - 0.453	0.429 - 0.436	= 0.703 hr^{-1}
		15	0.440 - 0.498	0.451 - 0.490	0.463 - 0.477	
		20	0.476 - 0.535	0.483 - 0.531	0.498 - 0.512	
		25	0.512 - 0.579	0.512 - 0.572	0.532 - 0.560	
		30	0.556 - 0.619	0.559 - 0.614	0.572 - 0.595	STD. DEV. =
		35	0.591 - 0.649	0.592 - 0.643	0.613 - 0.635	= 0.190
		40	0.622 - 0.666	0.628 - 0.664	0.642 - 0.655	
		45	0.653 - 0.697	0.654 - 0.694	0.660 - 0.679	
		50	0.667 - 0.729	0.675 - 0.723	0.691 - 0.703	
		55	0.698 - 0.774	0.699 - 0.770	0.713 - 0.748	SAMPLE SIZE =
		60	0.729 - 0.800	0.739 - 0.796	0.761 - 0.788	= 400
		65	0.778 - 0.827	0.785 - 0.822	0.795 - 0.812	
		70	0.807 - 0.865	0.810 - 0.857	0.820 - 0.844	
		75	0.832 - 0.908	0.843 - 0.904	0.857 - 0.877	
		80	0.872 - 0.938	0.877 - 0.935	0.904 - 0.924	
		85	0.924 - 0.965	0.926 - 0.962	0.938 - 0.950	
		90	0.954 - 0.982	0.957 - 0.981	0.966 - 0.977	
		95	0.982 - 0.989	0.982 - 0.989	0.983 - 0.987	

Table D-9 Probability distribution of $\lambda(m_f)/\lambda(m_f = 0.9)$ for Q = 0.01 cm^3/cm^2-s and m_f = 0.01

Total water flux cm^3/cm^2-s	Mass fraction aerosol remaining	Percentile	$\lambda(m_f)/\lambda(m_f = 0.9)$ 95% confidence	90% confidence	50% confidence	
0.01	0.01	5	0.261 - 0.287	0.264 - 0.286	0.276 - 0.283	MEAN =
		10	0.287 - 0.339	0.288 - 0.331	0.296 - 0.316	= 0.616 hr^{-1}
		15	0.320 - 0.368	0.326 - 0.364	0.342 - 0.356	
		20	0.356 - 0.414	0.358 - 0.407	0.369 - 0.402	
		25	0.395 - 0.462	0.403 - 0.451	0.408 - 0.436	
		30	0.430 - 0.502	0.435 - 0.493	0.449 - 0.477	STD. DEV. =
		35	0.471 - 0.536	0.475 - 0.531	0.491 - 0.515	= 0.227
		40	0.508 - 0.560	0.512 - 0.559	0.527 - 0.544	
		45	0.538 - 0.597	0.539 - 0.590	0.556 - 0.576	
		50	0.564 - 0.620	0.571 - 0.614	0.585 - 0.606	
		55	0.597 - 0.694	0.599 - 0.684	0.612 - 0.651	SAMPLE SIZE =
		60	0.625 - 0.726	0.643 - 0.723	0.676 - 0.705	= 400
		65	0.696 - 0.750	0.702 - 0.744	0.717 - 0.733	
		70	0.731 - 0.796	0.732 - 0.790	0.741 - 0.767	
		75	0.762 - 0.855	0.766 - 0.851	0.789 - 0.817	
		80	0.814 - 0.902	0.819 - 0.895	0.852 - 0.880	
		85	0.880 - 0.941	0.887 - 0.938	0.902 - 0.922	
		90	0.927 - 0.968	0.932 - 0.967	0.942 - 0.961	
		95	0.968 - 0.980	0.968 - 0.979	0.971 - 0.977	

Table D-10 Probability distribution of $\lambda(m_f)/\lambda(m_f = 0.9)$ for Q = 0.01 cm^3/cm^2-s and $m_f = 0.001$

Total water flux cm^3/cm^2-s	Mass fraction aerosol remaining	Percentile	$\lambda(m_f)/\lambda(m_f = 0.9)$ 95% confidence	90% confidence	50% confidence	
0.01	0.001	5	0.218 - 0.242	0.223 - 0.241	0.233 - 0.239	MEAN =
		10	0.241 - 0.291	0.242 - 0.283	0.257 - 0.271	= 0.577 hr^{-1}
		15	0.274 - 0.323	0.278 - 0.320	0.298 - 0.309	
		20	0.309 - 0.364	0.312 - 0.362	0.324 - 0.349	
		25	0.342 - 0.407	0.351 - 0.399	0.363 - 0.381	
		30	0.378 - 0.450	0.380 - 0.436	0.398 - 0.423	STD. DEV. =
		35	0.414 - 0.488	0.421 - 0.482	0.435 - 0.465	= 0.238
		40	0.454 - 0.512	0.462 - 0.509	0.478 - 0.498	
		45	0.490 - 0.545	0.493 - 0.537	0.504 - 0.521	
		50	0.514 - 0.581	0.520 - 0.574	0.532 - 0.554	
		55	0.545 - 0.655	0.550 - 0.639	0.569 - 0.610	SAMPLE SIZE =
		60	0.583 - 0.682	0.595 - 0.679	0.626 - 0.669	= 400
		65	0.659 - 0.717	0.662 - 0.708	0.677 - 0.688	
		70	0.684 - 0.762	0.687 - 0.755	0.705 - 0.733	
		75	0.722 - 0.824	0.733 - 0.812	0.753 - 0.786	
		80	0.782 - 0.881	0.788 - 0.866	0.814 - 0.856	
		85	0.856 - 0.923	0.862 - 0.922	0.879 - 0.904	
		90	0.910 - 0.958	0.915 - 0.957	0.927 - 0.950	
		95	0.958 - 0.973	0.958 - 0.973	0.962 - 0.970	

Table D-11 Probability distribution of $\lambda(m_f)/\lambda(m_f = 0.9)$ for Q = 0.002 cm^3/cm^2-s and $m_f = 0.5$

Total water flux cm^3/cm^2-s	Mass fraction aerosol remaining	Percentile	$\lambda(m_f)/\lambda(m_f = 0.9)$ 95% confidence	90% confidence	50% confidence	
0.002	0.5	5	0.688 - 0.719	0.694 - 0.719	0.700 - 0.714	MEAN =
		10	0.719 - 0.747	0.721 - 0.744	0.730 - 0.737	= 0.913 hr^{-1}
		15	0.739 - 0.773	0.741 - 0.771	0.750 - 0.765	
		20	0.764 - 0.786	0.767 - 0.785	0.773 - 0.781	
		25	0.779 - 0.811	0.781 - 0.808	0.785 - 0.801	
		30	0.796 - 0.829	0.800 - 0.823	0.808 - 0.816	STD. DEV. =
		35	0.814 - 0.847	0.815 - 0.845	0.822 - 0.837	= 0.606
		40	0.832 - 0.870	0.834 - 0.868	0.844 - 0.860	
		45	0.848 - 0.889	0.857 - 0.887	0.862 - 0.878	
		50	0.871 - 0.902	0.874 - 0.900	0.884 - 0.892	
		55	0.890 - 0.917	0.891 - 0.915	0.899 - 0.909	SAMPLE SIZE =
		60	0.903 - 0.932	0.907 - 0.929	0.914 - 0.920	= 400
		65	0.917 - 0.944	0.920 - 0.940	0.927 - 0.938	
		70	0.933 - 0.957	0.935 - 0.955	0.939 - 0.950	
		75	0.946 - 0.967	0.948 - 0.967	0.954 - 0.962	
		80	0.961 - 0.974	0.962 - 0.973	0.967 - 0.970	
		85	0.970 - 0.981	0.971 - 0.980	0.974 - 0.977	
		90	0.977 - 0.991	0.979 - 0.990	0.983 - 0.988	
		95	0.991 - 0.996	0.991 - 0.996	0.992 - 0.994	

Table D-12 Probability distribution of $\lambda(m_f)/\lambda(m_f = 0.9)$ for Q = 0.002 cm^3/cm^2-s and $m_f = 0.3$

Total water flux cm^3/cm^2-s	Mass fraction aerosol remaining	Percentile	$\lambda(m_f)/\lambda(m_f = 0.9)$ 95% confidence	90% confidence	50% confidence	
0.002	0.3	5	0.544 - 0.583	0.548 - 0.581	0.560 - 0.573	MEAN =
		10	0.582 - 0.616	0.584 - 0.615	0.595 - 0.606	= 0.838 hr^{-1}
		15	0.612 - 0.656	0.614 - 0.652	0.623 - 0.640	
		20	0.640 - 0.676	0.643 - 0.672	0.657 - 0.666	
		25	0.664 - 0.706	0.666 - 0.703	0.672 - 0.687	
		30	0.684 - 0.736	0.687 - 0.731	0.702 - 0.722	STD. DEV. =
		35	0.712 - 0.762	0.719 - 0.756	0.730 - 0.745	= 0.559
		40	0.739 - 0.788	0.742 - 0.785	0.754 - 0.775	
		45	0.766 - 0.817	0.768 - 0.815	0.782 - 0.802	
		50	0.789 - 0.842	0.795 - 0.836	0.814 - 0.826	
		55	0.819 - 0.864	0.824 - 0.861	0.833 - 0.854	SAMPLE SIZE =
		60	0.844 - 0.886	0.848 - 0.882	0.859 - 0.871	= 400
		65	0.867 - 0.905	0.870 - 0.900	0.875 - 0.895	
		70	0.889 - 0.920	0.893 - 0.919	0.900 - 0.914	
		75	0.909 - 0.935	0.913 - 0.932	0.918 - 0.927	
		80	0.926 - 0.954	0.927 - 0.952	0.932 - 0.943	
		85	0.943 - 0.971	0.947 - 0.968	0.954 - 0.962	
		90	0.965 - 0.981	0.966 - 0.981	0.972 - 0.978	
		95	0.981 - 0.992	0.983 - 0.992	0.986 - 0.989	

Table D-13 Probability distribution of $\lambda(m_f)/\lambda(m_f = 0.9)$ for Q = 0.002 cm^3/cm^2-s and m_f = 0.1

Total water flux cm^3/cm^2-s	Mass fraction aerosol remaining	Percentile	$\lambda(m_f)/\lambda(m_f = 0.9)$ 95% confidence	90% confidence	50% confidence	
0.002	0.1	5	0.382 - 0.428	0.384 - 0.417	0.395 - 0.407	MEAN =
		10	0.426 - 0.471	0.434 - 0.465	0.442 - 0.458	= 0.742 hr^{-1}
		15	0.461 - 0.510	0.465 - 0.505	0.473 - 0.493	
		20	0.493 - 0.537	0.498 - 0.534	0.511 - 0.524	
		25	0.523 - 0.579	0.525 - 0.566	0.535 - 0.556	
		30	0.547 - 0.628	0.552 - 0.620	0.564 - 0.598	STD. DEV. =
		35	0.588 - 0.652	0.597 - 0.646	0.617 - 0.636	= 0.510
		40	0.632 - 0.691	0.635 - 0.682	0.645 - 0.664	
		45	0.653 - 0.719	0.658 - 0.715	0.680 - 0.704	
		50	0.692 - 0.753	0.698 - 0.750	0.711 - 0.731	
		55	0.721 - 0.783	0.725 - 0.781	0.746 - 0.765	SAMPLE SIZE =
		60	0.755 - 0.815	0.760 - 0.811	0.775 - 0.800	= 400
		65	0.786 - 0.848	0.790 - 0.847	0.804 - 0.833	
		70	0.823 - 0.867	0.831 - 0.865	0.841 - 0.854	
		75	0.851 - 0.893	0.854 - 0.888	0.863 - 0.875	
		80	0.873 - 0.923	0.875 - 0.921	0.890 - 0.910	
		85	0.910 - 0.944	0.913 - 0.943	0.923 - 0.931	
		90	0.939 - 0.969	0.940 - 0.967	0.947 - 0.960	
		95	0.968 - 0.987	0.970 - 0.986	0.975 - 0.983	

Table D-14 Probability distribution of $\lambda(m_f)/\lambda(m_f = 0.9)$ for Q = 0.002 cm^3/cm^2-s and $m_f = 0.01$

Total water flux cm^3/cm^2-s	Mass fraction aerosol remaining	Percentile	$\lambda(m_f)/\lambda(m_f = 0.9)$ 95% confidence	90% confidence	50% confidence	
0.002	0.01	5	0.258 - 0.302	0.259 - 0.298	0.268 - 0.281	MEAN =
		10	0.302 - 0.350	0.303 - 0.338	0.313 - 0.330	= 0.648 hr^{-1}
		15	0.333 - 0.385	0.337 - 0.382	0.352 - 0.364	
		20	0.363 - 0.420	0.373 - 0.415	0.386 - 0.404	
		25	0.401 - 0.463	0.405 - 0.456	0.416 - 0.436	
		30	0.432 - 0.508	0.435 - 0.504	0.454 - 0.486	STD. DEV. =
		35	0.471 - 0.552	0.474 - 0.550	0.503 - 0.527	= 0.464
		40	0.514 - 0.590	0.523 - 0.588	0.548 - 0.568	
		45	0.553 - 0.628	0.556 - 0.617	0.584 - 0.599	
		50	0.592 - 0.658	0.595 - 0.654	0.609 - 0.638	
		55	0.628 - 0.698	0.635 - 0.692	0.649 - 0.668	SAMPLE SIZE =
		60	0.660 - 0.738	0.663 - 0.726	0.682 - 0.709	= 400
		65	0.700 - 0.772	0.708 - 0.771	0.720 - 0.750	
		70	0.741 - 0.800	0.749 - 0.799	0.771 - 0.784	
		75	0.777 - 0.826	0.781 - 0.819	0.798 - 0.810	
		80	0.809 - 0.870	0.811 - 0.868	0.820 - 0.858	
		85	0.859 - 0.904	0.862 - 0.900	0.870 - 0.890	
		90	0.895 - 0.944	0.899 - 0.941	0.910 - 0.927	
		95	0.943 - 0.975	0.945 - 0.974	0.957 - 0.972	

Table D-15 Probability distribution of $\lambda(m_f)/\lambda(m_f = 0.9)$ for Q = 0.002 cm^3/cm^2-s and m_f = 0.001

Total water flux cm^3/cm^2-s	Mass fraction aerosol remaining	Percentile	$\lambda(m_f)/\lambda(m_f = 0.9)$ 95% confidence	90% confidence	50% confidence	
0.002	0.001	5	0.214 - 0.251	0.216 - 0.242	0.225 - 0.236	MEAN =
		10	0.248 - 0.298	0.256 - 0.294	0.268 - 0.278	= 0.605 hr^{-1}
		15	0.287 - 0.337	0.292 - 0.330	0.301 - 0.316	
		20	0.316 - 0.369	0.318 - 0.366	0.337 - 0.354	
		25	0.352 - 0.419	0.355 - 0.406	0.367 - 0.389	
		30	0.382 - 0.459	0.386 - 0.453	0.406 - 0.431	STD. DEV. =
		35	0.421 - 0.512	0.429 - 0.509	0.446 - 0.474	= 0.440
		40	0.464 - 0.543	0.468 - 0.536	0.500 - 0.522	
		45	0.512 - 0.580	0.519 - 0.575	0.531 - 0.556	
		50	0.546 - 0.607	0.554 - 0.603	0.570 - 0.593	
		55	0.580 - 0.651	0.585 - 0.648	0.599 - 0.617	SAMPLE SIZE =
		60	0.607 - 0.686	0.610 - 0.682	0.639 - 0.667	= 400
		65	0.653 - 0.736	0.656 - 0.730	0.680 - 0.706	
		70	0.698 - 0.763	0.704 - 0.758	0.723 - 0.744	
		75	0.742 - 0.786	0.743 - 0.736	0.755 - 0.772	
		80	0.771 - 0.850	0.773 - 0.846	0.786 - 0.833	
		85	0.833 - 0.886	0.838 - 0.884	0.849 - 0.868	
		90	0.872 - 0.931	0.880 - 0.923	0.891 - 0.906	
		95	0.928 - 0.970	0.934 - 0.968	0.943 - 0.962	

DISTRIBUTION:

U.S. Nuclear Regulatory Commission (16)
Office of Nuclear Regulatory Research
Attn: E. Beckjord, NLS-007
T. Speis, NLS-007
W. Minners, NLS-360
T. L. King, NLS-358
L. Soffer, NLS-324
R. Lee, NLN-344
A. Reuben, NLN-344
M. Cunningham, NLS-372
F. Eltawila, NLN-344
J. Mitchell, NLS-314
A. Behbahani, NLN-344
R. Meyer, NLS-007
J. C. Ryder, NLS-007
S. B. Burson, NLS-324
S. Basu, NLS-344
B. Sheron, NLS-007
Washington, D.C. 20555

U.S. Nuclear Regulatory Commission (4)
Office of Nuclear Reactor Regulation
Attn: R. Palla, 10E4
R. Barrett, 10E4
W. Lyon, 8E23
J. Lee, 10D4
Washington, DC 20555

U.S. Department of Energy (2)
Office of Nuclear Safety
Attn: S. Blush
P. Worthington
1000 Independence Ave., S.W.
Washington, DC 20585

U.S. Department of Energy
NE-42
Attn: W. F. Pasedag
19901 Germantown Rd.
Germantown, MD 20585

U.S. Department of Energy
EM-36
Attn: H. Eckert
12800 Middlebrook Road
Germantown, MD 20874

U.S. Department of Energy (2)
Albuquerque Operations Office
Attn: C. E. Garcia, Director
For: C. B. Quinn
R. L. Holton
P.O. Box 5400
Albuquerque, NM 87185

Los Alamos National Laboratories
Attn: M. Stevenson
P.O. Box 1663
Los Alamos, NM 87545

Electric Power Research Institute (2)
Attn: A. Michiels
R. Sehgal
3412 Hillview Avenue
Palo Alto, CA 94303

University of California Los Angeles (4)
Nuclear Energy Laboratory
Attn: I. Caffon
D. Okrent
W. Kastenberg
G. Apostolakis
405 Hilgaard Avenue
Los Angeles, CA 90024

Brookhaven National Laboratory (6)
Attn: R. A. Bari
T. Pratt
N. Tutu
G. Greene
V. Mubay
R. Davis
130 BNL
Upton, NY 11973

Fauske and Associates, Inc.
Attn: R. Henry
16W070 West 83rd Street
Burr Ridge, IL 60952

Battelle Columbus Laboratory (4)
Attn: R. Denning
J. Gieseke
K. Lee
C. Alexander
505 King Avenue
Columbus, OH 43201

Department of Energy
Scientific and Tech. Info. Center
P.O. Box 62
Oak Ridge, TN 37831

EG&G Idaho
Willow Creek Building, W-3
Attn: R. Hobbins
P.O. Box 1625
Idaho Falls, ID 83415

Battelle Pacific Northwest Laboratory
Attn: M. Freshley
P.O. Box 999
Richland, WA 99352

Wang Lu
TVA
400 Commerce, WGC 157-CK
Knoxville, TN 37902

Professor R. Seale
Department of Nuclear Engineering
University of Arizona
Tucson, Arizona 85721

Oak Ridge National Laboratory (3)
Attn: T. S. Kress
S. Hodge
T. Wright
P.O. Box Y
Oak Ridge, TN 37830

S. Rosen
Nuclear Fuel Engineering
ABB Combustion Engineering
Nuclear Power
1000 Prospect Hill Road
P.O. Box 500
Windsor, CT 06095-0500

Alan Nelson
NUMARC
1776 I Street NW
Suite 300
Washington, DC 20006

Professor T. G. Theofanous
University of California Santa Barbara
Chemical and Nuclear Engineering Dept.
UC-Santa Barbara
Santa Barbara, CA 93106

D. Osetek
Los Alamos Technical Associates
Building 1, Suite 400
2400 Louisiana NE
Albuquerque, NM 87110

David Leaver
TENERA
1340 Saratoga-Sunnyvale Rd.
Suite 206
San Jose, CA 95129

FOREIGN DISTRIBUTION

Alan Jones
ISPRA
CEC Joint Research Center
21020 Varese
ITALY

Japan Atomic Energy Research Institute
Tokai Research Establishment
Attn: Dr. S. Matsuura, Deputy Director General
Tokai-mura, Naka-gun, Ibaraki-ken
319-11
JAPAN

Japan Atomic Energy Research Institute (4)
Severe Accident Research Laboratory
Attn: K. Soda
J. Sugimoto
N. Yamano
Y. Maruyama
Tokai-mura, Naka-gun, Ibaraki-ken
319-11
JAPAN

Japan Atomic Energy Research Institute
Reactor Accident Laboratory
Attn: Dr. T. Fujishiro, Head
Tokai-mura, Naka-gun, Ibaraki-ken
319-11
JAPAN

Technische Universitat Munchen
Attn: Professor H. Karwat
8046 Garching, Forschungagelande
Munich
GERMANY

Kernforschungszentrum Karlsruhe (4)
Attn: H. Alsmeyer
P. Hofmann
B. Kuczera
S. Hagen
Postfach 3640
75 Karlsruhe
GERMANY

Nucleare e delie Protezione Sanitaria (DISP) (2)
Attn: Mr. Manilia
Mr. G. Petrangeli
Ente Nazionnle Energie Alternative (ENEA)
Viale Regina Margherita, 125
Caselle Postale M. 2358
I-00100 Roma A. D.
ITALY

Dr. K. J. Brinkman
Reactor Centrum Nederland
1755 ZG Petten
THE NETHERLANDS

M. Jankowski
International Atomic Energy Agency
Division of Nuclear Reactor Safety
Wagranerstrasse 5
P.O. Box 100
A/1400 Vienna
AUSTRIA

Stratens Karnfraftinspektion (2)
Attn: L. Hammer
W. Frid
P.O. Box 27106
S-10252 Stockholm
SWEDEN

Studvik Energiteknik AB
Attn: K. Johansson
5-611 82 Nykoping
SWEDEN

Institute of Nuclear Energy Research
Attn: Sen-I Chang
P.O. Box 3
Lungtan
Taiwan 325
REPUBLIC OF CHINA

P. Fehrenbach
Atomic Energy Canada, Ltd.
Chalk River, Ontario
CANADA KOJ IJO

Korea Advanced Energy Research Institute
Attn: H. R. Jun
P.O. Box 7
Daeduk-Danji
Choong-Nam
KOREA

POSTECH
Dept. of Mechanical Eng.
Attn: Moo Hwan Kim
P.O. Box 125
Kyungbuk 790-600
KOREA

Md. C. Lecomte
CEN FAR
60-68 Av. du G. Leclerc-B.P.6
92265 Fontenay aux Roses Cedex
FRANCE

Dr. A. Meyer-Heine
CEN Cadarache
13108 Saint Paul Lez Durance
FRANCE

H. Bairiot, Chief
Department LWR Fuel
Belgonucleair
Rue de Champ'e Mars. 25
B-1050 Brussels
BELGIUM

J. E. Antill
Berkeley Nuclear Laboratory
Berkeley GL 139 PB
Gloucestershire, England
UNITED KINGDOM

W. G. Cunliffe
Bldg. 396
British Nuclear Fuels, Ltd.
Springfield Works
Salwick, Preston
Lancashire, England
UNITED KINGDOM

AEA Technology (7)
Attn: A. Nichols, 102/A50
T. Butland
B. Bowsher, 105A/A50
J. Mitchell, 01/A50
P. Smith, 215,A23
D. Sweet, 210/A32
D. Williams, 210/A32
Winfrith, Dorchester
Dorset DT2 8DH, England
UNITED KINGDOM

Itaru Kaneko
Chemical Techology Group
Nuclear Engineering Laboratory
Toshiba Corporation
4-1 Ukishima Cho, Kawasaki Ku
Kawasaki 210
JAPAN

Japan Atomic Energy Research Institute
Attn: K. Sato
Fukoku Seime Building
2-2-2, Uchisaiwai-cho, Chiyoda-ku, Tokyo
JAPAN

Mr. F. Abbey (2)
AEA Technology
Safety and Reliability Directorate
Wigshaw Lane
Culcheth
Cheshire WA3 4NE
UNITED KINGDOM

Simon J. Board
CEGB National Power
Barnett Way
Barnwood, Gloucestershire GL4 7RS
ENGLAND

Nigel E. Buttery
Central Elect. Gen. Board, Booths Hall
Chelford Road, Knutsford
Cheshire WA16 8QG
ENGLAND

Professor Agustin Alonso
E.T.S. Ingenieros Industriales
Jost Gutierrez Abascal 2
28006 Madrid
SPAIN

Jose Angel Martinez
Sub. Emplazamientos y Programas Loop
CONSEJO DE SEGURIDAD NUCLEAR
Justo Doradoll
28040 Madrid
SPAIN

Juan Bagues
CONSEJO DE SEGURIDAD NUCLEAR
SOR Angela de la Cruz No. 3
28056 Madrid
SPAIN

G. Caropreso
Dept. for Environmtl Protection & Health
ENEA CRE Casaccia
Via Anguillarese, 301
00100 Roma Ad.
ITALY

P. Ficara
Department for Thermal Reactors
ENEA CRE Casaccia
Via Anguillarese, 301
00100 Roma Ad.
ITALY

Klaus Trambauer
Gesellschaft Fuer Reaktorsicherheit
Forschungsgelande
D-8046 Garching
GERMANY

UKAEA (3)
Attn: D. Sweet
S. Kinnersly 203/A32
D. Williams 210/A32
Winfrith, Dorchester
Dorset DT2 8DH
UNITED KINGDOM

UKAEA Culham Laboratory
Attn: B. D. Turland E5.157
Abingdon
Oxfordshire OX14 3DB
UNITED KINGDOM

UKAEA
Reactor Development Division
Attn: T. Butland
Winfrith, Dorchester
Dorset DT2 8DH
UNITED KINGDOM

M. R. Hayns
AEA Reactor Services
B329
Harwell
Didcot
Oxfordshire OX11 ORA
UNITED KINGDOM

Japan Atomic Energy Research Institute
Severe Accident Research Laboratory
Attn: Dr. K. Soda, Head
Tokai-mura, Naka-gun, Ibaraki-ken
319-11
JAPAN

Japan Atomic Energy Research Institute
Reactivity Accident Laboratory
Attn: Toyoshi Fuketa
Tokai-Mura, Ibaraki-Ken
319-11
JAPAN

R. D. MacDonald
Atomic Energy Canada, Ltd.
Chalk River, Ontario
CANADA KOJ IJO

Atomic Energy Canda Ltd.
Attn: Vijay I. Ngth
Sheridan Park Res. Comm.
Mississauga, Ontario
Canada L5K 1B2

Oguz Akalin
Ontario Hydro
700 University Avenue
Toronto, Ontario
CANADA M5G 1X6

K. N. (Kannan) Tennankore
Safety Research Division
Whiteshell Nuclear Res. Establishment
Pinawa, Manitoba
CANADA ROE 1LO

J. Clive Wood
Safety Research Division
Whiteshell Nuclear Res. Establishment
Pinawa, Manitoba
CANADA ROE 1LO

Korea Adv. Energy Research Institute
Attn: Hee-Dong Kim
P.O. Box 7
Daeduk-Danji
Choong-Nam
KOREA

Chang K. Park
Korea Atomic Energy Research Institute
Korea Advanced Energy Research Institute
P.O. Box 7, Daeduk Danji
Taejon 305-353
KOREA

Jong In Lee
Severe Accident Assessment Department
Korea Institute of Nuclear Safety
P.O. Box 16, Daeduk-Danji
Daejeon, 305-353
KOREA

Institute of Nuclear Energy Research
Attn: Yi-Bin Chen
P.O. Box 3
Lungtan
Taiwan 32500
REPUBLIC OF CHINA

Dr. A. Tattegrain
CEN Cadarache
13108 Saint Paul lez Durance
FRANCE

Dr. G. Hache
CEN Cadarache
13108 Saint Paul lez Durance
FRANCE

Jacques Duco
Centre d'Etudes Nucleaires (IPSN-DAS)
Commissariat a l'Energie Atomique
Boite Postale No. 6
F-92265 Fontenay-aux-Roses Cedex
FRANCE

Maurice Gomolinski
Protection and Nuclear Safety Institute
Commissariat a l'Energie Atomique
Boite Postale No. 6
F-92265 Fontenay-aux-Roses Cedex
FRANCE

Michel Livolant
Inst. de Protection et de Surete Nucl.
Commisariat a l'Energie Atomique
Boite Postale No. 6
F-92265 Fontenay-aux Roses Cedex
FRANCE

Jorma V. Sandberg
Department of Nuclear Safety
Finnish Center Radiation & Nucl. Safety
P.O. Box 268
SF-00101 Helsinki
FINLAND

Lasse Mattila
Nuclear Engineering Laboratory
Technical Research Center of Finland
P.O. Box 169
SF-00181 Helsinki
FINLAND

S. Chakraborty
Swiss Federal Nucl. Safety Inspectorate
CH-5303 Wurenlingen
SWITZERLAND

J. Peter Hosemann
Light Water Reactor Safety Program
Paul Scherrer Institute
CH-5232 Villigen PSI
SWITZERLAND

Vladimir Asmolov
I.V. Kurchatov Institute of Atomic Energy
Moscow 123182
Kurchatov Square
CIS

SANDIA DISTRIBUTION

6400 N. R. Ortiz
6403 W. A. von Riesemann
6404 D. A. Powers (5)
6412 A. Camp
6413 F. T. Harper
6413 T. D. Brown
6413 J. C. Helton
6413 L. A. Miller
6414 J. Kelly
6415 K. D. Bergeron
6418 S. L. Thompson
6422 M. D. Allen
6422 N. Bixler
6422 J. E. Brockmann
6422 T. K. Blanchat
6422 T. Y. Chu
6422 R. M. Elrick
6422 T. J. Heames
6429 K. E. Washington
6429 D. C. Williams
6429 K. K. Murata
6501 J. V. Walker
6602 J. L. Sprung
7141 Technical Library (5)
7151 Technical Publications
8523 Central Technical Files

NRC FORM 335 (2-89) NRCM 1102 3201 3202

U.S. NUCLEAR REGULATORY COMMISSION

BIBLIOGRAPHIC DATA SHEET

(See instructions on the reverse)

1 REPORT NUMBER (Assigned by NRC. Add Vol., Supp., Rev., and Addendum Numbers, if any.)
NUREG/CR-5978
SAND92-2688

2 TITLE AND SUBTITLE

Source Term Attenuation by Water in the Mark I Boiling Water Reactor Drywell

3 DATE REPORT PUBLISHED
MONTH: September
YEAR: 1993

4 FIN OR GRANT NUMBER
L1484

5 AUTHOR(S)

D. A. Powers

6 TYPE OF REPORT
Technical

7 PERIOD COVERED (Inclusive Dates)

8 PERFORMING ORGANIZATION - NAME AND ADDRESS (If NRC, provide Division, Office or Region, U.S. Nuclear Regulatory Commission, and mailing address; if contractor, provide name and mailing address.)

Sandia National Laboratories
Albuquerque, NM 87185

9 SPONSORING ORGANIZATION - NAME AND ADDRESS (If NRC, type "Same as above"; if contractor, provide NRC Division, Office or Region, U.S. Nuclear Regulatory Commission, and mailing address.)

Division of Systems Research
Office of Nuclear Regulatory Research
U.S. Nuclear Regulatory Commission
Washington, D.C. 20555-0001

10 SUPPLEMENTARY NOTES

11 ABSTRACT (200 words or less)

Mechanistic models of aerosol decontamination by an overlying water pool during core debris/concrete interactions and spray removal of aerosols from a Mark I drywell atmosphere are developed. Eighteen uncertain features of the pool decontamination model and 19 uncertain features of the model for the rate coefficient of spray removal of aerosols are identified. Ranges for values of parameters that characterize these uncertain features of the models are established. Probability density functions for values within these ranges are assigned according to a set of rules. A Monte Carlo uncertainty analysis of the decontamination factor produced by water pools 30 and 50 cm deep and subcooled 0-70 K is preformed. An uncertainty analysis for the rate constant of spray removal of aerosols is done for water fluxes of 0.25, 0.01, and 0.001 cm^3 H_2O/cm^2-s and decontamination factors of 1.1, 2, 3.3, 10, 100, and 1000.

12 KEY WORDS/DESCRIPTORS (List words or phrases that will assist researchers in locating the report.)

Source term, water pools, aerosols, sprays, source term mitigation, drywell, core debris/concrete interactions Monte Carlo sampling, uncertainty analysis

13 AVAILABILITY STATEMENT
Unlimited

14 SECURITY CLASSIFICATION
(This Page) Unclassified
(This Report) Unclassified

15 NUMBER OF PAGES

16 PRICE

END

DATE
FILMED
12/9/93